Impacts of pumping on the distribution of arsenic in Bangladesh groundwater

M. Rajib Hassan Mozumder

Submitted in partial fulfillment of the
requirements for the degree of
Doctor of Philosophy
in the Graduate School of Arts and Sciences

COLUMBIA UNIVERSITY
2019

ABSTRACT

Impacts of pumping on the distribution of arsenic in Bangladesh groundwater

M. Rajib Hassan Mozumder

Chronic exposure to naturally occurring arsenic (As) in groundwater threatens the health of >150 million villagers in S/SE Asia. In Bangladesh, low As aquifers offer the best hope of reducing the exposure of 35-40 million remain exposed to elevated levels of As in drinking water (>10 µg/L). These low As aquifers could be affected, however, by massive pumping from shallow (<30 m) depths for growing rice and overexploitation of deeper aquifer for municipal water supply. The goal of this dissertation is to assess the impacts of groundwater pumping on the distribution in groundwater of dissolved As, reactive carbon, and redox-sensitive elements in anoxic aquifers of Bangladesh based on long-term hydrologic measurements, geochemical analyses, and numerical flow modeling.

In the second chapter, changes in the well-water As concentrations within a 25 km^2 area over a 10+ year timespan are assessed on the basis of continuous time series for 18 monitoring wells, a set of 271 wells resampled three times, and a large dataset obtained from blanket surveys of several thousand wells in the region. The two larger data sets both show a 10% decline in the initial areal mean As of 100 µg/L. This decline can be explained by flushing of As in the shallow aquifer by low-As recharge water, evidently compensated to some extent by the desorption of sediment-bound As. The presence of a large exchangeable pool of As in the sediment therefore seems to buffer changes in the distribution of As in the face of large perturbation in groundwater flow, albeit not enough to prevent some trends indicated by the detailed time series. The third chapter provides a complementary perspective on groundwater-sediment interactions by

quantifying the rates of adsorption and desorption of As with column experiments conducted in the field for two different types of sediments: grey reduced Holocene sands and orange oxidized Pleistocene sands. The data show that, contrary to widely held beliefs, retardation of As transport by adsorption is quite similar in Holocene and Pleistocene sediments, even if Holocene sands initially contain a much larger pool of easily mobilizable As. The field column experiments also showed significant changes in solid phase speciation that affected As retention within a timespan of only a few weeks. Detailed field observations and flow modeling in the fourth chapter examine how perturbed flow paths can draw either As or reactive carbon into a Pleistocene aquifer. A groundwater flow model, constrained by head measurements and isotopic tracer data shows that certain portions of the aquifer are becoming increasingly contaminated with As as a result of municipal pumping, but against a background of redox transformation in the aquifer that probably preceded this perturbation.

Overall, the research conducted for this thesis shows that alteration of the hydrological system due to local and regional forcing is affecting the distribution of As in groundwater. These changes do not affect all wells yet and, if they do, the increase in As concentrations observed so far are gradual because of the buffering capacity of the sediment. Lowering exposure by targeting low As aquifer should therefore definitely continue in Bangladesh, with particular attention paid to regular monitoring using vulnerability criteria this research has helped to identify.

TABLE OF CONTENTS

LIST OF FIGURES

model.

LIST OF TABLES

ACKNOWLEDGEMENTS

DEDICATION

To my wife Nadia and my parents Shahjahan and Hasina

who sacrificed the most to see me succeed ...

CHAPTER 1

INTRODUCTION

1.1. Scale of poisoning by arsenic

An estimated 830 million people in the world still lack safe water access. Ensuring easy, equitable access to clean drinking water and sanitation is one of the United Nation's sustainable development goals with an especial emphasis on testing water quality for fecal contaminants, arsenic (As), and fluoride (JMP/UNICEF, 2017). Elevated levels of As contaminates the drinking water of approximately 200 million people across the globe (Naujokas et al., 2013); half of the population exposed are from S/SE Asia (Fendorf et al., 2010) (Figure 1-1), drinking groundwater from tens of millions of wells containing As above the World Health Organization (WHO) guideline of 10 μg/L (WHO 1993; Fihser et al., 2017). In Bangladesh alone, about 35-40 million are exposed chronically to geogenic As, resulting in an increase in mortality (Argos et al., 2010; Flanagan et al., 2012), mainly due to cardiovascular disease (Chen et al., 2011) and various cancers (Smith et al., 2000; BGS/DPHE, 2001). Due to microbially contaminated surface water (e.g. pond, river) and lack of piped, chlorinated water supply systems, rural Bangladeshis heavily rely on groundwater for their domestic use. A large fraction of the 80% rural population of Bangladesh drinking daily from hand-pumped wells is exposed to elevated levels of As (Ahmed, 2011). The consumption of rice as staple food, which is often grown in soil irrigated with high As groundwater (Panaullah et al., 2009; Dittmar et al., 2007, 2010; Huhmann et al., 2017), could also be a significant, secondary exposure pathway (Duxbury et al., 2003). To date, blanket As testing campaigns that encourage safe well sharing (van Geen et al., 2002; 2014) and installation of deep community wells are the most popular forms of mitigation (van Geen et al.,

2003; Ahmed et al., 2006; Ravenscroft et al., 2013, 2014 2018) because groundwater As-removal technologies have proved currently not be sustainable (Ravenscroft et al., 2009). Although the sedimentary aquifers of S/SE Asia are contaminated with naturally occurring As, the extent and magnitude of As poisoning could potentially be exacerbated by large-scale hydrologic perturbations (Micheal et al., 2008; Winkel et al., 2011; van Geen 2013; Stahl et al., 2016; Knappette et al., 2016; Khan et al., 2016). This thesis is composed of three studies taking different approaches to address the issue of potential perturbations by pumping of the distribution of As in the subsurface.

1.2. Geogenic occurrence of Arsenic in alluvial aquifers

Geogenic As is commonly associated in alluvial sediments with sulfides and iron and manganese oxides (Smedley & Kinniburgh, 2002; Lowers et al., 2007). Scientists have for at least two decades been bewildered by the presence of high As (100s-1000s μg/L) in groundwater in contact with the aquifer sediment in some regions and not in others. The fluvio-deltaic sediments of Bangladesh and elsewhere in S/SE Asia contains a wide range but not exceptionally high levels of sediment-bound As comparable to average crustal concentrations of 2 mg/kg (Mason, 1966). Even without considering that sedimentary As concentrations are somewhat higher (up to 20 mg/kg) in fine-grained materials (e.g. clay) compared to sand (1-5 mg/kg of As), sandy aquifers contain more than enough As to potentially pose a health risk. A simple calculation shows, for instance, if only a hundredth of the total sorbed As (0.01 mg/kg) is transferred to groundwater in an uncontaminated aquifer with 30% porosity and a bulk density of 2.65 g/cm^3 (BGS/DPHE, 2001), the aqueous As concentration would rise to 62 μg/L, which is about 6 times higher than the WHO prescribed guideline of 10 μg/L of As in drinking water (Figure 1-2).

Bangladesh, the largest As contaminated delta in the world, receives its sediment supply from the

Himalayas drained by Ganges, Brahmaputra, and other rivers depositing thick sequences of dark gray, organic rich, Holocene alluvial sediment (Roy & Chatterjee, 2015). A hiatus in sediment supply is indicated by the weathered and oxidized Pliocene-Pleistocene *Dupi-Tila* orange sand that were subaerially exposed during the last glacial Maximum (Umitsu, 1987, 1994). The *Dupi-Tila* aquifer is typically low in As (BGS/DPHE, 2001; Burgess et al., 2011) and is often overlain by As elevated (frequently >100 µg/L) shallow alluvial aquifers separated by a clay aquitard. The depth to the top of the low-As Pleistocene aquifer varies locally as well as regionally as such the spatial prediction of As in groundwater remains challenging (Figure 1-3).

The general consensus is that As is released in groundwater in this part of the world through microbially mediated reductive dissolution of sediment bound iron-oxy-hydroxides fueled by the oxidation of organic carbon (Ahmed et al., 1998b; Nickson et al., 1998; Bhattacharya et al., 1997; BGS/DPHE, 2001; McArthur et al., 2001; Berg et al., 2001; Harvey et al., 2002; Oremland & Stolz, 2003; Ahmed et al., 2004; van Geen et al., 2004; Swartz et al., 2004; Oremland & Stolz, 2005). The color of sediment (reduced gray vs. less reduced orange), thus, provides the first line of evidence on the status of solid phase Fe reduction as a result of transformation of Fe(III) phases to mixed Fe(II)/Fe(III) phases and concomitant release of As into the solution (Horneman et al., 2004; von Brömssen et al., 2007). The reduction of As(V) to As(III), often considered less particle-bound and more toxic, is believed to follow the reductive dissolution of Fe(III) oxides (BGS/DPHE, 2001; Islam et al., 2004; Tufano & Fendorf 2008; Fendorf et al., 2010) (Figure 1-4). The reductive dissolution also release phosphate, competing with As for sorption sites on iron-oxy-hydroxide mineral surfaces, as other products of weathering and carbon metabolism such as silica and bicarbonate, respectively. Following the initial As release, the dissolved concentration of As in the aquifer is primarily maintained by the adsorption (desorption) of As

on (from) the remaining (i.e. undissolved) iron oxides and/or newly formed secondary mineral phases.

Microbial reduction of As(V) and/or Fe(III) and associated solid phase transformations require a supply of reactive organic carbon under anoxic condition (BGS/DPHE, 2001; McArthur et al., 2001, 2004). These generally follow the mineralization of organic carbon in the subsurface driven by the microbial respiration of O_2, the reduction of NO_3^- to NO_2^- and eventually N_2, and the reduction Mn-oxides to dissolved Mn^{2+} (Olson et al. 1981; Chappelle et al., 1987; Lovley et al., 1990). Subsequent steps as such the reduction of Fe(III)-oxides to soluble Fe^{2+}, SO_4^{2-} to S^{2-}, and production of CH_4 by methanogens and/or acetate fermentation often appear to co-occur in Bengal basin aquifers. More recently, Achaea catalyzed Fe mediated anaerobic oxidation of CH_4 has been postulated as a viable mechanism for the release of trace metals and/or metalloids in groundwater (Ettwig et al., 2016), which could potentially facilitate direct Fe(III) reduction and release As in Bangladesh groundwater with low SO_4 levels (Ravenscroft et al., 2009). On a regional scale, the shallow groundwater of Bangladesh is elevated in dissolved CH_4 of biogenic origin (Ahmed et al. 1998a; Harvey et al., 2002).

1.3. Anthropogenic influence on As pollution

1.3.1. *Hydrological consequences of pumping*

Massive pumping of groundwater could potentially exacerbate the magnitude and extent of As contamination in Asian megadeltas, although the extent to which it has is still debated (Michael & Voss, 2008; Mukherjee et al., 2011; Winkel et al., 2011; Burgess et al., 2012; van Geen et al., 2013; Stahl et al., 2016; Knappette et al., 2016; Khan et al., 2016; Postma et al., 2017). The two major human induced hydrologic perturbations in the Bengal Basin are typically shallow

irrigation pumping for growing rice and deeper groundwater abstraction for municipal water supply. Widespread shallow irrigation for growing rice is the main consumer of groundwater in rural Bangladesh since 1970s (Shamsudduha et al., 2011). Groundwater irrigation for *Boro* rice requires the rice fields to be submerged and require about a meter of water during the dry season, causing a drop in groundwater level that is usually but not always compensated by recharge during the monsoon (Ahmed, 2011). The municipal supply of groundwater is primarily met from low-As, deep Pleistocene aquifers in Dhaka metropolitan City, but overexploitation has caused groundwater levels to drop at a staggering rate of about 3 m/year (IWM & DWASA, 2011; Ahmed, 2011; Knappette et al., 2016; Khan et al., 2016). Deep groundwater meets about 90% of the current municipal supply for ~10 million City dwellers (DWASA, 2008) at a rate of 1.9×10^6 m^3/day (DWASA 2012) mainly through DWASA installed production wells tapping the *Dupi Tila* aquifers. Last several decades of overexploitation dewatered the upper *Dupi Tila* aquifer (Ahmed et al., 1999; Hoque et al., 2007), increased vertical leakage from polluted surface water bodies (Hassan et al., 1999), and gradually expanded the pumping cone of depression in adversely As-affected regions well beyond the urban periphery (Knappette et al., 2016; Khan et al., 2016). The expanding cone of depression around Dhaka has also started to limit access to groundwater with surface-mounted hand-pumps.

1.3.2. *Geochemical consequences of pumping*

The demands from both shallow and deep aquifers must have been compensated to some extent by recharge from surface water bodies (e.g. rivers, ponds) and may have enhanced a flux of reactive carbon from these sources that could have triggered additional release of As to groundwater (Harvey et al., 2002; Polizotto et al., 2005; Datta et al., 2009; Neumann et al., 2010; Lawson et al, 2013; Mihajlov et al., 2016; Desbarats et al, 2014; 2017). For instance, irrigation

pumping for growing rice could be expected to flush As from the shallow aquifer over time (BGS/DHPE, 2001; Harvey et al., 2003; McArthur et al., 2004; Harvey et al., 2006; Stute et al., 2007; van Geen et al., 2008; Shamsudduha et al., 2015). The magnitude of shallow aquifer contamination will then depend on the rate at which recharge water entrains and accumulates (newly) mobilized As along the flow path. The shallow recharge rate will rely on the presence or absence of conductive (permeable) layers (e.g. sand) at the surface (Aziz et al., 2008; Weinman et al., 2008). Over time, recharge low in As will continue to replace high As shallow groundwater (Stute et al., 2007; van Geen et al., 2008) and high As groundwater irrigated soil will continue to accumulate As (Meharg & Rahman, 2003). At the same time, shallow irrigation pumping could potentially increase the input of fresh reactive from near surface environments (e.g. sedimentary peat layers, ponds). This accelerated flux could drive reductive dissolution of Fe oxides and increase the scale of As pollution (Harvey et al., 2002; Neuman et al., 2010; Plizotto et al., 2005). These opposing consequences of human perturbation may have contributed to the complex spatiotemporal distribution of dissolved As in shallow aquifers of Bangladesh.

In spite of these potential perturbations, the relatively stable groundwater composition of the deep (>150 m) aquifers with typically low As have provided a sustainable mitigation option in many regions of the Bengal Basin (Ravenscroft et al., 2013, 2014, 2018; Mihajlov et al., 2016). However, as groundwater demand in Dhaka City is likely to increase in the foreseeable future, the Dhaka cone would continue to grow beyond the City limits and the likelihood of shallow high As/DOC groundwater intrusion to the deep aquifer would rise in response to an increase in lateral/vertical head gradients. The most affected regions will be the rural areas of Bangladesh where the deeper Plio-Pleistocene low-As aquifer is overlain by As contaminated shallow groundwater.

1.4. Predicting As transport

Basin scale groundwater flow models with simulated physical heterogeneity (Michael & Voss, 2008) indicate that preferential transport of As could contaminate the deep low-As aquifers under the current Dhaka pumping scenario (Khan et al., 2016). Similar models are utilized with chemical heterogeneity (differences in As sorption) to evaluate the spread of As contamination with respect to groundwater flow (Michael & Khan, 2016). The sustainability of deep low-As aquifers under enhanced flow rate, therefore, will primarily depend on the geologic (physical) distribution of sedimentary facies (sand and clay), sediment adsorption capacity (Radloff et al., 2011; van Geen et al., 2013) and future groundwater abstraction practices (Michael & Voss, 2008). For example, under the current pumping scenario, an assumed As partition coefficient (K_D) of only 1.2 L/kg would delay the migration of shallow As for thousands of years when only domestic pumps draw deep groundwater whereas the same model predicts shallow water intrusion in <1000 year if irrigation water were also drawn from deep water resources (Michael & Voss, 2008; Radloff et al., 2011).

1.5. Organization of this thesis

The over-arching goal of my research has been to identify sources, transport pathways, and sinks of As to groundwater in perturbed hydrologic systems. I examined how anthropogenic activities such as intensive groundwater pumping for irrigation and municipal supply may affect the subsurface chemical environment, altering groundwater geochemistry and the magnitude of As contamination. The change in the distribution of As in response to a shift in water use is investigated over a time scale of minutes to thousands of years and spatial scale of centimeters to tens of kilometers on the basis of field observations and model predictions. The study area is located in Araihazar, the most densely populated region of Bangladesh, perturbed by shallow

irrigation pumping as well as deep, Dhaka pumping. The area is located in a geologically transitional zone, providing an unique outset for geoscientists and biomedical researchers alike to track how pumping induced changes influence the heterogeneous distribution of As and how this evolution has impacted human health.

In **Chapter 2**, I exploit a unique data set of two large well testing campaigns conducted a decade apart in the same 25 sq. km area to determine the spatiotemporal variability of shallow (<30 m deep) As concentrations based on geostatistical analysis. After addressing the challenges of comparing the two data sets, I present several lines of evidence from the repeated surveys to challenge the notion that shallow groundwater As are necessarily stable over time. This is significant because changing levels in drinking water sources would influence As exposure. The spatial variability and assumed temporal stability of well-water As concentrations among neighboring shallow wells in the study area has a leading As avoidance by well switching and sharing, but this practice may not be sustainable if well concentrations are less stable than previously recognized. Both long-term and short-term variations in As were assessed and the observed changes are attributed to widespread irrigation pumping for growing rice.

Chapter 3 of this thesis examines the extent to which adsorption of As delays transport relative to groundwater flow. To understand the potential differences in As retention for different sediments, I conducted a 3 weeklong field column experiment with both Holocene gray sand and Pleistocene orange sand under controlled conditions. The novelty of my experiment lies in the use of unaltered shallow groundwater directly from a well to elute cored sediment columns collected and maintained under anoxic condition in the field. Contrary to the widely held belief that Fe(III)-dominated Pleistocene sands sorb more As than Fe(II+III) sands, the results indicate that As retardation is comparable in the two types of sediment. Adsorption was kinetically

limited under the conditions of the experiments and could be explained by a unique set of rate constants derived from a 1D numerical solute transport model. Although the main purpose of the experiment was to compare As sorption between two major types of aquifer sands, the columns also underwent biogeochemical transformation in response to iron and sulfur reduction at the later phase that affected As partitioning. These changes were quantified using synchrotron-based Fe and As K-edge X-ray absorption spectral analysis.

Chapter 4 presents a detailed hydrogeological investigation based environmental tracers and isotopic analyses to assess the vulnerability of low-As intermediate (40-75 m deep) Pleistocene aquifers under the influence of municipal (Dhaka) pumping across a 3 sq. km area. The sustainability of drawing low-As water from this intermediate aquifer is important because rural Bangladeshis exploit the aquifer widely as a low-cost alternative to deeper, more expensive wells that are typically installed only by the government. The study was motivated by the repeated failure of a community well tapping the intermediate aquifer for which As concentrations increased over time. This chapter explores two possible hydrologic pathways of As contamination of safe aquifers located just below the interface between generally contaminated Holocene aquifer and typically low-As Pleistocene aquifers. The first considers the role of *recharge windows* (breaks in clay aquitard) as potential conduits for the intrusion of shallow groundwater elevated with As/DOC/CH_4 to the Pleistocene confined (clay capped) aquifer in the face of massive depressurization at depth due to Dhaka pumping. The second pathway considers the role of the clay aquitard itself as a potential source of reactive carbon that had driven the release of reduction of Fe oxides and release of As over geologic timescales, and a process that may have been accelerated more recently by Dhaka pumping. A 3D numerical groundwater flow model was constructed with boundary conditions derived from existing reference heads to

9

explain the past, present, and future As pollution scenarios.

The field-driven research contained in this thesis is representative of the current status of our understanding of the distribution of As in groundwater and its sensitivity to hydrological perturbations. The approach combines fairly routine field observations conducted over a long time or over large areas with some of the most sophisticated spectroscopic techniques available today. I hope the outcome will be of interest to geochemists, geologists, hydrogeologists, and water resources managers investigating the As crisis in Bangladesh and similar fluvio-deltaic settings in S/SE Asia where reductive dissolution of iron oxide is the dominant As release mechanism. Each of the three chapters is organized as a separate article and has its own abstract and references.

1.6. References

Ahmed K. M. (2011) Groundwater contamination in Bangladesh. In *Water Resources Planning and Management* (eds. K. Hussey and R. Q. Grafton). Cambridge University Press, Cambridge. pp. 529–560. Available at: https://www.cambridge.org/core/books/water-resources-planning-and-management/groundwater-contamination-in-bangladesh/78D816AC68854C29717A4A735052EC74.

Ahmed K. M., Bhattacharya P., Hasan M. A., Akhter S. H., Alam S. M. M., Bhuyian M. A. H., Imam M. B., Khan A. A. and Sracek O. (2004) Arsenic enrichment in groundwater of the alluvial aquifers in Bangladesh: an overview. *Appl. Geochem.* **19**, 181–200.

Ahmed K. M., Hasan M. K., Burgess W. G., Dottridge J., Ravenscroft P. and van Wonderen J. (1999) The Dupi Tila aquifer of Dhaka, Bangladesh: hydraulic and hydrochemical response to intensive exploitation. In *Groundwater in the urban environment: selected city profiles.* (ed. P. J. Chilton). Balkema, Rotterdam. pp. 19–30. Available at: http://discovery.ucl.ac.uk/169447/ [Accessed October 19, 2018].

Ahmed K. M., Hoque M., Hasan M. K., Ravenscroft P. and Chowdhury L. R. (1998a) Occurrence and origin of water well methane gas in Bangladesh. *J. Geol. Soc. India* **51**, 697–708.

Ahmed K. M., Imam M. N., Akhter S. H., Hasan M. A., Alam M. M., Chowdhury S. Q., Burgess W. G., Nickson R., McArthur J. M., Hasan M. K., Ravenscroft P. and Rahman M. (1998b) Mechanism of arsenic release to groundwater: geochemical and mineralogical evidence. In International Conference on Arsenic Pollution on Groundwater in Bangladesh: Causes, Effects, and Remedies. Dhaka Community Hospital, Dhaka, Bangladesh.

Ahmed M. F., Ahuja S., Alauddin M., Hug S. J., Lloyd J. R., Pfaff A., Pichler T., Saltikov C., Stute M. and Geen A. van (2006) Ensuring Safe Drinking Water in Bangladesh. *Science* **314**, 1687–1688.

Argos M., Kalra T., Rathouz P. J., Chen Y., Pierce B., Parvez F., Islam T., Ahmed A., Rakibuz-Zaman M., Hasan R., Sarwar G., Slavkovich V., Geen A. van, Graziano J. and Ahsan H. (2010) Arsenic exposure from drinking water, and all-cause and chronic-disease mortalities in Bangladesh (HEALS): a prospective cohort study. *The Lancet* **376**, 252–258.

Aziz Z., van Geen A., Stute M., Versteeg R., Horneman A., Zheng Y., Goodbred S., Steckler M., Weinman B., Gavrieli I., Hoque M. A., Shamsudduha M. and Ahmed K. M. (2008) Impact of local recharge on arsenic concentrations in shallow aquifers inferred from the

electromagnetic conductivity of soils in Araihazar, Bangladesh. *Water Resour. Res.* **44**, W07416.

Berg M., Tran H. C., Nguyen T. C., Pham H. V., Schertenleib R. and Giger W. (2001) Arsenic Contamination of Groundwater and Drinking Water in Vietnam: A Human Health Threat. *Environ. Sci. Technol.* **35**, 2621–2626.

Bhattacharya P., Chatterjee D. and Jacks G. (1997) Occurrence of Arsenic-contaminated Groundwater in Alluvial Aquifers from Delta Plains, Eastern India: Options for Safe Drinking Water Supply. *Int. J. Water Resour. Dev.* **13**, 79–92.

von Brömssen M., Jakariya M., Bhattacharya P., Ahmed K. M., Hasan M. A., Sracek O., Jonsson L., Lundell L. and Jacks G. (2007) Targeting low-arsenic aquifers in Matlab Upazila, Southeastern Bangladesh. *Sci. Total Environ.* **379**, 121–132.

Burgess W. G., Hasan M. K., Rihani E., Ahmed K. M., Hoque M. A. and Darling W. G. (2011) Groundwater quality trends in the Dupi Tila aquifer of Dhaka, Bangladesh: sources of contamination evaluated using modelling and environmental isotopes. *Int. J. Urban Sustain. Dev.* **3**, 56–76.

Chapelle F. H., Zelibor J. L., Grimes D. J. and Knobel L. L. (1987) Bacteria in deep coastal plain sediments of Maryland: A possible source of CO2 to groundwater. *Water Resour. Res.* **23**, 1625–1632.

Chen Y., Graziano J. H., Parvez F., Liu M., Slavkovich V., Kalra T., Argos M., Islam T., Ahmed A., Rakibuz-Zaman M., Hasan R., Sarwar G., Levy D., Geen A. van and Ahsan H. (2011) Arsenic exposure from drinking water and mortality from cardiovascular disease in Bangladesh: prospective cohort study. *BMJ* **342**, d2431.

Datta S., Mailloux B., Jung H.-B., Hoque M. A., Stute M., Ahmed K. M. and Zheng Y. (2009) Redox trapping of arsenic during groundwater discharge in sediments from the Meghna riverbank in Bangladesh. *Proc. Natl. Acad. Sci.* **106**, 16930–16935.

Desbarats A. J., Koenig C. E. M., Pal T., Mukherjee P. K. and Beckie R. D. (2014) Groundwater flow dynamics and arsenic source characterization in an aquifer system of West Bengal, India. *Water Resour. Res.* **50**, 4974–5002.

Desbarats A. J., Pal T., Mukherjee P. K. and Beckie R. D. (2017) Geochemical Evolution of Groundwater Flowing Through Arsenic Source Sediments in an Aquifer System of West Bengal, India. *Water Resour. Res.* **53**, 8715–8735.

Dittmar J., Voegelin A., Roberts L. C., Hug S. J., Saha G. C., Ali M. A., Badruzzaman A. B. M. and Kretzschmar R. (2010) Arsenic Accumulation in a Paddy Field in Bangladesh:

Seasonal Dynamics and Trends over a Three-Year Monitoring Period. *Environ. Sci. Technol.* **44**, 2925–2931.

Dittmar J., Voegelin A., Roberts L. C., Hug S. J., Saha G. C., Ali M. A., Badruzzaman A. B. M. and Kretzschmar R. (2007) Spatial Distribution and Temporal Variability of Arsenic in Irrigated Rice Fields in Bangladesh. 2. Paddy Soil. *Environ. Sci. Technol.* **41**, 5967–5972.

DPHE and BGS (2001) *Arsenic contamination of groundwater in Bangladesh.*, BGS, Keyworth.

Duxbury J. M., Mayer A. B., Lauren J. G. and Hassan N. (2003) Food chain aspects of arsenic contamination in Bangladesh: effects on quality and productivity of rice. *J. Environ. Sci. Health Part A Tox. Hazard. Subst. Environ. Eng.* **38**, 61–69.

DWASA (2012) *Annual Report 2011–2012.*, Dhaka Water Supply and Sewerage Authority, Dhaka, Bangladesh, Dhaka. Available at: http://dwasa.org.bd/annual-reports/.

DWASA (2008) *Management Information Report for the month of May 2008.*, Dhaka Water Supply and Sewerage Authority, Dhaka, Bangladesh, Dhaka.

Ettwig K. F., Zhu B., Speth D., Keltjens J. T., Jetten M. S. M. and Kartal B. (2016) Archaea catalyze iron-dependent anaerobic oxidation of methane. *Proc. Natl. Acad. Sci.* **113**, 12792–12796.

Fendorf S., Michael H. A. and Geen A. van (2010) Spatial and Temporal Variations of Groundwater Arsenic in South and Southeast Asia. *Science* **328**, 1123–1127.

Fisher A. T., López-Carrillo L., Gamboa-Loira B. and Cebrián M. E. (2017) Standards for arsenic in drinking water: Implications for policy in Mexico. *J. Public Health Policy* **38**, 395–406.

Flanagan S., Johnston R. and Zheng Y. (2012) Arsenic in tube well water in Bangladesh: health and economic impacts and implications for arsenic mitigation. *Bull. World Health Organ.*, 839–46.

van Geen A., Ahmed E. B., Pitcher L., Mey J. L., Ahsan H., Graziano J. H. and Ahmed K. M. (2014) Comparison of two blanket surveys of arsenic in tubewells conducted 12 years apart in a 25 km2 area of Bangladesh. *Sci. Total Environ.* **488**–**489**, 484–492.

van Geen A., Ahsan H., Horneman A. H., Dhar R. K., Zheng Y., Hussain I., Ahmed K. M., Gelman A., Stute M., Simpson H. J., Wallace S., Small C., Parvez F., Slavkovich V., Loiacono N. J., Becker M., Cheng Z., Momotaj H., Shahnewaz M., Seddique A. A. and Graziano J. H. (2002) Promotion of well-switching to mitigate the current arsenic crisis in Bangladesh. *Bull World Health Organ* **80**, 732–7.

van Geen A., Bostick B. C., Thi Kim Trang P., Lan V. M., Mai N.-N., Manh P. D., Viet P. H., Radloff K., Aziz Z., Mey J. L., Stahl M. O., Harvey C. F., Oates P., Weinman B., Stengel C., Frei F., Kipfer R. and Berg M. (2013) Retardation of arsenic transport through a Pleistocene aquifer. *Nature* **501**, 204–207.

van Geen A., Rose J., Thoral S., Garnier J. M., Zheng Y. and Bottero J. Y. (2004) Decoupling of As and Fe release to Bangladesh groundwater under reducing conditions. Part II: Evidence from sediment incubations. *Geochim. Cosmochim. Acta* **68**, 3475–3486.

van Geen A., Zheng Y., Goodbred S., Horneman A., Aziz Z., Cheng Z., Stute M., Mailloux B., Weinman B., Hoque M. A., Seddique A. A., Hossain M. S., Chowdhury S. H. and Ahmed K. M. (2008) Flushing History as a Hydrogeological Control on the Regional Distribution of Arsenic in Shallow Groundwater of the Bengal Basin. *Environ. Sci. Technol.* **42**, 2283–2288.

Harvey C. F., Swartz C. H., Badruzzaman A. B., Keon-Blute N., Yu W., Ali M. A., Jay J., Beckie R., Niedan V., Brabander D., Oates P. M., Ashfaque K. N., Islam S., Hemond H. F. and Ahmed M. F. (2002) Arsenic mobility and groundwater extraction in Bangladesh. *Science* **298**, 1602–6.

Hasan M. K., Burgess W. and Dottridge J. (1999) The vulnerability of the Dupi Tila aquifer of Dhaka, Bangladesh. *IAHS Publ. No 259 Proc. IUGG Symp. HS5 Birm.*, 8.

Hoque M. A., Burgess W. G., Shamsudduha M. and Ahmed K. M. (2011) Delineating low-arsenic groundwater environments in the Bengal Aquifer System, Bangladesh. *Appl. Geochem.* **26**, 614–623.

Hoque M., Hoque M. M. and Ahmed K. (2007) Declining groundwater level and aquifer dewatering in Dhaka metropolitan area, Bangladesh: causes and quantification. *Hydrogeol. J.* **15**, 1523–1534.

Horneman A., Van Geen A., Kent D. V., Mathe P. E., Zheng Y., Dhar R. K., O'Connell S., Hoque M. A., Aziz Z., Shamsudduha M., Seddique A. A. and Ahmed K. M. (2004) Decoupling of As and Fe release to Bangladesh groundwater under reducing conditions. Part 1: Evidence from sediment profiles. *Geochim. Cosmochim. Acta* **68**, 3459–3473.

Huhmann B. L., Harvey C. F., Uddin A., Choudhury I., Ahmed K. M., Duxbury J. M., Bostick B. C. and van Geen A. (2017) Field Study of Rice Yield Diminished by Soil Arsenic in Bangladesh. *Environ. Sci. Technol.* **51**, 11553–11560.

Islam F. S., Gault A. G., Boothman C., Polya D. A., Charnock J. M., Chatterjee D. and Lloyd J. R. (2004) Role of metal-reducing bacteria in arsenic release from Bengal delta sediments. *Nature* **430**, 68–71.

IWM and DWASA (2011) *Establishment of Groundwater Monitoring System in Dhaka City for Aquifer Systems and DWASA Production Wells, Draft Final Report.*, Institute of Water Modeling and Dhaka Water Supply and Sewerage Authority, Dhaka.

JMP and UNICEF (2017) Progress on drinking water, sanitation and hygiene: 2017 update and SDG baselines.

Khan M. R., Koneshloo M., Knappett P. S. K., Ahmed K. M., Bostick B. C., Mailloux B. J., Mozumder R. H., Zahid A., Harvey C. F., Geen A. van and Michael H. A. (2016) Megacity pumping and preferential flow threaten groundwater quality. *Nat. Commun.* **7**, 12833.

Knappett P. S. K., Mailloux B. J., Choudhury I., Khan M. R., Michael H. A., Barua S., Mondal D. R., Steckler M. S., Akhter S. H., Ahmed K. M., Bostick B., Harvey C. F., Shamsudduha M., Shuai P., Mihajlov I., Mozumder R. and van Geen A. (2016) Vulnerability of low-arsenic aquifers to municipal pumping in Bangladesh. *J. Hydrol.* **539**, 674–686.

Lawson M., Polya D. A., Boyce A. J., Bryant C., Mondal D., Shantz A. and Ballentine C. J. (2013) Pond-Derived Organic Carbon Driving Changes in Arsenic Hazard Found in Asian Groundwaters. *Environ. Sci. Technol.*, 130620151836005.

Lovley D. R., Chapelle F. H. and Phillips E. J. P. (1990) Fe(III)-reducing bacteria in deeply buried sediments of the Atlantic Coastal Plain. *Geology* **18**, 954–957.

Lowers H. A., Breit G. N., Foster A. L., Whitney J., Yount J., Uddin M. N. and Muneem A. A. (2007) Arsenic incorporation into authigenic pyrite, Bengal Basin sediment, Bangladesh. *Geochim. Cosmochim. Acta* **71**, 2699–2717.

Mason B. H. (1966) *Principles of geochemistry.*, Wiley, New York.

McArthur J. M., Banerjee D. M., Hudson-Edwards K. A., Mishra R., Purohit R., Ravenscroft P., Cronin A., Howarth R. J., Chatterjee A., Talukder T., Lowry D., Houghton S. and Chadha D. K. (2004) Natural organic matter in sedimentary basins and its relation to arsenic in anoxic ground water: the example of West Bengal and its worldwide implications. *Appl. Geochem.* **19**, 1255–1293.

McArthur J. M., Ravenscroft P., Safiulla S. and Thirlwall M. F. (2001) Arsenic in groundwater: Testing pollution mechanisms for sedimentary aquifers in Bangladesh. *Water Resour. Res.* **37**, 109–117.

McArthur J. M., Sikdar P. K., Leng M. J., Ghosal U. and Sen I. (2018) Groundwater Quality beneath an Asian Megacity on a Delta: Kolkata's (Calcutta's) Disappearing Arsenic and

Present Manganese. *Environ. Sci. Technol.* Available at:
https://pubs.acs.org/doi/full/10.1021/acs.est.7b04996 [Accessed November 25, 2018].

Meharg A. A. and Rahman M. M. (2003) Arsenic Contamination of Bangladesh Paddy Field
Soils: Implications for Rice Contribution to Arsenic Consumption. *Environ. Sci.
Technol.* **37**, 229–234.

Michael H. A. and Khan M. R. (2016) Impacts of physical and chemical aquifer heterogeneity on
basin-scale solute transport: Vulnerability of deep groundwater to arsenic contamination
in Bangladesh. *Adv. Water Resour.* **98**, 147–158.

Michael H. A. and Voss C. I. (2008) Evaluation of the sustainability of deep groundwater as an
arsenic-safe resource in the Bengal Basin. *Proc. Natl. Acad. Sci.* Available at:
http://www.pnas.org/content/early/2008/06/16/0710477105 [Accessed March 31, 2014].

Mihajlov I., Stute M., Schlosser P., Mailloux B. J., Zheng Y., Choudhury I., Ahmed K. M. and
van Geen A. (2016) Recharge of low-arsenic aquifers tapped by community wells in
Araihazar, Bangladesh, inferred from environmental isotopes. *Water Resour. Res.* **52**,
3324–3349.

Mukherjee A., Fryar A. E., Scanlon B. R., Bhattacharya P. and Bhattacharya A. (2011) Elevated
arsenic in deeper groundwater of the western Bengal basin, India: Extent and controls
from regional to local scale. *Appl. Geochem.* **26**, 600–613.

Naujokas M. F., Anderson B., Ahsan H., Aposhian H. V., Graziano J. H., Thompson C. and Suk
W. A. (2013) The broad scope of health effects from chronic arsenic exposure: update on
a worldwide public health problem. *Environ. Health Perspect.* **121**, 295.

Neumann R. B., Ashfaque K. N., Badruzzaman A. B. M., Ashraf Ali M., Shoemaker J. K. and
Harvey C. F. (2010) Anthropogenic influences on groundwater arsenic concentrations in
Bangladesh. *Nat. Geosci* **3**, 46–52.

Nickson R., McArthur J., Burgess W., Ahmed K. M., Ravenscroft P. and Rahman M. (1998)
Arsenic poisoning of Bangladesh groundwater. *Nature* **395**, 338.

Olson G. J., Dockins W. S., McFeters G. A. and Iverson W. P. (1981) Sulfate-reducing and
methanogenic bacteria from deep aquifers in montana. *Geomicrobiol. J.* **2**, 327–340.

Oremland R. S. and Stolz J. F. (2005) Arsenic, microbes and contaminated aquifers. *Trends
Microbiol.* **13**, 45–49.

Oremland R. S. and Stolz J. F. (2003) The Ecology of Arsenic. *Science* **300**, 939–944.

Panaullah G. M., Alam T., Hossain M. B., Loeppert R. H., Lauren J. G., Meisner C. A., Ahmed Z. U. and Duxbury J. M. (2009) Arsenic toxicity to rice (Oryza sativa L.) in Bangladesh. *Plant Soil* **317**, 31.

Polizzotto M. L., Harvey C. F., Sutton S. R. and Fendorf S. (2005) Processes conducive to the release and transport of arsenic into aquifers of Bangladesh. *Proc. Natl. Acad. Sci. U. S. A.* **102**, 18819–18823.

Postma D., Mai N. T. H., Lan V. M., Trang P. T. K., Sø H. U., Nhan P. Q., Larsen F., Viet P. H. and Jakobsen R. (2017) Fate of Arsenic during Red River Water Infiltration into Aquifers beneath Hanoi, Vietnam. *Environ. Sci. Technol.* **51**, 838–845.

Radloff K. A., Zheng Y., Michael H. A., Stute M., Bostick B. C., Mihajlov I., Bounds M., Huq M. R., Choudhury I., Rahman M. W., Schlosser P., Ahmed K. M. and van Geen A. (2011) Arsenic migration to deep groundwater in Bangladesh influenced by adsorption and water demand. *Nat. Geosci.* **4**, 793–798.

Ravenscroft P. (2007) *Predicting the global extent of arsenic pollution of groundwater and its potential impact on human health.*, UNICEF, Cambridge, UK.

Ravenscroft P., Kabir A., Hakim S. A. I., Ibrahim A. K. M., Ghosh S. K., Rahman M. S., Akhter F. and Sattar M. A. (2014) Effectiveness of public rural waterpoints in Bangladesh with special reference to arsenic mitigation. *J. Water Sanit. Hyg. Dev.* **4**, 545–562.

Ravenscroft P., McArthur J. M. and Hoque M. A. (2013) Stable groundwater quality in deep aquifers of Southern Bangladesh: The case against sustainable abstraction. *Sci. Total Environ.* **454–455**, 627–638.

Ravenscroft P., McArthur J. M. and Rahman M. S. (2018) Identifying multiple deep aquifers in the Bengal Basin: Implications for resource management. *Hydrol. Process.* **32**, 3615–3632.

Roy A. B. and Chatterjee A. (2015) Tectonic framework and evolutionary history of the Bengal Basin in the Indian subcontinent. *Curr. Sci. 00113891* **109**, 271–279.

Shamsudduha M., Taylor R. G., Ahmed K. M. and Zahid A. (2011) The impact of intensive groundwater abstraction on recharge to a shallow regional aquifer system: evidence from Bangladesh. *Hydrogeol. J.* **19**, 901–916.

Shamsudduha M., Taylor R. G. and Chandler R. E. (2015) A generalized regression model of arsenic variations in the shallow groundwater of Bangladesh. *Water Resour. Res.* **51**, 685–703.

Smedley P. L. and Kinniburgh D. G. (2002) A review of the source, behaviour and distribution of arsenic in natural waters. *Appl. Geochem.* **17**, 517–568.

Smith A. H., Elena O. Lingas and Rahman M. (2000) Contamination of drinking-water by arsenic in Bangladesh: a public health emergency. *Bull World Health Organ* **78**, 1093–103.

Stahl M. O., Harvey C. F., Geen A. van, Sun J., Trang P. T. K., Lan V. M., Phuong T. M., Viet P. H. and Bostick B. C. (2016) River bank geomorphology controls groundwater arsenic concentrations in aquifers adjacent to the Red River, Hanoi Vietnam. *Water Resour. Res.* **52**, 6321–6334.

Swartz C. H., Blute N. K., Badruzzman B., Ali A., Brabander D., Jay J., Besancon J., Islam S., Hemond H. F. and Harvey C. F. (2004) Mobility of arsenic in a Bangladesh aquifer: Inferences from geochemical profiles, leaching data, and mineralogical characterization. *Geochim. Cosmochim. Acta* **68**, 4539–4557.

Tufano K. J. and Fendorf S. (2008) Confounding Impacts of Iron Reduction on Arsenic Retention. *Environ. Sci. Technol.* **42**, 4777–4783.

Umitsu M. (1994) Late quaternary sedimentary environments and landforms in the Ganges Delta. *Sediment. Geol.* **83**, 177–186.

Umitsu M. (1987) Quaternary sedimentary environment and landform evolution in the Bengal lowland. *Geogr Rev Jpn* **B 60**, 164–78.

Weinman B., Goodbred S. L., Zheng Y., Aziz Z., Steckler M., van Geen A., Singhvi A. K. and Nagar Y. C. (2008) Contributions of floodplain stratigraphy and evolution to the spatial patterns of groundwater arsenic in Araihazar, Bangladesh. *Geol. Soc. Am. Bull.* **120**, 1567–1580.

WHO (1993) *Guidelines for drinking-water quality.*, World Health Organization, Geneva. Available at: http://apps.who.int/iris/bitstream/handle/10665/259956/9241544600-eng.pdf;jsessionid=6A88AB5DA4633E395E762B07AC27953A?sequence=1.

Winkel L. H. E., Trang P. T. K., Lan V. M., Stengel C., Amini M., Ha N. T., Viet P. H. and Berg M. (2011) Arsenic pollution of groundwater in Vietnam exacerbated by deep aquifer exploitation for more than a century. *Proc. Natl. Acad. Sci.* **108**, 1246–1251.

Figure 1-1. Population at risk from arsenic poisoning in the S/SE Asian (after Ravenscroft 2007).
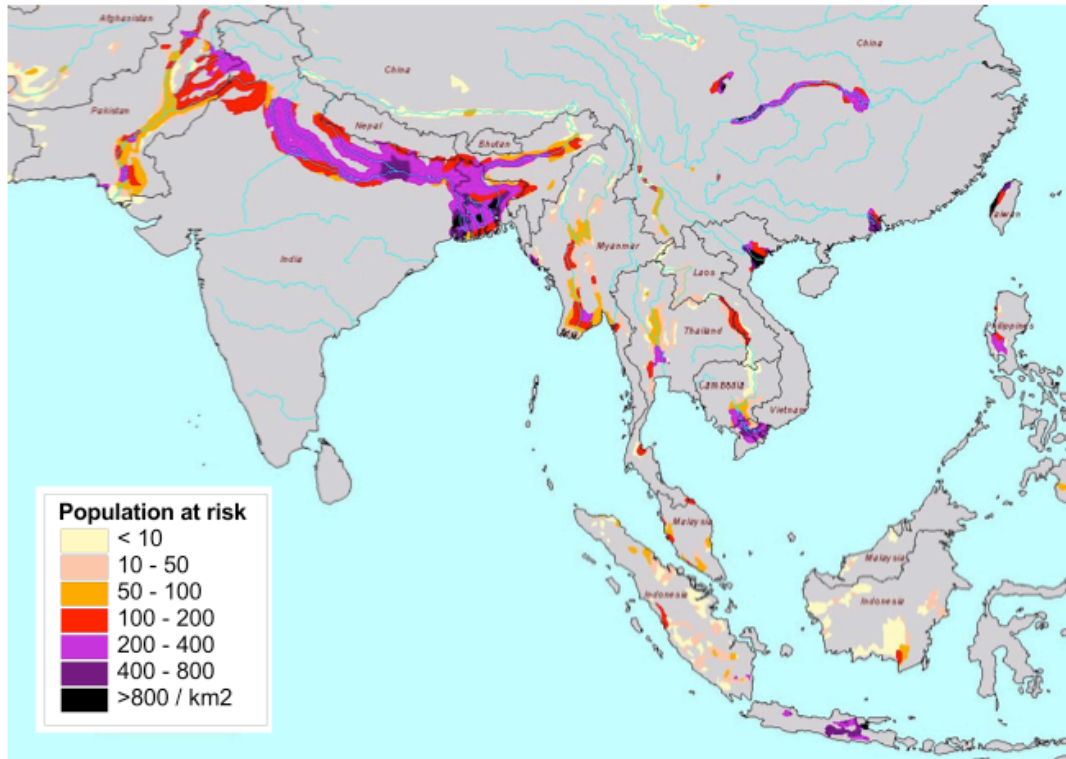
Figure 1-2. A schematic diagram showing how complete dissolution of even a small amount of solid phase As (1 mg/kg) may result very high dissolved As levels (7,950 ug/L) in Bangladesh aquifers (after BGS/DPHE, 2001).

As in
groundwater
7950 µg L^{-1}

25% water
(by volume)

dissolve/
desorb

As in sediment
1 mg kg^{-1}

75% sand
(by volume)
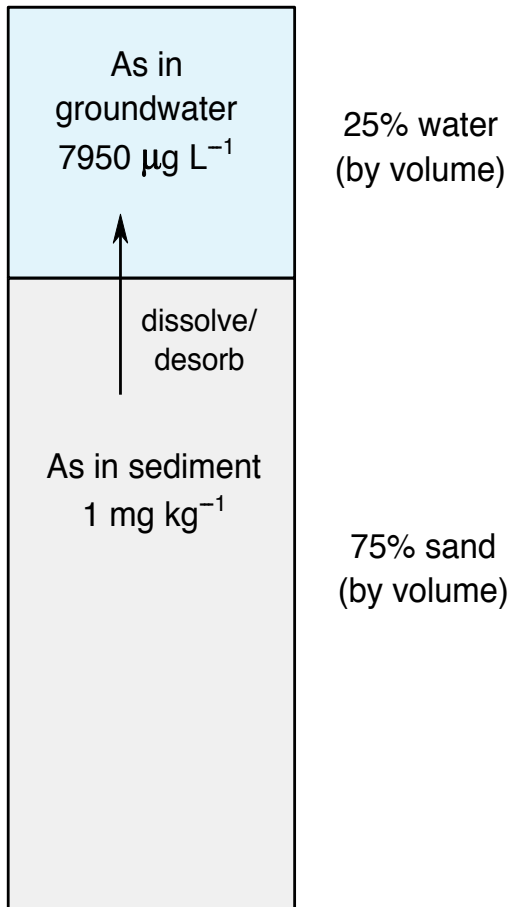
Figure 1-3. Schematic diagrams showing the distribution of Holocene gray sediment (pre-Last Glacial Maxima (LGM) about 20 ka) and Pleistocene orange sediments (post-LGM) in a basin scale (after McArthur et al., 2018). Also shown a cross-section of outcropping low-As aquifer in the capital of Bangladesh and its patchy occurrence further away from the Plio-Pleistocene uplifted Terrace (after Hoque et al., 2011).
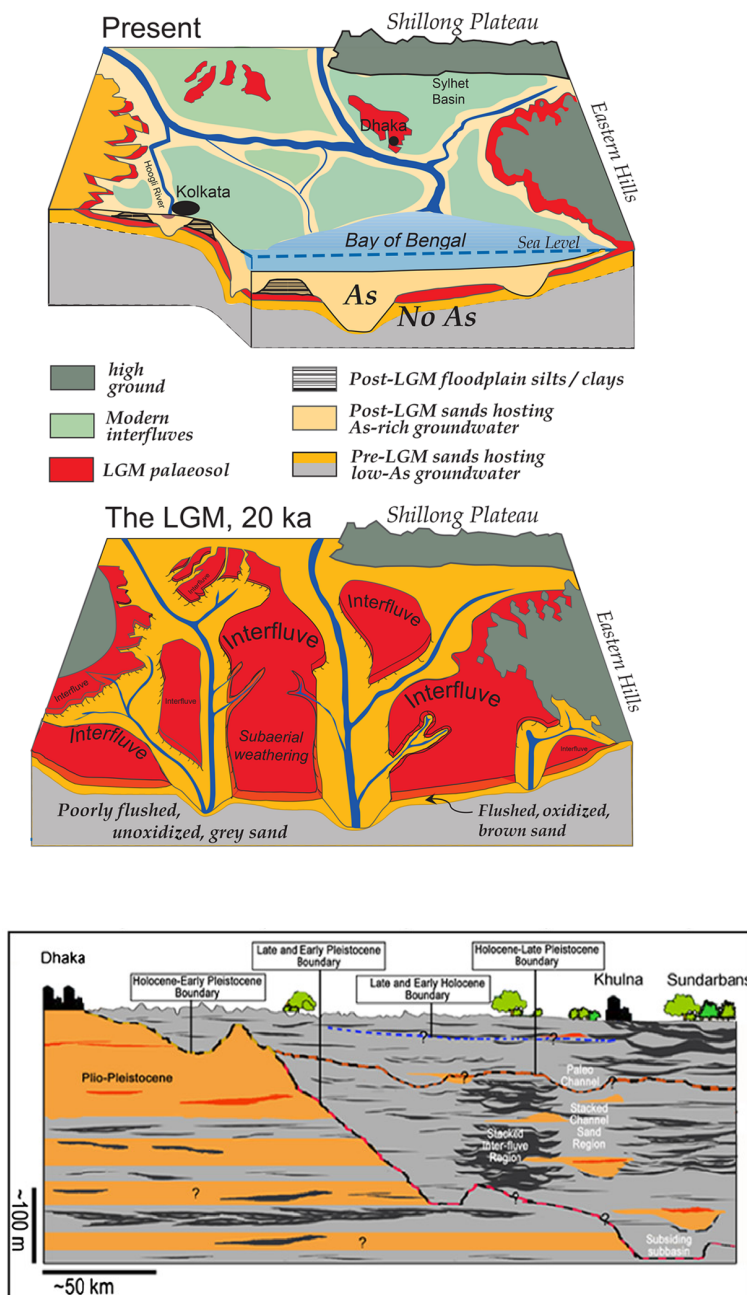
Figure 1-4. Schematic diagrams showing three possible As release pathways in the anoxic groundwater of Bangladesh through electron accepting microbial processes driven by the oxidation of organic carbon (after Oremland & Stolz, 2005).
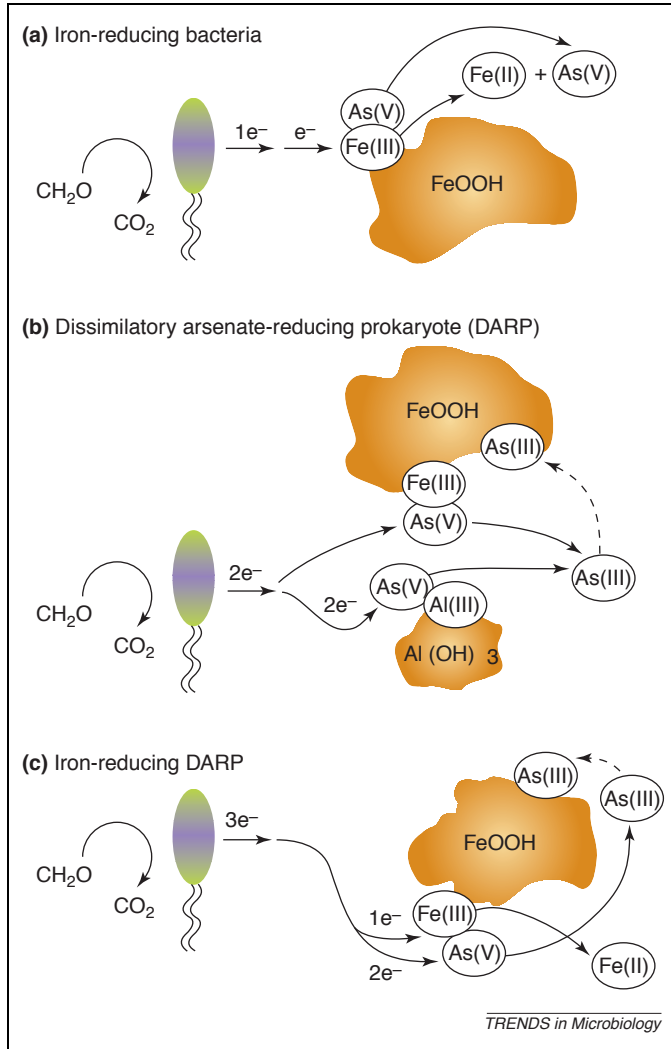
CHAPTER 2

FLUSHING OF ARSENIC OUT OF SHALLOW AQUIFERS BY IRRIGATION PUMPING IN BANGLADESH

M. Rajib Mozumder[1*], Charles F. Harvey[2], Brian J. Mailloux[3], Benjamin C. Bostick[1], Tyler Ellis[1], Therese Chen[3], Kazi M. Ahmed[4], & Alexander van Geen[1*]

[1]Lamont-Doherty Earth Observatory of Columbia University, Palisades, NY, USA

[2]Parsons Laboratory, Civil and Environmental Engineering, Massachusetts Institute of Technology, Cambridge, MA, USA

[3]Environmental Sciences, Barnard College, New York, NY, USA

[4]Department of Geology, University of Dhaka, Dhaka, Bangladesh

Abstract

The contamination of millions of shallow wells across South and Southeast Asia with geogenic arsenic (As) is spatially very heterogeneous, with concentrations often vary 10-100 fold between neighboring wells. The most effective way of reducing As exposure, testing wells in the field and switching to a nearby well on the basis of these tests, takes advantage of this variability. The approach has been brought into question, however, by increases in As concentrations documented in a limited number of shallow wells. To evaluate the extent and magnitude of such variations, we compare here the distribution of As in aquifers <30 m deep inferred from (i) two blanket testing campaigns of several thousand household wells conducted a decade apart within the same 25 km^2 area, (ii) concentrations of As for a subset of 271 household wells in the same area that could be unambiguously re-identified on three occasions over 15 years, and (iii) more detailed time series of As in 18 shallow monitoring wells over the same period. This unique combination of observations consistently shows a modest decline in As concentrations at the intermediate to higher end of the range attributed to flushing of the shallow aquifer by enhanced recharged induced by irrigation pumping. There is some indication also of a small rise in lower As concentrations, reinforcing the need for continued well testing.

2.1. Introduction

Millions of people across South and Southeast Asia are chronically exposed to toxic As levels by drinking water from contaminated shallow wells[1]. The most affected country is Bangladesh, with an estimated population of 40 million people still exposed as of 2013 to groundwater As levels above the World Health Organization (WHO) guideline of 10 μg/L[2,3]. Well testing and the installation of deep community wells have initially reduced exposure by encouraging households to switch their consumption to these low-As wells but these efforts have stagnated[4–6]. The present study addresses the sustainability of drinking from shallow (<30 m) low-As wells to reduce exposure following an anticipated new well testing campaign. These shallow aquifers are tapped by a majority of the 10 million household wells in Bangladesh and by most irrigation wells in Bangladesh.

Previous testing has revealed the highly heterogeneous spatial distribution of As in groundwater of Bangladesh, both laterally and with depth[3,7–9]. This heterogeneous distribution complicates prediction but also often makes it practical to share a safe well within walking distance, provided As concentrations do not fluctuate over time. Limited monitoring over time has shown that, by and large, concentrations of As in groundwater are stable, even in shallow aquifers[3,10–12]. For reasons that are not fully understood, there is a small but significant increase in As concentrations as a function of well age[1,8,13,14]. More recently, McArthur et al.[15] demonstrated with 8 years of monitoring of a limited number of wells in a neighboring portion of the Bengal basin in India that As concentrations in wells near geologic transitions can increase or decrease over time. It is presently unclear to what extent such observation challenges the notion that As

concentrations in a well will remain stable over time in spite of massive perturbations of groundwater flow patterns in the region by irrigation pumping to grow rice.

Elevated As concentrations in shallow groundwater pre-date the onset of groundwater pumping[3,16], but irrigation pumping for growing rice has without a doubt perturbed the hydrology of shallow aquifers throughout the Bengal basin[1,17–19]. Over the course of a year, irrigation pumping during the dry winter season is compensated by recharge at the beginning of each summer monsoon. This means the residence time of groundwater relative to recharge has been shortened by irrigation pumping from centuries to decades. It is still unclear if and how this perturbation impacted the complex set of biogeochemical interactions that regulate groundwater As concentrations in shallow aquifers. On one hand, recharge accelerated by irrigation pumping could gradually flush As out of shallow aquifers, at the cost of accumulating As in paddy soil[14,20–22]. Depending on the extent to which exchange occurs between groundwater and the much larger pool of As in aquifer sediment, several decades of irrigation pumping could already have considerably reduced average As concentrations in shallow aquifers[17,23,24,36]. At the same time, an inflow of reactive dissolved organic carbon induced by irrigation pumping could have triggered and additional release of As to groundwater and possibly an increase in concentrations[25–27]. In this study, we document the net impact of these factors on the basis of two surveys of thousands of wells in the same area conducted in 2000-01 and 2012-13. Because most of the wells originally surveyed were replaced by the time of the second survey, we complement these results with data from repeated sampling of a smaller subset of wells that remained in place. (Fig. 2-1).

2.2. Evolution of the spatial distribution of As in groundwater

The first large set of well-water samples was collected for laboratory analysis in 2000-01 from all 4,574 shallow (<30 m) wells within a 25 km^2 portion of Araihazar upazila, Bangladesh. A second round of blanket testing of 8,229 shallow wells using field kits was conducted in the same area in 2012-13. The increase in the number of shallow wells installed in the study area reflects the continued popularity of tubewells as a source of drinking water. The lifetime of a well is on the order of a decade and a majority of wells was therefore replaced during this interval[6]. Many of the metal tags attached to wells to re-identify them also fell off over time even if the well was not replaced. A direct comparison of As concentrations is therefore possible only for a subset of 271 private shallow wells that remained in use from 2000-01 through 2014, and again in 2015 when they were sampled a third time. We also report here more detailed changes in As concentrations for a set of 18 shallow wells purposely installed to monitoring the aquifer at the beginning of the study. We have to rely on spatial averaging of As concentrations to compare the larger data sets; the comparisons are based on resampling the same wells, albeit a smaller number of them.

The field kit is very useful for distinguishing wells that meet the WHO guideline from wells with an As content that exceeds it by an order of magnitude or more, but the kit misclassifies a considerable proportion in the intermediate range relative to Bangladesh standard of 50 μg/L for As in drinking water[6]. In spite of this limitation, the data show that the villages that were generally low in As in 2000-01 still were in 2012-13 and the same applies to high-As villages or villages with a very mixed distribution of As (Fig. 2-1a-b). After replacing the field kit data with laboratory measurements using a Monte Carlo approach (Supp. Mat. Fig. 2-S1), the data indicate

an increase from 15% in 2000-01 to 20% in 2012-13 in the proportion of wells that meet the WHO guideline of 10 μg/L of As. The proportion of wells in the range of 50-100 μg/L also increased from 20 to 25%. However, the proportion of wells containing >100 μg/L As declined from 40 to 30% over the same period (Fig. 2-S2a, c). The kit data, overall, therefore show a lowering of exposure, although far from sufficient to mitigate the serious health consequences of drinking water with such still high As levels on a daily basis.

To compare the two large-scale surveys spatially, the study area was divided into 348 blocks 300 m by 300 m in size (Fig. 2-1a-c). The block size was set to half of the spatial autocorrelation distance[28] for As in the study area (Fig. 2-S4). Both smaller and larger block dimensions lead to similar conclusions (Fig. 2-S6). Average As concentrations for each block and the entire area were determined by block kriging, a statistical method for weighing spatial data[29,30]. Kriging ensures that the larger numbers of wells that were installed in low-As areas compared to high-As areas do not disproportionally contribute to the spatial averages (Fig. 2-S2b, d & Fig. 2-S8). The kriged results for the entire study area indicate a mean As concentration of 110±32 μg/L (±standard error of the mean) in 2000-01 and 99±21 μg/L in 2012-13. The 11% decline in mean As concentration over the decade is statistically significant according to a modified paired-t-test (see Methods).

When pairwise block averages are compared, almost a third of the blocks (116 of 348) show significant differences between groundwater As levels over a 10-year period. The changes are asymmetric, with blocks showing a decrease twice as common a blocks showing an increase (Fig. 2-3). The prevalence of blocks showing a decrease in As concentration was confirmed by

examining the histograms of observed differences. To do so, histograms of the orthogonal

distances of the block average As data from the 1:1 line (unchanged) were determined. These

indicate that the data that fall below the line (histogram, h_b) are drawn from a wider distribution

compared to the data above the line (h_a) (Fig. 2-S7). We employed a grid search method[42] to

determine the most probable distribution i.e. the *expected or theoretical* histogram (h_T) and

compared that with the two observed histograms constructed from orthogonal distance analyses.

Comparison of h_a, h_b, and h_T confirm with 99.99% confidence that h_a and h_b did not come from

the same distribution; i.e. the scatter about the 1:1 line is statistically significant. Similarly, a

weighted least-squares regression that minimizes residuals by considering errors in block

average As concentrations in 2000-01 and 2012-13 yields a slope of 0.65 with 95% confidence

intervals of 0.58-0.72. The intercept of this regression is only slightly positive at 17 µg/L

(95%CI of 17-30 µg/L).

We rely on the data from individual wells that were analyzed in laboratory on both occasions to

address some of the limitation of the large data set. A subset of 271 household wells were tested

in 2000-01 were sampled again in 2014 and 2015. The one-year interval between the last two

sampling constrain the changes in As concentrations that can occur over relatively short time

scales and provides a reference for the longer-term changes. Taking into account analytical errors

in both the 2014 and the 2015 in a weighted regression, the slope of a regression of the two data

sets is indistinguishable from one (0.93-1.00 95%CI). There are some outliers even for this short

interval, which we attributed to actual changes in groundwater composition rather than

measurement or sampling error. For the same set of wells, the slope of the weighted regression of

As concentrations in 2015 as a function of 2001 is 0.89 (0.83-0.94 95%CI). The spatial average

of As concentration for the 271 wells determined by block kriging also declines by 10%, from 100 μg/L in 2000-01 to 90 μg/L in 2015, which is also significant based on a paired t-test (Methods).

The purposely-installed monitoring wells provide the most detailed perspective of changes in As concentrations over time, albeit for only 18 wells. In spite of short term variability in some of the records, the data show gradual increases in As concentrations for 7 wells, 6 of which started at As concentrations below the areal mean of 100 μg/L. Conversely, 5 wells show a decline in As concentrations, 3 of which with initial As concentrations above 100 μg/L. The remaining 6 wells do not show systematic changes in As concentrations over time (Fig. 2-4).

In summary, the two large blanket testing campaigns and the 271 wells resampled indicate a 10% decline in the overall content of As in the shallow aquifer. For reasons that are presently unclear, the slope of the block-to-block comparison of 0.65 of 2000-01 and 2012-13 averages is considerably below the slope of the well-to-well comparison of 0.87. From a public health perspective, perhaps most significant is that out of the 8 monitoring wells that initially met the local standard of 50 μg/L As in drinking water, 6 wells indicate a slight decrease in concentration and 6 an increase in As that also led to exceeding the local standard in 3 cases. This suggests that the rise in block averages at the low end of the As spectrum cannot be ignored, despite the limitations of the field kit used for the second round of testing.

2.3. Impacts of irrigation pumping

Concentrations of As generally increase with depth in shallow aquifers (Fig. 2-S9), but the observed changes in As cannot be explained by a systematic shift in the depth at which wells were re-installed (Fig. 2-S10). Accelerated recharge due to irrigation pumping is a more plausible explanation for the modest decline in shallow groundwater As concentrations documented in the study area. More than 85% of the groundwater pumped in Bangladesh is used for *Boro* rice cultivation during the winter dry season[34]. In Araihazar, a dense network of ~10 irrigation wells/km^2 extracts 100 times more water than is withdrawn with hand-pumps for domestic consumption[31]. Growing Boro rice under flooded conditions requires ~1 m/yr of groundwater[1,19,32] and rice paddies cover approximately 50% of the study area (Fig. 2-S12). This water is derived primarily from a 30 m-thick shallow aquifer (Fig. 2-S11), that contains 7.5 m of water assuming 25% porosity. Irrigation pumping of 0.5 m/yr across the area is equivalent to an annual withdrawal of ~7% (0.5 m/yr divided by 7.5 m) of groundwater from the shallow aquifer, corresponding to a residence time of only 15 years. Irrigation pumping does not deplete shallow aquifers because of annual recharge during the summer monsoon. The estimated recharge rate is consistent with the average recharge rate of 0.5±0.4 m/yr measured over this period at 9 sites within the study area using the tritium-helium dating method[20,33] (Fig. 2-S13).

A simple flushing model shows that accelerated flushing of the shallow aquifer without any exchange of As between groundwater and aquifer sediment would result in a decline in average As in the shallow aquifer much larger than indicated by both the large scale surveys and the individual wells (Fig. 2-5). Assuming that recharged surface water contains no As, the predicted decline to 50% of the average concentrations observed in 2000 clearly did not occur by 2010.

31

The same model also implies that As concentrations in shallow groundwater of the area would have had to be considerably higher in 1990, which is around the time that most farmers started to pump groundwater for irrigating rice paddies during winter. A more realistic model takes into account that the pool of As in the aquifer sediments is considerably larger than in groundwater and that exchange between the two pools be considered at equilibrium and determined by an empirical distribution coefficient which is independently and reasonably well constrained[21]. This modified model predicts a decline in average As for the shallow aquifer that is consistent with the observations and, more generally, a much more gradual since irrigation pumping started in earnest (Fig. 2-5).

Flushing of the shallow aquifer by irrigation pumping provides a plausible explanation for the decline in average As but not the observed increase in some block averages and some individual wells. One possibility is that enhanced recharged supplied more reactive carbon to stimulate the microbial dissolution of iron oxides where much of the sedimentary As is concentrated[17-18,23,25-27]. Another possibility is enhanced lateral mixing and the resulting homogenization caused by asynchronous irrigation pumping[18]. This mixing scenario is consistent with a trend in block-averaged As data showing that concentrations have tended to increase in blocks surrounded by higher-As blocks and concentrations often decrease in blocks surrounded by lower-As blocks between 2000-01 and 2012-13 (Fig. 2-S14). The relative importance of these two processes causing some well-As concentrations to rise cannot be determined on the basis of the available data.

2.4. Implications for future exposure and mitigation

The data presented in this study provide no reason to reconsider advice given to villagers across Bangladesh to drink from wells that low for As, even if the test dates to a decade ago. Fluctuations in groundwater As concentrations induced by irrigation pumping appear to be buffered to a considerable extent by exchange with a pool of As residing on the sediment. One implication is that the As content of wells high in As is not declining as rapidly as it would have without exchange with the sediment. On the other hand, exchange with aquifer sands provides considerable protection to the subset of wells that are low in As. The main reason the rural population of Bangladesh continues to be exposed is not that concentration of As have increased over time but because the vast majority of wells have been reinstalled since the last blanket testing campaign that ended over a decade ago and those reinstalled wells have never been tested[6]. The recent allocation of funds by the government of Bangladesh to a new blanket testing campaign is therefore a very welcome development.

2.5. Method Summary

Groundwater samples from the original survey of 2000-01 were analyzed a first time for As in the laboratory by graphite furnace atomic absorption (GFAA) using a method with a detection limit of 5 µg/L and overall reproducibility of about 10%[8]. A subset of 608 samples containing up to 5 µg/L As was subsequently re-analyzed by inductively coupled plasma mass spectrometry (ICPMS) to reduce the detection limit to 0.1 µg/L[37]. The 2012-13 blanket survey was carried out using the Econo-Quick field kit (Industrial Test Systems, Rock Hill, South Carolina, USA, Cat. No. 481298) based on visual readings of a test strip at 9 discrete levels[6]. The kit readings were converted to equivalent laboratory concentrations by bootstrapping[38] on the basis of 944 quality-

control samples analyzed with the kit and in the laboratory (Fig. 2-S1). We used one of many

equally probable Monte-Carlo realizations of the imputed (bootstrapped) 2012-13 ICP-MS data

for our interpretation. The inter-calibrated As concentrations were block kriged[29,30] after spatial

structure analyses (Fig. 2-S5) using the 'gstat' package in R[39]. The block kriging method does

not take into account measurement error[43] because of computational complexity and

unavailability of reliable source codes at this time (personal communication with Prof. Edzer

Pebesma, Institute for Geoinformatics, University of Muenster).

A total of 656 individual wells, 550 of which were shallow (<30 m), were selected for

resampling a decade after the first survey on the basis of the ID recorded on a small tag attached

to each pump in 2000-01, a deviation of <0.0001 decimal degrees (100 m) in latitude or

longitude and a difference of <15 m in the recorded depth between the two surveys. In 2014, a

subset of 357 of the pre-selected shallow wells were relocated and resampled after confirmation

by the household of their installation date. These samples were analyzed for As by ICPMS, as

were the corresponding 327 samples stored since 2000-01. After excluding 19 outliers (Fig. 2-

S3), a final set of 308 pairs of ICPMS measurements were retained. A subset of 271 of the 308

wells were resampled again in 2015 and analyzed on ICPMS and used for evaluating changes in

As for individual wells over the last 15 years. At 4 locations in the study area, a total of 18

shallow wells (5-29 m deep) were monitored for the duration of 15 years (2001-2016). The As

data for long-term tend analyses were also measured with ICPMS.

The significance of changes in the mean As concentration of the entire area was assessed

separately at the block level and for the individual wells using a paired- t-test after adjusting for

effective sample size[40] on the basis of global autocorrelation. The global autocorrelation coefficient determined from Moran's I statistic[41] was ~0.6 for both 2001 and 2012 block average As concentrations and ~0.3 for both 2001 and 2014 well As concentrations. The effective sample size (N^*) was determined by: $N^*[(1-I)/(1+I)]$; where N is the total number of blocks or wells and I = Moran's I coefficient for global autocorrelation; in the case of the blocks, $N^* = 348*0.25 = 87$ and for the individual wells, $N^* = 166$. The modified paired t-test rejects the null hypothesis (i.e. no difference in the mean As concentration for the study area) at the block level (t-statistic = -3.87; $p < 0.001$) as well as for resampled wells (t-statistic = -2.84; $p < 0.01$).

2.6. References

1.   Ravenscroft, P., Brammer, H. & Richards, K. *Arsenic Pollution: a global synthesis*. (Wiley-Blackwell, 2009).

2.   BBS & UNICEF. *Bangladesh Multiple Indicator Cluster Survey 2012-2013*. (Bangladesh Bureau of Statistics United Nations Children's Fund, 2015).

3.   DPHE & BGS. *Arsenic contamination of groundwater in Bangladesh*. (BGS, 2001).

4.   Ahmed, M. F. *et al.* Ensuring safe drinking water in Bangladesh. *Science* **314,** 1687–1688 (2006).

5.   Chen, Y. *et al.* Reduction in urinary arsenic levels in response to arsenic mitigation efforts in Araihazar, Bangladesh. *Environ. Health Perspect.* **115,** 917–923 (2007).

6.   van Geen, A. *et al.* Comparison of two blanket surveys of arsenic in tubewells conducted 12 years apart in a 25 km^2 area of Bangladesh. *Sci. Total Environ.* **488–489,** 484–492 (2014).

7.   Dhar, R. K. *et al.* Groundwater arsenic calamity in Bangladesh. *Current Science* **73,** 48–59 (1997).

8.   van Geen, A. *et al.* Spatial variability of arsenic in 6000 tube wells in a 25 km^2 area of Bangladesh. *Water Resour. Res.* **39,** No. 5, 1140, doi:10.1029/2002WR001617 (2003).

9.   Jakariya, M. *et al.* Screening of arsenic in tubewell water with field test kits: Evaluation of the method from public health perspective. *Sci. Total Environ.* **379,** 167–175 (2007).

10.   van Geen, A. *et al.* Promotion of well-switching to mitigate the current arsenic crisis in Bangladesh. *Bull World Health Organ* **80,** 732–7 (2002).

11.   Cheng, Z., van Geen, A., Seddique, A. A. & Ahmed, K. M. Limited temporal variability of arsenic concentrations in 20 wells monitored for 3 years in Araihazar, Bangladesh. *Environ. Sci. Technol.* **39,** 4759–4766 (2005).

12.   Dhar, R. K. *et al.* Temporal variability of groundwater chemistry in shallow and deep aquifers of Araihazar, Bangladesh. *J. Contam. Hydrol.* **99,** 97–111 (2008).

13.   Burgess, W. G., Burren, M., Perrin, J. & Ahmed, K. M. Constraints on sustainable development of arsenic-bearing aquifers in southern Bangladesh. Part 1: A conceptual model of arsenic in the aquifer. *Geol. Soc. Lond. Spec. Publ.* **193,** 145–163 (2002).

14.   McArthur, J. M. *et al.* Natural organic matter in sedimentary basins and its relation to arsenic in anoxic ground water: the example of West Bengal and its worldwide implications. *Appl. Geochem.* **19,** 1255–1293 (2004).

15.   McArthur, J. M. *et al.* Migration of As, and 3H/3He ages, in groundwater from West Bengal: Implications for monitoring. *Water Res.* **44,** 4171–4185 (2010).

16.   Fendorf, S., Michael, H. A. & van Geen, A. Spatial and temporal variations of groundwater arsenic in South and Southeast Asia. *Science* **328,** 1123–1127 (2010).

17.   Harvey, C. F. *et al.* Arsenic mobility and groundwater extraction in Bangladesh. *Science* **298,** 1602–6 (2002).

18.   Harvey, C. F. *et al.* Groundwater dynamics and arsenic contamination in Bangladesh. *Chem. Geol.* **228,** 112–136 (2006).

19.   Shamsudduha, M., Taylor, R. G., Ahmed, K. M. & Zahid, A. The impact of intensive groundwater abstraction on recharge to a shallow regional aquifer system: evidence from Bangladesh. *Hydrogeol. J.* **19,** 901–916 (2011).

20.   Stute, M. *et al.* Hydrological control of As concentrations in Bangladesh groundwater. *Water Resour. Res.* **43,** W09417 (2007).

21.   van Geen, A. *et al.* Flushing history as a hydrogeological control on the regional distribution of arsenic in shallow groundwater of the Bengal basin. *Environ. Sci. Technol.* **42,** 2283–2288 (2008).

22.   Postma, D. *et al.* A model for the evolution in water chemistry of an arsenic contaminated aquifer over the last 6000 years, Red River floodplain, Vietnam. *Geochim. Cosmochim. Acta* (2016). doi:10.1016/j.gca.2016.09.014

23.   Klump, S. *et al.*, Groundwater dynamics and arsenic mobilization in Bangladesh assessed using noble gases and tritium. *Environ. Sci. Technol.* **40**, 243-250 (2006).

24.   Polizzotto, M. L., Harvey, C. F., Sutton, S. R. & Fendorf, S. Processes conducive to the release and transport of arsenic into aquifers of Bangladesh. *Proc. Natl. Acad. Sci. U. S. A.* **102,** 18819–18823 (2005).

25.   Neumann, R. B. *et al.* Anthropogenic influences on groundwater arsenic concentrations in Bangladesh. *Nat. Geosci* **3,** 46–52 (2010).

26.   Mailloux, B. J. *et al.* Advection of surface-derived organic carbon fuels microbial reduction in Bangladesh groundwater. *Proc. Natl. Acad. Sci.* **110,** 5331–5335 (2013).

27.   Whaley-Martin, K. J. *et al.* Stimulation of microbially mediated arsenic release in Bangladesh aquifers by young carbon indicated by radiocarbon analysis of sedimentary bacterial lipids. *Environ. Sci. Technol.* **50,** 7353–7363 (2016).

28.   Hengl, T. Finding the right pixel size. *Comput. Geosci.* **32,** 1283–1298 (2006).

29.   Cressie, N. A. C. Geostatistics in statistics for spatial data. in *Statistics for Spatial Data* (J. Wiley, 1993).

30.   Isaaks, E. H. & Srivastava, R. M. *An Introduction to Applied Geostatistics*. (Oxford University Press, 1990).

31.   Zheng, Y. *et al.* Geochemical and hydrogeological contrasts between shallow and deeper aquifers in two villages of Araihazar, Bangladesh: Implications for deeper aquifers as drinking water sources. *Geochim. Cosmochim. Acta* **69,** 5203–5218 (2005).

32.   Meharg, A. A. & Rahman, M. M. Arsenic contamination of Bangladesh paddy field soils: Implications for rice contribution to arsenic consumption. *Environ. Sci. Technol.* **37,** 229–234 (2003).

33.   Radloff, K. A. *et al.* Reversible adsorption and flushing of arsenic in a shallow, Holocene aquifer of Bangladesh. *Appl. Geochem.* (2015). doi:10.1016/j.apgeochem.2015.11.003

34.   Ahmed K. M. (2011) Groundwater contamination in Bangladesh. In *Water Resources Planning and Management* (eds. K. Hussey and R. Q. Grafton). Cambridge University Press, Cambridge. pp. 529–560.

35.	Ravenscroft, P., McArthur, J. M. & Hoque, M. A. Stable groundwater quality in deep aquifers of Southern Bangladesh: The case against sustainable abstraction. *Sci. Total Environ.* **454–455,** 627–638 (2013).

36.	Shamsudduha M., Taylor R. G. and Chandler R. E. (2015) A generalized regression model of arsenic variations in the shallow groundwater of Bangladesh. *Water Resour. Res.* **51**, 685–703.

37.	Cheng, Z., Zheng, Y., Mortlock, R. & Geen, A. van. Rapid multi-element analysis of groundwater by high-resolution inductively coupled plasma mass spectrometry. *Anal. Bioanal. Chem.* **379,** 512–518 (2004).

38.	Menke, W. & Menke, J. 11 - Are my results significant? in *Environmental Data Analysis with MatLab* (eds. Menke, W. & Menke, J.) 217–238 (Elsevier, 2012).

39.	Pebesma, E. J. Multivariable geostatistics in S: the gstat package. *Comput. Geosci.* **30,** 683–691 (2004).

40.	DALE, M. R. T. & FORTIN, M.-J. Spatial autocorrelation and statistical tests in ecology. *Écoscience* **9,** 162–167 (2002).

41.	Cliff, A. D. & Ord, J. K. *Spatial Processes: Models & Applications*. (Pion, 1981).

42.	Menke, W.; Menke, J. 4 - The Power of Linear Models. In *Environmental Data Analysis with Matlab (Second Edition)*; Menke, W., Menke, J., Eds.; Academic Press, 2016; pp 67–89. https://doi.org/10.1016/B978-0-12-804488-9.00004-5.

43. Hipel, K. W.; McLeod, A. I. Time Series Modelling of Water Resources and Environmental Systems; Developments in water science; Elsevier: Amsterdam ; New York, 1994.

44.	Kang, J.; Jin, R.; Li, X.; Zhang, Y. Block Kriging With Measurement Errors: A Case Study of the Spatial Prediction of Soil Moisture in the Middle Reaches of Heihe River Basin. *IEEE Geosci. Remote Sens. Lett.* 2017, 14 (1), 87–91. https://doi.org/10.1109/LGRS.2016.2628767.

45.	Terry Therneau (2018). deming: Deming, Thiel-Sen and Passing-Bablock Regression. R package version 1.3. https://CRAN.R-project.org/package=deming

Acknowledgements

Author contributions

Field and laboratory data were collected by K.M.A., T.E., T.C., M.R.M. and A.v.G. Analysis of the data was conducted by M.R.M. with input from C.F.H., B.J.M., B.C.B., and A.v.G. M.R.M. drafted the paper, which was edited by all co-authors.

Competing financial interests

The authors have none to report.
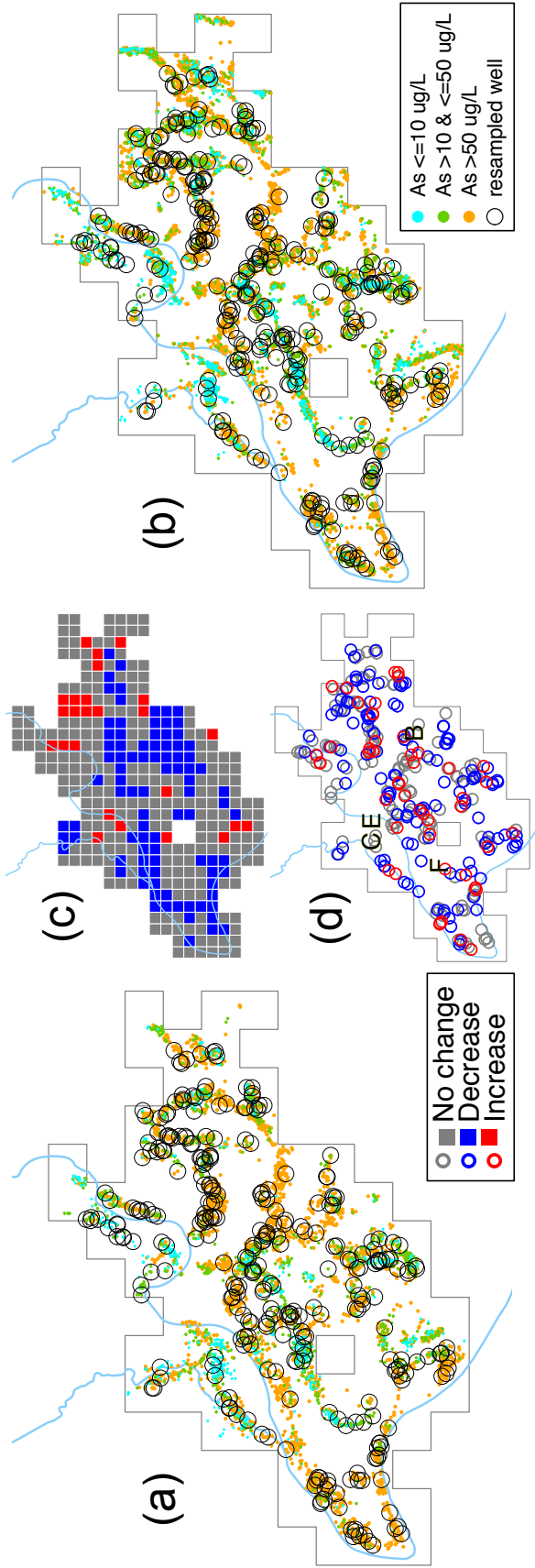
Figure 2-1. Spatial evolution in the distribution of As in shallow (<30 m) groundwater within a 25 km² area. (a) Small color-coded dots indicate the location of 4,574 wells sampled in 2000-01 and analyzed in the laboratory. Larger open circles indicate the location of a subset of 271 wells that were unambiguously re-identified in 2015. Also shown is the 300 m by 300 m grid used to calculate block averages. (b) Arsenic data for the same area for 8,229 wells, originally tested with a field kit in 2012-2013 color-coded as in (a), after inter-calibration against laboratory measurements. (c) Difference in block-averaged As concentrations color-coded according to the direction and significance of the change. (d) Difference in As concentrations for the 271 resampled wells color-coded as in (c). Also shown are the 4 locations (site-B, C, E, and F) where long-term measurements are available (See Fig. 2-4).

40
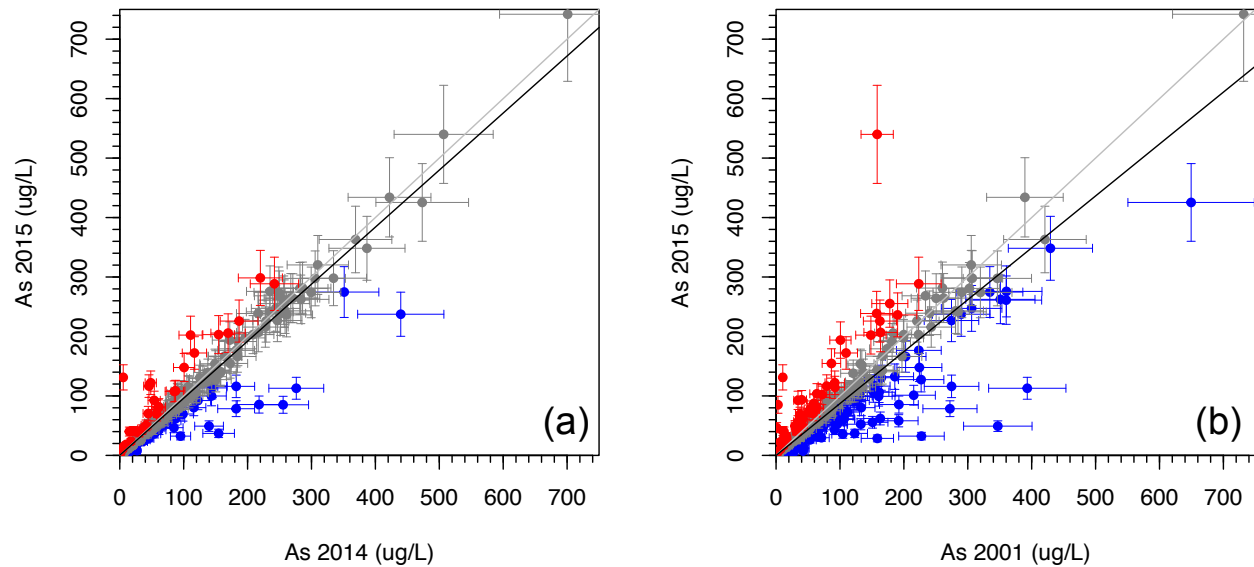
Figure 2-2. Changes in As concentrations in the individual wells. (a) Changes in groundwater As concentrations between 2015 and 2014 measured in the laboratory for 271 resampled wells. Significance of differences in As concentrations was established on the basis of the error calculated for each measurement at 3σ level using the formula: $\sigma_{sing} = \sigma_{meas} + 0.5$ μg/L where the measurement error, $\sigma_{meas} = 5\%$ of individual ICP-MS measurement. Deming regression[45] on the individual well As data yields an intercept of 0.21 [95% confidence intervals: -0.20 & 0.81] and a slope of 0.95 [95% confidence intervals: 0.93 & 0.99], shown as a solid black line. Deming regression minimizes the sum of distances in both the x and y direction. The continuous gray line shows the one-to-one correspondence. (b) As concentrations in 2015 as a function of concentrations in 2001 for the same 271 wells. The intercept and slope of the regression in this case is -0.095 [95% confidence intervals: -0.95 & 0.76] and 0.87 [95% confidence intervals: 0.83, 0.92], respectively.

41
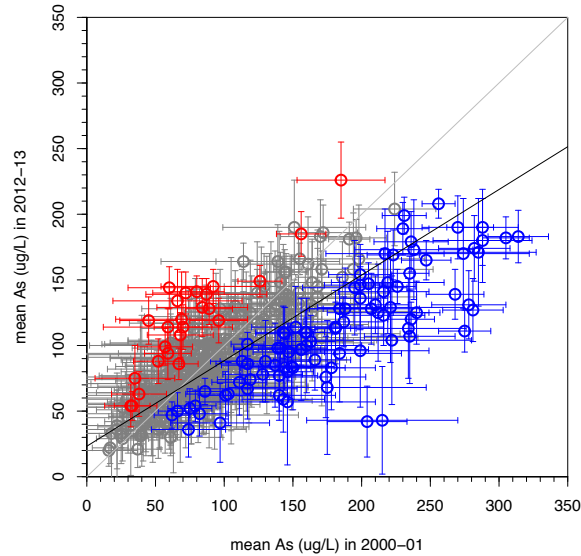
Figure 2-3. Changes in As concentrations at the block level. Concentrations of As in 2012-13 averaged by kriging for 348 blocks as a function of average As concentrations in 2000-01 in the same blocks. The differences are color-coded according to the direction of the change and statistical significance determined by the overlap of standard error of the mean (i.e. square root of the block kriging variance). The diagonal gray line represents the one-to-one line. Deming regression[45] shown with a darker solid line provides an intercept of 23.25 [95% confidence intervals: 16.8 & 29.7] and a slope of 0.65 [95% confidence intervals: 0.58 & 0.72].
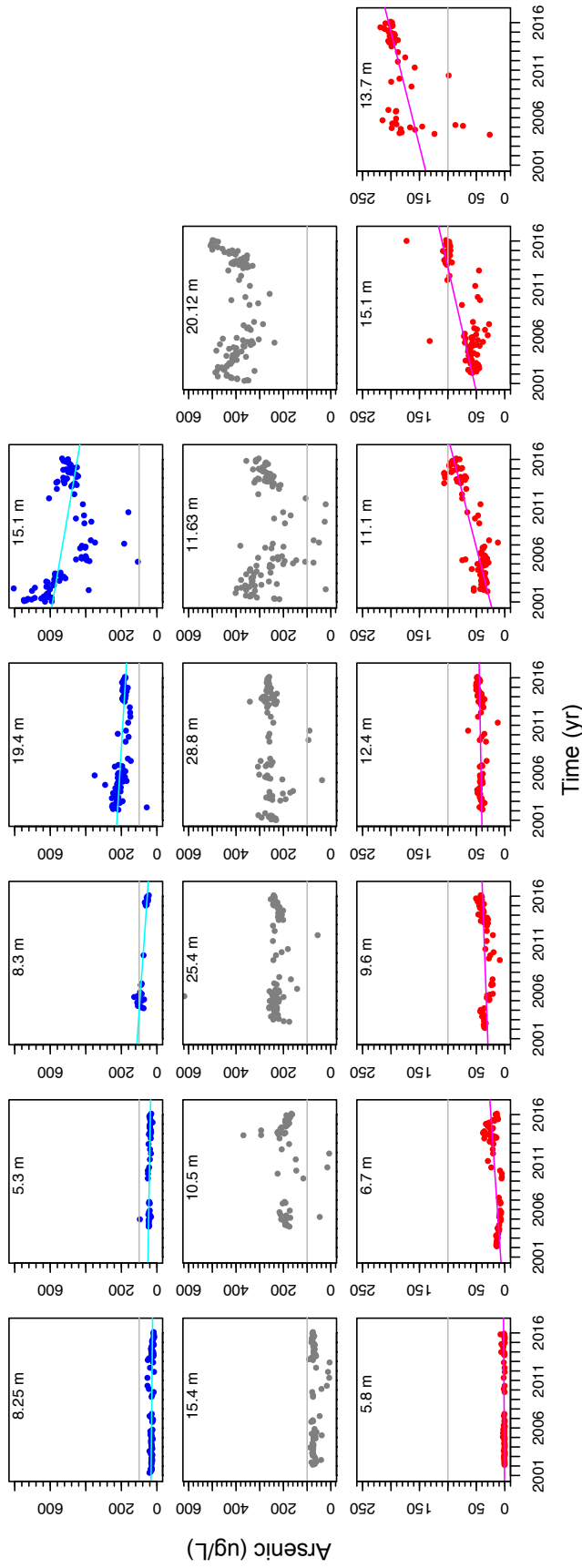
Figure 2-4. Time-series of As in the shallow aquifer of Araihazar, Bangladesh. Linear trends are shown for the time series that pass a Mann-Kendall's trend test[43] to determine the monotonic relationships between time and As concentrations (p<0.05). No systematic pattern is detected between depth (indicated at the top of each plot) and change in As. The wells are located at lettered site-B (8.25, 11.63, 15.1, 20.1, and 28.8 m), site-F (5.8, 11.1, 15.1, 19.4, and 25.4 m), site-C (6.7, 9.6, 12.4, and 15.4 m), and site-E (5.3, 8.3, 10.5, and 13.7 m).
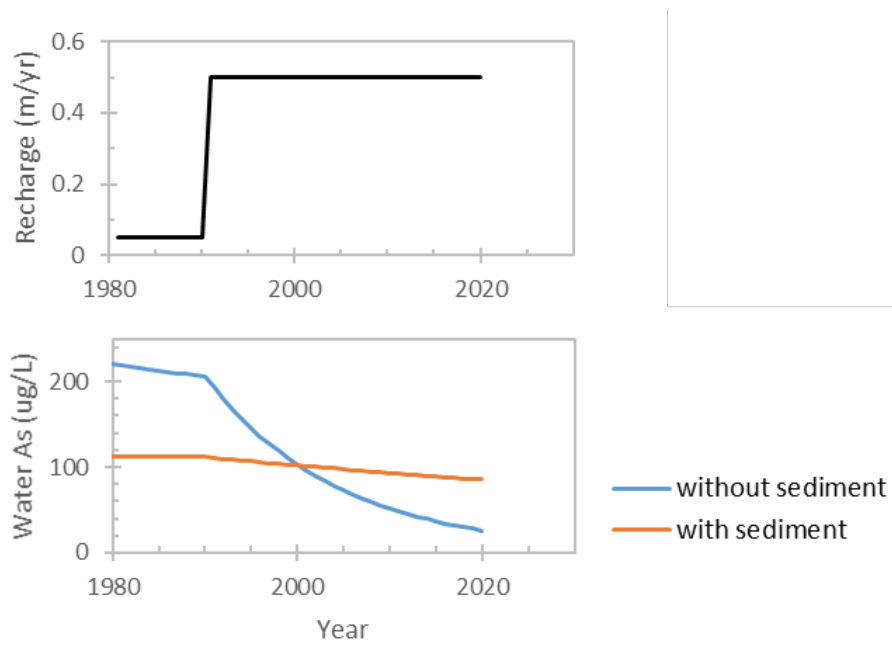
Figure 2-5. A flushing model of As for the shallow aquifer. The recharge rate with surface water free of As is increased by a factor of 10 (from 0.05 to 0.5 m/yr) in 1990. A porosity of 25% is assumed for the 30 m-thick shallow aquifer. A distribution coefficient of 4 L/kg[21] was used for the case illustrating exchange of As between groundwater and aquifer sediment. The model is tuned to a concentration of 100 µg/L As in 2000.

2.7. Supporting Materials
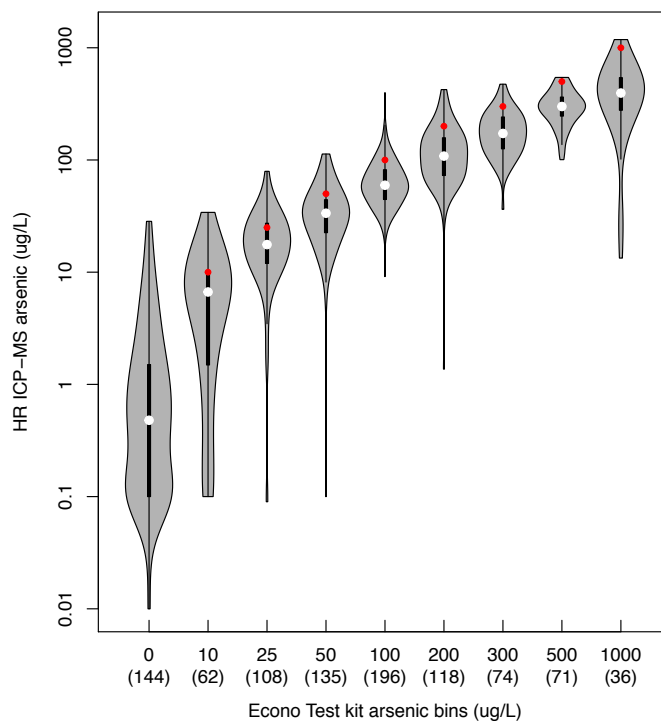
Figure 2-S1. Inter-calibration of laboratory and field-kit results for arsenic. Samples from a subset of 944 wells were analyzed with the ITS Econo-Quick field kit[1] in 2012-13 and later by ICPMS in the laboratory[2]. Soon after the stipulated 10 min reaction time, test trips were compared by the village-health workers to the kit's reference chart and classified visually as containing 0, 10, 25, 50, 100, 200, 300, 500, or 1000 µg/L As. The above box plots (black) display the ICPMS measurements corresponding to each of these bins on a log scale and indicate some overlap (the number of measurements for each bin is listed in parentheses below the nominal As concentration). Probability density of ICP-MS data for each bin (gray) is also shown with the box plots. The average concentrations measured by ICPMS value for the aforementioned 9 bins are: 2±1, 7±2, 20±3, 37±4, 68±6, 129±14, 188±20, 306±25, and 422±80 µg/L As, respectively. These results confirm that the kit on average overestimates As concentrations in groundwater by about a factor of two above 50 µg/L As. To convert kit results to equivalent ICPMS measurements, each of the 8,229 kit readings was assigned an ICPMS concentration by bootstrapping, i.e. by random resampling with duplication of all the ICPMS within that bin[3]. The imputed ICPMS data were used for spatial analysis and comparison with the 2000-01 survey.
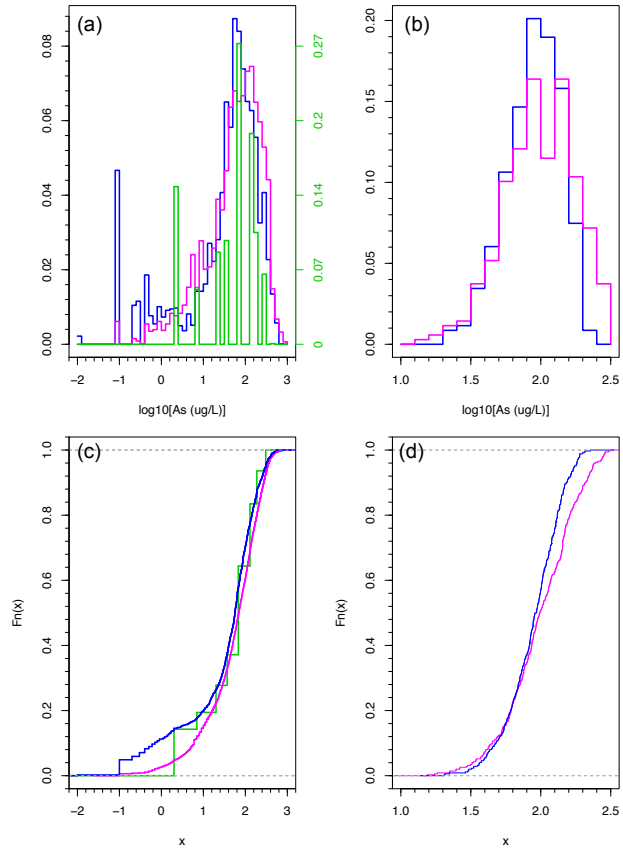
Figure 2-S2. Changes in the distribution of arsenic concentrations over time. (a) histograms of As concentrations on a log-scale for 4,574 well samples collected in 2000-01 and analyzed by GFAA (pink), 8,229 well samples collected in 2012-13 and analyzed with the field kit using averaged ICPMS data for each of the 9 bins (green), and the same 8,229 well samples using imputed concentrations drawn from ICPMS measurements for each of the 9 bins (blue). Area under each histogram normalized to one. (b) histograms of As concentrations on a log-scale for 348 blocks within the same study area generated by block-kriging (**Fig. 2-S6**) for 2000-01 (pink) and 2012-13 (blue). (c) empirical cumulative distribution function corresponding to histrograms in (a). (d) empirical cumulative distribution function corresponding to histrograms in (c).
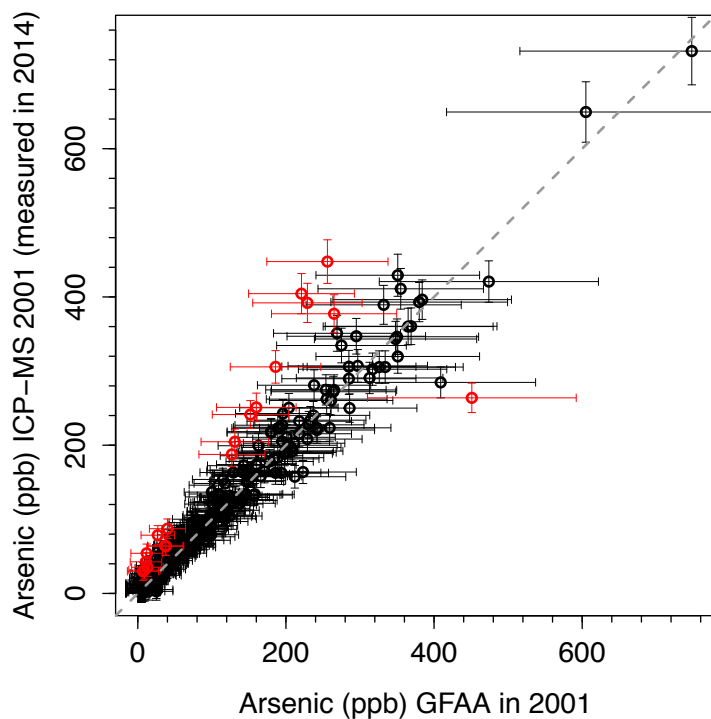
Figure 2-S3. Consistency of laboratory measurements for well samples analyzed by GFAA in 2000-01 and reanalyzed by ICPMS in 2014. Samples collected within the study area in 2000-01 and were analyzed a first time by graphite-furnace atomic-absorption (GFAA) spectrometry[4]. Samples containing up to 5 μg/L were then reanalyzed by ICPMS[2]. To check for consistency, the archived 2000-01 samples from the subset of 331 wells that were sampled a second time in 2014 were reanalyzed by ICPMS in 2014. The standard error for each measurement was calculated using the expression: $\sigma_{sing} = \sqrt{(\theta^2\sigma_{cal}^2 + \sigma_{meas}^2)}$; where, σ_{meas} is the absolute measurement error based on reproducibility (4 and 7 μg/L for GFAA and ICPMS, respectively), σ_{cal} the relative error in calibration (0.10 and 0.02), and θ is the As concentration for an individual sample[2,4]. Only 17 archived samples, shown above in red, did not meet a consistency criterion based on 3σ overlapping error bars for individual 2001 GFAA and 2014 ICP-MS measurements.
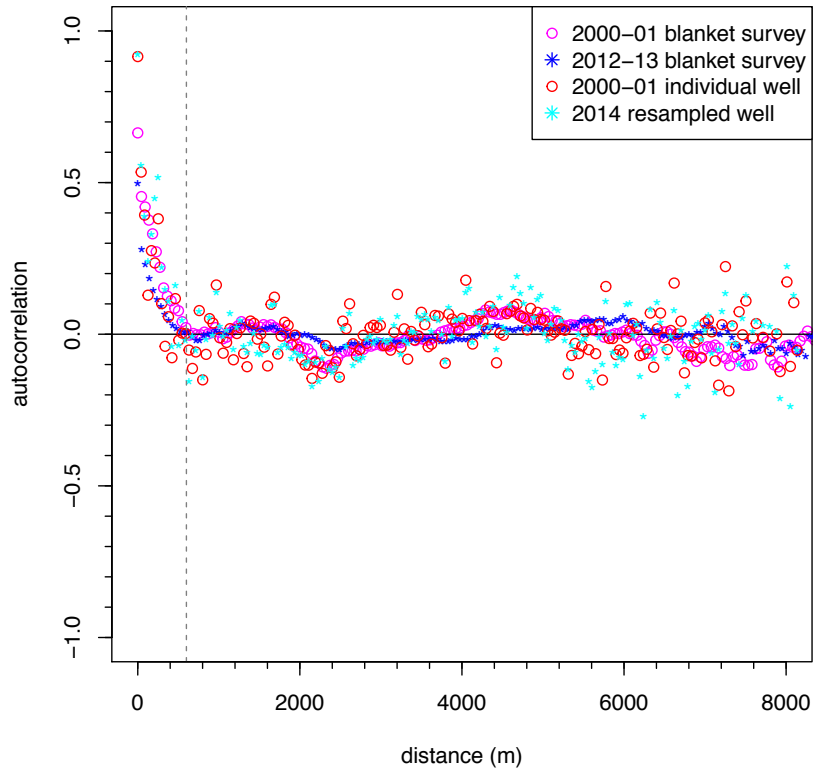
Figure 2-S4. Spatial dependence of groundwater arsenic (As) concentrations in the study area. Correlograms of As indicate a positive spatial autocorrelation (spatial dependence) up to a distance of 600 m (h). The largest block size was created as 600 X 600 m^2, followed by 300 X 300 m^2 and 150 X 150 m^2. The legible grid size is <=h/2 after Hengl[13].
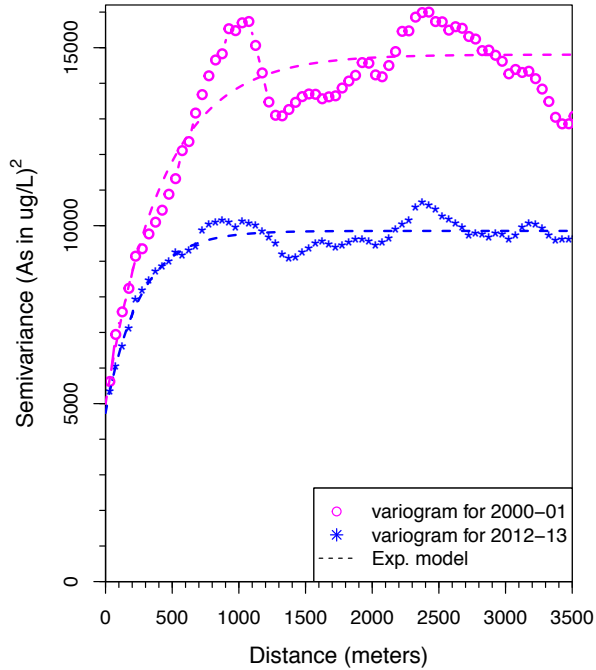
Figure 2-S5. Spatial structure analysis of well-water As concentrations measured in 2000-01 and 2012-13. Variography of 2000-01 lab-measured As concentrations (*open magenta circles*) and 2012-13 imputed lab concentrations (*blue stars*) with a lag spacing (h) of 50 m using the 'gstat' package[5] of the R programming language. The experimental semivariograms were fitted with exponential model: $\gamma(h) = C_0 + C\ (1\text{-}exp(\text{-}h/a))$; where, C_0 is the *nugget effect* , a is *range*, and $(C+C_0)$ is known as the *sill*.
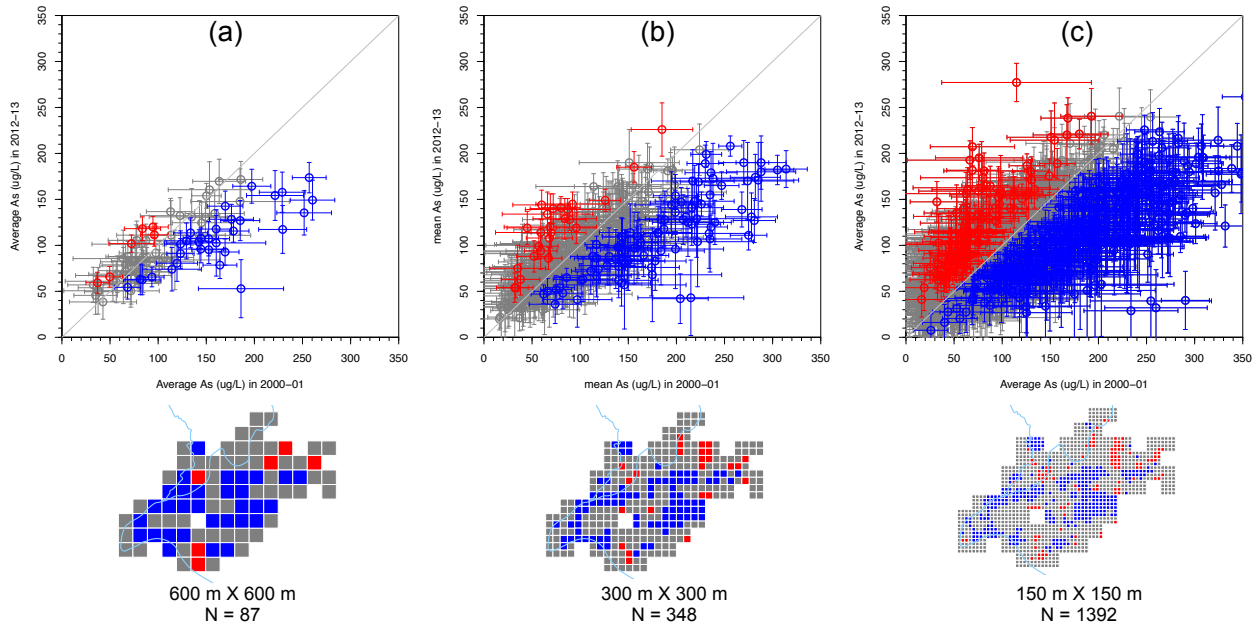
Figure 2-S6. Sensitivity of analysis to block size. Average As concentrations were calculated for blocks four times larger (a) 600 m X 600 m and (c) four times smaller (150 m X 150 m) for comparison with the main scenario (b). Whereas only minor regional patterns of changes in As concentration are sensitive to block size, the overall trends of rising concentrations at the low end and declining concentrations at high end remains the same about the 1:1 Line (gray)..The largest block configuration (600 X 600) was generated considering two criteria: (i) the spatial autocorrelation distance (Fig. 2-S4) of As in the study area as the length of each side of the square blocks and (ii) each block must contain tested wells from both surveys; each block of the largest configuration were disaggregated to produce the finer grids.
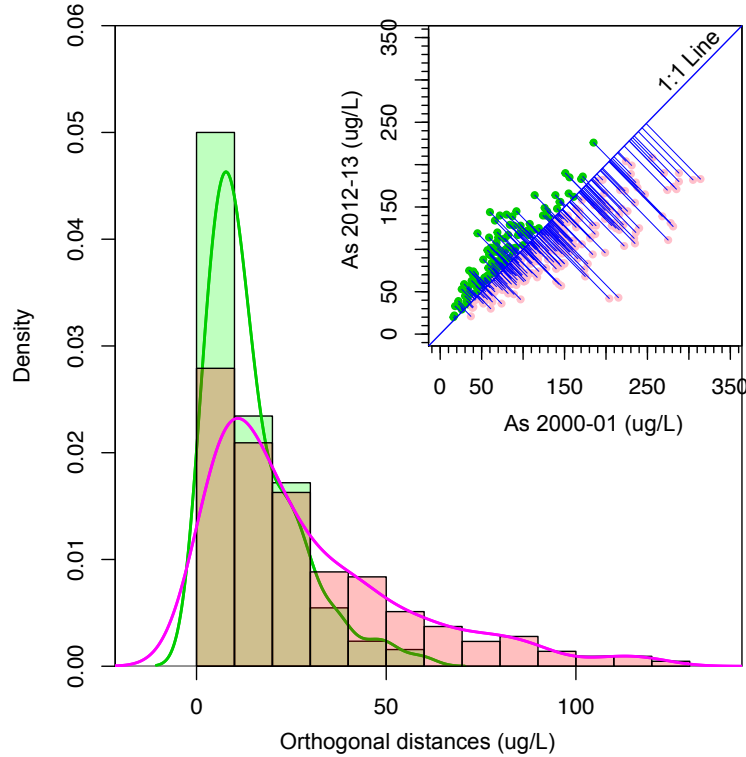
Figure 2-S7. Statistical test validating changes in As at the block level over the last decade. Overlapping density and histogram plots of the orthogonal distances from the 1:1 line (inset figure showing orthogonal distances). The histogram above the 1:1 line is h_a (green) and below the line is h_b (pink). The overlapping zone between histograms h_a and h_b is also indicated (brown). A Pearson's chi-squared test[3] can be used to test the significance of this asymmetry against the Null Hypothesis that the block average As data are drawn from a symmetric distribution; however, the form of this distribution is not known. Therefore, we have used a grid search method[12] to search through all possible histograms arising from symmetric distributions, and to select the one that is the most probable (h_T). Not surprisingly, it has a histogram that "splits the difference" between two observed histograms h_a and h_b. We used 5-bin histograms for the grid search method: h_a = [111, 19, 2, 0, 0], h_b = [128, 51, 20, 12, 5], and h_T = [114, 36, 13, 8, 3] to reduce the number of degrees of freedom. The Null Hypothesis can be rejected to 99.99999% certainty based on Pearson's χ^2 test, indicating that the asymmetric scatter is statistically significant. The same statistical test for the 271 individual wells rejects the Null Hypothesis with a certainty of 99.99998%. The Matlab script associated with the χ^2 test is provided at the end of the supporting document.
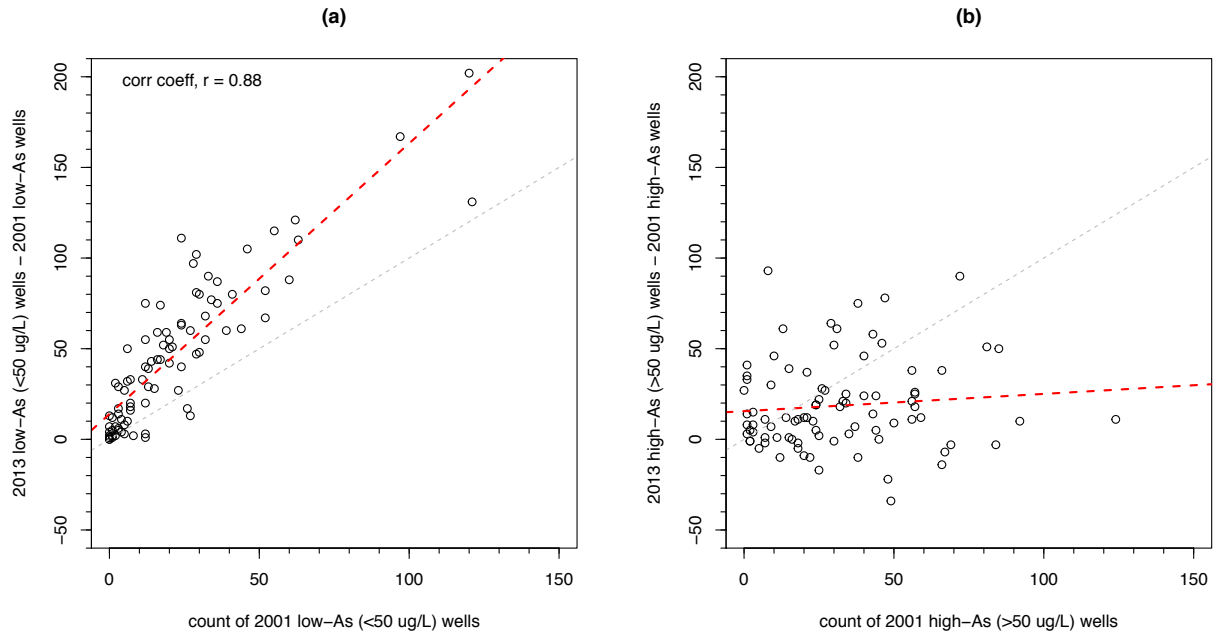
Figure 2-S8. Change in the number of wells at the block level (n = 87; 600 m X 600 m)

between 2000-01 and 2012-13. The observations show (a) an approximate doubling of the

number of wells installed in low-As blocks and (b) a lower average increase that is independent

of the initial number of wells in high-As blocks.
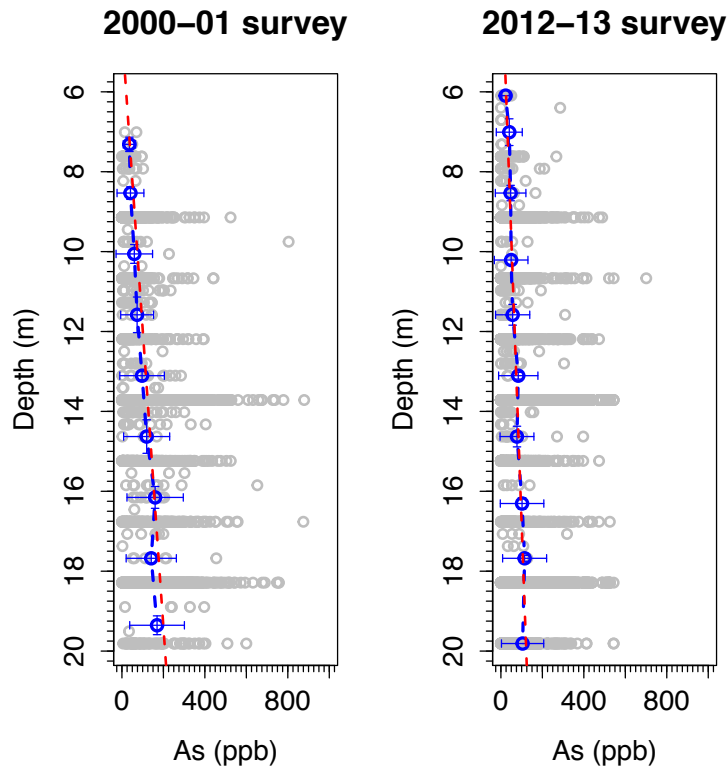
Figure 2-S9. Depth dependence of As concentrations in shallow groundwater. Both surveys shows a gradual, albeit noisy, increase in As concentrations with depth within the shallow aquifer of the study area. The discretized distribution of well depths indicates that most owner recall their well's depth in 5 ft intervals. After binning the data in 5 ft depth intervals and averaging, the data indicate an increase of 14±4 μg/L and 7±1 μg/L per meter in 2000-01 and 2012-13, respectively.
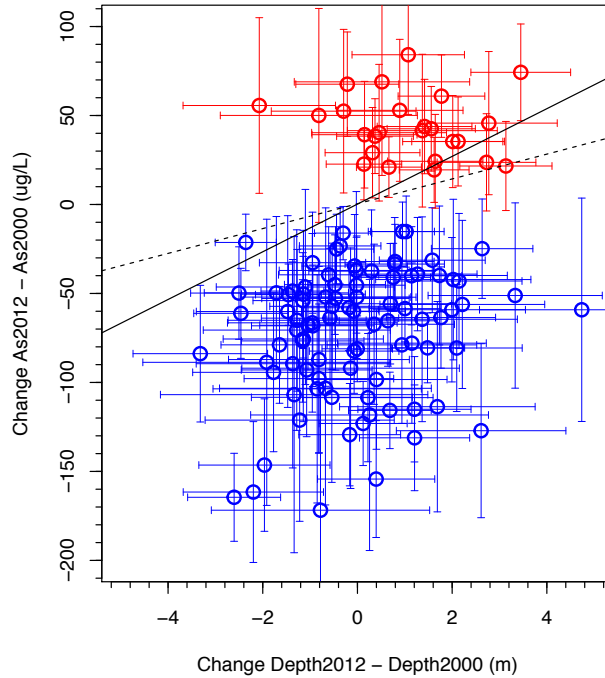
Figure 2-S10. Influence of well-depth on As concentrations. Changes in block-averaged As concentrations attributable to changes in block-averaged depth would follow the slopes defined in Fig. 2-S8 for 2000-01 (solid line) and 2012-13 (dotted line). Increases in As concentrations for a few blocks corresponding to the area between the two lines in the upper right corner of the graph could possibly be due to an increase in well depth but most of the declines in block-level As concentrations are not consistent with a decrease in well depth. The error bars indicate standard error of average As and average depth at block level.
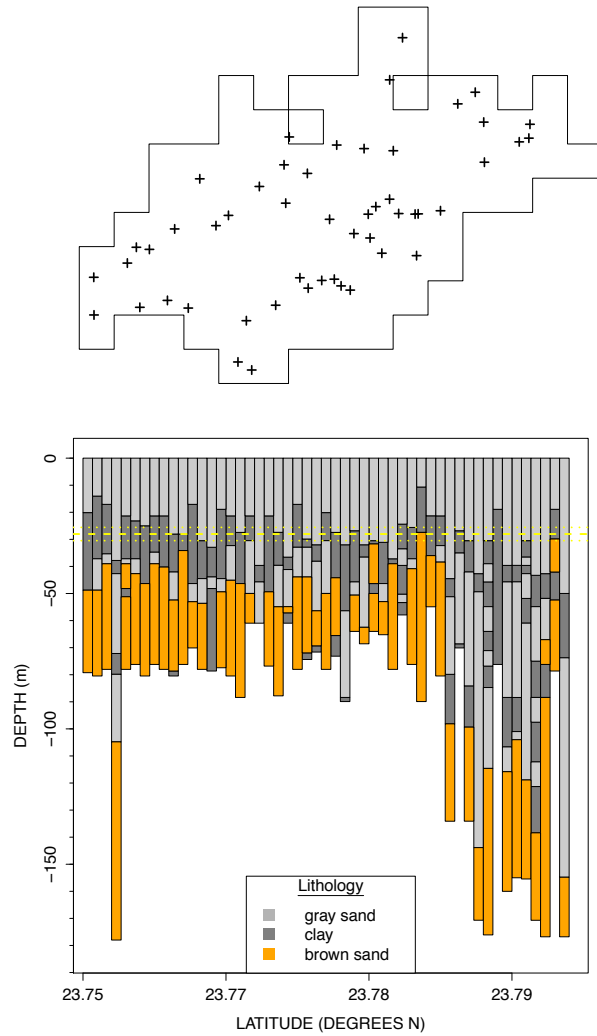
Figure 2-S11. Depth of the shallow aquifer in Araihazar. Profiles of sediment type based on drill cuttings collected at 2 ft intervals from a total of 51 sites within the 25 km^2 study area. The average thickness of the upper sandy aquifer tapped by all irrigation wells in the area of 28±3 m is indicated by a horizontal yellow line. The sediment cuttings were retrieved by indigenous hand-flapper method[6].
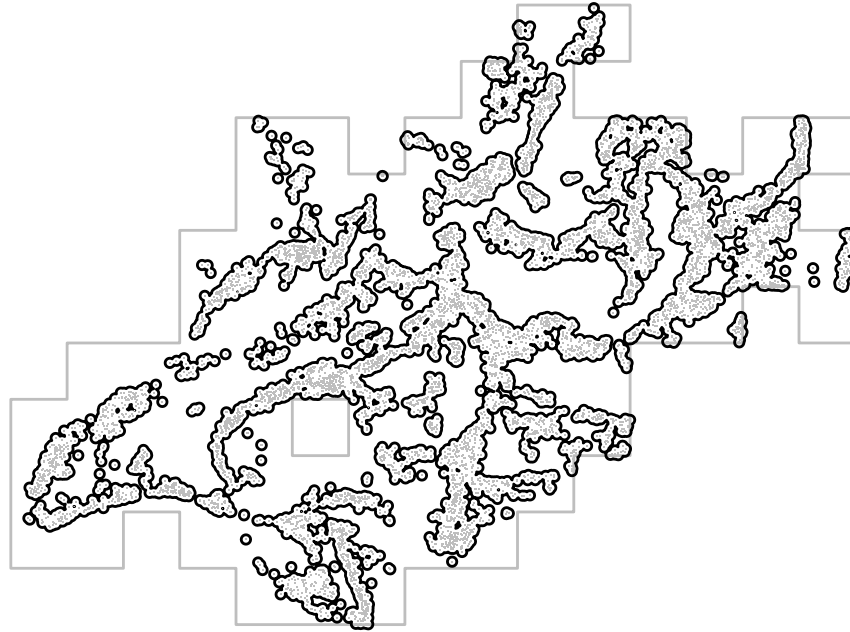
Figure 2-S12. Fraction of land within study area used for agriculture. The vast majority of hand-pumped tubewells are installed in villages rather than agricultural fields and their location can therefore be used to delineate settled areas. In order to calculate by difference the proportion of land used for agriculture, buffers with a radius of 50 m were drawn around each of the 8,229 wells surveyed during 2012-13 and merged. Under the justified assumption that most of the non-settled area is used to grow Boro rice during the winter season, we estimate that 1 m of groundwater is pumped each year to irrigate 50% of the study area.
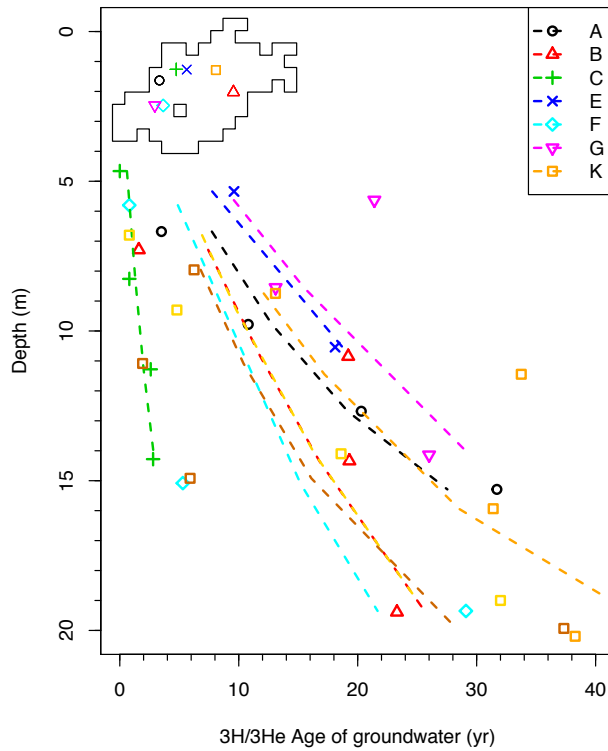
Figure 2-S13. Depth distribution of groundwater ages within the shallow aquifer. Using the tritium-helium method, the time elapsed since surface recharge was measured for a total of 32 depth intervals distributed across 9 sites[7,8]. The profile of groundwater ages was converted to recharge rates at each site by using the model of Vogel[9], as described by Schlosser et al.[10], which takes into account the local thickness of the shallow aquifer. The average recharge rate based on the 9 sites is 0.47±0.4 m/yr and is consistent with the rate inferred from requirement for growing Boro rice[11].
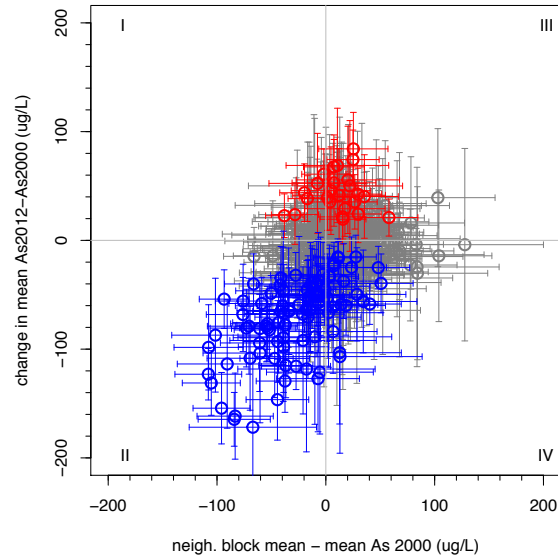
Figure 2-S14. Changes in block-averaged As concentrations in relation to neighboring blocks. For each of the 348 blocks, the average of the block-average As concentration of the nearest neighbors (max^m of 8) was calculated. This average is displayed as a function of the observed changes in block-As concentrations for each central block. The general trend is consistent with lateral exchange of groundwater As, with increases in As concentrations associated with higher As concentrations in neighboring blocks and vice-versa. The error bars indicate standard error of the mean. The 4 quadrants indicate: (I) blocks with increased As concentrations surrounded by lower block average concentrations; (II) blocks with decreased As concentrations surrounded by lower block average concentrations; (III) blocks with increased As concentrations surrounded by higher block average concentrations; and (IV) blocks with decreased As concentrations surrounded by higher block average concentrations.

Matlab script associated with χ^2 test explained in Figure 2-S7. The description of the *chi2pdf* function can be accessed here: https://www.mathworks.com/help/stats/chi2pdf.html

```matlab
clear all;

%set working directory
cd('/Users/Rajib/Documents/Rajib/Columbia_ARAIHAZAR/...')

a = load('blocks348_above_one_line.txt');
Na = length(a);
b = load('blocks348_below_one_line.txt');
Nb = length(b);
N = Na+Nb;
No2 = floor(N/2);

Nbins = 5;
binmin = 0;
binmax = 125;
Dbins = (binmax-binmin)/Nbins;
bins = binmin + Dbins*[0:Nbins]';

ha = histc( a, bins );
ha = ha(1:end-1);
hb = histc( b, bins );
hb = hb(1:end-1);

figure(1);
clf;
hold on;
set(gca,'LineWidth',2);
set(gca,'FontSize',14);
axis( [binmin, binmax, 0, 200] );
for i=[1:Nbins]
    plot( [bins(i),bins(i),bins(i+1),bins(i+1)]', [0,ha(i),ha(i),0]', 'k-', 'LineWidth', 2 );
    plot( [bins(i),bins(i),bins(i+1),bins(i+1)]', [0,hb(i),hb(i),0]', 'r-', 'LineWidth', 2 );
end

nu = (2*Nbins)-1;
pvmin = 1.0;
h0min = [1, 1, 1, 1, 1];
step = 1;
for i1 = [0:step:No2]
for i2 = [0:step:No2]
for i3 = [0:step:No2]
for i4 = [0:step:No2]
    k=No2-(i1+i2+i3+i4);
    if( k > 0 )
        h0 = [ i1, i2, i3, i4, k ]';
        c1 = sum((( ha - h0) .^ 2) ./ h0);
        c2 = sum((( hb - h0) .^ 2) ./ h0);
        pv = 1 - chi2pdf(c1+c2,nu);
        if( pv < pvmin )
            pvmin = pv;
            h0min = h0;
        end
    end
end
end
fprintf('%d %d\n', i1, i2);
end
end
fprintf('ha: %d %d %d %d %d\n', ha(1), ha(2), ha(3), ha(4), ha(5) );
fprintf('hb: %d %d %d %d %d\n', hb(1), hb(2), hb(3), hb(4), hb(5) );
fprintf('HT: %d %d %d %d %d\n', h0min(1), h0min(2), h0min(3), h0min(4), h0min(5) );

fprintf('Piersons p-value %f\n', pvmin);
```

References

1.   George C. M. *et al.* Evaluation of an arsenic test kit for rapid well screening in Bangladesh. *Environ. Sci. Technol.* **46**, 11213–11219 (2012).

2.   van Geen, A. *et al.* Reliability of a commercial kit to test groundwater for srsenic in Bangladesh. *Environ. Sci. Technol.* **39,** 299–303 (2005).

3.   Menke, W. & Menke, J. in *Environmental Data Analysis with MatLab* (eds. Menke, W. & Menke, J.) 217–238 (Elsevier, 2012).

4.   van Geen A., Zheng Y., Versteeg R., Stute M., Horneman A., Dhar R., Steckler M., Gelman A., Small C., Ahsan H., Graziano J. H., Hussain I. and Ahmed K. M. (2003) Spatial variability of arsenic in 6000 tube wells in a 25 km2 area of Bangladesh. *Water Resour. Res.* **39**. No. 5, 1140, doi:10.1029/2002WR001617 (2003).

5.   Pebesma, E. J. Multivariable geostatistics in S: the gstat package. *Comput. Geosci*. 30, **683–691** (2004).

6.   Horneman, A. *et al.* Decoupling of As and Fe release to Bangladesh groundwater under reducing conditions. Part 1: Evidence from sediment profiles. *Geochim. Cosmochim. Acta* **68,** 3459–3473 (2004).

7.   Stute, M. *et al.* Hydrological control of As concentrations in Bangladesh groundwater. *Water Resour. Res.* **43,** W09417 (2007).

8.   Radloff, K. A. *et al.* Reversible adsorption and flushing of arsenic in a shallow, Holocene aquifer of Bangladesh. *Appl. Geochem.* (2016).

9.   Vogel, J. C. Investigation of groundwater flow with radiocarbon: Isotopes in hydrology. in *Conference on Isotopes in Hydrology* 355–368 (International Atomic Energy Agency, 1967).

10.   Schlosser, P., Stute, M., Sonntag, C. & Munnich, K. O. Tritiogenic ^{3}He in shallow groundwater. *Earth Planet. Sci. Lett.* **94,** 245–256 (1989).

11.   Meharg A. A. and Rahman M. M. Arsenic contamination of Bangladesh paddy field soils: Implications for rice contribution to arsenic consumption. *Environ. Sci. Technol.* **37**, 229–234 (2003).

12.   Menke, W.; Menke, J. 4 - The Power of Linear Models. In *Environmental Data Analysis with Matlab (Second Edition)*; Menke, W., Menke, J., Eds.; Academic Press, 2016; pp 67–89. https://doi.org/10.1016/B978-0-12-804488-9.00004-5.

13.   Hengl, T. Finding the right pixel size. *Comput. Geosci.* **32,** 1283–1298 (2006).

CHAPTER 3

SIMILAR ARSENIC RETARDATION IN GRAY HOLOCENE AND ORANGE PLEISTOCENE SANDS IN BANGLADESH: EVIDENCE FROM COLUMN EXPERIMENTS CONDUCTED IN THE FIELD

Rajib H. Mozumder[1*], Benjamin C. Bostick[1], Magdi Selim[2], Atikul Islam[3], Elizabeth M. Shoenfelt[1,4], Tyler Ellis[1], Brian J. Mailloux[5], Imtiaz Choudhury[3], Kazi M. Ahmed[3] & Alexander van Geen[1]

[1]Lamont-Doherty Earth Observatory of Columbia University, NY 10964, USA

[2]School of Plant, Environmental, and Soil Sciences, Louisiana State University AgCenter, Baton Rouge, LA, 70803, USA

[3]University of Dhaka, Dhaka-1000, Bangladesh

[4]Massachusetts Institute of Technology, Cambridge, MA 02139, USA

[5]Barnard College, New York, NY-10027, USA

*Corresponding author: mozumder@ldeo.columbia.edu

Now at: Gradient, 20 University Rd, Cambridge, MA 02138

Abstract

Transport by groundwater flow has the potential to introduce arsenic (As) in previously uncontaminated aquifers. The extent to which As transport is retarded by adsorption is particularly relevant in Bangladesh where low-As wells offer the best chance of reducing chronic exposure to As of a large rural population dependent on groundwater. In this study, column experiments were conducted with intact cores in the field for up to 3 weeks to measure As retardation. Freshly collected cores of reduced (gray) sediment of Holocene age as well as oxidized (orange) sediment of Pleistocene age were eluted at pore-water velocities of 40-230 cm/day with high-As, anoxic groundwater pumped directly from a well. Gray columns released As from the very beginning of the experiments but the largest increase in eluted As for both grey and orange sands occurred after about 50 pore volumes. The early release of As from gray sand and some dependence of As breakthrough on flow rate was reproduced with a reversible multi-reaction transport model with an initial pool of weakly retained As. Over time, redox transformations affected Fe and As speciation in the columns and enhanced both sulfate and As retention.

3.1. Introduction

Millions of people in South and Southeast Asia are exposed to high arsenic (As) in their drinking water pumped from alluvial aquifers[1–3]. Anoxic Holocene aquifers composed of gray sands often contain naturally elevated levels of As (>100 μg/L) released by the microbial reduction of iron(oxy)hydroxides[3–7]. Pleistocene aquifers in the region are also anoxic today but were in some areas subaerially exposed during the last glacial maxima[8]. These aquifers contain orange sand coated with Fe(III) oxides and are typically low (<10 μg/L) in As[3]. A sizeable pool of As (<1-5 mg/kg) is adsorbed on both the gray and orange sediments[9,10]. It is therefore the partitioning of As between groundwater and aquifer sediment that largely determines whether an aquifer is toxic to human health.

The partitioning of As between the solid and aqueous phase has been expressed and modeled in various ways. Most widely used is the sorption partition coefficient K_D, the ratio of the As concentration in the solid phase divided by the As concentration in the dissolved phase. This approximation is often effective at describing transport under near-equilibrium conditions[11]. This assumption is less appropriate when groundwater flow is faster, for example where groundwater flow is accelerated by pumping for irrigation or the municipal supply of large cities[12–16]. The partition coefficient K_D may also be sensitive to the concentration of competing ions in groundwater. Surface complexation models[17] can include equilibrium and kinetically limited models of adsorption, and are also often applied to As transport, particularly to predict the sensitivity of As partitioning to oxyanions such as phosphate, bicarbonate, and silica[3,18–22]. Several laboratory and field investigations have suggested that As transport is a non-equilibrium

or rate-limited process[23–26]. An equilibrium assumption may therefore significantly underestimate the time required to clean up a contaminated site[27].

The risk of contamination of low-As aquifers by nearby high-As sources will depend on the direction of groundwater flow and sorption characteristics of sediment in contact with high-As as well as low-As groundwater. It has been suggested that the As sorption capacity of gray Holocene sand is limited and thus As supplied to these sediments would be transported at the same rate as groundwater[12,19]. However, considerable As adsorption has been measured with laboratory batch experiments and field studies using gray sand aquifers[3,10,12,19,21,28–30]. The wide range of measured K_D's of 0.15 to 46 L/kg derived from these experiments corresponds to retardation factors of 2 to 300, assuming an aquifer material bulk density of 1.8 g/cc and a porosity of 30%. It is unclear to what extent this range reflects variations in experimental conditions, sediment properties or preservation, or other factors.

The extent of adsorption of As to orange sediment also appears to vary widely, and potentially differs from adsorption to gray sands[20,31–34]. Laboratory studies conducted in batch mode generally indicate higher K_D values (20-70 L/kg; retardation of 120-420) compared to grey sands. Some laboratory experiments, however, may have been affected by prolonged storage, repacking of sediment, and the use of artificial groundwater that is not representative[20,32,35]. Field-based studies are not affected by storage but are subject to different uncertainties such as the direction and rate of groundwater flow. These indicate a lower K_D of 1-10 L/kg for originally orange sand that, in some cases, turned grey and therefore lower retardation factors of 7-60[31,33,34].

If retardation of As transport through orange sediments is greater than for grey sand, this could provide significant protection against intrusion of high As groundwater from reducing aquifers. Batch adsorption experiments conducted under carefully controlled conditions suggest, however, that As adsorption to Holocene gray and Pleistocene orange sediment may not be that different after all[21]. In order to address this unresolved issue under closer to ambient conditions, high-As groundwater from a shallow well was eluted for the present study at different rates through a series of columns containing intact, fresh gray and orange aquifer sediment and measured in the field under anaerobic conditions. We hypothesized that orange sands would have greater retention than gray sands, and thus more effectively protect low-As aquifers from the intrusion of As-containing groundwater under typical field conditions.

3.2. Materials and Methods

3.2.1. *Sediment coring and column preparation*

Sediment cores containing Holocene gray sand and Pleistocene orange sand were collected in Araihazar, Bangladesh, immediately before the experiment (Figure 3-S1). Intact cores were retrieved (30 cm long, 1.6 cm inner dia.) using a hammer-driven soil corer (AMS SST soil recovery probe 424.45) from drilling depths between 40 and 60 ft. Immediately after retrieval, the cores were refrigerated in nitrogen-flushed Mylar bags that were heat-sealed after adding oxygen absorbers (IMPAK sorbent systems). Within 24 hours, and inside a nitrogen inflated glove chamber (Glas-Col04408-38), a total of 15 (8 gray and 7 orange sand) undisturbed sediment columns, 7.5 cm in length, were prepared from the central portion of the recovered cores using a precision tube cutter. The inlets and outlets of the columns were enclosed with custom made plugs after inserting a thin (1-2 mm) layer of glass wool to prevent the transport of

fine particles. A column packed with pure sand (40-100 mesh, ACROS Organics 370942500) was also prepared in parallel as a control.

3.2.2. *Experimental setup*

The gray and orange sediment columns along with a control sand column containing 99.8% SiO_2 and 0.01% iron oxide (as specified by the manufacturer) were eluted with groundwater directly at the wellhead from a shallow well screened from 60 to 65 ft below ground surface, a depth where As concentrations typically peak in the study area (Figure 3-S1). The influent groundwater was pumped continuously into a bag (50 L capacity) shaped like a pyramid that was kept overflowing through a narrow opening at the top to ensure a constant supply of anoxic groundwater (Figure 3-1). The storage bag was placed at a higher elevation than the columns to ensure uninterrupted, steady flow in the event of a pump stoppage or electricity failure. The custom-made bag (Ready Containment LLC) facilitated escape of bubbles (probably carbon dioxide and/or methane) that tend to cling to the corners of a regular container. Groundwater from the storage bag reached a manifold that divided the flow into the columns at different rates using peristaltic pumps (Ismatec and Gilson Minipuls 3) and various tubing diameters. The columns were housed in custom-made anoxic chambers (modified from Becton-Dickinson#260672) with pouches that consume oxygen (Becton-Dickinson#260678) and anaerobic indicator strips (Becton-Dickinson#271051). The columns were placed inside the chamber in their natural orientation, with the groundwater entering the top of each column (Figure 3-1).

These columns used a wide range of flow velocities designed to be sufficient for column breakthrough over an experimental period short enough to minimize biological transformations that can affect transport, while also being slow enough to approximate typical groundwater flow velocities. The Darcian velocity was calculated by dividing the average volume of samples by the cross-sectional area of columns (2 cm^2) and average time interval and ranged from 0.5 to 3 cm/hr. Most of the columns (n=8) were eluted either at an average pore water velocity (PWV) of 154±10 cm/day (fast) or 75±10 cm/day (slow) (Table 3-S1). In addition, one orange sand column was eluted at 40 cm/day and one column of grey sand was eluted at 230 cm/day.

3.2.3. Sampling and onsite measurements

Column effluents were collected in a manually operated fraction collector in acid leached (10% HCl) 15 ml vials every 3 hours for the first 10 days (8 times a day) of the experiment, followed by every 12 hours for 2 weeks (2 times a day). The volume of each sample was documented at the time of collection. Every other sample was acidified in the field with TraceMetal grade HCl. Some of the remaining samples remained unacidified for anion analysis, while others were acidified later in the lab with Optima grade HCl for cation analysis. Towards the end of the experiment (day 20), groundwater flow into the storage bag was interrupted and the retained water in the bag was spiked with sodium bromide (Fisher#S255-500) and sodium phosphate monobasic dihydrate (Fisher#S381-500). A subset of columns was sampled more frequently on that day (Figure 3-S2).

The influent groundwater was sampled daily at an outlet before it reached the storage bag and from the bottom of the storage bag (Figure 3-1). Dissolved oxygen concentration in the influent

water was tested daily with a visual kit (Chemetrics 0-40 ppb). The input water was also monitored daily for pH, ORP (oxidation-reduction potential), electrical conductivity, and temperature using Oakton probes (UX-35650-10 & UX-35634-30). A pH flow-through cell (UX-05662-48) was used to measure pH in a subset of column effluents. Arsenic speciation cartridges (Metalsoft Center, Highland Park, NJ) were used in the field to separate As(V) from As(III) in the influent water as well as in a subset of column effluents immediately after collection[36]. Samples for dissolved organic carbon (DOC) and dissolved inorganic carbon (DIC) were collected in 22 ml clear glass vials (Sigma-Aldrich 27173 Supelco). The DOC samples were acidified to 0.1% HCl while DIC samples were left unacidified.

3.2.4. Sediment analyses

Sediments from control cored sections and experimental columns were analyzed from the same interval. Of the experiments performed, a total of 10 sediment columns (6 gray and 4 orange sand columns) were successfully completed, and 5 were compromised due to repeated flow interruption (Table 3-S1). Flow interrupted columns contained very high fraction of fine-grained silt and/or clay particles. Most of the successful experimental columns were composed of fine to medium grained sand.

X-ray fluorescence (XRF) and sediment phosphate extraction

Cuttings (10-15 mm thick) collected while drilling the sediment cores were packed in Saran wrap and analyzed through a single layer with a handheld XRF (InnovX Delta) in the instrument's soil mode for bulk As concentration. Each sample was analyzed under 3-beam soil mode for a total of 3 minutes (40, 120, 20 sec for the 3 beams, respectively). The internal calibration of the

instrument was verified by analyzing reference NIST standards (SRM 2709, 2710, and 2711) in

between samples. As a measure of the exchangeable As content of the sediment, 1 g of gray or

orange sand (n= 8) immersed in 55 mL N_2-flushed solution of 1 M Na_2HPO_4 solution was

adjusted to a pH of 5 for 24 hours[9]. The extraction was conduced in an anaerobic chamber

(Coy#120001) and the solutions filtered through 0.45 μm media.

X-ray absorption spectroscopy (XAS)

Iron (Fe) and arsenic (As) K-edge X-ray absorption spectra were collected in fluorescence mode

at the Stanford Synchrotron Radiation Lightsource (SSRL) on beamlines 4-1 and 11-2. Fe

spectra were collected using either 32 or 100-element Ge detectors windowed on the Fe $K_α$

fluorescence peak, and using a 3μx Mn filter. Spectra were calibrated to using a Fe metal foil

(7112.0 eV). Arsenic spectra were performed by windowing on the As $K_α$ fluorescence peak, and

using a 3μx Ge filter.

Spectral analysis was performed using Matthew Newville's Larch Data Analysis Tools for X-ray

Spectroscopy implemented in Python as detailed in Shoenfelt et al.[37]. Larch code and

documentation is available at http://xraypy.github.io/xraylarch/. Fe(II) content and mineral

composition were determined by linear combination fitting using the best-fit 5 of 10 reference

compounds (pyrite, siderite, goethite, hematite, magnetite, biotite, hornblende, augite, nontronite,

ferrihydrite). For this fitting, we used the k^3-weighted chi function from k=2 to k=8-12 $Å^{-1}$

depending on the quality of the sample data, optimized for the background spline function to end

at a node. Errors in mineral composition, usually within 5% of total Fe, LCF are determined in

Larch based on sensitivity analysis and fitting quality. This method is effective for most iron minerals, but ferrihydrite in fitting also includes reactive, nanocrystalline goethite; thus, ferrihydrite in fits should be considered as representative of a larger spectrum of reactive Fe(III)oxyhydroxides[38].

Arsenic XANES spectra were analyzed with Sixpack using 4 reference standards, As_2S_3, As(III) adsorbed on ferrihydrite, As(V) adsorbed on ferrihydrite, and FeAsS. Of these, FeAsS was not needed in any fit. To fit the white line most accurately, reference spectra were collected using As loadings that were comparable to natural samples (10 mg As/kg). Errors in fractional As content are usually within 3% for most samples, and occasionally somewhat higher for samples with very low As concentrations (<2-3 mg As/kg).

3.2.5. *Analysis of groundwater and sediment extracts*

All acidified (1% HCl) samples collected from the input well, storage tank, column effluents, and sediment extracts were analyzed for P, S, Fe, Mn, As, Na, K, Ca, Mg, Ba, and Sr using high-resolution inductively coupled plasma-mass spectrometry (HR ICP-MS) with a detection limit of 0.1 μg/L accounting for all dilutions[39]. The results from the HR ICP-MS were replicated for a subset of groundwater samples with a precision of <5%. The accuracy and precision of the measurements were within ±10% when compared to known laboratory standards. The anions Br^- and Cl^- were analyzed using a Dionex Integrion HPIC System (Dionex, Thermo Scientific) with an AS-18 column, which has detection limits of 0.05 ppm and a precision of ±5% at typical concentrations. DOC and DIC samples were analyzed with a Shimadzu Carbon Analyzer with ±5% precision at Lamont-Doherty Earth Observatory.

3.2.6. Column transport parameterization

The transport models used measured experimental flow rates for each column. The average bulk density ρ (range between 1.7 and 1.9 g/cc) of the columns was determined from oven dried sediment weight divided by the volume of dry sediment column (Table 3-S1). The porosity θ (range between 0.29 and 0.34) was then estimated as: θ = 1- ρ/2.65 assuming a particle density of 2.65 g/cm^3. The dispersion coefficient (D) was determined (1.5 and 3 cm^2/hr for slow and fast PWV, respectively) by fitting the bromide (Br$^-$) breakthrough curve using the analytical solution for one-dimensional advection-dispersion equation assuming conservative transport of Br$^-$ (i.e. a retardation factor of 1) in the sand columns (Figure 3-S4).

3.2.7. Model formulation

We use a two-phase reversible non-linear kinetic model[40] to simulate the observed column breakthrough curves, after modifying it to accommodate an initial exchangeable As concentration. This model is necessary because column elution data cannot be explained with a simple K_D model. A single set of rate constants is used to describe As elution in gray or orange sediments. We use the one dimensional advection-dispersion equation (ADE) to formulate the transport of arsenic in the sediment columns[41]:

$$\theta \frac{\partial C}{\partial t} + \rho \frac{\partial S}{\partial t} = \theta D \frac{\partial^2 C}{\partial^2 x} - v \frac{\partial C}{\partial x}$$

where, θ indicates the porosity of sand columns (dimensionless), ρ is the sediment bulk density (g/cm^3), C represents solute concentration (mg/L), S indicates the total sorbed concentration (mg/kg), D is the hydrodynamic dispersion coefficient (cm^2/hour), v represents the pore water

velocity (cm/hour), which is Darcy's velocity divided by θ and x is the length of column (cm).

When the retention and release of solute is strongly time-dependent, kinetic reactions are employed instead of local equilibrium assumption. A two-phase reversible non-linear kinetic model was used to simulate the observed column breakthrough curves:

$$\rho \frac{\partial S_1}{\partial t} = \theta k_1 C^n - \rho k_2 S_1$$

$$\rho \frac{\partial S_2}{\partial t} = \theta k_3 C^n - \rho k_4 S_2$$

$$S = S_1 + S_2$$

where, the parameters k_1 and k_3 are the forward rate constant (hr^{-1}), k_2 and k_4 are the reverse rate constants (hr^{-1}), and n is the reaction order which is also a measure of variability in sorption sites in terms of arsenic retention[24,40]. The sorbed phase S_1 is assumed to react rapidly with the aqueous phase at concentration C (hence, k_1 and k_2 are larger) whereas sorbed phase S_2 is assumed to react slowly with the dissolved phase C (small k_3 and k_4).

This two-phase, fully reversible kinetically-limited reaction model assumes: (a) any initial release of arsenic is due to desorption from an initial, rapidly exchanged pool of sorbed As; (b) the pool of sorbed arsenic (S) in the sediment is comprised of two components: the first phase (S1) is the fast reacting phosphate extractable arsenic and the second phase (S2) is a slow reacting phase, which is the difference between the bulk sediment arsenic concentration (S) and S1 (Table 3-S2). There are pseudo-first order kinetic rate constants, and initial adsorbed pools of

72

As in the model of As retention. The adsorbed pools of As in S1 and S2 are estimated based on total As and laboratory phosphate extractions.

3.2.8. Determination of rate constants

The rates of As exchange between the solid and dissolved phase in the columns were estimated using a numerical model at a time-step discretization of 0.05 hr and column length discretization of 0.1 cm using the Gaussian elimination method[40,42]. An input As concentration of 320 μg/L, porosity of 0.32, and bulk density of 1.80 g/cc was used for all columns. The only variable transport parameters were the measured flow velocities and corresponding dispersion coefficient. The Freundlich parameter (n), which is the dimensionless reaction order, was set to 0.4 for all sediment columns. A single and unique set of forward (k_1, k_3) and reverse rate (k_2, k_4) constants were used to describe the eluent concentrations for all columns in each sediment group (gray and orange). The best fit was derived by minimizing the sum of squared error between observed and predicted eluent concentrations at different PWV.

3.3. Results

3.3.1. Sediment properties

Bulk As concentrations measured by XRF in the gray Holocene sediment ranged between 2.0±0.6 and 4.2±0.6 mg/kg (n =7) (Table 3-S2). Iron (Fe) and calcium (Ca) concentrations averaged 1.5±0.4 % and 6,900±120 mg/kg, respectively. As a proxy for the redox state of surficial Fe oxides, the difference in diffuse spectral reflectance (ΔR = 530 nm – 520 nm) of column sands was recorded with a Minolta CM-600d spectrophotometer. The difference in

reflectance at those wavelengths ranged between 0.06±0.005 % (mean ± σ for triplicate measurements for an individual sample) and 0.34±0.04 % and averaged 0.22±0.08 (n=11), which corresponds to about 80% Fe(II) in the hot-acid leachable fraction of Fe(II+III) oxides in the sediment[43]. Bulk As concentrations in the orange sediment ranged from 1.8±0.6 to 3.0±0.5 mg/kg (n = 7). Overall, the orange sediment contained a higher concentration of Fe (2.4±0.3%) and a lower concentration of Ca (4400±100 mg/kg) than gray sediment. The reflectance difference ΔR for the orange sands ranged between 0.73±0.05 % and 1.46±0.02 %, with an average of 1.1±0.3 (n=10), which indicates the lack of any detectable Fe(II) in the fraction of hot-acid leachable Fe oxides (Table 3-S2).

The proportions of Fe(II) measured by XAS analysis in gray and orange sediment were 83±12% and 12±5% (n =2), respectively (Figure 3-4a, Figure 3-S12a). The most abundant Fe mineral classes in the gray sediment were Fe silicates (41±4% biotite and 35±4% and hornblende), with small proportion of goethite (10±5%) and reactive Fe oxides (10±5%). In contrast, the orange sediment was primarily composed of reactive Fe oxides (41±5%), goethite (30±5%), and hornblende (27±5%).

Phosphate extractable As was used to differentiate labile and nonlabile As pools. The gray sediment contains an average of 3 mg/kg of total sorbed As, and about half of that is P-extractable. In contrast, the orange sediment contains an average of 2 mg/kg of As, of which only about 0.3 mg/kg is P extractable. Therefore, both model parameters S1 and S2 are set to 1.5 mg/kg for gray sediments. For orange sediment columns, S1 and S2 are 0.3 and 1.7 mg/kg, respectively (Table 3-S2).

74

3.3.2. *Influent groundwater composition*

The source groundwater selected to elute the sediment columns was consistently high in dissolved As (320±11 µg/L) and Fe (7±0.4 mg/L) over the course of the experiment (Figure 3-S2). The water contained moderately high levels of manganese (3 mg/L Mn), phosphate (1.5 mg/L as P), sulfate (3 mg/L as S), and bicarbonate (104 mg/L as dissolved inorganic carbon/DIC). There was no detectable dissolved oxygen in the groundwater, the ORP readings (-105 to -134 mV) remained negative, and the pH consistent at 7.0±0.1 throughout the experimental period. The composition of groundwater remained unaltered in the overflowing storage bag; paired t-tests for the mean of daily samples of As, Fe, Mn, S, and P in direct samples and the bag (n = 18 each) were equivalent and constant over the experiment (p-value > 0.05). There was no detectable oxygen in groundwater in the storage bag (DO kit reading of 0 ppb). Based on speciation columns, most (>90%) As was present as As(III) in groundwater collected from the well and storage bag (n=8 each).

Three shallower wells were installed in the vicinity of the input well at 20, 45, and 55 ft depths to better understand local geochemical variability (Figure 3-S1). The vertical profiles indicate a general trend of increasing As, P, and dissolved inorganic carbon (DIC) and decreasing Fe concentrations with depth. However, S concentrations of 3 mg/L in the input well was considerably higher than in the two shallower high As wells (<1 mg/L S). The dissolved organic carbon (DOC) concentration in the input groundwater was 3 mg/L.

3.3.3. *Elution of arsenic and other redox sensitive elements*

Pleistocene Orange sediment columns

Concentration of As remained below 10 µg/L in the eluent for about 40 pore volumes in the two low-flow columns (82 cm/day) of orange sand but only 10-20 pore volumes in the higher flow column (156 cm/day) and the column eluted at the slowest PWV (40 cm/day) (Figure 3-2a-c). Concentrations of As in the eluent reached the input concentration of 300 µg/L after about 100 pore volumes in the fast flow column but did not exceed 250 µg/L in the two slow flow columns. Eluent As concentration in the slowest flow column reached a maximum of 150 µg/L after 40 PV. In spite of an input concentration of 7 mg/L, it is not until about 150 pore volumes that Fe concentrations in the eluent temporarily rose above 1 mg/L (Figure 3-2d-f). In contrast, S levels in the eluent started immediately about 20% above the inflow concentration of 3 mg/L and dropped precipitously to <0.5 mg/L after about 110 pore volume in the fast flow column, after 80 PV in the slow flow column, and after only 20 PV in the slowest flow column (Figure 3-2g-i). Concentration of P in the inflow was 1.5 mg/L but the eluent rarely rose above 0.20 mg/L throughout the experiment with orange columns (Figure 3-2j-l).

Gray sediment columns

Concentrations of As in the first 50 pore volumes of eluent from the grey columns were consistently higher than for the orange columns and varied between 10 and 200 µg/L (Figure 3-3a-c). For the 4 high flow columns (150-230 cm/day), As concentrations gradually increased to reach the inflow concentration of 300 µg/L at about 60-70 pore volumes and up to about 500 µg/L at about 80 pore volumes. For the 2 slow-flow columns of grey sand (75 cm/day), eluent As concentrations reached 300 ug/L at about 40 pore volumes. In all 6 columns of grey sand,

concentrations of As subsequently became more variable and generally did not exceed the inflow concentration. In contrast to elution of the orange columns, concentrations of Fe in the eluent reached inflow concentration of 7 mg/L after 70 and 30 pore volumes in the fast and slow following columns of grey sand, respectively (Figure 3-3d-f). Concentration of Fe in eluent from the grey columns reached 15-20 mg/L about 10-20 pore volumes later and declined to become variable, while more rarely exceeding the inflow concentration. As in the case of the orange columns, concentrations of S in eluent from the grey columns started immediately at 3.5 mg/L, somewhat higher than the inflow, and dropped precipitously below 0.5 mg/L within about 100 and 40 pore volumes for the fast and slow-flow columns of grey sand, respectively (Figure 3-3g-i). Unlike the orange columns, concentrations of P in eluent from the grey columns gradually rose up to levels in the inflow of 1.5 mg/L for the fast-flowing columns and about half the inflow concentration in the slow flowing columns after about 100 pore volumes (Figure 3-3j-l).

Control sand column

Arsenic and Fe concentrations in eluent from the pure sand column reached levels of the inflow within about 10 PV and then showed fluctuations around an average that is slightly below that of the input (Figure 3-S3a-b). Concentration of P in the eluent took about 50 pore volumes to reach about 2/3 of the inflow concentration and then became more variable (Figure 3-S3d). As in the case of orange and grey columns, concentrations of S started a little above concentration in the inflow and then declined steadily to <0.5 mg/L after about 100 pore volumes (Figure 3-S3c). Unlike the gray and orange sediment columns, the decline in S in the control sand column was not accompanied by a decline in As concentrations.

3.3.4. *Changes in Fe and As speciation*

Iron (Fe) speciation was measured at the inlet and outlet of each column at the end of the experiment to identify changes in Fe speciation that occurred relative to controls. Results are somewhat variable due to small variations in the redox state of these small volume samples, but generally indicate that there was an increase in the Fe(II) content in columns over the course of the experiment (Figure 3-4a & 3-S10a). In orange sands, the fraction of Fe(II) increased by about 10% at the column inlet, but was not significantly different from controls at the outlet (Figure 3-4a). This modest change was accompanied by an obvious change in sediment color to dark brown or black at the inlet (Figure 3-S11). In contrast, the outlet of gray sands gained marginally more Fe(II) (a few percent) than controls or the inlets (Figure 3-S12a). These changes coincide with the development of darker sediments in the inlet for orange sediments, but without obvious color change in gray sediments.

The oxidation state of As in the sediment changed over the course of the experiment. Most of the As present in the gray sediment was As(III), while the orange sediments contained a roughly equal mixture of As(III) and As(V). At the termination of the experiment, the fraction of As(V) had decreased considerably in most columns. Although groundwater contained primarily As(III), much of the As retained in the columns at the end of the experiment in orange columns was present as arsenic sulfide (Figure 3-4b, Table 3-S3). In gray sands, arsenic sulfides also were produced, and there was some evidence for oxidation because the fraction of As(V) also increased (Figure 3-S12b, Table 3-S3). It is unknown whether this oxidation reflects natural sediment processes or is caused by small amounts of oxidation prior to measurement (<0.5 μg/kg

As needs to explain the observed fractional change in As(V) content). However, As(V) oxidation has been observed in other systems undergoing reduction[44–46].

3.4. Discussion

3.4.1. *Modeling arsenic transport*

The eluent and solid phase data combined indicate that As transport was affected by adsorption and desorption and, at later stages of the experiment, by changes in Fe and S redox status that also resulted in changes in aqueous Fe and sulfate levels. In most of the columns, a decline in effluent As concentration occurred when S in the effluent reached <10% of the input level (Figure 3-1, 3-2). To quantify the transport and retention of As unaffected by sulfate reduction detectable in the eluent, we limit the fitting of the model to the initial breakthrough observed in many columns, i.e. within 40-100 PV depending on flow rate.

Two key considerations affect the selection of a model to describe adsorption in these experiments. First, the initial incomplete adsorption of As early in the experiment (and prior to breakthrough) indicates that there is an initial pool of weakly retained As present in the solid phase that is susceptible to desorption. This initial desorption was primarily observed in gray sand columns. Second, differences in the As breakthrough as a function of PV in the fast- and slow-flow columns indicates that adsorption is kinetically limited. Given kinetic limitation, it is best to describe As transport in these columns as a function of time rather than pore volume. The breakthrough of As takes place earlier at fast PWV as a function of time, while slower flow allows for increased reaction times, increased adsorption, and delayed breakthrough (Figure 3-5).

This result is analogous to flow-interruption experiments where a reduction in flow velocity reduces the in-situ dissolved concentration by enhanced adsorption[23,25,47].

3.4.2. Model derived As adsorption-desorption rates

The forward and reverse rate constants determined for the gray sediment columns associated with S1 are 6 h^{-1} (k_1) and 0.17 h^{-1} (k_2), and for S2 are 0.01 h^{-1} (k_3) and 0.008 h^{-1} (k_4), respectively. The forward and reverse rate constants determined for the orange sand columns for S1 are three fold smaller ($k_1 = 2$ h^{-1} and $k_2 = 0.057$ h^{-1}). The rates k_3 and k_4 applied for gray sediment are also used for orange sediment columns. These rate constants are comparable to the sorption and desorption coefficients determined for As(III) in earlier studies. The sorption rate constants derived for As(III) for soils from West Virginia[48,49] based on a modified Freundlich equation ranged between 0.5 and 1.7 h^{-1} whereas desorption rates varied between 4×10^{-6} and 0.0077 h^{-1}. Sorption and desorption rate constants derived from experiments with three Spanish soils ranged from 0.2–1.93 h^{-1} and from 0.0001–0.027 h^{-1}, respectively[50].

The assigned initial average sorbed phase concentration and the assumption of two-phase partitioning are somewhat arbitrary. Breakthrough in the sediment columns were also predicted assuming a single phase (i.e. S = S1 when S2 = 0 mg/kg) with a single set of rate constants (associated with S1), but a single phase model cannot predict As concentrations beyond the influent level as observed in the case of all gray sediment columns, nor can it describe persistent partial breakthrough similar to what is observed at the onset of the experiment (Figure 3-S5). The same model was used to predict variation in the observed initial release of As with variable phosphate extractable phase (Table 3-S2). Expectedly, an increase in the initially sorbed As

increased the initial release of As (Figure 3-S6). A single a single set of rate constants with variable sorbed concentrations also was ineffective to describe transport in the gray sand columns.

We also assessed if As breakthrough in both the gray and orange sediment columns could be predicted with one unique set of rate constants. We took the average of the forward and reverse rate constants of gray and orange sand columns derived from the main scenario while keeping all other model parameters (e.g. sorbed phase) consistent (Figure 3-S7). We also used a constant sorbed phase across all sediment groups along with a unique set of rate constants (Figure 3-S8), but none of these approaches matched the As breakthrough at different PWV.

Although solid-phase speciation was not used to constrain modeling because it was obtained later in the experiment, the modeled solid-phase concentrations increase in a way similar to the observations. The kinetic model indicates a net increase in total sorbed As in the columns over time, with the fast-reacting phase increasingly loaded with As and the slow-reacting phase being depleted before reaching a new equilibrium (Figure 3-S9).

3.5. Implications

The field-based column experiments took some effort to set up but allowed us to study the reactive transport of As through sediment with fewer perturbations than most previous experiments (Figure 3-1). The approach should be applicable to other settings where groundwater is difficult to preserve and sediments are susceptible to redox transformations. Adsorption of As on both gray and orange sands was kinetically limited, leading to incomplete

adsorption and desorption that was more strongly expressed in columns with faster flow rates. Disequilibrium condition may have stemmed from eluting the columns at pore water velocities (PWV) higher than natural groundwater flow rate. Groundwater flow at the lowest PWV (40 cm/day) in our experiments (Figure 3-2) was still almost an order magnitude faster than mean flow rate estimated from the residence time of groundwater based on tritium-helium dating technique, and adjusting model conditions to this lower value increases adsorption, and starts to approach equilibrium based (flow rate independent) transport, however, slower transport conditions also facilitate increased biogeochemical transformations, implying that these transformations also are probably significant in affecting As transport.

The best model describing the observed partitioning has equivalent ratios of forward and reverse rate constants (k_1/k_2 = 6 h^{-1}/0.2 h^{-1} for gray and 2 h^{-1}/0.06 h^{-1} for orange sediment), implying that the equilibrium retention on both gray Holocene and orange Pleistocene sediment is similar. However, the rate constants for adsorption and desorption on gray sands were three-fold higher than for orange sands, allowing As to desorb more easily from the sediments. This has three implications under field conditions: (a) the conversion of orange to gray sediments will not appreciably change equilibrium-based As solute transport, (b) equilibrium transport conditions may be more widely applicable to gray sand than to orange sand aquifers, and (c) the desorption of a weakly bound pool of sediment As may be more important than transport in causing groundwater As contamination in perturbed systems.

The transport of As in Bangladesh groundwater was initially retarded by a factor of 30-35 relative to the flow of groundwater by both gray and orange sediment. This corresponds to a

partition coefficient, K_D of 5.7 L/kg, similar to partition coefficients determined with batch equilibration experiments for Holocene gray sediment in Bangladesh[10] and with field observations for Pleistocene sands that were reduced over time in West Bengal, India, and near Hanoi in Vietnam[34,51]. No complete breakthrough of As was observed in the slow-flow orange sediment columns (Figure 3-2b-c). This could reflect some form of irreversible adsorption or precipitation, or just be a result of the limited duration of these experiments – slow flow enhances As retention and also leads to the biogeochemical transformations that affect As partitioning.

Although orange and gray sands retard As to a similar degree, only the grey sands contained a large pool of As that desorbed throughout the experiments. This desorption may have been triggered by the high levels of phosphate found in the input groundwater (about 1.5 mg/L P) combined with accelerated flow relative to ambient conditions. Four-times higher phosphate levels added to groundwater in the later stages of the experiment and resulted in a rapid but short pulse of As released into solution (Figure 3-S2d & 3-S10).

The experiments were designed to minimize redox changes and the associated mineral transformations that result from them so that we could isolate the effect of adsorption and desorption on transport. Nevertheless, redox changes occurred within about 1 week in column experiments, affecting the speciation of retained As, and the concentration of As, Fe and S in the effluent (Figure 3-4 & 3-S12). Even in the sand control experiment, inflow sulfate was lost in the column. The field columns all contained As sulfides by the end of the experiments and showed changes in Fe mineralogy. The changes observed in the later phases of the column

experiment are not the focus of this manuscript, but imply that these redox changes also should be considered to fully understand As mobility in sediments affected by groundwater flow.

There are broad practical implications of this study in aquifers contaminated with As in S/SE Asia. Despite substantial retardation of As with respect to groundwater flow, the adsorption capacity of both the orange Pleistocene and gray Holocene sediment is limited. A high retardation factor implies that As concentrations in groundwater is likely to remain stable over time. However, there is a risk of contamination of low As aquifers in the face of continuous inflow of high As water in the long-term or accelerated groundwater flow in the short-term. The latter is substantiated by the fact that earlier breakthrough in our experiments were observed at higher PWV (Figure 3-5). The current As mitigation practices that rely on low-As groundwater resources in S/SE Asia may, therefore, remain effective for decades unless the aquifers are significantly perturbed by pumping[14].

3.6. References

(1)   Fendorf, S.; Michael, H. A.; Geen, A. van. Spatial and Temporal Variations of Groundwater Arsenic in South and Southeast Asia. *Science* **2010**, *328* (5982), 1123–1127. https://doi.org/10.1126/science.1172974.

(2)   Ravenscroft, P.; Brammer, H.; Richards, K. *Arsenic Pollution: A Global Synthesis*; Wiley-Blackwell, 2009.

(3)   DPHE; BGS. *Arsenic Contamination of Groundwater in Bangladesh*; Survey, B. G., Series Ed.; BGS: Keyworth, 2001.

(4)   Bhattacharya, P.; Chatterjee, D.; Jacks, G. Occurrence of Arsenic-Contaminated Groundwater in Alluvial Aquifers from Delta Plains, Eastern India: Options for Safe Drinking Water Supply. *Int. J. Water Resour. Dev.* **1997**, *13* (1), 79–92. https://doi.org/10.1080/07900629749944.

(5)   Ahmed, K. M.; Imam, M. N.; Akhter, S. H.; Hasan, M. A.; Alam, M. M.; Chowdhury, S. Q.; Burgess, W. G.; Nickson, R.; McArthur, J. M.; Hasan, M. K.; et al. Mechanism of Arsenic Release to Groundwater: Geochemical and Mineralogical Evidence; Dhaka Community Hospital, Dhaka, Bangladesh, 1998.

(6)   Nickson, R. T.; McArthur, J. M.; Ravenscroft, P.; Burgess, W. G.; Ahmed, K. M. Mechanism of Arsenic Release to Groundwater, Bangladesh and West Bengal. *Appl. Geochem.* **2000**, *15* (4), 403–413.

(7)   Berg, M.; Tran, H. C.; Nguyen, T. C.; Pham, H. V.; Schertenleib, R.; Giger, W. Arsenic Contamination of Groundwater and Drinking Water in Vietnam: A Human Health Threat. *Environ. Sci. Technol.* **2001**, *35* (13), 2621–2626. https://doi.org/10.1021/es010027y.

(8)   Umitsu, M. Late Quaternary Sedimentary Environments and Landforms in the Ganges Delta. *Sediment. Geol.* **1994**, *83* (3–4), 177–186. https://doi.org/10.1016/0037-0738(93)90011-S.

(9)   Zheng, Y.; van Geen, A.; Stute, M.; Dhar, R.; Mo, Z.; Cheng, Z.; Horneman, A.; Gavrieli, I.; Simpson, H. J.; Versteeg, R.; et al. Geochemical and Hydrogeological Contrasts between Shallow and Deeper Aquifers in Two Villages of Araihazar, Bangladesh: Implications for Deeper Aquifers as Drinking Water Sources. *Geochim. Cosmochim. Acta* **2005**, *69* (22), 5203–5218. https://doi.org/10.1016/j.gca.2005.06.001.

(10)   van Geen, A.; Zheng, Y.; Goodbred, S.; Horneman, A.; Aziz, Z.; Cheng, Z.; Stute, M.; Mailloux, B.; Weinman, B.; Hoque, M. A.; et al. Flushing History as a Hydrogeological Control

on the Regional Distribution of Arsenic in Shallow Groundwater of the Bengal Basin. *Environ. Sci. Technol.* **2008**, *42* (7), 2283–2288. https://doi.org/10.1021/es702316k.

(11)   Baes, C. F.; Sharp, R. D. A Proposal for Estimation of Soil Leaching and Leaching Constants for Use in Assessment Models. *J. Environ. Qual.* **1983**, *12* (1), 17–28. https://doi.org/10.2134/jeq1983.00472425001200010003x.

(12)   Harvey, C. F.; Swartz, C. H.; Badruzzaman, A. B.; Keon-Blute, N.; Yu, W.; Ali, M. A.; Jay, J.; Beckie, R.; Niedan, V.; Brabander, D.; et al. Arsenic Mobility and Groundwater Extraction in Bangladesh. *Science* **2002**, *298* (5598), 1602–1606. https://doi.org/10.1126/science.1076978.

(13)   Hoque, M.; Hoque, M. M.; Ahmed, K. Declining Groundwater Level and Aquifer Dewatering in Dhaka Metropolitan Area, Bangladesh: Causes and Quantification. *Hydrogeol. J.* **2007**, *15* (8), 1523–1534. https://doi.org/10.1007/s10040-007-0226-5.

(14)   Michael, H. A.; Voss, C. I. Evaluation of the Sustainability of Deep Groundwater as an Arsenic-Safe Resource in the Bengal Basin. *Proc. Natl. Acad. Sci.* **2008**. https://doi.org/10.1073/pnas.0710477105.

(15)   Knappett, P. S. K.; Mailloux, B. J.; Choudhury, I.; Khan, M. R.; Michael, H. A.; Barua, S.; Mondal, D. R.; Steckler, M. S.; Akhter, S. H.; Ahmed, K. M.; et al. Vulnerability of Low-Arsenic Aquifers to Municipal Pumping in Bangladesh. *J. Hydrol.* **2016**, *539*, 674–686. https://doi.org/10.1016/j.jhydrol.2016.05.035.

(16)   Khan, M. R.; Koneshloo, M.; Knappett, P. S. K.; Ahmed, K. M.; Bostick, B. C.; Mailloux, B. J.; Mozumder, R. H.; Zahid, A.; Harvey, C. F.; Geen, A. van; et al. Megacity Pumping and Preferential Flow Threaten Groundwater Quality. *Nat. Commun.* **2016**, *7*, 12833. https://doi.org/10.1038/ncomms12833.

(17)   Dzombak, D. A.; Morel, F. M. M. *Surface Complexation Modeling : Hydrous Ferric Oxide*; Wiley: New York, c1990.

(18)   Appelo, C. A. J.; Van Der Weiden, M. J. J.; Tournassat, C.; Charlet, L. Surface Complexation of Ferrous Iron and Carbonate on Ferrihydrite and the Mobilization of Arsenic. *Environ. Sci. Technol.* **2002**, *36* (14), 3096–3103. https://doi.org/10.1021/es010130n.

(19)   Swartz, C. H.; Blute, N. K.; Badruzzman, B.; Ali, A.; Brabander, D.; Jay, J.; Besancon, J.; Islam, S.; Hemond, H. F.; Harvey, C. F. Mobility of Arsenic in a Bangladesh Aquifer: Inferences from Geochemical Profiles, Leaching Data, and Mineralogical Characterization.

Geochim. Cosmochim. Acta **2004**, *68* (22), 4539–4557.
https://doi.org/10.1016/J.Gca.2004.04.020.

(20)   Stollenwerk, K. G.; Breit, G. N.; Welch, A. H.; Yount, J. C.; Whitney, J. W.; Foster, A. L.; Uddin, M. N.; Majumder, R. K.; Ahmed, N. Arsenic Attenuation by Oxidized Aquifer Sediments in Bangladesh. *Sci. Total Environ.* **2007**, *379* (2), 133–150.
https://doi.org/10.1016/j.scitotenv.2006.11.029.

(21)   Thi Hoa Mai, N.; Postma, D.; Thi Kim Trang, P.; Jessen, S.; Hung Viet, P.; Larsen, F. Adsorption and Desorption of Arsenic to Aquifer Sediment on the Red River Floodplain at Nam Du, Vietnam. *Geochim. Cosmochim. Acta* **2014**, *142*, 587–600.
https://doi.org/10.1016/j.gca.2014.07.014.

(22)   Rathi, B.; Neidhardt, H.; Berg, M.; Siade, A.; Prommer, H. Processes Governing Arsenic Retardation on Pleistocene Sediments: Adsorption Experiments and Model-Based Analysis. *Water Resour. Res.* **2017**, *53* (5), 4344–4360. https://doi.org/10.1002/2017WR020551.

(23)   Zhang, H.; Magdi Selim, H. Second-Order Modeling of Arsenite Transport in Soils. *J. Contam. Hydrol.* **2011**, *126* (3), 121–129. https://doi.org/10.1016/j.jconhyd.2011.08.002.

(24)   Zhang, H.; Selim, H. M. Kinetics of Arsenate Adsorption−Desorption in Soils. *Environ. Sci. Technol.* **2005**, *39* (16), 6101–6108. https://doi.org/10.1021/es050334u.

(25)   Zhang, H.; Selim, H. M. Reaction and Transport of Arsenic in Soils: Equilibrium and Kinetic Modeling. In *Advances in Agronomy*; Academic Press, 2008; Vol. 98, pp 45–115.
https://doi.org/10.1016/S0065-2113(08)00202-2.

(26)   Darland, J. E.; Inskeep, W. P. Effects of Pore Water Velocity on the Transport of Arsenate. *Environ. Sci. Technol.* **1997**, *31* (3), 704–709. https://doi.org/10.1021/es960247p.

(27)   Bethke, C. M.; Brady, P. V. How the Kd Approach Undermines Ground Water Cleanup. *Groundwater* **2000**, *38* (3), 435–443. https://doi.org/10.1111/j.1745-6584.2000.tb00230.x.

(28)   Itai, T.; Takahashi, Y.; Seddique, A. A.; Maruoka, T.; Mitamura, M. Variations in the Redox State of As and Fe Measured by X-Ray Absorption Spectroscopy in Aquifers of Bangladesh and Their Effect on As Adsorption. *Appl. Geochem.* **2010**, *25* (1), 34–47.
https://doi.org/10.1016/j.apgeochem.2009.09.026.

(29)   Jung, H. B.; Bostick, B. C.; Zheng, Y. Field, Experimental, and Modeling Study of Arsenic Partitioning across a Redox Transition in a Bangladesh Aquifer. *Environ. Sci. Technol.* **2012**, *46* (3), 1388–1395. https://doi.org/10.1021/es2032967.

(30)   Radloff, K. A.; Zheng, Y.; Stute, M.; Weinman, B.; Bostick, B.; Mihajlov, I.; Bounds, M.; Rahman, M. M.; Huq, M. R.; Ahmed, K. M.; et al. Reversible Adsorption and Flushing of Arsenic in a Shallow, Holocene Aquifer of Bangladesh. *Appl. Geochem.* **2015**. https://doi.org/10.1016/j.apgeochem.2015.11.003.

(31)   McArthur, J. M.; Nath, B.; Banerjee, D. M.; Purohit, R.; Grassineau, N. Palaeosol Control on Groundwater Flow and Pollutant Distribution: The Example of Arsenic. *Environ. Sci. Technol.* **2011**, *45* (4), 1376–1383. https://doi.org/10.1021/es1032376.

(32)   Robinson, C.; Brömssen, M. von; Bhattacharya, P.; Häller, S.; Bivén, A.; Hossain, M.; Jacks, G.; Ahmed, K. M.; Hasan, M. A.; Thunvik, R. Dynamics of Arsenic Adsorption in the Targeted Arsenic-Safe Aquifers in Matlab, South-Eastern Bangladesh: Insight from Experimental Studies. *Appl. Geochem.* **2011**, *26* (4), 624–635. https://doi.org/10.1016/j.apgeochem.2011.01.019.

(33)   Radloff, K. A.; Zheng, Y.; Michael, H. A.; Stute, M.; Bostick, B. C.; Mihajlov, I.; Bounds, M.; Huq, M. R.; Choudhury, I.; Rahman, M. W.; et al. Arsenic Migration to Deep Groundwater in Bangladesh Influenced by Adsorption and Water Demand. *Nat. Geosci.* **2011**, *4* (11), 793–798. https://doi.org/10.1038/ngeo1283.

(34)   van Geen, A.; Bostick, B. C.; Thi Kim Trang, P.; Lan, V. M.; Mai, N.-N.; Manh, P. D.; Viet, P. H.; Radloff, K.; Aziz, Z.; Mey, J. L.; et al. Retardation of Arsenic Transport through a Pleistocene Aquifer. *Nature* **2013**, *501* (7466), 204–207. https://doi.org/10.1038/nature12444.

(35)   Dhar, R. K.; Zheng, Y.; Saltikov, C. W.; Radloff, K. A.; Mailloux, B. J.; Ahmed, K. M.; van Geen, A. Microbes Enhance Mobility of Arsenic in Pleistocene Aquifer Sand from Bangladesh. *Env. Sci Technol* **2011**, *45* (7), 2648–2654. https://doi.org/10.1021/es1022015.

(36)   Meng, X.; Korfiatis, G. P.; Jing, C.; Christodoulatos, C. Redox Transformations of Arsenic and Iron in Water Treatment Sludge during Aging and TCLP Extraction. *Environ. Sci. Technol.* **2001**, *35* (17), 3476–3481. https://doi.org/10.1021/es010645e.

(37)   Shoenfelt, E. M.; Winckler, G.; Lamy, F.; Anderson, R. F.; Bostick, B. C. Highly Bioavailable Dust-Borne Iron Delivered to the Southern Ocean during Glacial Periods. *Proc. Natl. Acad. Sci.* **2018**, 201809755. https://doi.org/10.1073/pnas.1809755115.

(38)   Sun, J.; Mailloux, B. J.; Chillrud, S. N.; van Geen, A.; Thompson, A.; Bostick, B. C. Simultaneously Quantifying Ferrihydrite and Goethite in Natural Sediments Using the Method of

Standard Additions with X-Ray Absorption Spectroscopy. *Chem. Geol.* **2018**, *476*, 248–259. https://doi.org/10.1016/j.chemgeo.2017.11.021.

(39)   Cheng, Z.; Zheng, Y.; Mortlock, R.; Geen, A. van. Rapid Multi-Element Analysis of Groundwater by High-Resolution Inductively Coupled Plasma Mass Spectrometry. *Anal. Bioanal. Chem.* **2004**, *379* (3), 512–518. https://doi.org/10.1007/s00216-004-2618-x.

(40)   Selim, H. M. *Transport & Fate of Chemicals in Soils: Principles & Applications*; 2014.

(41)   Lapidus, L.; Amundson, N. R. Mathematics of Adsorption in Beds. VI. The Effect of Longitudinal Diffusion in Ion Exchange and Chromatographic Columns. *J. Phys. Chem.* **1952**, *56* (8), 984–988. https://doi.org/10.1021/j150500a014.

(42)   Carnahan, B.; Luther, H. A.; Wilkes, J. O. *Applied Numerical Methods*; Wiley: New York, 1969.

(43)   Horneman, A.; Van Geen, A.; Kent, D. V.; Mathe, P. E.; Zheng, Y.; Dhar, R. K.; O'Connell, S.; Hoque, M. A.; Aziz, Z.; Shamsudduha, M.; et al. Decoupling of As and Fe Release to Bangladesh Groundwater under Reducing Conditions. Part 1: Evidence from Sediment Profiles. *Geochim. Cosmochim. Acta* **2004**, *68* (17), 3459–3473. https://doi.org/10.1016/J.Gca.2004.01.026.

(44)   Saalfield, S. L.; Bostick, B. C. Changes in Iron, Sulfur, and Arsenic Speciation Associated with Bacterial Sulfate Reduction in Ferrihydrite-Rich Systems. *Environ. Sci. Technol.* **2009**, *43* (23), 8787–8793. https://doi.org/10.1021/es901651k.

(45)   Sultana, M.; Mou, T. J.; Sanyal, S. K.; Diba, F.; Mahmud, Z. H.; Parvez, A. K.; Hossain, M. A. Investigation of Arsenotrophic Microbiome in Arsenic-Affected Bangladesh Groundwater. *Groundwater* **2017**, *55* (5), 736–746. https://doi.org/10.1111/gwat.12520.

(46)   Gu, Y.; Nostrand, J. D. V.; Wu, L.; He, Z.; Qin, Y.; Zhao, F.-J.; Zhou, J. Bacterial Community and Arsenic Functional Genes Diversity in Arsenic Contaminated Soils from Different Geographic Locations. *PLOS ONE* **2017**, *12* (5), e0176696. https://doi.org/10.1371/journal.pone.0176696.

(47)   Brusseau, M. L.; Rao, P. S. C.; Jessup, R. E.; Davidson, J. M. Flow Interruption: A Method for Investigating Sorption Nonequilibrium. *J. Contam. Hydrol.* **1989**, *4* (3), 223–240. https://doi.org/10.1016/0169-7722(89)90010-7.

(48)   Elkhatib, E. A.; Bennett, O. L.; Wright, R. J. Arsenite Sorption and Desorption in Soils. *Soil Sci. Soc. Am. J.* **1984**, *48* (5), 1025–1030. https://doi.org/10.2136/sssaj1984.03615995004800050015x.

(49)   Elkhatib, E. A.; Bennett, O. L.; Wright, R. J. Kinetics of Arsenite Sorption in Soils. *Soil Sci. Soc. Am. J.* **1984**, *48* (4), 758–762. https://doi.org/10.2136/sssaj1984.03615995004800040012x.

(50)   Barrachina, A. C.; Carbonell, F. B.; Beneyto, J. M. Kinetics of Arsenite Sorption and Desorption in Spanish Soils. *Commun. Soil Sci. Plant Anal.* **1996**, *27* (18–20), 3101–3117. https://doi.org/10.1080/00103629609369764.

(51)   McArthur, J. M.; Ravenscroft, P.; Banerjee, D. M.; Milsom, J.; Hudson-Edwards, K. A.; Sengupta, S.; Bristow, C.; Sarkar, A.; Tonkin, S.; Purohit, R. How Paleosols Influence Groundwater Flow and Arsenic Pollution: A Model from the Bengal Basin and Its Worldwide Implication. *Water Resour. Res.* **2008**, *44* (11), W11411. https://doi.org/10.1029/2007WR006552.

Figure 3-1. A schematic of the experimental setup. High arsenic groundwater from the shallow aquifer was pumped continuously in an overflowing bag and channeled under controlled flow rates to elute undisturbed sediment cores housed in custom made anoxic chambers. The figure is not drawn to scale.
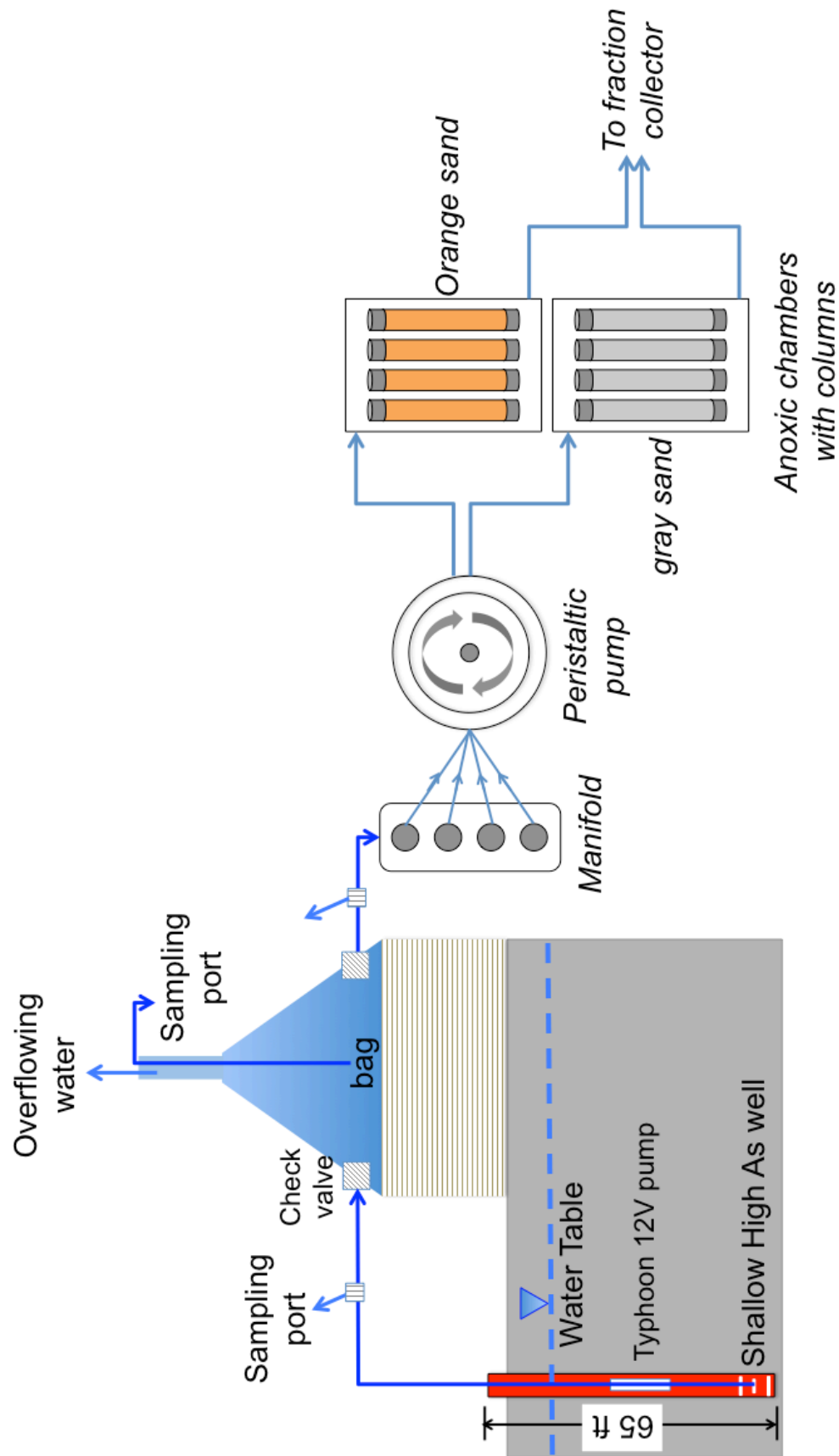
Figure 3-2. Arsenic (a, b, and c), iron (d, e, and f), sulfur (g, h, and i), and phosphorus (j, k, and l) in the effluents of orange Pleistocene sediment columns. Arsenic and other redox-sensitive parameters plotted as a function of pore volume at a pore-water velocity of 156 cm/day (top panel, n=1), 81.6 cm/day (middle panel, n= 2), and 40 cm/day (bottom panel, n = 1). Input groundwater concentrations of each analyte are indicated by the dashed line in each plot. The blue shading in the background of As corresponds to the portion of breakthrough curve with eluent S level within 10% of the input concentration .The same vertical axes of Figure 3-3 are maintained for the ease of comparison.

Figure 3-2.

...concentrations of each analyte are indicated by the dashed line in each plot. The PWA of the top two panels are comparable to that of...

Pore volume

Figure 3-4. Change in the fraction of solid phase iron (II) and arsenic (As) speciation in the orange sediment columns following elution with high-arsenic groundwater. (a) The percentage of Fe(II) in the inlets and outlets of columns were compared with average Fe(II) content (n =2) in the control sediment (blue). The thick portion of the absolute error represents relative error between samples that is largely due to variation in the determination of inflection edge position; i.e. the relative error for comparing the change in the proportion of Fe(II) between samples. The absolute errors in oxidation state are larger and result from inaccuracies in edge position caused primarily by calibration errors between samples and references; (b) XANES spectra of As for the same color-coded cores retrieved between 42 and 51 ft depth (Table 3-S1). The gray background (11875-11877 eV) shows the peak of normalized absorbance in the control as a reference for comparison with the rest of the columns (Table 3-S3). The outlets of the columns are shown as dashed lines. The outlet sample at 51 ft eluted at the slowest flow rate is not representative.

(a) Fe–XAS

(b) As–XANES
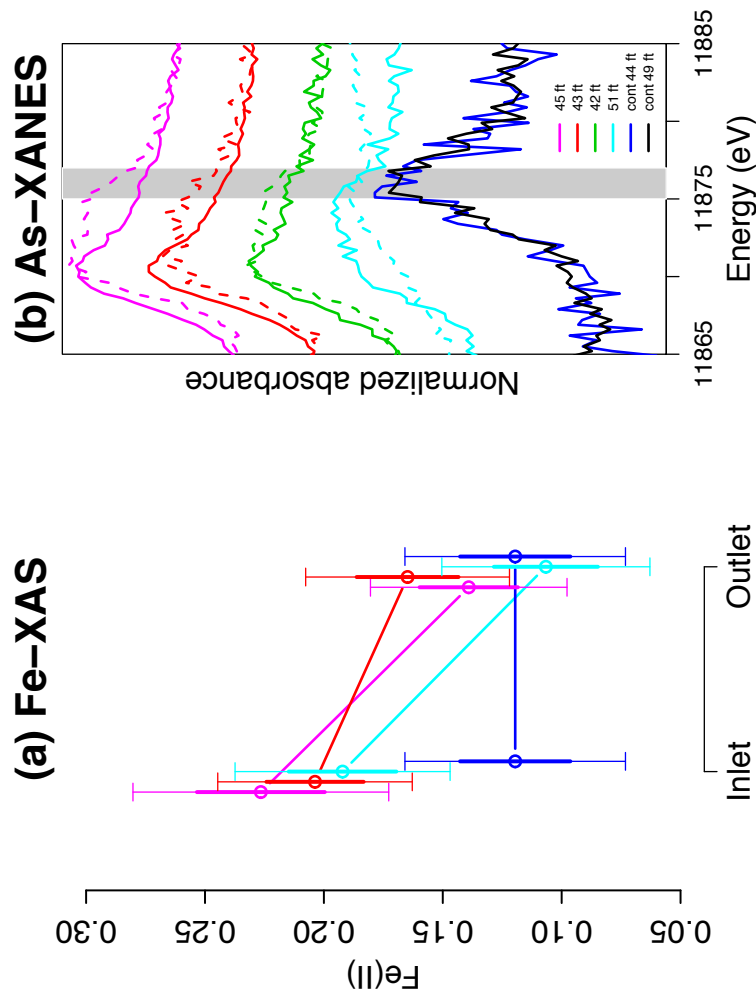
Figure 3-5. Time-dependent evolution of arsenic (As) for a two phase, reversible kinetic model. Relative concentration of arsenic plotted against time at varying PWV for orange (a) and gray (b) sediment columns. Also shown the predicted nonequilibrium transport of As (dotted lines) invariant of kinetic rate constants within each sediment group. Same symbols from Figure 3-2 and 3-3 are retained with an outline color corresponding to Darcian velocity (see legend). Simulated breakthrough curves for three representative flow-velocities are shown (Table 3-S1). Effluents collected after SO$_4$ level started to decline below the input level are outlined/dotted only.

96
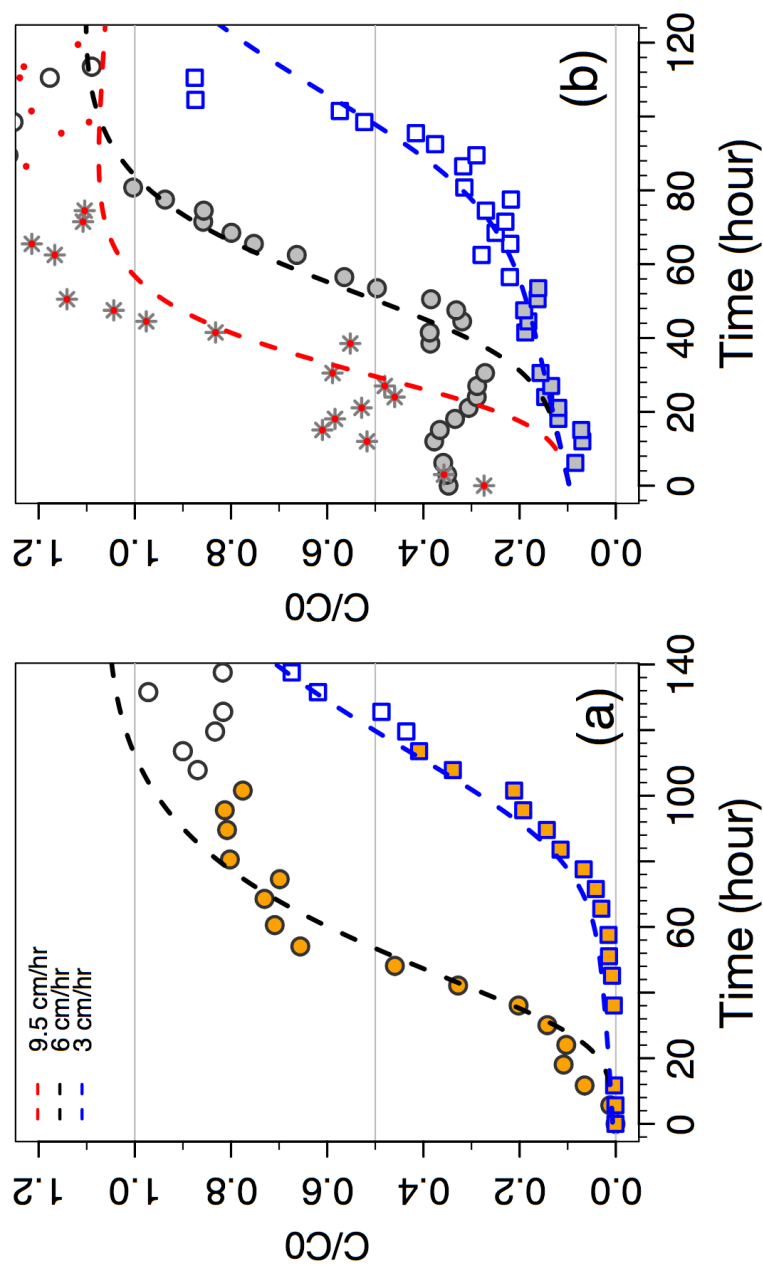
3.7. Supporting Materials

Figure 3-S1. Coring locations of gray Holocene and Pleistocene orange sediments. Spatial map indicating the location of drilling sites in Araihazar in central Bangladesh (inset) over blanket arsenic test results (van Geen et al. 2014) grouped into <=10 ug/L (cyan), >10 to 50 ug/L (green), and >50 ug/L (red). The orange sediment site is located in the NW part of the area (90.6352°, 23.8542°) with a higher proportion of low As wells (<10 ug/L) installed in Pleistocene aquifer whereas the gray sediment coring site is located in a high As region at central Araihazar (90.6577°, 23.7909°); Depth profiles of lithology (sand or clay) and diffuse spectral reflectance (Horneman et al. 2004) of the sediment samples retrieved from Pleistocene material (a) and Holocene material (b) are shown. The dashed lines indicate coring depth interval for gray sediment (44-57 ft) and orange sediment (42 - 51 ft). Also shown are the depth profiles of (c) arsenic, (d) iron, (e) sulfur, (f) phosphate and (g) dissolved inorganic carbon (DIC) concentrations in the input well screened at 60-65 ft and co-located shallow wells screened at 20-25, 45-50, and 55-60 ft below ground surface.
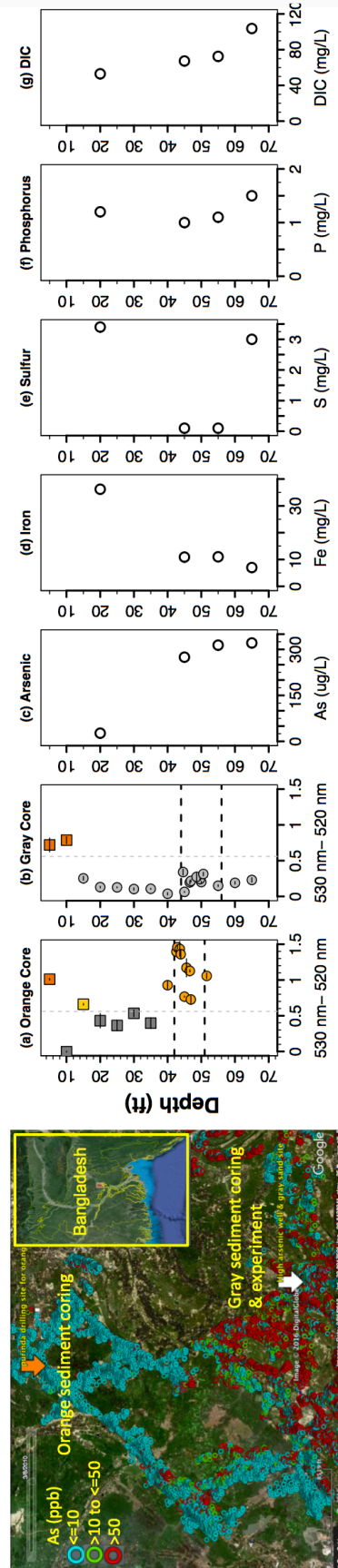
97

Figure ... the concentrations of ... in the ... (y) ... storage bag (green), over time.
Arsenic (a), iron (b), sulfur (c), phosphorus (d), arsenite (e), manganese (f), chloride (g), bromide (h), pH and oxidation-reduction potential (ORP) in the influent groundwater. The storage bag was spiked with phosphorus and bromide on day 20 of the experiment (vertical dotted line).
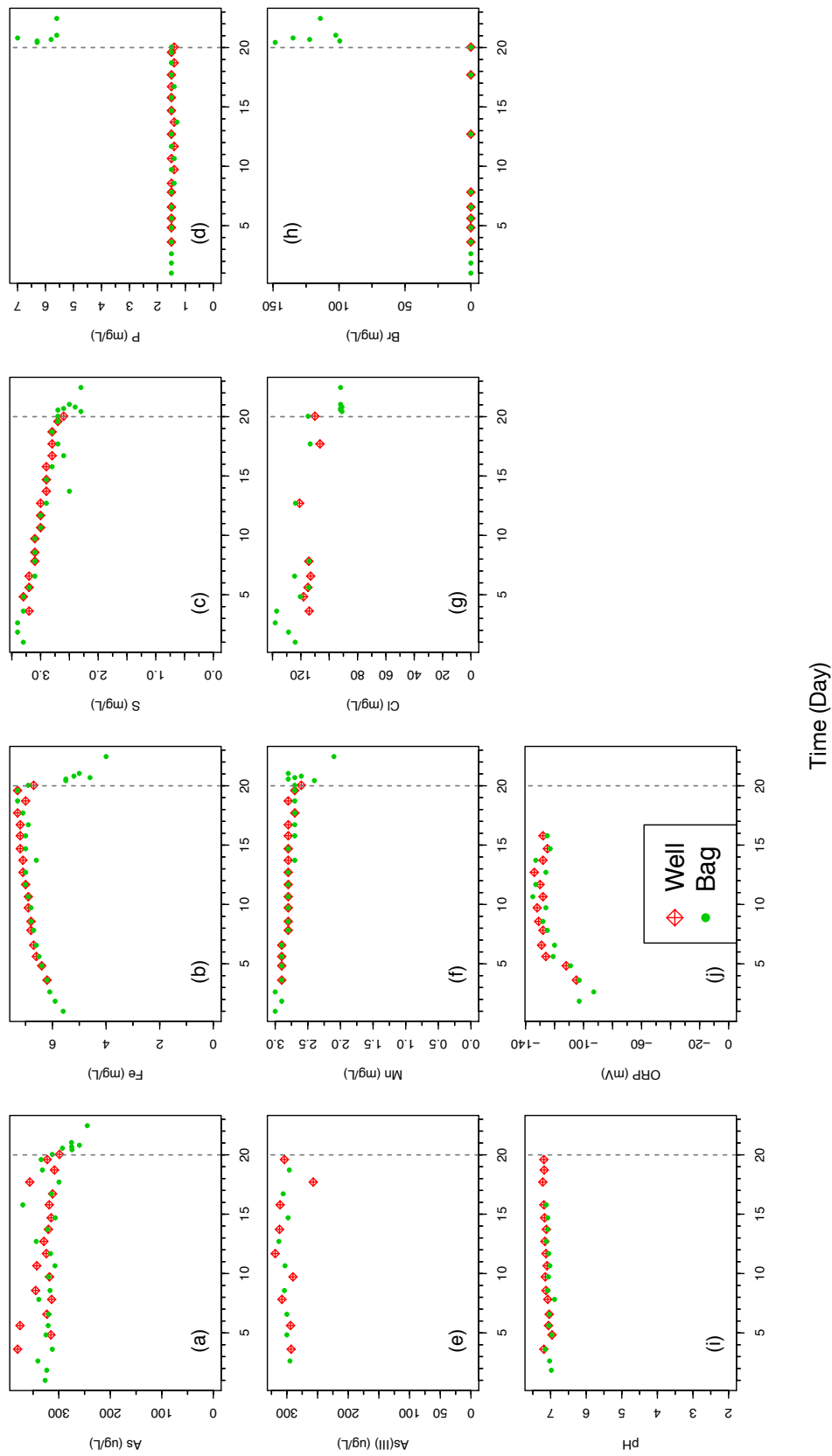
Figure 3-S3. Concentrations of arsenic (a), iron (b), sulfur (c) and phosphorus (d) in the control sand column plotted as a function of pore volume at fast PWV.
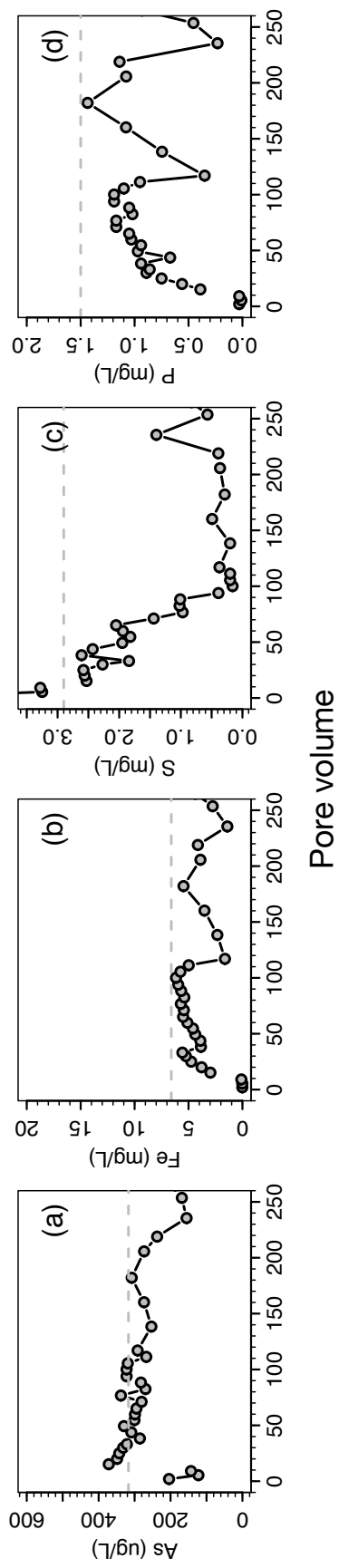
Figure 3-S4. Determination of dispersion coefficient, D with bromide (Br⁻) tracer injection. The influent groundwater originally containing very low Br⁻ concentration (0.1 mg/L) was artificially spiked to ~140 mg/L (Figure 3-S2) to observe the breakthrough of Br⁻ under field condition. The breakthrough of Br⁻ was modeled using an analytical solution for 1D advection-dispersion equation (van Genuchten and Alves, 1982) assuming a partition coefficient, K_D of 0 (retardation factor of 1) for a range of D values. The best fit was derived by reducing the sum of squared error between observed and predicted relative concentrations of Br⁻ at fast (a) and slow (b) PWV. The colors of the observations indicate the sediment color.
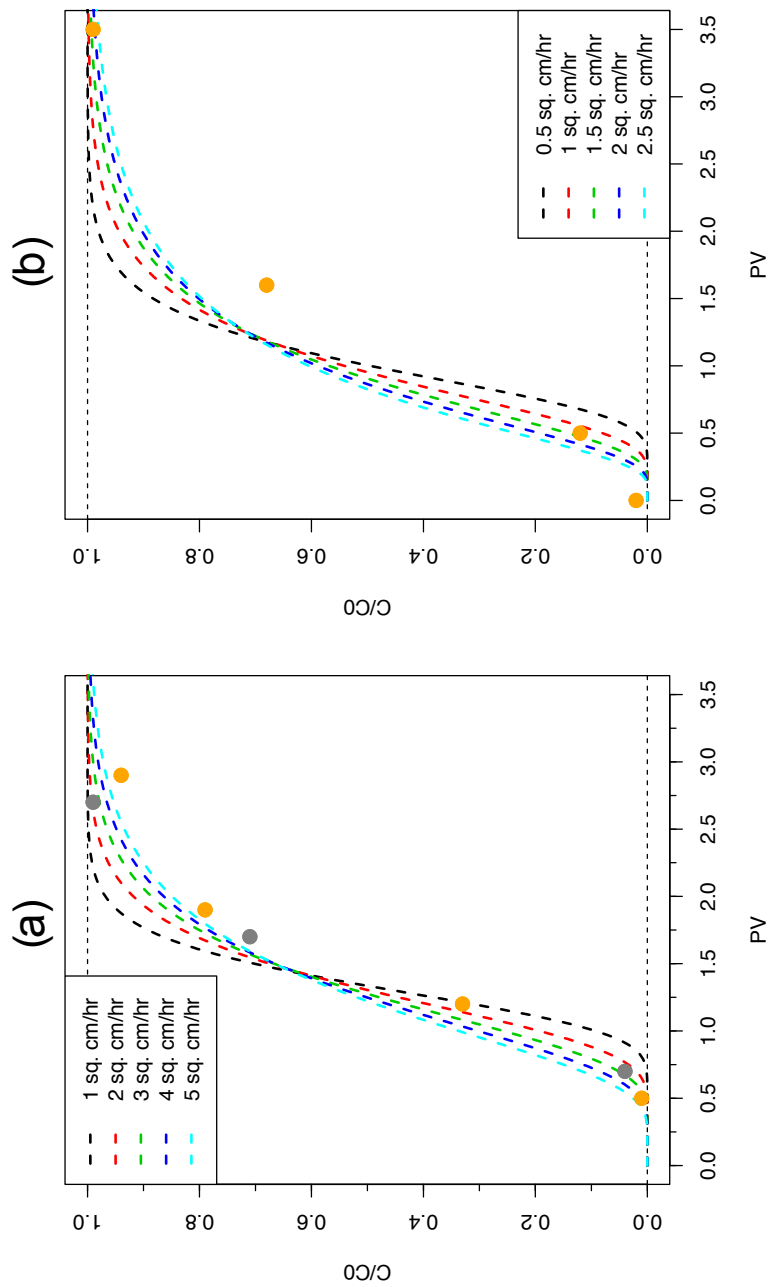
Figure 3-S5. Modeling arsenic (As) transport assuming a single solid phase. Relative concentration of arsenic plotted against time at varying PWV for orange (a) and gray (b) sediment columns along with predicted concentrations (dotted lines) that are invariant of kinetic rate constants. The assigned initial solid phase As concentration in the orange and gray sediment columns is 0.5 and 2 mg/kg, respectively. The forward and reverse rate constants used for the gray sediment columns are 6 h^{-1} (k_1) and 0.17 h^{-1} (k_2), respectively and for orange sediment columns are 2 h^{-1} (k_1) and 0.07 h^{-1} (k_2), respectively. The symbol/color coding is as described in Figure 3-5.
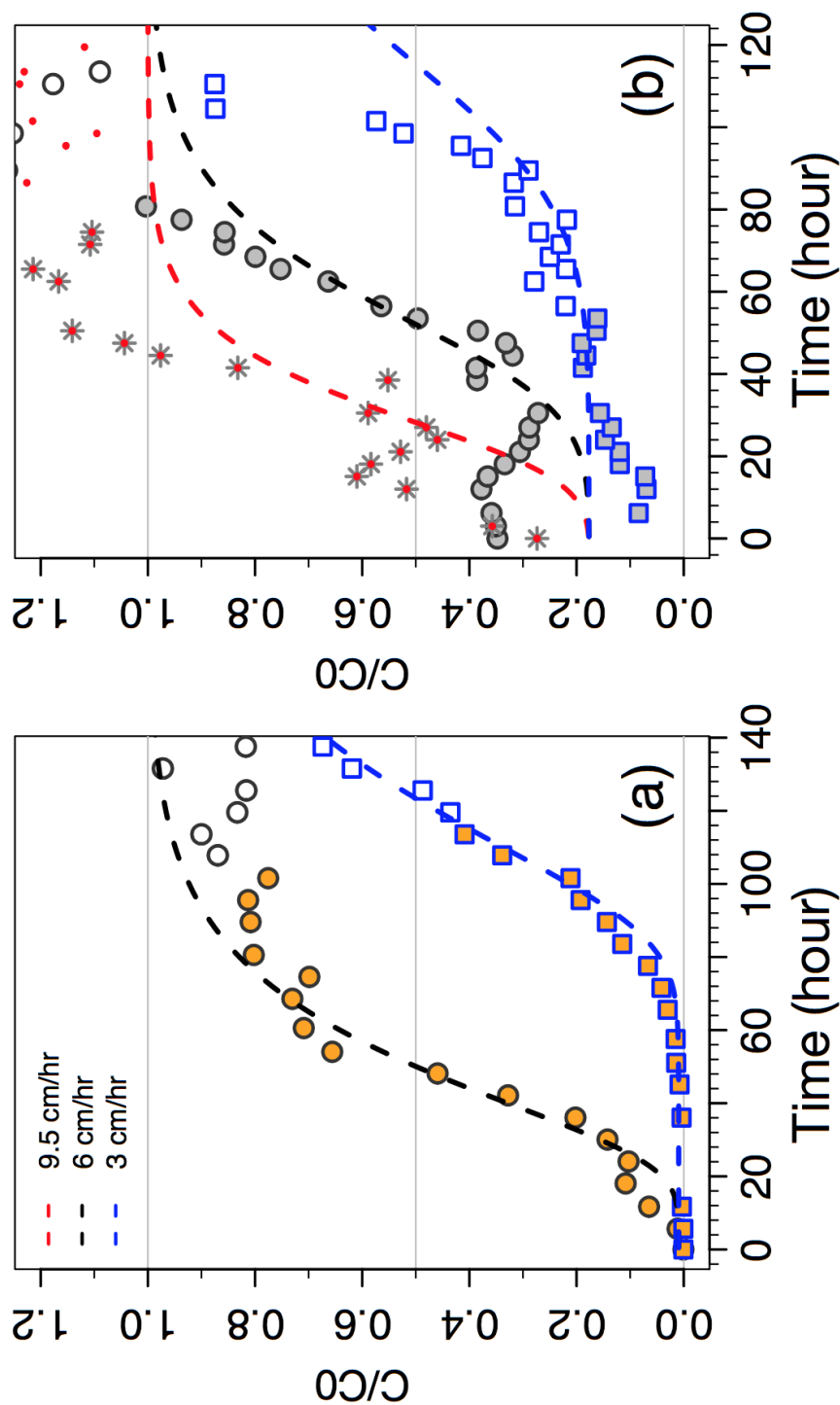
Figure 3-S6. Transport model sensitivity to the initial total sorbed arsenic (As) concentration. The single solid phase As concentration in the gray sediment columns is increased with increasing PWV: 1.5 mg/kg (blue), 2 mg/kg (black), and 2.5 mg/kg (red) while the forward and reverse rate constants are kept unchanged (6 h^{-1} and 0.17 h^{-1}). The symbol/color coding is as described in Figure 3-5b.
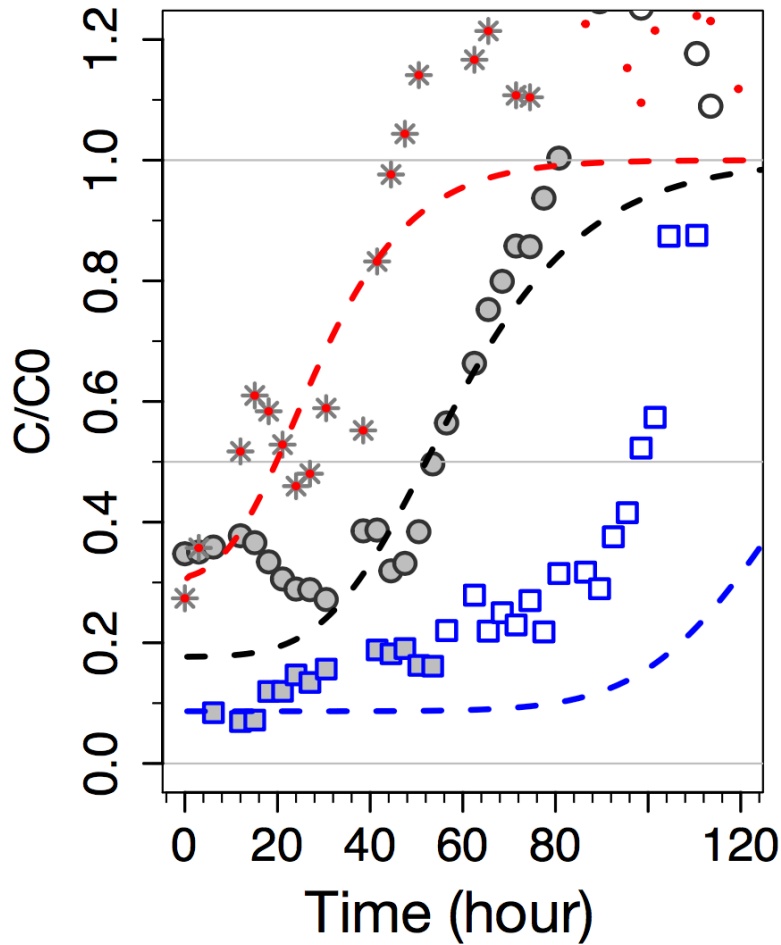
Figure 3-S7. Transport model simulations with the same rate constants across all sediment groups. Relative concentration of arsenic plotted against time at varying PWV for orange (a) and gray (b) sediment columns along with predicted concentrations (dashed lines) with the same forward and reverse rate constants. The forward and reverse rate constants used in this case for both the gray and orange sediment columns are: 4 h^{-1} (k$_1$) and 0.13 h^{-1} (k$_2$), which is the average for the main case scenario (Figure 3-5) for gray sand columns (6 h^{-1} and 0.2 h^{-1}) and orange sediment columns (2 h^{-1} and 0.057 h^{-1}). All other model parameters are kept same as the main scenario.

103
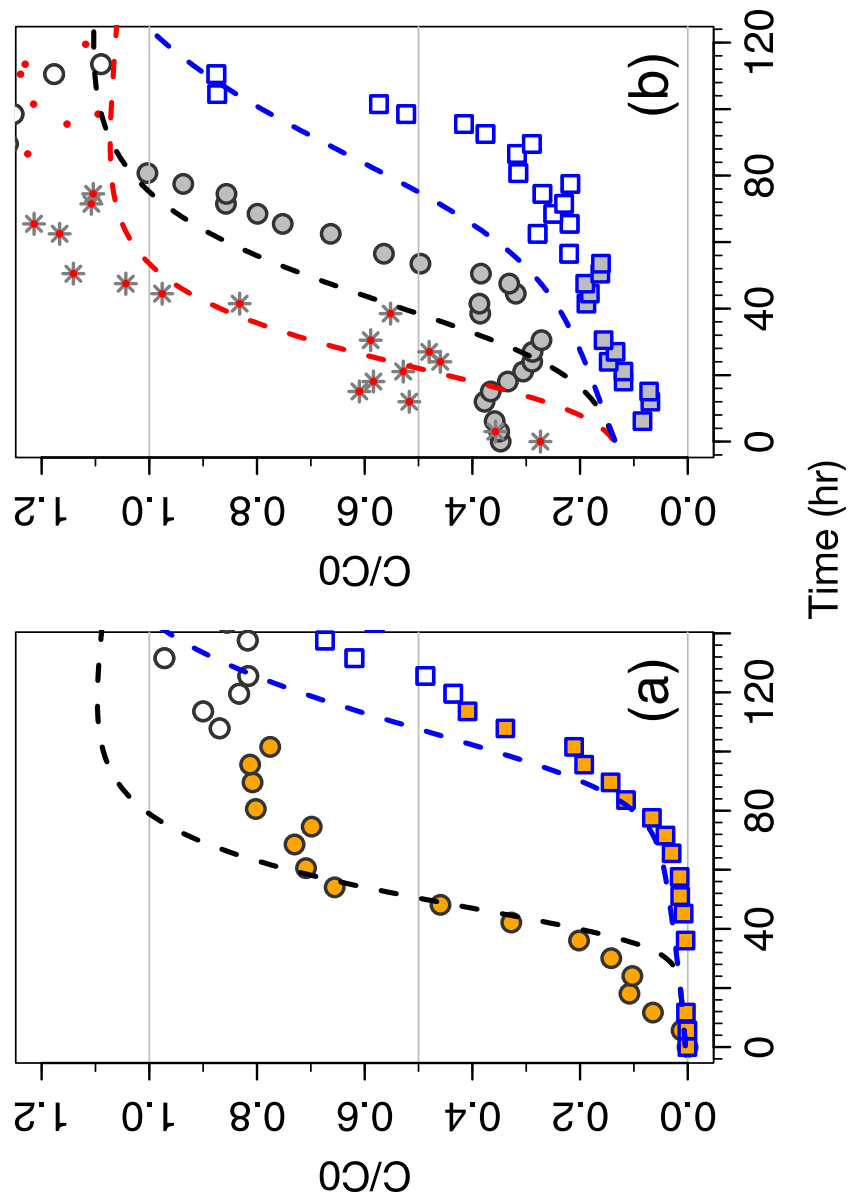
Figure 3-S8. Transport model simulations with the same rate constants and initial solid phase concentrations across all sediment groups. Relative concentration of arsenic plotted against time at varying PWV for orange and gray sediment columns along with predicted concentrations (dashed lines). An initial kinetic sorbed phase of 1 mg/kg is applied for both phases. The forward and reverse rate constants associated with the first phase are 3 h^{-1} (k_1) and 0.8 h^{-1} (k_2) and for the second phase are 0.01 h^{-1} and 0.008 h^{-1}, respectively.
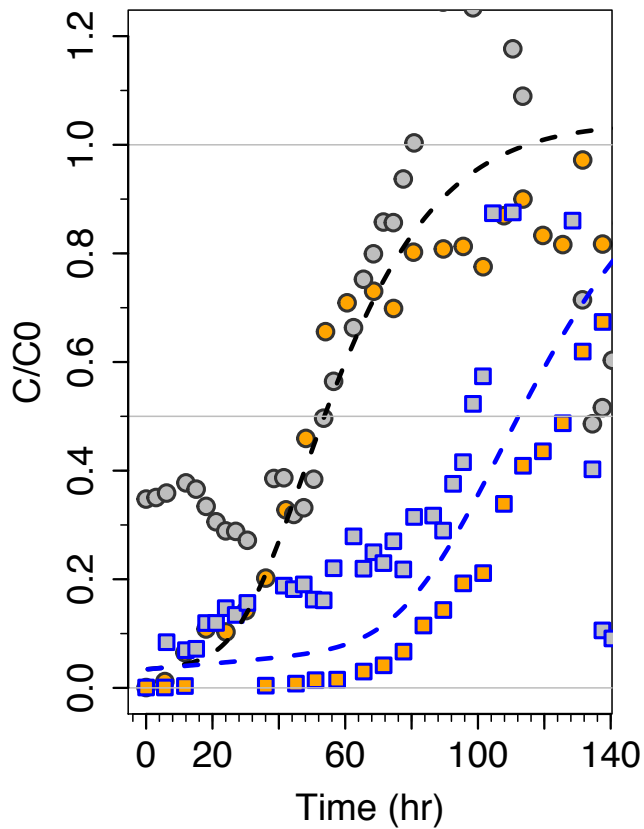
Figure 3-S9. The evolution of solid phase arsenic (As) concentrations predicted by a two-phase, reversible kinetic model. Simulated adsorption of As in the orange (a, b) and gray (c, d) sediment columns at fast (solid lines) and slow (dotted lines) pore-water velocities. The top panel (a, c) shows the evolution of total sorbed As and the bottom panel (b, d) indicates the increasing fast reacting phase, S1 and depleting slow reacting phase, S2 at ~1 cm interval along the length of the column. The rate of As loading is higher at fast PWV; in other words, if the rate constants are proportionally reduced for a given initial sorbed concentration, the rate of As loading in the columns will be slower and more time will be required for As breakthrough. Following elution, the observed total sorbed As concentrations in the columns increased by 1.4 to 9 fold, averaging 6.7 ± 0.3 mg/kg for the orange sediment columns (n=8) and 4.7 ± 1.2 mg/kg in the inlets of the gray sediment column (n=5), consistent with the simulated net increase in sorbed As concentration.
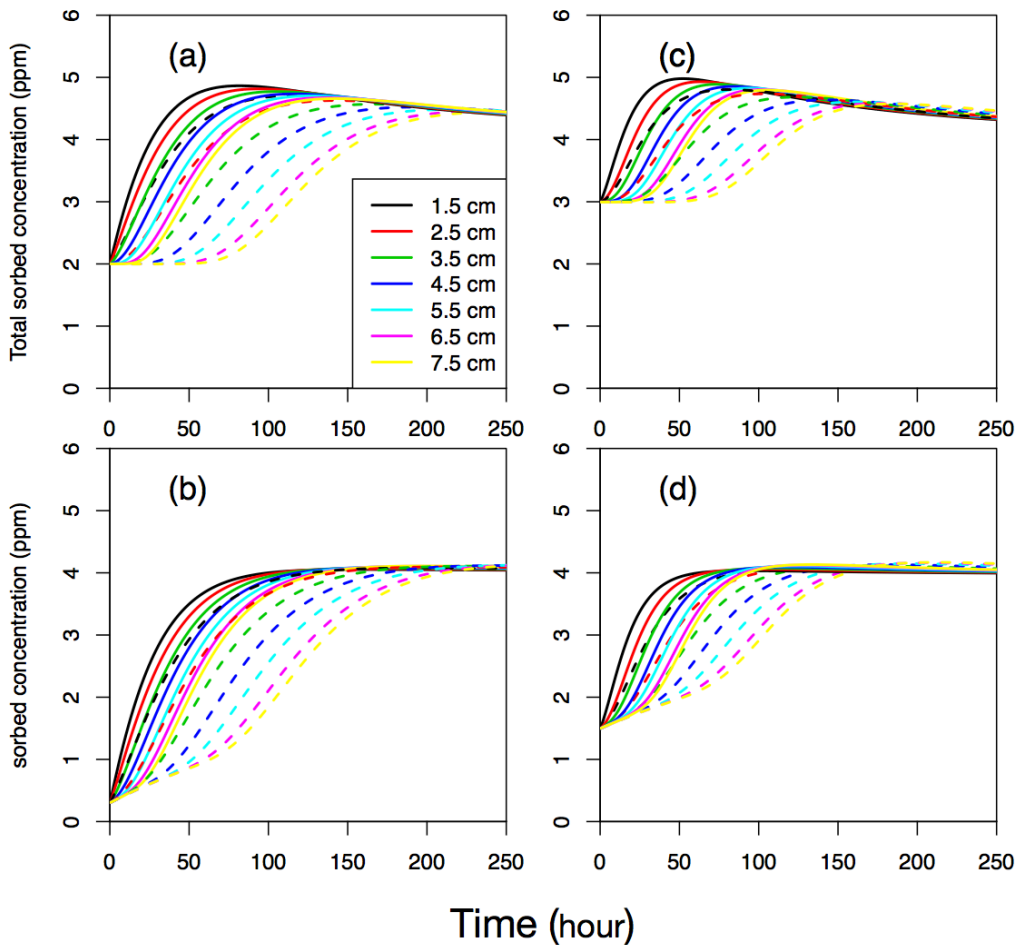
Figure 3-S10. The effect of phosphate spiking in a gray sediment column. Groundwater in the storage bag was artificially elevated to ~ 6 mg/L of P (a) by the end of the experiment (Figure 3-S2) that released additional arsenic (b) and iron (c) to the influent. The vertical line separates groundwater samples collected a few pore-volumes before and after P spiking, respectively.
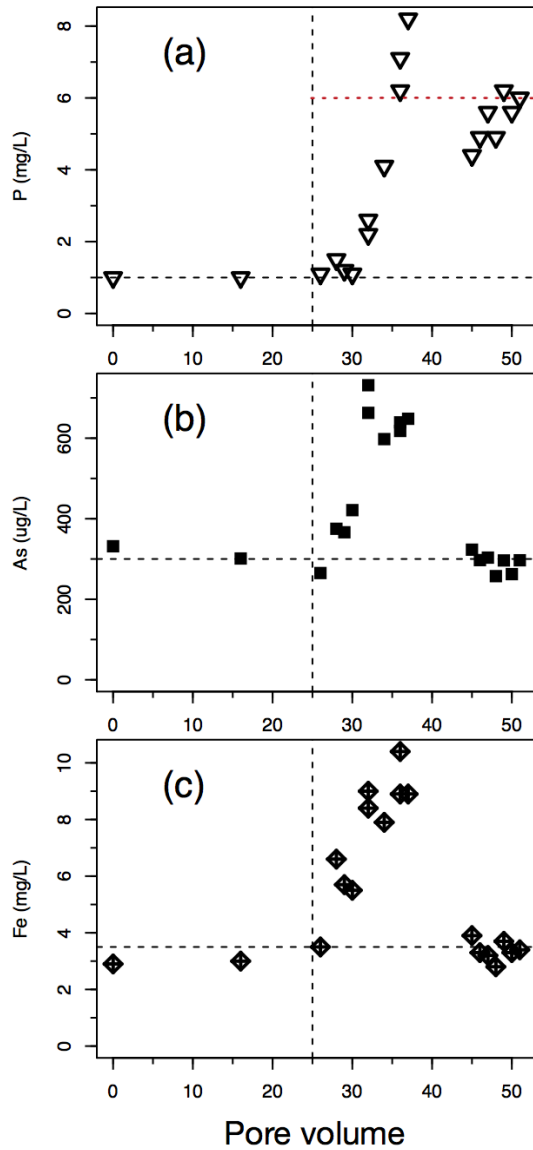
Figure 3-S11. Evidence of color change in an orange sediment column. The color of sediment is darker towards the inlet than in the outlet, which implies reduction of solid phase iron and sulfur during the experimental period. The color in the inset picture was normalized with the reference white balance.
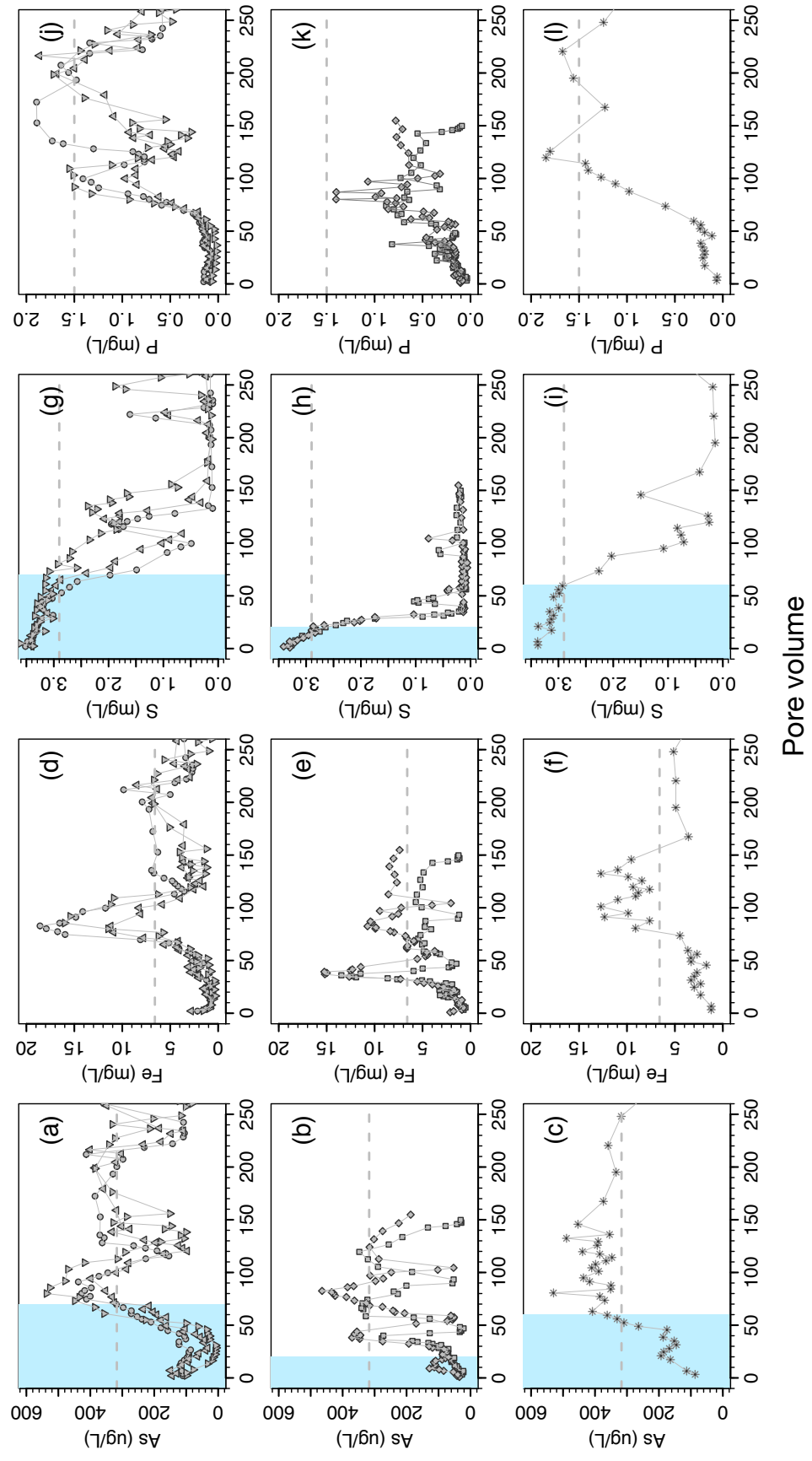
Figure 3-S12. Change in the fraction of solid phase iron (II) and arsenic (As) speciation in the gray sediment columns following elution with high-arsenic groundwater. (a) The percentage of Fe(II) in the inlets and outlets of columns were compared with average Fe(II) content (n =2) in the control sediment (blue); (b) XANES spectra of As for the same color-coded cores retrieved between 44 and 56 ft depth (Table 3-S1). The gray background (11872-11875 eV) shows the peak of normalized absorbance in the controls as a reference to compare with the rest of the columns (Table 3-S3). The associated linear combination fitting results are presented in Table 3-S3.
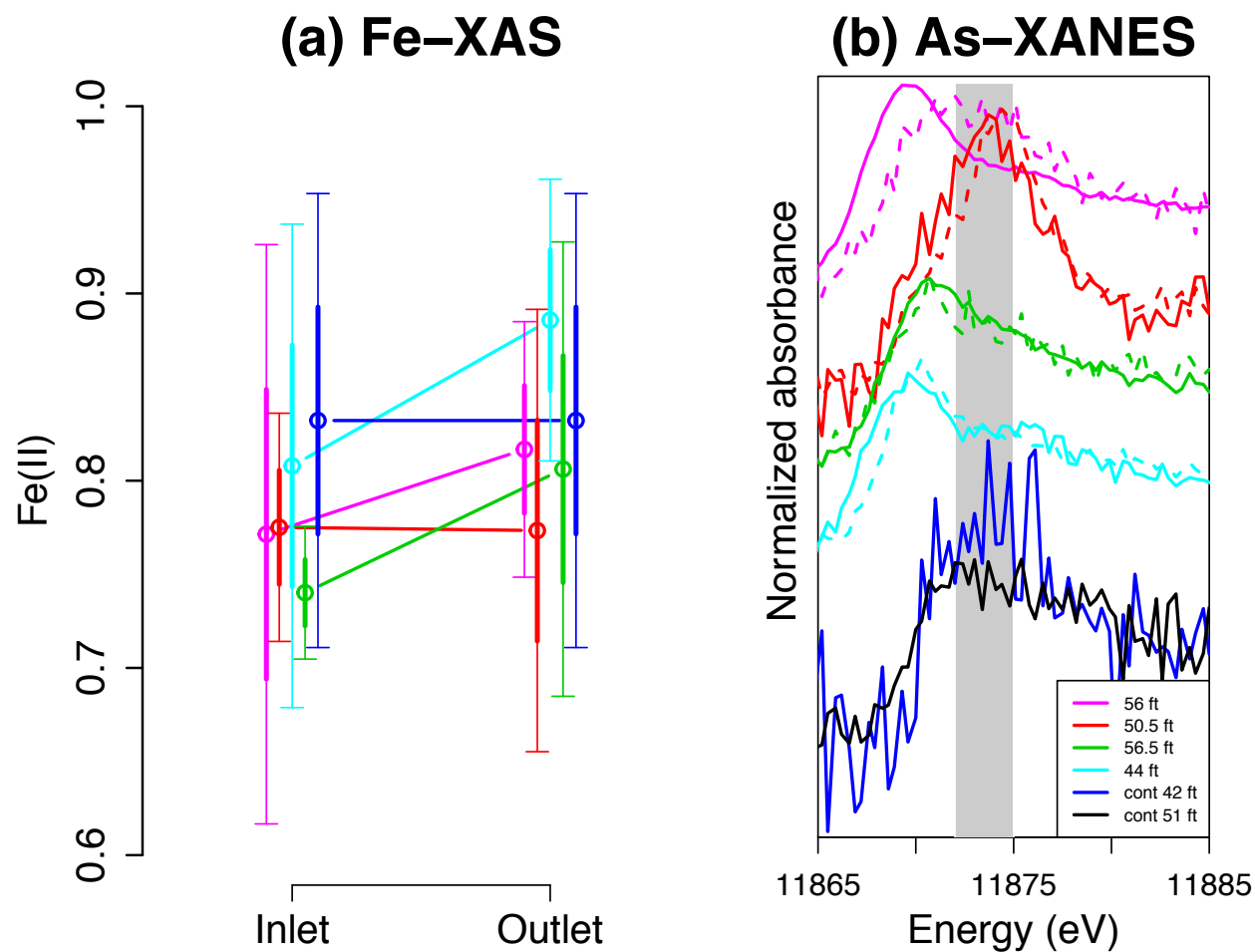
Table 3-S1. Column transport parameters for gray and orange sediments.

Coring depth	dry weight	Length	Volume	Bulk Density	Porosity	Pore volume	Darcy's flux	Pore water velocity
ft	g	cm	cm^3	g/cm^3	cm^3/cm^3	mL	cm/hr	cm/day
				Gray sand column				
56	27.4	7.5	15.1	1.82	0.31	4.72	3.0	230*
50	27.4	7.5	15.1	1.82	0.31	4.74	2.0	156*
50.5	26.2	7.5	15.1	1.74	0.34	5.18	2.0	140
48	26.6	7.0	14.1	1.89	0.29	4.03	2.0	165
56.5	28.3	7.5	15.1	1.88	0.29	4.41	0.8	66*
44	28.8	7.5	15.1	1.91	0.28	4.23	0.9	73
				Orange sand column				
45	27.6	7.5	15.1	1.83	0.31	4.67	2.0	155*
42	29.2	7.8	15.7	1.86	0.30	4.66	1.0	81*
43	27.0	7.5	15.1	1.79	0.32	4.89	1.1	81
51	27.9	7.5	15.1	1.85	0.30	4.56	0.5	40

*Observations simulated in **Figure 5**

Table 3-S2. Bulk chemical properties of the gray and orange sediment.

Coring depth ft	As mg/kg	As +/- mg/kg	P-ext. As %	Ca mg/kg	Ca +/- mg/kg	Fe %
			Gray sediment cuttings			
35	2.4	0.6	NA	8311	146	1.8
40	<LOD	1.7	NA	9617	148	1.7
45	4.2	0.6	NA	5781	124	2.1
50	<LOD	1.6	NA	3529	88	0.8
55	2.1	0.5	NA	8573	140	1.2
60	2.4	0.5	NA	5336	107	1.1
65	<LOD	1.6	NA	6472	116	1.2
42	1.9	0.5	0.23	7492	131	1.1
47	<LOD	1.6	0.88*	6201	124	1.6
AC12 ??	2.4	0.5	0.41	8896	148	1.3
54	4.1	0.6	0.41	6106	129	2.9
Average	*3*	*0.6*	*0.5*	*6938*	*127*	*1.5*
			Orange sediment cuttings			
42	<LOD	1.8	NA	3369	98	2.4
42	<LOD	1.7	NA	3602	106	2.4
43	3	0.5	NA	4526	111	2.5
43	<LOD	1.8	NA	4975	124	3.2
45	<LOD	1.9	NA	4355	118	3.8
46	2.6	0.6	NA	4492	113	2.1
51	2.1	0.6	NA	4673	114	3.0
41	2.8	0.6	0.10	2480	86	1.9
48	1.8	0.6	0.16	4572	110	2.0
50	2.3	0.6	0.20	4864	116	2.8
44	1.8	0.6	0.15	5206	116	2.6
Average	*2*	*0.6*	*0.15*	*4402*	*109*	*2.4*

Table 3-S3. Linear combination fitting results of As XANES spectra for the orange and gray sediment columns.

		Orange sediment columns			Grays sediment columns	
Depth	speciation	Inlet	Outlet	Depth	Inlet	Outlet
	As V sorbed	*11%*	*13%*		*3%*	*16%*
45 ft	*As III sorbed*	*4%*	*82%*	**56 ft**	*0%*	*36%*
	AsS sorbed	*85%*	*4%*		*97%*	*48%*
Res. Chi sq.		0.05	0.16		0.14	0.14
	As V sorbed	*7%*	*19%*		*25%*	*31%*
43 ft	*As III sorbed*	*11%*	*37%*	**50.5 ft**	*75%*	*69%*
	AsS sorbed	*83%*	*43%*		*0%*	*0%*
Res. Chi sq.		0.05	0.04		0.42	0.38
	As V sorbed	*31%*	*55%*		*12%*	*24%*
51 ft	*As III sorbed*	*26%*	*0%*	**56.5 ft**	*21%*	*4%*
	AsS sorbed	*42%*	*45%*		*68%*	*73%*
Res. Chi sq.		0.02	0.02		0.02	0.03
	As V sorbed	*20%*	*20%*		*15%*	*13%*
42 ft	*As III sorbed*	*17%*	*33%*	**44 ft**	*0%*	*0%*
	AsS sorbed	*62%*	*47%*		*85%*	*87%*
Res. Chi sq.		0.01	0.03		0.17	0.01
	As V sorbed	*76%*	*76%*		*0%*	*0%*
Cont 44 ft	*As III sorbed*	*24%*	*24%*	**Cont 42 ft**	*100%*	*100%*
	AsS sorbed	*0%*	*0%*		*0%*	*0%*
Res. Chi sq.		0.19	0.19		0.34	0.34
	As V sorbed	*89%*	*89%*		*28%*	*28%*
Cont 49 ft	*As III sorbed*	*11%*	*11%*	**Cont 51 ft**	*11%*	*11%*
	AsS sorbed	*0%*	*0%*		*60%*	*60%*
Res. Chi sq.		0.02	0.02		0.03	0.03

CHAPTER 4

ORIGIN OF GROUNDWATER ARSENIC IN A PLEISTOCENE AQUIFER DEPRESSURIZED BY MUNICIPAL PUMPING IN BANGLADESH

M.R.H. Mozumder[1]*, H.M. Michael[2], I. Mihajlov[1], B.C. Bostick[1], M.R. Khan[2,3], B. J. Mailloux[4], K.M. Ahmed[3], I. Choudhury[3], P.S.K. Knappett[5], T. Koffman[1], T. Ellis[1], K. Whaley-Martin[7], R. San Pedro[7], G. Slater[7], T. Koffman[1], M. Stute[1, 4], P. Schlosser[1,6] & A. van Geen[1]

[1]Lamont-Doherty Earth Observatory of Columbia University, Palisades, New York, USA

[2]University of Delaware, Newark, DE, USA

[3]University of Dhaka, Dhaka-1000, Bangladesh

[4]Barnard College, New York, NY 10027, USA

[5]Texas A&M University, College Station, Texas, USA

[6]Arizona State University, Tempe, AZ, USA

[7]McMaster University, Hamilton, Ontario, Canada

*Corresponding author: mozumder@ldeo.columbia.edu

Now at: Gradient, 20 University Rd, Cambridge, MA 02138

Abstract

Across South Asia, millions of villagers have reduced their exposure to high arsenic (As) groundwater by switching to low As wells. Isotopic tracers and flow modeling are used in this study to reconstruct the evolution of a semi-confined aquifer of Pleistocene (>10 kyr) age in Bangladesh that is generally low in As but has been perturbed by massive pumping about 25 km for the municipal supply of Dhaka. A 10-15 m thick clay aquitard caps much of the intermediate aquifer (>40-90 m bgs) in the 3 km^2 study area, with some interruptions by younger channel sand deposits indicative of river scouring. Water levels in the intermediate aquifer below the clay-capped areas are 1-2 m lower than in the high-As aquifer above the clay layer. Similar water levels in the shallow and intermediate aquifer where the clay layer is missing suggest a pattern of downward flow and lateral advection into the semi-confined aquifer that is consistent with ^{3}H-^{3}He ages, stable isotope data, and flow modeling. An accompanying influx of As and/or reactive carbon that triggers the reductive dissolution of sedimentary iron oxides could explain an association below capped portions of the Pleistocene aquifer of elevated As and methane concentrations within layers of grey sand. Alternatively, diffusion of reactive carbon from the clay layer itself could have reduced initially orange sands over longer time scales. Regardless of the mechanism, steadily rising As concentrations in three monitoring wells in the intermediate aquifer are most likely due to Dhaka pumping.

4.1. Introduction

Groundwater contamination with As threatens the health of more than 200 million people around the world who are exposed to As in drinking water above the World Health Organization (WHO) guideline of 10 μg/L (WHO, 1993; Ravenscroft et al., 2009). Bangladesh, part of the largest river delta in the world (Morgan and McIntire, 1959), represents the worst case scenario with a rural population of about 100 million relying on naturally polluted sedimentary aquifers containing As levels that often exceed the WHO guideline by a factor of ten to a hundred (Smith et al., 2000, BGS/DPHE, 2001; Ahmed et al., 2004). Spatial heterogeneity complicates the prediction of the distribution of As in the shallow (<50 m deep) Holocene (<12 kyr) aquifers of Bangladesh (van Geen et al., 2003) but older, deeper (>100 m) Pleistocene aquifers are consistently low in As in many parts of the region (BGS/DPHE, 2001; Michael and Voss, 2008; Burgess et al., 2010; Ravenscroft et al., 2013; Mihajlov et al., 2016; Choudhury et al. 2016; Lapworth et al., 2018). Aquifers in the geologic transition (50-100 m) are often also low in As and are increasingly exploited by local drillers contracted privately by individual households (Gelman et al., 2004; van Geen et al., 2006; von Brömssen et al, 2007; Hossain et al, 2014). These intermediate aquifers could, however, be more vulnerable to contamination in response to changing groundwater flow patterns than deep groundwater (McArthur et al, 2008, 2011, 2016; Hoque et al., 2012). Studying the geochemical and hydrologic processes that regulate groundwater As within this intermediate zone over time is therefore particularly relevant to private initiatives to reduce exposure. Government policy so far has relied primarily on nationwide installation of deep tube-wells (Ravenscroft et al., 2009, 2013, 2014, 2018) that are too costly for most households. In addition, these deep (>150 m) tubewells are often poorly allocated and not truly accessible to the public (van Geen et al., 2015).

114

Elevated levels of As (>100 µg/L) in shallow groundwater across the Ganges-Brahmaputra Delta have been widely attributed to microbially-mediated reductive dissolution of sediment-bound iron(oxy)hydroxides (Bhattacharya et al., 1997; Ahmed et al., 1998b; Nickson et al., 1998; McAurthur et al., 2001; BGS/DPHE, 2001; Berg et al., 2001; Oremland & Stolz, 2003; Ahmed et al., 2004; van Geen et al., 2004; Swartz et al., 2004; Islam et al., 2004; Oremland & Stolz, 2005). There is, however, still no consensus about the source of labile carbon that is necessary for such reduction to take place (Olson et al. 1981; Chappelle et al., 1987; Lovely et al., 1990). Buried peat/coal fragments elevated in total organic carbon that are deposited extensively in the Bengal Basin during the last marine transgression could be an important source (McArthur et al., 2001, 2004; Rotiroti et al., 2014). A shallow marine environment during the Holocene transgression also favored the deposition of a thick sequence of clay that typically separates shallow high-As groundwater from the confined low-As aquifers. However, the clay aquitard itself may contain 1-3 orders of magnitude higher levels of dissolved organic carbon (DOC) than the sandy aquifers (Leenheer et al., 1974; Hendry & Wassenaar, 2005) which may diffuse to the underlying aquifer (Thorstenson et al., 1979; Hendry and Schwartz 1990; Chapelle and McMahon 1991, McMahon & Chapelle, 1991; McMahon, 2001; Krumholz et al., 1997) and modify biogeochemical composition of groundwater at the aquifer-aquitard interface (Thurman, 1985; McMahon & Chapelle, 1991; Aravena et al., 1995; Crum et al., 1996; Aravena et al., 2004; Hendry & Wassenaar, 2005). Advection of young reactive carbon with surface recharge and groundwater flow has been invoked as an alternative source of reductants fueling the contamination of low-As aquifers (Polizotto et al., 2005, 2008; Klump et al., 2006; Neumann et al., 2010; Mailloux et al., 2013; Lawson et al., 2013; Stahl et al., 2016).

Hydrology is likely to play an important role in redistributing As and carbon in a perturbed aquifer system (Michael &Voss 2008; Fendorf et al., 2010; Burgess et al., 2010; Mukherjee et al., 2011; Winkel et al., 2011; van Geen et al. 2013; Mihajlov et al., 2016; MacDonald et al., 2016; Desbarats et al, 2014; 2017; Postma et al. 2017; Huang et al., 2018). The shallow aquifer of Bangladesh is perturbed by widespread irrigation pumping for growing rice (Harvey et al., 2002, 2006; Shamsudduha et al., 2011, 2015; Ahmed, KM 2011) but water levels typically recover rapidly at the beginning of the summer monsoon. In confined deeper aquifers within a 20-30 km radius of Dhaka, instead, water levels have been falling rapidly under the influence of deep pumping for the city's municipal since the 1980s (Ahmed et al., 1999; Hoque et al., 2007; IWM & DWASA, 2011; Ahmed, KM 2011; Knappett et al., 2016; Khan et al., 2016). The Dhaka cone of depression has continued to expand beyond the city limits and it has been suggested that this might draw As and/or dissolved organic carbon into aquifers previously low in As (Knappett et al., 2016; Khan et al., 2016).

Deep groundwater depletion is experienced by many other megacities around the world (Konikow & Kenedy, 2005; Wada et al., 2010; Werner et al., 2013; Famiglietti, 2014). Overpumping can affect the composition of groundwater on a large scale. A statistical analysis of a large number of wells in the US has shown an association between proximity of an aquitard and elevated levels of As in domestic wells (Erickson & Barnes, 2005). Overexploitation of groundwater has also been shown to mobilize significant amount of sedimentary dissolved organic carbon (Graham et al., 2015). Finally, dropping water levels have been invoked to explain groundwater contamination with As on a larger scale in the vicinity of compacted clay aquitards (Erban et al., 2013; Smith et al., 2018).

116

Large-scale (10s-100s of km) numerical models have previously been used to assess the risk of anthropogenic contamination of deep (>150 m) low-As groundwater by downward advection (Michael &Voss 2008; Jusseret et al., 2009; Hoque & Burgess, 2012; Sahu et al., 2013; von Brömssen et al, 2014; Michael & Khan, 2016; Radloff et al., 2011; Khan et al., 2016; Hoque et al., 2017). However, such models have not been widely applied at finer resolution to understand local flow patterns backed by detailed, long-term hydrogeochemical observations. We do so in this study by documenting the distal impact of Dhaka pumping on the local hydrology and distribution of As of a vulnerable intermediate aquifer (>40-100 m) within a ~3 km^2 area of Araihazar, Bangladesh. We rely on a groundwater flow model constrained by head measurements and geochemical data to shed light on the processes that evidently already led to the contamination of some portions of the intermediate aquifer and use this model also to make predictions.

4.2. Geologic setting

The 3 km^2 study area (between 23.7856, 90.6229 and 23.7714, 90.6430) is a part of a larger 25 km^2 area in Araihazar upazila, Bangladesh, where the on-going Health Effects of Arsenic Longitudinal Study was launched in 2000 (Figure 1c; Ahsan et al., 2006).

The site is located ~25 km east of the capital Dhaka and within the eastern perimeter of the expanding cone of depression induced by deep pumping (Khan et al., 2016; Knappett et al., 2016) (Figure 4-1). The occurrence of As in Araihazar and the rest of the country have been shown to be geogenic (BGS/DPHE, 2001; Ravenscroft et al., 2009). Low-As aquifers are largely associated with less reduced Pleistocene sediment that are exposed in Dhaka City (Figure 4-1a-b); but beyond the city limits, low-As aquifers are generally overlain by more reduced Holocene,

high-As aquifers (Horneman et al., 2004; Hoque et al., 2011). The top of the Pleistocene aquifer was weathered (oxidized) during the last glacial maxima (20 ka BP) when the sediment was subaerially exposed and flushed by meteoric water as the sea level was at least 100 m lower than present day (Umitsu 1994). In the northwestern portion of Araihazar, the oxidized, orange sand aquifer outcrops as the *Madhupur Terrace* (Morgan and McIntire, 1959). The same formation is buried under organic rich recent floodplain sediments of the Meghna and old Brahmaputra river system in the east/southeast. Valley fill, channel migration, and avulsion of rivers and their distributaries (Morgan and McIntire, 1959; van Geen et al., 2003; Zheng et al., 2005; Weinman et al., 2008; Pickering et al., 2014) over the course of geologic time-scale have partially eroded the sediments in the study area and resulted in the patchy occurrence of orange, oxidized deposits at variable depths further away from the uplifted Madhupur Terrace (Figure 4-1). Due to increasing popularity of the low-As intermediate aquifer (40-90 m) in Araihazar, the number of private wells tapping the Pleistocene orange sand quadrupled between 2001 and 2018 (Figure 4-S1).

4.3. Methods

4.3.1. *Monitoring nests*

Drilling and installation

Beyond the previously described 15 monitoring wells in the study area (Horneman et al., 2004; Zheng et al., 2005; Stute et al., 2007; Dhar et al., 2008), a total of 30 new locations were drilled and 10 nests consisting of 2-5 monitoring wells installed (Table 4-1) between June 2012 and January 2017 (Figure 4-2a). The new monitoring wells at site T, S, SS, N, Q, R, W, J, L, and D were installed between 9 and 195 m below ground level (bgl). The manual percussion ("hand

118

flapper") drilling technique (Horneman et al., 2004) was employed to install the shallow (< 40 m bgl) and intermediate (>40-80 m) wells with a 1.5 m screened interval at the bottom. Both sand and clay drill cuttings retrieved at regular intervals of 1.5 m were preserved for sediment analysis. In addition to 4 existing deep wells (> 80 m; Mihajlov et al., 2016) in the study area, 3 deep wells were installed by the rotary drilling direct circulation ("donkey") method (Mihajlov et al., 2016) with a screened interval of 6 m. The depth of all installed wells was verified with a graduated water-level tape. Each monitoring well is constructed with a 5 cm diameter galvanized iron casing pipe erected above the ground surface, followed by a series of connected 5-6 m long PVC pipes that extend down to the maximum depth of drilling.

Water level monitoring

Hydraulic heads were monitored with a water-level meter (Solinst Model 101 P2 probe part#100289) from the TOC of each monitoring well at regular intervals (on the third week of each month) between 2012 and 2018. The nests were leveled relative to each other within ±2 cm based on closure using a 500-ft long transparent tube filled with water. All relative water level elevations were then converted to absolute water level elevations (i.e. elevation above mean sea-level) with respect to site-B piezometers (Figure 4-2a) for which absolute elevation was determined in 2003 using differential Global Positioning System (GPS) survey with a precision of ±3 cm (Zheng et al. 2005).

Pressure transducers (Model 3001, Levelogger Edge, Solinst Canada Ltd., Georgetown, Ontario, Canada) were deployed in 25 monitoring wells to record groundwater pressure fluctuations. The loggers were attached to the TOC with a thin stainless steel wire of a length adjusted to keep

them submerged throughout the year and within the detection range of the loggers. Barologgers (Barologger Edge, Solinst, Georgetown, Canada) were also deployed in a similar fashion but above the high water level to record atmospheric pressure in two different wells. Both levelloggers and barologgers were set to measure water and atmospheric pressure fluctuations at concurrent 20 min intervals. Pressure transducer data were converted to water level following the two-step process described by Knappett et al., 2016. Barologger-corrected water level data were compared with manual water level measurements to verify consistency over the duration of the deployments.

Onsite chemical measurements and water sampling

After measuring groundwater level in the undisturbed water column, at least one well volume was purged with a submersible pump (Typhoon P-10200) for 10-50 minutes depending on well depth. Groundwater samples were collected from sand formations in 2012-17 after groundwater pH, oxidation-reduction potential (ORP), temperature, and electrical conductivity (EC) readings with Oakton probes (UX-35650-10 & UX-35634-30) placed in a flow-through cell had stabilized. Groundwater samples were collected from clay layers by squeezing pore-water at site-S and M in February 2016 using a press or mechanical squeezer (Manheim, 1966).

Polyethylene liquid scintillation vials (20 mL Wheaton Fisher 986706) with PolySeal caps were used to sample groundwater for cation and anion analyses. Groundwater samples for stable water isotope (^{2}H and ^{18}O) analyses were collected in 20 mL scintillation glass vials with urea PolySeal caps (Wheaton Fisher 986546) in February 2016 and January 2017. Samples for tritium (^{3}H) were collected in 500 ml Amber Boston round bottles (Qorpak GLA00896) with polycone lined

cap (Qorpak 00190) in June 2012, May 2016, and Feb 2017. A subset of 6 wells from nest T, R, and S was sampled in duplicate in Jan 2018 for noble-gas analyses (helium, He and neon, Ne) in crimped copper tubes (0.3" diameter, 30" length weighing approximately 40 cm^3 of water) following the prescribed protocol (https://water.usgs.gov/lab/3h3he/sampling/).

Samples for dissolved organic carbon (DOC) and dissolved inorganic carbon (DIC) analyses were collected in 22 mL clear glass vials (Sigma-Aldrich 27173 Supelco) assembled with PTFE/silicone septum attached screw caps (Sigma-Aldrich 27021 Supelco) in February 2016 and January 2017. The DOC samples were acidified to 0.1% HCl in the field immediately after collection. DIC vials were overfilled to avoid a headspace and were not acidified. For radiocarbon dating of DIC and DOC, groundwater samples were collected in 250 mL bottles (Qorpak™ GLA00815) with PolyCone Lined Cap. The DIC radiocarbon samples were preserved with 0.02% $HgCl_2$ and the radiocarbon DOC samples with 0.1% HCl.

To determine methane (CH_4) concentrations in groundwater, 60 mL groundwater samples collected with a syringe were injected through septa into pre-evacuated, burnt serum glass bottles fixed with Hg_2Cl and shipped upside-down for laboratory methane analyses of site-SS, M and B nest samples in January 2017 and site-T, R, S, N, Q, D, J, L nest samples in January 2018. Measurement of the stable carbon and hydrogen isotope ratios of CH_4 was performed on a selected subset of groundwater samples.

Groundwater analysis

Concentrations of major cations and redox-sensitive trace elements Na, K, Ca, Mg, P, Fe, Mn, Sr, and Ba were measured by high-resolution inductively coupled plasma-mass spectrometry (HR ICP-MS) on acidified (1% Optima grade HCl) groundwater samples (Cheng et al., 2004; van Geen et al., 2007). In the case of As, the precision was on the order of 5% and the detection limit based on the variability of the blank <0.1 µg/L. Base cations were measured with a precision of ±10% based on a laboratory and NIST-traceable standard. Concentrations of the major groundwater anions Br, F, and Cl were measured using a Dionex Integrion HPIC System (Dionex, Thermo Scientific) with an AS-18 column, which has a detection limit of 0.05 mg/L and a precision of ±5% at environmental concentrations. Elemental concentrations reported in Table 4-1 indicate the median when time-series data are available.

Stable isotopes of ^{18}O and ^{2}H were analyzed with a Picarro Isotopic Water Analyzer at Lamont-Doherty Earth Observatory with a precision of ±0.002-0.065‰ for ^{18}O and ±0.03F-0.71‰ for ^{2}H (Table 4-1). Working standards for the Picarro are stored in stainless steel casks under argon and measured yearly against the primary standards VSMOW2, GISP, and SLAP provided by IAEA in Vienna. An aliquot of an independent standard (not used for normalization) is run with each set of samples. Repeatability of ocean water measurements was ±0.03-0.05‰ (Walker et al., 2016).

Samples for tritium (^{3}H) were analyzed using the ^{3}He ingrowth technique from the decay of ^{3}H (Bayer et al., 1989; Ludin et al., 1998). The analytical precision for ^{3}H measurements was ±0.01-0.1 TU with a detection limit of 0.05-0.10 TU, where 1 TU corresponds to one ^{3}H atom per 10^{18}

[1]H atoms. Two internal tritium standards have reproducibility of 1.1-1.5% (for ~8TU tap water) and <50% (for ~0.12 TU ocean water). Noble gas concentrations and ^{3}He/^{4}He ratio were determined by mass spectrometry (Ludin et al., 1998; Stute et al., 2007) with a precision of ±0.05-0.10% for ^{4}He and Ne concentrations and ±0.3-0.5% for ^{3}He/^{4}He ratios. Long-term reproducibility of air equilibrated water standards for ^{4}He was 0.3-0.7%, for Ne was 0.3-0.8% and for ^{3}He/^{4}He was 0.3-0.5%.

Both the DOC (n = 30) and DIC samples (n = 45) were analyzed in triplicate (three injections for each sample) on a Shimadzu Carbon Analyzer with a precision of ±5% at Lamont-Doherty Earth Observatory. Groundwater methane (CH$_4$) concentrations were measured by injecting 50-1000 µL of headspace from the bottles using a SRI 8610C gas-chromatographer with a 0.91 m by 2.1 mm silica gel column coupled to a flame ionization detector. Measurements were made in triplicates (RSD ≤10%) to compare with the calibration curves. PeakSimple Chromatography Software 3.29 (SRI Instruments) was used for peak analyses and integrations. Analyses of δ^{13}C and ^{2}H of CH$_4$ were performed by a GC-IRMS (Agilent 6890) at McMaster University (Whaley-Martin, 2017).

4.3.2. Analysis of sediment cuttings

Drill cuttings (primarily sand and clay) were wrapped with transparent plastic food wrap upon retrieval. A Konica Minolta CM-600d spectrophotometer was used to measure the difference in diffuse spectral reflectance between 530 and 520 nm (Horneman et al., 2004) through the plastic wrap soon after the samples were retrieved. The measurements were made in triplicates by the spectrophotometer and recorded for three different spots on each cuttings sample. Magnetic

susceptibility was measured at Lamont-Doherty Earth Observatory on sediment cuttings with a magnetic susceptibility meter (Model MS2, Bartington instrument, Oxford, England). A handheld X-ray fluorescence analyzer (InnovX Delta) was used in the 3-beam soil mode to determine bulk As, Fe, and Ca concentrations in the sediment cuttings. Reference NIST standards SRM 2709, 2710, and 2711 were also analyzed by XRF at least at the beginning and end of each run to check calibration. Analysis of subset of powdered sand samples (n=19) from one of the sites by XRF confirmed that grain-size did not affect the bulk concentrations.

A total of 45 pulverized, oven dried drill cuttings of clay and occasionally encountered peat/charcoal layers from 6 sites collected from 3-73 m depth range were prepared for total carbon (TC) and inorganic carbon (IC) analyses. The samples were analyzed on the solid sample module (SSM) of Shimadzu Carbon Analyzer (TOC-Vcsn) by dry combustion at 900°C in the TC furnace and at 200°C in the IC furnace after acidifying the sample. The difference between the TC and IC is reported as total organic carbon (TOC). A subset of 20 drill cuttings from clay, peat or buried wood fragments retrieved between 32 m and 74 m depth interval at 9 locations were sent to NOSAMS for radiocarbon dating of organic carbon (Elder et al., 1998). A subset of 4 clay cuttings was sent to the Particle Technology Lab (Downers Grove, IL) for porosity determination using the mercury intrusion method (Diamond, 1970) on an AutoPore IV 9500.

4.3.3. *Pumping test*

Two pumping tests were performed at site-M. The first test was performed by pumping from the fully penetrating pumping well A (M_A) in the shallow aquifer for approximately 24 hours (January 17-18, 2011). The second test was performed by pumping the entire vertical extent of

the intermediate aquifer from the fully penetrating pumping well B (M_B) for approximately 48 hours (January 19-21, 2011). A locally purchased irrigation pump (1.75 horsepower, 1 atm maximum lift) was powered by a generator to maintain a constant flow rate of ~200 L/min (58 m^3/d), measured by a flow meter (McMaster-Carr) connected in-line to a PVC tube carrying the pump outflow.

Hydraulic heads in multi-level observation wells and pumping well C were monitored simultaneously by Solinst pressure loggers at 2-second intervals for the first 70 min of the tests, and at 1-minute intervals for the remainder of the pumping tests and a 24-hr recovery period after pumping ended. A barometric pressure logger recorded atmospheric pressure changes on site at the same time intervals. Several pressure loggers were deployed for weeks prior to and after the pumping tests to monitor the seasonal declining hydraulic head trend and atmospheric pressure changes.

4.3.4. *Groundwater modeling*

A small-scale (3 km^2) MODFLOW (Harbaugh, 2005) groundwater flow model was constructed on the basis of local stratigraphy and reference heads extracted from the homogeneous case of an existing large-scale (11,025 km^2) transient model of Khan et al. (2016) (Figure 4-1), which was originally developed from the basin-scale (362,700 km^2) model after Michael and Voss (2008). The local model has a refined grid size of 50 × 50 m and cell thickness of 1 m. The model comprises 202 layers, with 41 cells in the east-west direction and 29 cells in the north-south direction.

The topmost and bottommost layers represent model top and bottom boundaries, respectively.

Because the effect of Dhaka pumping is primarily along the East-West direction (Knappett et al.,

2016 & Khan et al., 2016), side boundary conditions at the model perimeter are imposed in the

farthest cells in the east as well as in the west. No-flow boundaries were assigned in the north

and south of the model domain.

Recharge was specified along the top 1 m of the model with a spatially uniform rate of 0.5 m/yr

for the pumping scenario and 0.05 m/yr for the pre-pumping scenario. A drain was also specified

along the model top to prevent heads from exceeding the land surface elevation. The current rate

(0.5 m/yr) of recharge is consistent with regional estimates (Stute et al., 2007; Michael & Voss,

2009; Shamsudduha et al., 2011; Khan et al., 2016) as well as estimates on the basis of ^{3}H/^{3}He

ages of shallow groundwater in Araihazar, Bangladesh (Stute et al., 2007). To assess the impact

of top boundary condition, an alternative model with a constant head boundary was also run

because little spatial variation in shallow groundwater head is observed in the study area (Figure

4-S2). The simulation result remains the same whether a uniform recharge or a constant head is

specified at the model top. A storage coefficient of 0.1 was assigned only to the top layer of cells

to simulate specific yield under unconfined conditions while using a more computationally

efficient confined aquifer in MODFLOW (e.g., Khan et al., 2016). For the rest of the model

layers, a specific storage value of 1×10^{-4} was used (Khan et al., 2016).

The general head boundary (GHB) package was used to set hydraulic boundaries on the sides

and the bottom of the model. GHB is implemented to overcome three challenges: (i) no natural

126

boundary (e.g. river) is present in close proximity to the study area; (ii) a prescribed-head with an infinite source of water may not be suitable when local pumping is invoked; and (iii) the stratigraphy is well constrained only within the study area and the heterogeneity outside the modeled domain is uncertain. When knowledge of the regional flow system is well defined, the utilization of reference heads and conductance from the regional model allow the use of GHB with some confidence. GHB allows groundwater flow into and out of the model domain by simulating the ambient regional groundwater flux across the boundary.

The reference heads for the GHB were taken by interpolating the coarsely gridded (1 km × 1 km × 5 m) simulated heads from the 66 model layers of Khan et al. (2016). Because there is a linear relationship between head at the boundary and flux through the boundary in GHB package, the reference hydraulic heads for the pumping condition were extracted at the maximum distance from the edge of the model area. This is where the reference heads linearly drop in the west and linearly increase in the east. The distance of the reference heads from the east and west boundary cells of our model was 1 km. Beyond that distance, the reference heads declined nonlinearly in the west due to Dhaka pumping and plateaued in the east at the Meghna River (Figure 4-S3). Likewise, the GHB at the bottom of the model was assigned at 200 m with the reference heads extracted from 300 m. The conductance was calculated at the sides of the model as: and at the bottom as: ; where, A is the cross-sectional area perpendicular to flow direction, which is 50 × 1 m^2 for the side boundaries and 50 × 50 m^2 for the bottom boundary; L is the distance (sediment thickness) of 1000 m on the sides and 100 m at the bottom; K_h and K_v are the horizontal and vertical hydraulic conductivity, respectively.

Heterogeneity and anisotropy

A three-dimensional (3D) lithofacies model of the study area was generated in Rockware15

software (Rockworks^{TM}) by interpolating between 33 drilling logs at 1.5 m vertical resolution

that were confirmed at 12 locations when additional piezometers were installed (Figure 4-S4, 4-

5). The model was conditioned against each of the drilling logs to closely mimic subsurface

heterogeneity. The model consists of two major lithofacies: sand and clay. Boundary conditions

were employed on the sides of this refined heterogeneous 3D field to assess how the hydraulic

head distribution varies as a function of the thickness of a clay aquitard, typically encountered

25-30 m below ground surface (Figure 4-S4). The applied horizontal hydraulic conductivity of

the sand facies is 2×10^{-4} and clay facies is 9×10^{-9} m/sec, consistent with pumping test results

(Figure 4-S6) and are within the range of typical values for these sediment types. The model is

considered heterogeneous up to a depth of 75 m and homogeneous between 75 and 200 m depth

range (Figure 4-S7). The depth for the heterogeneous portion of the model corresponds to the

maximum depth local drillers could reach with hand-percussion technique. The cuttings retrieved

by hand-percussion drilling make a reliable distinction between sand- and clay-sized particles up

to a depth of 75 m, whereas the direct-circulation technique (donkey-drilling) usually produces

unreliable mixed cuttings. A vertical anisotropy (K_h/K_v) of 100, representing effects of

heterogeneity beneath the scale of representation, was calibrated from measured hydraulic heads.

The facies values in the homogeneous portions of the model were assigned equivalent K_h and K_v

values derived by simulating Darcy's flow horizontally and vertically across the heterogeneous

domain (Khan et al., 2016). The model was calibrated manually with an overall root mean

squared error of about 0.5 m (Figure 4-S8).

Domestic and irrigation pumping

The pre-pumping case does not consider deep Dhaka pumping or shallow irrigation pumping. The pumping case includes both. The spatial distribution of domestic hand-pumps in the study area was gathered from a blanket testing campaign conducted in 2012-13 (van Geen et al., 2014). A total of 1,274 domestic hand-pumps were identified and tested for As in the 3 km^2 area (Figure 4-2b). Only 5 deep wells whose depths exceeded the model domain's maximum of 200 m were excluded. A 2 m screened depth interval was assumed for all domestic hand pumps. The rate of pumping was determined on the basis of previously estimated domestic water demand of 10 L per person per day (Zheng et al., 2005) and a 5-person household sharing each well, resulting 50 L of withdrawal per well per day.

The location of 37 irrigation wells in the study area was determined in 2014 (Figure 4-2b). Their maximum depths ranged from 15 to 26 m, with an average screened interval of 5 m. The pumping rate of the most popular low-cost 2 horsepower submersible irrigation pump (100 QRm 3/16 #85054) was determined by matching the name of the manufacturer of the pump in the local market. The maximum flow rate of 70 L/min indicated by the manufacturer was used to calculate the rate of irrigation pumping. Since irrigation pumps are active for 4 months per year and each pump runs for half a day on average, based on conversations with local farmers, about 17% of the maximum pumping rate (11.7 L/min) was used for each pump for the steady-state model simulation. To avoid unusual drawdown due to pumping from clay horizons, the screened depth interval of each of the irrigation pump was restricted to the sand facies. For both domestic and irrigation withdrawals, the Well Package of MODFLOW was used to assign the negative

pumping rate after dividing the calculated rate by the total number of model layers that intersect corresponding screened depth interval.

Transport of arsenic

Advective transport of As was simulated by particle tracking using MODPATH version 6 (Pollock D.W., 2012) to estimate the travel time required for groundwater and As to reach the recharge source in the absence of retardation. Particles were tracked backward from site-S intermediate aquifer and were allowed to travel over a prescribed time interval of 50 years for the pumping scenario and 500 years for the prepumping scenario. Initially, particles were placed at the top of 20 vertically connected cells across the entire thickness of the intermediate aquifer (45-65 m). MODPATH was used with a retardation factor of 1 to determine the transport of As at the rate of groundwater flow. A porosity of 30% was considered for the confined aquifer for MODPATH simulations.

The MT3DMS package (Zheng and Wang, 1999) was used to simulate advective-dispersive transport of As in groundwater to predict As distribution and transport when accounting for adsorption (e.g., Michael and Khan, 2016). For simplicity, a constant (relative) concentration (C/C_0) of 1 was applied to the model top, and zero flux along the east and west boundaries. An initial concentration of 1 was applied in the shallow aquifer (up to a depth of 20 m) and 0 was applied to the rest of the aquifer. In this case, retardation factors of 5, 10, and 30 were applied for all lithofacies assuming a linear isotherm to predict the volumetric spread of As pollution in the intermediate aquifer under different sorption scenarios (Figure 4-S9). A partition coefficient, K_D of 1.5 L/kg translates into a retardation factor (R_f) of 10 when a porosity of 0.3 and bulk density

of 1.8 g/cc are assumed. A constant longitudinal dispersivity value of 10 m and transverse

dispersivities of 0.01 and 0.001 m (Michael and Khan, 2016) were assigned. Forward

simulations were performed with and without the effect of Dhaka pumping for 50 and 500 years,

respectively.

4.4. Results

4.4.1. Hydrostratigraphy

A clay aquitard of variable thickness typically separates the shallow and intermediate aquifers in

Araihazar, as it does in many regions of Bengal basin. In our 3 km^2 study area, this aquitard is up

to 24 m thick but almost entirely absent at two drilling sites R and T (Figure 4-2b, Figure 4-S4).

The top of this aquitard, where present, is generally encountered at 25-30 m depth (Figure 4-S4).

The intermediate aquifer (>40-80 m) located below this aquitard is semi-confined. In most cases,

depending on location, a second harder clay layer was encountered in the 65-80 m depth range

and could not be penetrated with the local driller's hand-percussion method (Figure 4-S4). This

hard clay layer is considered the bottom of the intermediate aquifer. Pumping test results within

this semi-confined aquifer yielded an average hydraulic conductivity value (K) of 1×10^{-4} m/sec

and storativity (S) of 6.2×10^{-4} (dimensionless) (Figure 4-S6, Table S1), which is typical for

confined aquifers composed of medium- to fine-grained sand.

The shallow aquifer (< 30 m) in the study area consists of a fining-upward sequence of gray

channel sands capped by surface clay at 29 out of 33 drill sites (Figure 4-2b & 4-S4), below

which groundwater As levels are generally elevated (Figure 4-S1). The intermediate aquifer

below the deeper clay layer shows inter-fingering gray and orange sand sequences (Figure 4-4 &

4-S4). At 24 of the 33 drill sites, the upper part of the intermediate aquifer sand is gray (reduced) in color. For 12 out of 33 drill sites, there is also a gray sand layer in the intermediate aquifer that is sandwiched between orange (oxidized) sands at a depth that varies from one drill site to the other. At 5 of the 33 drill sites, the bottom of the clay layer capping the intermediate aquifer is oxidized, reddish brown in color, and has been described elsewhere as a paleosol (McArthur et al., 2004; 2008; 2011) that protects the orange intermediate aquifer (Figure 4-S4). The difference in diffuse spectral reflectance between 530 and 520 nm recorded on a total of 461 sediment cuttings of gray sand and clay averages 0.2±0.1%. The difference in reflectance for drill cuttings retrieved from the oxidized orange/reddish sand and clay sequences averages 0.9±0.2% (n = 111).

The integrated proportion of clay relative to sand within the upper 50 m at each drill site varies spatially varies from 3 -73% (Figure 4-2b). At 5 of the 33 drill sites, the integrated proportion of clay is ≤20%. These sites, where the intermediate aquifer is clearly separated from the shallow aquifer, are located mostly on the periphery of the study area.

4.4.2. The Holocene-Pleistocene transition

Oxidized orange sediments are generally considered of Pleistocene age across the Bengal Basin (Ahmed et al., 2004; McArthur et al. 2004). We refine this assessment in our study area on the basis of organic radiocarbon dating of clay or peat and profiles of magnetic susceptibility and bulk concentration of calcium (Ca) in sediment based on the cuttings (Figure 4-3a-b, e-h). Radiocarbon ages of 23 clay cuttings from between 32 and 78 m depth range from 6.5 to 36.5 kyr (Figure 4-S4b). Overall the data show the expected increase in age with depth, but also that

the depth of the Holocene-Pleistocene boundary can vary significantly within a distance of a few 100 m. At scoured site T near the southern boundary of the study area, which is representative of 5 other locations (Figure 4-2b), the confining clay layer is missing and Holocene gray sands extend all the way down to 53 m depth. At site S, representative of 25 similar locations with clay layer instead, the intermediate aquifer is capped by a Pleistocene oxidized paleosol as shallow as 37 m depth (Figure 4-3a-b).

Profiles of magnetic susceptibility and Ca help define the Holocene-Pleistocene transition at each site (Figure 4-3e-f). The contribution of magnetite and other magnetic minerals to Holocene sediments is variable but distinctly higher than for Pleistocene sediments (BGS/DPHE 2001; Horneman et al., 2004). The bulk Ca content of Holocene sands is also higher than for Pleistocene intervals (Figure 4-3g-h). This has been attributed, respectively, to the partial reduction of Fe oxides forming magnetite and the authigenic precipitation of carbonate in supersaturated Holocene sediment (McArthur et al., 2008; van Geen et al., 2013). The two authigenic phases evidently never formed or were not preserved during subaerial exposure of Pleistocene sediments during the last sea-level low stands.

Unlike Ca or weathering-sensitive sediment constituents such strontium (Sr), the solid phase arsenic (As) content of Holocene and Pleistocene sands is comparable. The average As concentrations of the Holocene gray and Pleistocene orange sand is 3 ± 1 mg/kg (n = 100) and 2 ± 1 mg/kg (n = 21), respectively based on measurements from 6 sites drilled in the study area. Arsenic concentrations in clay are typically higher (up to 7-15 mg/kg) than in sand cuttings but there is no noticeable difference between Holocene and Pleistocene clay. In contrast to Ca, the

133

bulk Fe concentration of Pleistocene (1.0±0.3%, n = 21) and Holocene gray sand (1.2±0.4%, n = 100) is comparable.

The gray Holocene aquifer contains wood fragments and peat- or charcoal-like fragments in the study area (Figure 4-S4) of a type that has been dated extensively in other parts of the country (Umitsu, 1993; Goodbred & Kuehl, 2000). In our study area, a total of 16 buried peat/wood layers were discovered during drilling in 14 out of the 33 logs within the 6-52 m depth interval. The concentrations of total organic carbon (TOC) measured in 7 such peat fragments from 5 locations ranged from 12-50% by weight with an average of 30±10%, contrasting with an average of about 0.5±0.2% (maximum of 3.1%) measured on 38 clay cuttings retrieved from 6 locations in the study area. The TOC (%) for gray Holocene clay is systematically higher than 0.1% whereas the orange Pleistocene clay sequences typically contain <0.1% (Figure 4-S10).

4.4.3. *Groundwater chemistry*
Clay-capped intermediate aquifers

Sites S and SS are two comparable sites 150 m apart in the center of the study area where the intermediate aquifer is capped by a stiff, confining clay layer (Figure 4-2, Figure 4-4a-l). At site S, the top half of the confining clay layer is reduced, gray and of Holocene age and the bottom half is oxidized and of Pleistocene age (Figure 4-3a-b). The top and bottom sands of the Pleistocene aquifer are orange and low in As (<5 µg/L) whereas the reduced, gray middle of the aquifer is elevated in As (40±5 µg/L). This reduced portion of the aquifer with elevated As at site S is also higher in dissolved organic carbon (DOC), dissolved methane (CH_4), and bomb-produced tritium (^3H) in comparison to the oxidized portions of the aquifer above and below

134

(Figure 4-4a-c, e). Groundwater stable isotope composition in the reduced, gray sand is similar to that of shallow groundwater at this site (Figure 4-4d). The southward extension of the reduced portion of the intermediate aquifer at Site SS is less elevated in As (15 ± 2 µg/L) with barely detectable (> 0.1 TU) ^{3}H, but DOC and CH$_4$ levels are comparable to those in the reduced portions of the intermediate aquifer at site S. In grey sand just below the clay layer at site SS, both As and CH$_4$ concentrations are higher at 70 µg/L and 1200 µmol/L, respectively.

Site M, located 450 m south of site S (Figure 4-2a), has been studied extensively in the wake of the repeated failure (i.e. a rise in As) of a community well installed in the intermediate aquifer that served the neighboring villagers (van Geen et al. 2006; Mihajlov et al. in prep.). Long-term monitoring of two wells at site M, where the intermediate aquifer is capped by thick clay, indicates elevated levels of As (80 ± 29 & 350 ± 21 µg/L), DOC (~4 mg/L), and CH$_4$ concentrations (1200 ± 100 & 690 ± 70 µmol/L). In contrast, the wells installed in the oxidized, lower portion of the aquifer (>55 m) are low in both As and CH$_4$ (Figure 4-4m-o, q). Unlike at site S, ^{3}H was not detected in the well immediately below the confining clay layer at site-M. The stable isotopic composition of groundwater derived from gray sand beneath the thick clay varies by 1.5‰ at this site.

Clay pore waters at site-S and M are elevated in As (maximum of 190 µg/L) and contain an order of magnitude higher DOC concentrations (maximum of 49 mg/L with an average of 20 ± 5 mg/L) than well w ater (Figure 4-4a-b, m-n). The stable isotopic composition of clay pore water in both grey and orange clay at site S is comparable to that of the shallow aquifer (Figure 4-4d, j, p). Groundwater just below the orange clay is more depleted by about 2‰ at this site. In contrast,

the stable isotope composition of grey clay water at site M is similar to that of groundwater in gray sand just below the clay.

The age of groundwater containing detectable ^{3}H (>0.1 TU) in the intermediate aquifer ranges from 11 to 49 yr at site-M (n=9) and 45-47 yr at site-S (n=2) (Table 4-2). With the exception of well S2 and M3.5, the ^{3}H+^{3}He content of these samples, which is unaffected by ^{3}H decay, accounts for <70% of the predicted value based on a smoothed version of ^{3}H input to the atmosphere since 1950 (Figure 4-S11). This indicates that most of these samples are mixtures of old groundwater recharged before bomb-^{3}H input with younger groundwater containing bomb-^{3}H.

Intermediate aquifers without a clay cap

The composition of groundwater as a function of depth at the two sandy sites R and T, 700 m to the west and 750 m to the south of site M, is somewhat featureless compared to sites SS, S, and M (Figure 4-2 & 4-5). The gray sandy aquifer at sites R and T is elevated in As (> 50 μg/L) to a depth of 55 m (Figure 4-5a & g). At greater depth, groundwater in contact with orange Pleistocene sands contains <5 μg/L of As. The DOC concentration at site-T is somewhat higher at 4 mg/L in an intermediate well installed immediately below a peat layer, whereas all monitoring wells at site R are consistently low (0.5 mg/L) in DOC (Figure 4-5b, h). Methane concentrations in groundwater at the sandy sites are lower than in the gray sand layers where the intermediate aquifer is capped by clay, by a factor of 10 and 100 at sites T and R, respectively (Figure 4-5c & i).

The stable isotope compositions of groundwater in the shallow and intermediate aquifer at sandy sites R and T, including orange sands at depth, is similar to that of the shallow aquifer (Figure 4-5d & j). Bomb-produced ^{3}H also penetrates the intermediate aquifers to the depth of orange sand at all sandy sites (Figure 4-5e,k). The estimated age of groundwater in the intermediate aquifer based on the ^{3}H/^{3}He method at site-T and R ranges from 14 to 24 yr and 22-38 yr, respectively (Table 4-2). The distribution of ^{3}H+^{3}He relative to predicted bomb input show no indication of mixing of young and old groundwater in these samples (Figure 4-S11).

Long-term changes in As concentrations in the intermediate aquifer

Two intermediate wells at clay-capped sites M and B monitored for more than 5 years indicate a steady increase in As concentrations, a third well at site S shows steady As levels, while fourth indicates a slight decline in As (Figure 4-6a). Both wells with rising As were installed beneath the gray confining clay layer, coincidentally at the same depth of 41 m. Well M1-4 at the clay-capped site-M, which is devoid of ^{3}H and has a similar isotopic and conservative solute composition to that of overlying clay water (Figure 4-4p, 4-S12), shows a steady increase in As from 40 μg/L in Feb 2011 to 150 μg/L in Oct 2017. At a slightly lower rate, groundwater As in well B5 has been rising steadily from 20 μg/L in Oct 2002 to 110 μg/L in Dec 2017 (only data since 2011 shown). Rather than a thick clay layer, the transition between the shallow and intermediate aquifer at site B is characterized by multiple thinner clay layers (Zheng et al., 2005). At the sandy site T, As concentrations in one intermediate well screened near a peat layer rose have been fluctuating widely and rising since July 2015 (Figure 4-6b). Other monitoring wells in the intermediate aquifer in the study area show either constant concentrations or variable concentrations without a clear trend or connection to seasonal variations in water level.

4.4.4. Groundwater heads

Hydraulic heads were monitored in the study area for 6 years in 52 piezometers. The data are subdivided into shallow (8-40 m, n = 17), intermediate (40-90 m, n = 30), and deep (>90-195 m, n = 5) aquifer in accordance with the local stratigraphy. Seasonal variations in water level of about 4 m in amplitude parallel each other at different depths, with the highest heads recorded during the monsoon (August-September) and the lowest levels in March-April (Figure 4-S13a-b). In the shallow and intermediate aquifer, water levels average 4.1±0.2 (±1σ) and 2.5±0.8 above mean sea level respectively. Across all locations, the average vertical head differences between a pair of shallow and an intermediate wells from the same nest ranges between 1.3 and 2.8 m (n = 21) and averages 2±0.5 m (±1σ) in *clay-capped* sites such as S, SS, and M (Figure 4-4). The corresponding vertical head gradient across the confining unit varies from 0.03-0.07. In contrast, the average vertical head differences between a shallow and an intermediate well at sandy sites such as T and R ranges from 0.01 to 0.6 m (n = 7) and averages 0.3±0.2 m (Figure 4-5). These results indicate that water level in the intermediate aquifer decreases as a function of increasing thickness of the confining clay aquitard (Figure 4-S14).

Head data for the intermediate aquifer suggest groundwater flowing from sandy areas to the south towards the clay-capped areas to the north. The average hydraulic head along the south-north transect within the intermediate aquifer (52-59 m bgs) decreases from about 3.76 m at the sandy site well-T3 to 2.58 m at the 12 m thick clay-capped site well-M1-4a to 1.73 m at the 17 m clay capped site well-S2 (Figure 4-4, 4-5, Figure 4-2). Pressure transducer data indicate that the

138

groundwater level in the deep aquifer is declining at a rate of 0.5 m per year in the study area (Figure 4-S13c).

4.4.5. Groundwater flow modeling

The model reproduces the generalized local flow pattern under the influence of local and municipal pumping in Dhaka city (Figure 4-1b). Model-derived estimates indicate that Dhaka pumping induces a 1.2 m drop in average hydraulic head at 195 m depth in the study area, from -0.26 m amsl in the east to -1.45 m amsl in the west over a distance of 1.9 km (Figure 4-7b). The drop in head in the deep aquifer across the study area is propagated upward more effectively at the clay-capped sites compared to the sandy sites (Figure 4-7a). The highest simulated head observed in the intermediate aquifer (55 m bgs) at the recharge window site-T is 3.1 m amsl and matches the observations. The head drops by about 0.45 m at the clay-capped site-M (2.6 m amsl), 300 m north of site-T and by another 0.45 m at the clay-capped site-S (2.2 m amsl), 450 m north of site-M. Despite a westerly flow in the deep aquifer (Knappett et al., 2016; Khan et al., 2016), the local heterogeneity gives rise to a different local flow pattern in the intermediate aquifer.

The pre-pumping simulation results along the T-M-S transect indicates a head drop of only 0.13 m over a distance of 750 m, corresponding to a lateral gradient of 0.00017 between site-T and S, which is almost an order of magnitude lower than the simulated present day gradient of 0.0012. The predicted vertical head gradients across the confining unit under pre-pumping scenario are 0.009 and 0.013 at the clay-capped site-S and M, respectively. These results suggest that Dhaka

pumping has significantly increased the rate of lateral and vertical transport of groundwater As in the study area over the last half century.

4.5. Discussion

4.5.1. *Source of As and carbon in the intermediate aquifer*

Half of the 30 monitoring wells installed in the intermediate aquifer for this study were screened in gray sands and the other half in orange sands. With the exception of W4 (7.6 ug/L As) and B-CW (0.4 μg/L), the intermediate wells installed in gray sand contained >10 μg/L As. With again two exceptions, J2 and Q2 containing 10 and 39 μg/L As, respectively, intermediate wells installed in orange sand layers contain ≤5 μg/L As (Table 4-1). Although ^{3}H was detected (>0.1 TU) in 17 out of 30 monitoring wells screened between 41 and 72 m bgs (Table 4-2), no systematic relationship was observed between ^{3}H, As, and sand color across sites (Figure 4-S15). Therefore, recent recharge of shallow groundwater in portions of the intermediate aquifer is not directly associated with elevated As concentrations in the Pleistocene layers that were reduced and turned gray.

Previous studies have shown that the radiocarbon content of labile bacterial DNA and phospholipid fatty acids in shallow aquifers of the study area is much closer to that of groundwater DOC than to that of organic carbon in the sediment (Mailloux et al., 2013; Whaley-Martin, 2016). Despite their high TOC content (12-50%), the peat or charcoal fragments encountered in 42% (n = 33) of the boreholes (Figure 4-S4a) therefore do not appear to be the main source of reactive carbon. With the exception of one study (Dunnivant et al., 1992), most field observations suggest DOC is strongly adsorbed (Sengupta et al., 2008; Datta et al., 2011;

Mailloux et al., 2013). On the other hand, certain micro-organisms have more recently been shown to oxidize CH_4 while reducing Fe oxides in the absence of sulfate (Amos et al., 2012; Ettwig et al., 2016). Methane could therefore be an alternative source of reactive carbon that is transported at the rate of groundwater flow (Cahill, 2017).

Concentrations of As and CH_4 generally track each other in the intermediate aquifer of our study area (Figure 4-S15, Table 4-3). In the clay-capped intermediate aquifer at site-S, SS, and M nest of wells, high groundwater As is generally associated with elevated levels of CH_4 (Figure 4-4c, i, o). About 50% of the wells tapping the gray Pleistocene sediment contain elevated levels of CH_4 (>200-1,239 μmol/L) with the exception of 3 installed in sandy sites. All wells tapping the orange Pleistocene aquifer contain very low levels of CH_4 (<60 μmol/L). The depleted $\delta^{13}C$-CH_4 (<-58±5‰) and δ^2H-CH_4 are typical of biogenic CH_4 (Fuex, 1977; Whiticar & Faber, 1986 Simpkin & Parkin, 1993). The association of As relative to 10 μg/L, CH_4 relative to 100 μmol/L, and sand color relative to a 0.5% reflectance difference suggest microbially-mediated anaerobic oxidation of CH_4 by Fe oxides may have contributed to the release As to the intermediate aquifer (Figure 4-S15).

4.5.2. *Reduction of Fe oxides by lateral advection of reactive carbon*

The inter-fingering of gray and orange sediment in the Pleistocene aquifer is an indication that layers that were once oxidized were probably reduced due to lateral advection of reactive carbon with groundwater. For instance, sites S, SS, and 8 other similar sites drilled in their vicinity indicate a high As (measured at 2 sites) gray portion of the aquifer sandwiched between two layers of orange sand (Figure 4-4 & 4-S4). We cannot rule out an alternation in preservation of

orange, gray, followed again by orange sands over time but lateral advection of high As and DOC water that reduced an originally orange sand layer provides a simpler explanation, as previously proposed for a different setting (van Geen et al., 2013).

Under the current pumping scenario, the model predicts a time frame of 30 and 50 years for recently recharged groundwater near the sandy site-T to reach the clay-capped monitoring nests at sites M and S (Figure 4-8b) along the predominant south-north flow path. Detectable levels of ^{3}H were measured in 8 of the 11 analyzed intermediate monitoring wells at sites T, M, SS, and S (Figure 4-8a). There is no systematic relation between groundwater ages measured by the ^{3}H/^{3}He method and the distance from the recharge window traveled by groundwater. However, the estimated ages tend to be younger near sandy sites T and R (Figure 4-6a, Table 4-2). A number of groundwater samples with >10 µg/L As in the intermediate aquifer could not be dated because they did not contain ^{3}H. Of the 4 samples with >10 µg/L As that could be dated (S1, S2, R1, T3), only S1 shows a clear indication of mixing with older groundwater (Figure 4-S11). This suggests even if the release of As in the intermediate aquifer is not linked to recharge, it was associated with fairly recent and rapid plug flow. In comparison, the pre-pumping scenario predicts 300-500 years for groundwater from groundwater to travel across the same distance from Site T to Site S (Figure 4-8d).

Numerous incubation studies have shown that, even without lateral transport of As, the reduction of orange sands would be sufficient to raise As concentrations to the observed level (van Geen et al., 2004; Dhar et al., 2011). In addition, most studies show that As is significantly retarded relative to groundwater flow by adsorption to aquifer sands, even reduced gray sands (DPHE and

142

BGS, 2001; Harvey et al., 2002; Swartz et al., 2004; Stollenwerk et al., 2007; van Geen et al., 2008; McArthur et al., 2008; McArthur et al., 2010; McArthur et al., 2011; Robinson et al., 2011; Itai et al., 2010; Radloff et al., 2011; Jung et al., 2012; van Geen et al., 2013; Hoa Mai et al., 2014; Radloff et al., 2015). The model is consistent with local release of As within the Pleistocene aquifer instead of advection from the shallow aquifer. For a retardation factor of 10, the relative As concentration front (C/C_0) of 0.1 within the intermediate aquifer extends a maximum distance of 200 m north of the recharge area in 50 years (Figure 4-9b). For a retardation of 30, which is more consistent with adsorption experiments conducted in the field (Chapter 2 of this dissertation), a shallow source of As to the intermediate aquifer is even less likely (Figure 4-9c). Under the pre-pumping scenario, the distribution of As observed today in the intermediate aquifer can be reproduced along the same transect if the model is run forward for 200-400 years, depending on retardation factor (Figure 4-10).

The proportion of intermediate aquifer (>40-80 m bgs) that would be As contaminated ($C/C_0 \geq 0.1$) after a century of pumping is estimated to be 10% for a retardation factor of 10 (Figure 4-11). The simulations in three-dimensional space indicate that the plume of As would migrate downward through sandy recharge areas and would continue to propagate laterally in the semi-confined intermediate aquifer. Intermediate wells near recharge windows are more vulnerable to the lateral intrusion of As from the shallow aquifer along the margins of the clay. Arsenic concentrations in wells that are further away from the recharge windows would more likely be controlled by a local supply of reactive carbon.

4.5.3. Reduction of Fe oxides by advection and diffusion of clay derived DOC

Clay pore water contains 1 order of magnitude higher DOC level compared to the <1-4 mg/L DOC concentration in the intermediate aquifer (Figure 4-4b,n). The field observations therefore suggest vertical leakage of DOC as an alternative mechanism to lateral advection for reducing orange aquifer sands. The advective flux of groundwater and carbon from the shallow aquifer has increased by an order of magnitude due to Dhaka pumping. In the absence of Dhaka pumping, the downward transport of reactive DOC could potentially have occurred by molecular diffusion (Desaulniers et al., 1981, 1986; Hendry & Wassenaar, 2000; Hendry et al., 2003). In that case, the pattern of grey Pleistocene sands could be the result of slow redox transformations over the course of the Holocene (Figure 4-7, 4-9). Simple calculations of both transport processes in one dimension suggest that the impact of Dhaka pumping on the advective flux of reactive carbon from the clay layer is comparable to that for the diffusive flux. However, the estimated flux of reactive carbon for each process can only convert about 0.01 cm thick orange sand to gray sand each year (**See Supplementary discussion**).

The thickness of the gray, reduced portion of the aquifer immediately underlying the gray clay aquitard at site-M, SS and its 22 analogs vary between 1 and 24 m in the study area, averaging 8±6 m (Figure 4-S4a). Therefore, the average of 8 m thick intermediate aquifer in contact with clay is unlikely to have been reduced by a downward flux of DOC from a single depth. The observations could instead reflect a downward flux of DOC causing reduction of Fe oxides combined with lateral flow below a clay layer whose depth varies considerably from one site to the other (Figure 4-S4a).

144

4.5.4. Evolution of groundwater composition in the face of pumping

A combination of mechanisms appears to be required to explain the observed evolution of groundwater chemistry in the intermediate aquifer of the study area. The hydrology has evolved since the expansion of Dhaka drawdown cone, resulting in a distinct magnification of lateral and vertical head gradients driven by heterogeneity in the local geology. Both lateral and vertical intrusion of shallow groundwater in portions of the intermediate aquifer is evident based on isotopic signature of ^{3}H, δ^{18}O, and δ^2H (Figure 4-4, 4-5). While the vertical intrusion of shallow groundwater elevated in DOC (from clay) partially explain the reduction and rise of As in the upper gray portion of the Pleistocene aquifer, lateral migration of As, DOC, and/or CH_4 has to be invoked to explain elevated As concentrations in gray sand layers that are sandwiched between orange sand.

It is not entirely clear why the rise in groundwater As at some of the sites is more rapid at some sites than at others (Figure 4-6). The three fold difference in the magnitude of increases in As concentrations at well M1-4 (16 μg/L per year) and well-B5 (6 μg/L per year) may well be connected to the variation in advective/diffusive fluxes of groundwater. The thickness of clay and the vertical head gradient estimated across the clay at site-M is almost three times greater than that at site-B. The vertical (advective) flux at the bottom of the clay at site-M introduces 0.5 L of groundwater per square meter per year, which is about three fold higher than that at site B (0.2 L) for a K_v of 9×10^{-11} m/sec. Finally, the model estimated lateral flux of groundwater estimated at the screened depth for well-M1-4 is about 3 times higher than that at well B5. These site-specific estimates suggest that accelerated fluxes of groundwater may enhance the supply of reactive carbon and increase As concentrations over time. The third well with elevated levels of

DOC (4 mg/L) and CH$_4$ (90±5 μmol/L) at site-T that also showed a rapid increase in groundwater As over the past 3 years (Figure 4-5a-c; 4-6b) might have been impacted by its proximity to a peat layer.

4.6. Conclusion

This detailed study based on direct field observations and modeling in small area of Bangladesh provides sheds new light on the way local groundwater flow patterns can affect groundwater composition in response to pumping. The inferred reduction of intermediate aquifer sands from Fe (III)-dominated orange to Fe(II)-dominated grey that leads to the release of As to groundwater probably started several thousand years ago but has been accelerated by Dhaka pumping (Figure 4-8, 4-9, 4-10). Slow, diffused flux of DOC from clay and other organic rich sediments probably conditioned the aquifer over longer geologic time scales. The relative contribution of the natural downward flow of DOC from clay layers and accelerated flow of lateral CH$_4$ is not fully resolved. What is clear is that the intermediate aquifers tapped by a growing number of private households to reduce their exposure to As over the past decade (Figure 4-S1) is vulnerable and needs to be closely monitored. The risks of promoting private well installations to lower As exposure relative to government funding of a smaller number of public deep wells therefore need to be carefully weighed.

Acknowledgements

4.7. References

Ahmed K. M. (2011) Groundwater contamination in Bangladesh. In *Water Resources Planning and Management* (eds. K. Hussey and R. Q. Grafton). Cambridge University Press, Cambridge. pp. 529–560. Available at: https://www.cambridge.org/core/books/water-resources-planning-and-management/groundwater-contamination-in-bangladesh/78D816AC68854C29717A4A735052EC74.

Ahmed K. M., Bhattacharya P., Hasan M. A., Akhter S. H., Alam S. M. M., Bhuyian M. A. H., Imam M. B., Khan A. A. and Sracek O. (2004) Arsenic enrichment in groundwater of the alluvial aquifers in Bangladesh: an overview. *Appl. Geochem.* **19**, 181–200.

Ahmed K. M., Hasan M. K., Burgess W. G., Dottridge J., Ravenscroft P. and van Wonderen J. (1999) The Dupi Tila aquifer of Dhaka, Bangladesh: hydraulic and hydrochemical response to intensive exploitation. In *Groundwater in the urban environment: selected city profiles.* (ed. P. J. Chilton). Balkema, Rotterdam. pp. 19–30. Available at: http://discovery.ucl.ac.uk/169447/ [Accessed October 19, 2018].

Ahmed K. M., Hoque M., Hasan M. K., Ravenscroft P. and Chowdhury L. R. (1998a) Occurrence and origin of water well methane gas in Bangladesh. *J. Geol. Soc. India* **51**, 697–708.

Ahmed K. M., Imam M. N., Akhter S. H., Hasan M. A., Alam M. M., Chowdhury S. Q., Burgess W. G., Nickson R., McArthur J. M., Hasan M. K., Ravenscroft P. and Rahman M. (1998b) Mechanism of arsenic release to groundwater: geochemical and mineralogical evidence. In International Conference on Arsenic Pollution on Groundwater in Bangladesh: Causes, Effects, and Remedies. Dhaka Community Hospital, Dhaka, Bangladesh.

Ahmed M. F., Ahuja S., Alauddin M., Hug S. J., Lloyd J. R., Pfaff A., Pichler T., Saltikov C., Stute M. and Geen A. van (2006) Ensuring Safe Drinking Water in Bangladesh. *Science* **314**, 1687–1688.

Ahsan H., Chen Y., Parvez F., Argos M., Hussain A. I., Momotaj H., Levy D., Geen A. van, Howe G. and Graziano J. (2006) Health Effects of Arsenic Longitudinal Study (HEALS): Description of a multidisciplinary epidemiologic investigation. *J. Expo. Sci. Environ. Epidemiol.* **16**, 191–205.

Amos R. T., Bekins B. A., Cozzarelli I. M., Voytek M. A., Kirshtein J. D., Jones E. J. P. and Blowes D. W. (2012) Evidence for iron-mediated anaerobic methane oxidation in a crude oil-contaminated aquifer. *Geobiology* **10**, 506–517.

Aravena R., Wassenaar L. I. and Plummer L. N. (1995) Estimating 14C Groundwater Ages in a Methanogenic Aquifer. *Water Resour. Res.* **31**, 2307–2317.

Aravena R., Wassenaar L. I. and Spiker E. C. (2004) Chemical and carbon isotopic composition of dissolved organic carbon in a regional confined methanogenic aquifer. *Isotopes Environ. Health Stud.* **40**, 103–114.

Bayer R., Schlosser P., Bönisch G., Rupp H., Zaucker F. and Zimmek G. (1989) *Performance and Blank Components of a Mass Spectrometric System for Routine Measurement of Helium Isotopes and Tritium by the 3He Ingrowth Method: Vorgelegt in der Sitzung vom 1. Juli 1989 von Otto Haxel.*, Springer-Verlag, Berlin Heidelberg. Available at: //www.springer.com/us/book/9783540517108 [Accessed July 31, 2018].

Berg M., Tran H. C., Nguyen T. C., Pham H. V., Schertenleib R. and Giger W. (2001) Arsenic Contamination of Groundwater and Drinking Water in Vietnam: A Human Health Threat. *Environ. Sci. Technol.* **35**, 2621–2626.

Bhattacharya P., Chatterjee D. and Jacks G. (1997) Occurrence of Arsenic-contaminated Groundwater in Alluvial Aquifers from Delta Plains, Eastern India: Options for Safe Drinking Water Supply. *Int. J. Water Resour. Dev.* **13**, 79–92.

von Brömssen M., Jakariya M., Bhattacharya P., Ahmed K. M., Hasan M. A., Sracek O., Jonsson L., Lundell L. and Jacks G. (2007) Targeting low-arsenic aquifers in Matlab Upazila, Southeastern Bangladesh. *Sci. Total Environ.* **379**, 121–132.

von Brömssen M., Markussen L., Bhattacharya P., Ahmed K. M., Hossain M., Jacks G., Sracek O., Thunvik R., Hasan M. A., Islam M. M. and Rahman M. M. (2014) Hydrogeological investigation for assessment of the sustainability of low-arsenic aquifers as a safe drinking water source in regions with high-arsenic groundwater in Matlab, southeastern Bangladesh. *J. Hydrol.* **518**, 373–392.

Burgess W. G., Hoque M. A., Michael H. A., Voss C. I., Breit G. N. and Ahmed K. M. (2010) Vulnerability of deep groundwater in the Bengal Aquifer System to contamination by arsenic. *Nat. Geosci.* **3**, 83–87.

Cahill A. G., Steelman C. M., Forde O., Kuloyo O., Ruff S. E., Mayer B., Mayer K. U., Strous M., Ryan M. C., Cherry J. A. and Parker B. L. (2017) Mobility and persistence of methane in groundwater in a controlled-release field experiment. *Nat. Geosci.* **10**, 289–294.

Chapelle F. H. and McMahon P. B. (1991) Geochemistry of dissolved inorganic carbon in a Coastal Plain aquifer. 1. Sulfate from confining beds as an oxidant in microbial CO2 production. *J. Hydrol.* **127**, 85–108.

149

Chapelle F. H., Zelibor J. L., Grimes D. J. and Knobel L. L. (1987) Bacteria in deep coastal plain sediments of Maryland: A possible source of CO2 to groundwater. *Water Resour. Res.* **23**, 1625–1632.

Cheng Z., Zheng Y., Mortlock R. and Geen A. van (2004) Rapid multi-element analysis of groundwater by high-resolution inductively coupled plasma mass spectrometry. *Anal. Bioanal. Chem.* **379**, 512–518.

Choudhury I., Ahmed K. M., Hasan M., Mozumder M. R. H., Knappett P. S. K., Ellis T. and van Geen A. (2016) Evidence for Elevated Levels of Arsenic in Public Wells of Bangladesh Due To Improper Installation. *Groundwater* **54**, 871–877.

Crum R. H., Murphy E. M. and Keller C. K. (1996) A non-adsorptive method for the isolation and fractionation of natural dissolved organic carbon. *Water Res.* **30**, 1304–1311.

Datta S., Neal A. W., Mohajerin T. J., Ocheltree T., Rosenheim B. E., White C. D. and Johannesson K. H. (2011) Perennial ponds are not an important source of water or dissolved organic matter to groundwaters with high arsenic concentrations in West Bengal, India. *Geophys. Res. Lett.* **38**, L20404.

Desaulniers D. E., Cherry J. A. and Fritz P. (1981) Origin, age and movement of pore water in argillaceous Quaternary deposits at four sites in southwestern Ontario. *J. Hydrol.* **50**, 231–257.

Desaulniers D. E., Kaufmann R. S., Cherry J. A. and Bentley H. W. (1986) 37Cl-35Cl variations in a diffusion-controlled groundwater system. *Geochim. Cosmochim. Acta* **50**, 1757–1764.

Desbarats A. J., Koenig C. E. M., Pal T., Mukherjee P. K. and Beckie R. D. (2014) Groundwater flow dynamics and arsenic source characterization in an aquifer system of West Bengal, India. *Water Resour. Res.* **50**, 4974–5002.

Desbarats A. J., Pal T., Mukherjee P. K. and Beckie R. D. (2017) Geochemical Evolution of Groundwater Flowing Through Arsenic Source Sediments in an Aquifer System of West Bengal, India. *Water Resour. Res.* **53**, 8715–8735.

Dhar R. K., Zheng Y., Saltikov C. W., Radloff K. A., Mailloux B. J., Ahmed K. M. and van Geen A. (2011) Microbes Enhance Mobility of Arsenic in Pleistocene Aquifer Sand from Bangladesh. *Environ. Sci. Technol.* **45**, 2648–2654.

Dhar R. K., Zheng Y., Stute M., van Geen A., Cheng Z., Shanewaz M., Shamsudduha M., Hoque M. A., Rahman M. W. and Ahmed K. M. (2008) Temporal variability of groundwater

chemistry in shallow and deep aquifers of Araihazar, Bangladesh. *J. Contam. Hydrol.* **99**, 97–111.

Diamond S. (1970) Pore Size Distributions in Clays. *Clays Clay Miner.* **18**, 7–23.

DPHE and BGS (2001) *Arsenic contamination of groundwater in Bangladesh.*, BGS, Keyworth.

Dunnivant F. M., Jardine P. M., Taylor D. L. and McCarthy J. F. (1992) Transport of Naturally Occurring Dissolved Organic Carbon in Laboratory Columns Containing Aquifer Material. *Soil Sci. Soc. Am. J.* **56**, 437–444.

Elder K. L., McNichol A. P. and Gagnon A. R. (1998) Reproducibility of seawater, inorganic and organic carbon 14C results at NOSAMS. *Radiocarbon* **40**, 223–230.

Erban L. E., Gorelick S. M., Zebker H. A. and Fendorf S. (2013) Release of arsenic to deep groundwater in the Mekong Delta, Vietnam, linked to pumping-induced land subsidence. *Proc. Natl. Acad. Sci.* **110**, 13751–13756.

Erickson M. L. and Barnes R. J. (2005) Well characteristics influencing arsenic concentrations in ground water. *Water Res.* **39**, 4029–4039.

Ettwig K. F., Zhu B., Speth D., Keltjens J. T., Jetten M. S. M. and Kartal B. (2016) Archaea catalyze iron-dependent anaerobic oxidation of methane. *Proc. Natl. Acad. Sci.* **113**, 12792–12796.

Famiglietti J. S. (2014) The global groundwater crisis. *Nat. Clim. Change*. Available at: https://www.nature.com/articles/nclimate2425 [Accessed October 19, 2018].

Fendorf S., Michael H. A. and Geen A. van (2010) Spatial and Temporal Variations of Groundwater Arsenic in South and Southeast Asia. *Science* **328**, 1123–1127.

Fuex A. N. (1977) The use of stable carbon isotopes in hydrocarbon exploration. *J. Geochem. Explor.* **7**, 155–188.

Gelman A., Trevisani M., Lu H. and van Geen A. (2004) Direct data manipulation for local decision analysis as applied to the problem of arsenic in drinking water from tube wells in Bangladesh. *Risk Anal* **24**, 1597–612.

Goodbred Jr S. L. and Kuehl S. A. (2000) The significance of large sediment supply, active tectonism, and eustasy on margin sequence development: Late Quaternary stratigraphy and evolution of the Ganges–Brahmaputra delta. *Sediment. Geol.* **133**, 227–248.

Graham P. W., Baker A. and Andersen M. S. (2015) Dissolved Organic Carbon Mobilisation in a Groundwater System Stressed by Pumping. *Sci. Rep.* **5**, 18487.

Harbaugh A. W. (2005) *MODFLOW-2005, The U.S. Geological Survey Modular Ground-Water Model—the Ground-Water Flow Process.*, U.S. Geological Survey.

Harvey C. F., Ashfaque K. N., Yu W., Badruzzaman A. B. M., Ali M. A., Oates P. M., Michael H. A., Neumann R. B., Beckie R., Islam S. and Ahmed M. F. (2006) Groundwater dynamics and arsenic contamination in Bangladesh. *Chem. Geol.* **228**, 112–136.

Harvey C. F., Swartz C. H., Badruzzaman A. B., Keon-Blute N., Yu W., Ali M. A., Jay J., Beckie R., Niedan V., Brabander D., Oates P. M., Ashfaque K. N., Islam S., Hemond H. F. and Ahmed M. F. (2002) Arsenic mobility and groundwater extraction in Bangladesh. *Science* **298**, 1602–6.

Hendry M. J., Ranville J. R., Boldt-Leppin B. E. J. and Wassenaar L. I. (2003) Geochemical and transport properties of dissolved organic carbon in a clay-rich aquitard. *Water Resour. Res.* **39**. Available at: https://agupubs.onlinelibrary.wiley.com/doi/abs/10.1029/2002WR001943 [Accessed September 4, 2018].

Hendry M. J. and Schwartz F. W. (1990) The Chemical Evolution of Ground Water in the Milk River Aquifer, Canada. *Groundwater* **28**, 253–261.

Hendry M. J. and Wassenaar L. I. (2000) Controls on the distribution of major ions in pore waters of a thick surficial aquitard. *Water Resour. Res.* **36**, 503–513.

Hendry M. J. and Wassenaar L. I. (2005) Origin and migration of dissolved organic carbon fractions in a clay-rich aquitard: 14C and δ13C evidence. *Water Resour. Res.* **41**. Available at: https://agupubs.onlinelibrary.wiley.com/doi/abs/10.1029/2004WR003157 [Accessed September 6, 2018].

Hoque M. A. and Burgess W. G. (2012) 14C dating of deep groundwater in the Bengal Aquifer System, Bangladesh: Implications for aquifer anisotropy, recharge sources and sustainability. *J. Hydrol.* **444**, 209–220.

Hoque M. A., Burgess W. G. and Ahmed K. M. (2017) Integration of aquifer geology, groundwater flow and arsenic distribution in deltaic aquifers – A unifying concept. *Hydrol. Process.* **31**, 2095–2109.

Hoque M. A., Burgess W. G., Shamsudduha M. and Ahmed K. M. (2011) Delineating low-arsenic groundwater environments in the Bengal Aquifer System, Bangladesh. *Appl. Geochem.* **26**, 614–623.

Hoque M., Hoque M. M. and Ahmed K. (2007) Declining groundwater level and aquifer dewatering in Dhaka metropolitan area, Bangladesh: causes and quantification. *Hydrogeol. J.* **15**, 1523–1534.

Horneman A., Van Geen A., Kent D. V., Mathe P. E., Zheng Y., Dhar R. K., O'Connell S., Hoque M. A., Aziz Z., Shamsudduha M., Seddique A. A. and Ahmed K. M. (2004) Decoupling of As and Fe release to Bangladesh groundwater under reducing conditions. Part 1: Evidence from sediment profiles. *Geochim. Cosmochim. Acta* **68**, 3459–3473.

Hossain M., Bhattacharya P., Frape S. K., Jacks G., Islam M. M., Rahman M. M., von Brömssen M., Hasan M. A. and Ahmed K. M. (2014) Sediment color tool for targeting arsenic-safe aquifers for the installation of shallow drinking water tubewells. *Sci. Total Environ.* **493**, 615–625.

Huang K., Liu Y., Yang C., Duan Y., Yang X. and Liu C. (2018) Identification of Hydrobiogeochemical Processes Controlling Seasonal Variations in Arsenic Concentrations Within a Riverbank Aquifer at Jianghan Plain, China. *Water Resour. Res.* **54**, 4294–4308.

Islam F. S., Gault A. G., Boothman C., Polya D. A., Charnock J. M., Chatterjee D. and Lloyd J. R. (2004) Role of metal-reducing bacteria in arsenic release from Bengal delta sediments. *Nature* **430**, 68–71.

Itai T., Takahashi Y., Seddique A. A., Maruoka T. and Mitamura M. (2010) Variations in the redox state of As and Fe measured by X-ray absorption spectroscopy in aquifers of Bangladesh and their effect on As adsorption. *Appl. Geochem.* **25**, 34–47.

IWM and DWASA (2011) *Establishment of Groundwater Monitoring System in Dhaka City for Aquifer Systems and DWASA Production Wells, Draft Final Report.*, Institute of Water Modeling and Dhaka Water Supply and Sewerage Authority, Dhaka.

Jung H. B., Bostick B. C. and Zheng Y. (2012) Field, Experimental, and Modeling Study of Arsenic Partitioning across a Redox Transition in a Bangladesh Aquifer. *Environ. Sci. Technol.* **46**, 1388–1395.

Jusseret S., Tam V. T. and Dassargues A. (2009) Groundwater flow modelling in the central zone of Hanoi, Vietnam. *Hydrogeol. J.* **17**, 915–934.

Khan M. R., Koneshloo M., Knappett P. S. K., Ahmed K. M., Bostick B. C., Mailloux B. J., Mozumder R. H., Zahid A., Harvey C. F., Geen A. van and Michael H. A. (2016) Megacity pumping and preferential flow threaten groundwater quality. *Nat. Commun.* **7**, 12833.

Klump S., Kipfer R., Cirpka O. A., Harvey C. F., Brennwald M. S., Ashfaque K. N., Badruzzaman A. B. M., Hug S. J. and Imboden D. M. (2006) Groundwater Dynamics and Arsenic Mobilization in Bangladesh Assessed Using Noble Gases and Tritium. *Environ. Sci. Technol.* **40**, 243–250.

Knappett P. S. K., Mailloux B. J., Choudhury I., Khan M. R., Michael H. A., Barua S., Mondal D. R., Steckler M. S., Akhter S. H., Ahmed K. M., Bostick B., Harvey C. F., Shamsudduha M., Shuai P., Mihajlov I., Mozumder R. and van Geen A. (2016) Vulnerability of low-arsenic aquifers to municipal pumping in Bangladesh. *J. Hydrol.* **539**, 674–686.

Konikow L. F. and Kendy E. (2005) Groundwater depletion: A global problem. *Hydrogeol. J.* **13**, 317–320.

Krumholz L. R., McKinley J. P., Ulrich G. A. and Suflita J. M. (1997) Confined subsurface microbial communities in Cretaceous rock. *Nature* **386**, 64–66.

Lapworth D. J., Zahid A., Taylor R. G., Burgess W. G., Shamsudduha M., Ahmed K. M., Mukherjee A., Gooddy D. C., Chatterjee D. and MacDonald A. M. (2018) Security of Deep Groundwater in the Coastal Bengal Basin Revealed by Tracers. *Geophys. Res. Lett.* **45**, 8241–8252.

Lawson M., Polya D. A., Boyce A. J., Bryant C., Mondal D., Shantz A. and Ballentine C. J. (2013) Pond-Derived Organic Carbon Driving Changes in Arsenic Hazard Found in Asian Groundwaters. *Environ. Sci. Technol.*, 130620151836005.

Leenheer J. (1974) Occurrence of dissolved organic carbon in selected groundwater samples in the United States. *US Geol. Surv. J. Res.*, 361–369.

Lovley D. R., Chapelle F. H. and Phillips E. J. P. (1990) Fe(III)-reducing bacteria in deeply buried sediments of the Atlantic Coastal Plain. *Geology* **18**, 954–957.

Ludin A., Weppernig R., Bönisch G. and Schlosser P. (1998) Mass spectrometric measurement of helium isotopes and tritium in water samples. , 41.

MacDonald A. M., Bonsor H. C., Ahmed K. M., Burgess W. G., Basharat M., Calow R. C., Dixit A., Foster S. S. D., Gopal K., Lapworth D. J., Lark R. M., Moench M., Mukherjee A., Rao M. S., Shamsudduha M., Smith L., Taylor R. G., Tucker J., Steenbergen F. van and Yadav S. K. (2016) Groundwater quality and depletion in the Indo-Gangetic Basin mapped from *in situ* observations. *Nat. Geosci.* **9**, 762–766.

Mailloux B. J., Trembath-Reichert E., Cheung J., Watson M., Stute M., Freyer G. A., Ferguson A. S., Ahmed K. M., Alam M. J., Buchholz B. A., Thomas J., Layton A. C., Zheng Y.,

Bostick B. C. and van Geen A. (2013) Advection of surface-derived organic carbon fuels microbial reduction in Bangladesh groundwater. *Proc. Natl. Acad. Sci.* **110**, 5331–5335.

Manheim F. T. (1966) A Hydraulic Squeezer for Obtaining Interstitial Water from Consolidated and Unconsolidated Sediments. *US Geol. Surv. Prof. Pap.* **550.C**, 256–261.

McArthur J. M., Banerjee D. M., Hudson-Edwards K. A., Mishra R., Purohit R., Ravenscroft P., Cronin A., Howarth R. J., Chatterjee A., Talukder T., Lowry D., Houghton S. and Chadha D. K. (2004) Natural organic matter in sedimentary basins and its relation to arsenic in anoxic ground water: the example of West Bengal and its worldwide implications. *Appl. Geochem.* **19**, 1255–1293.

McArthur J. M., Banerjee D. M., Sengupta S., Ravenscroft P., Klump S., Sarkar A., Disch B. and Kipfer R. (2010) Migration of As, and 3H/3He ages, in groundwater from West Bengal: Implications for monitoring. *Water Res.* **44**, 4171–4185.

McArthur J. M., Ghosal U., Sikdar P. K. and Ball J. D. (2016) Arsenic in Groundwater: The Deep Late Pleistocene Aquifers of the Western Bengal Basin. *Environ. Sci. Technol.* **50**, 3469–3476.

McArthur J. M., Nath B., Banerjee D. M., Purohit R. and Grassineau N. (2011) Palaeosol Control on Groundwater Flow and Pollutant Distribution: The Example of Arsenic. *Environ. Sci. Technol.* **45**, 1376–1383.

McArthur J. M., Ravenscroft P., Banerjee D. M., Milsom J., Hudson-Edwards K. A., Sengupta S., Bristow C., Sarkar A., Tonkin S. and Purohit R. (2008) How paleosols influence groundwater flow and arsenic pollution: A model from the Bengal Basin and its worldwide implication. *Water Resour. Res.* **44**, W11411.

McArthur J. M., Ravenscroft P., Safiulla S. and Thirlwall M. F. (2001) Arsenic in groundwater: Testing pollution mechanisms for sedimentary aquifers in Bangladesh. *Water Resour. Res.* **37**, 109–117.

McMahon P. (2001) Aquifer/aquitard interfaces: mixing zones that enhance biogeochemical reactions. *Hydrogeol. J.* **9**, 34–43.

McMahon P. B. and Chapelle F. H. (1991) Microbial production of organic acids in aquitard sediments and its role in aquifer geochemistry. *Nature* **349**, 233–235.

Michael H. A. and Khan M. R. (2016) Impacts of physical and chemical aquifer heterogeneity on basin-scale solute transport: Vulnerability of deep groundwater to arsenic contamination in Bangladesh. *Adv. Water Resour.* **98**, 147–158.

Michael H. A. and Voss C. I. (2009) Controls on groundwater flow in the Bengal Basin of India and Bangladesh: regional modeling analysis. *Hydrogeol. J.* **17**, 1561.

Michael H. A. and Voss C. I. (2008) Evaluation of the sustainability of deep groundwater as an arsenic-safe resource in the Bengal Basin. *Proc. Natl. Acad. Sci.* Available at: http://www.pnas.org/content/early/2008/06/16/0710477105 [Accessed March 31, 2014].

Mihajlov I., Stute M., Schlosser P., Mailloux B. J., Zheng Y., Choudhury I., Ahmed K. M. and van Geen A. (2016) Recharge of low-arsenic aquifers tapped by community wells in Araihazar, Bangladesh, inferred from environmental isotopes. *Water Resour. Res.* **52**, 3324–3349.

Mihajlov I., Mozumder M.R.H., Bostick B.C., Stute M., Mailloux B., Knappett P.S.K., Choudhury I., Ahmed K.M., Schosser P., & van Geen A.*. Arsenic contamination of Bangladesh aquifers exacerbated by clay layers (in prep.).

Morgan J. P. and McINTIRE W. G. (1959) QUATERNARY GEOLOGY OF THE BENGAL BASIN, EAST PAKISTAN AND INDIA. *Geol. Soc. Am. Bull.* **70**, 319.

Mukherjee A., Fryar A. E., Scanlon B. R., Bhattacharya P. and Bhattacharya A. (2011) Elevated arsenic in deeper groundwater of the western Bengal basin, India: Extent and controls from regional to local scale. *Appl. Geochem.* **26**, 600–613.

Neumann R. B., Ashfaque K. N., Badruzzaman A. B. M., Ashraf Ali M., Shoemaker J. K. and Harvey C. F. (2010) Anthropogenic influences on groundwater arsenic concentrations in Bangladesh. *Nat. Geosci* **3**, 46–52.

Nickson R., McArthur J., Burgess W., Ahmed K. M., Ravenscroft P. and Rahman M. (1998) Arsenic poisoning of Bangladesh groundwater. *Nature* **395**, 338.

Olson G. J., Dockins W. S., McFeters G. A. and Iverson W. P. (1981) Sulfate-reducing and methanogenic bacteria from deep aquifers in montana. *Geomicrobiol. J.* **2**, 327–340.

Oremland R. S. and Stolz J. F. (2005) Arsenic, microbes and contaminated aquifers. *Trends Microbiol.* **13**, 45–49.

Oremland R. S. and Stolz J. F. (2003) The Ecology of Arsenic. *Science* **300**, 939–944.

Pickering J. L., Goodbred S. L., Reitz M. D., Hartzog T. R., Mondal D. R. and Hossain M. S. (2014) Late Quaternary sedimentary record and Holocene channel avulsions of the Jamuna and Old Brahmaputra River valleys in the upper Bengal delta plain. *Geomorphology* **227**, 123–136.

Polizzotto M. L., Harvey C. F., Sutton S. R. and Fendorf S. (2005) Processes conducive to the release and transport of arsenic into aquifers of Bangladesh. *Proc. Natl. Acad. Sci. U. S. A.* **102**, 18819–18823.

Polizzotto M. L., Kocar B. D., Benner S. G., Sampson M. and Fendorf S. (2008) Near-surface wetland sediments as a source of arsenic release to ground water in Asia. *Nature* **454**, 505–508.

Pollock D. W. (2012) *User Guide for MODPATH Version 6 - A Particle-Tracking Model for MODFLOW.*, USGS.

Radloff K. A., Zheng Y., Michael H. A., Stute M., Bostick B. C., Mihajlov I., Bounds M., Huq M. R., Choudhury I., Rahman M. W., Schlosser P., Ahmed K. M. and van Geen A. (2011) Arsenic migration to deep groundwater in Bangladesh influenced by adsorption and water demand. *Nat. Geosci.* **4**, 793–798.

Radloff K. A., Zheng Y., Stute M., Weinman B., Bostick B., Mihajlov I., Bounds M., Rahman M. M., Huq M. R., Ahmed K. M., Schlosser P. and van Geen A. (2015) Reversible adsorption and flushing of arsenic in a shallow, Holocene aquifer of Bangladesh. *Appl. Geochem.* Available at: http://www.sciencedirect.com/science/article/pii/S0883292715300706 [Accessed October 23, 2016].

Ravenscroft P., Brammer H. and Richards K. (2009) *Arsenic Pollution: a global synthesis.*, Wiley-Blackwell. Available at: http://dx.doi.org/10.1002/9781444308785.ch1.

Ravenscroft P., Kabir A., Hakim S. A. I., Ibrahim A. K. M., Ghosh S. K., Rahman M. S., Akhter F. and Sattar M. A. (2014) Effectiveness of public rural waterpoints in Bangladesh with special reference to arsenic mitigation. *J. Water Sanit. Hyg. Dev.* **4**, 545–562.

Ravenscroft P., McArthur J. M. and Hoque M. A. (2013) Stable groundwater quality in deep aquifers of Southern Bangladesh: The case against sustainable abstraction. *Sci. Total Environ.* **454–455**, 627–638.

Ravenscroft P., McArthur J. M. and Rahman M. S. (2018) Identifying multiple deep aquifers in the Bengal Basin: Implications for resource management. *Hydrol. Process.* **32**, 3615–3632.

Robinson C., Brömssen M. von, Bhattacharya P., Häller S., Bivén A., Hossain M., Jacks G., Ahmed K. M., Hasan M. A. and Thunvik R. (2011) Dynamics of arsenic adsorption in the targeted arsenic-safe aquifers in Matlab, south-eastern Bangladesh: Insight from experimental studies. *Appl. Geochem.* **26**, 624–635.

Rotiroti M., Sacchi E., Fumagalli L. and Bonomi T. (2014) Origin of Arsenic in Groundwater from the Multilayer Aquifer in Cremona (Northern Italy). *Environ. Sci. Technol.* **48**, 5395–5403.

Sahu P., Michael H. A., Voss C. I. and Sikdar P. K. (2013) Impacts on groundwater recharge areas of megacity pumping: analysis of potential contamination of Kolkata, India, water supply. *Hydrol. Sci. J.* **58**, 1340–1360.

Sengupta S., McArthur J. M., Sarkar A., Leng M. J., Ravenscroft P., Howarth R. J. and Banerjee D. M. (2008) Do Ponds Cause Arsenic-Pollution of Groundwater in the Bengal Basin? An Answer from West Bengal. *Environ. Sci. Technol.* **42**, 5156–5164.

Shamsudduha M., Taylor R. G., Ahmed K. M. and Zahid A. (2011) The impact of intensive groundwater abstraction on recharge to a shallow regional aquifer system: evidence from Bangladesh. *Hydrogeol. J.* **19**, 901–916.

Shamsudduha M., Taylor R. G. and Chandler R. E. (2015) A generalized regression model of arsenic variations in the shallow groundwater of Bangladesh. *Water Resour. Res.* **51**, 685–703.

Simpkins W. W. and Parkin T. B. (1993) Hydrogeology and redox geochemistry of CH4 in a Late Wisconsinan Till and Loess Sequence in central Iowa. *Water Resour. Res.* **29**, 3643–3657.

Smith A. H., Elena O. Lingas and Rahman M. (2000) Contamination of drinking-water by arsenic in Bangladesh: a public health emergency. *Bull World Health Organ* **78**, 1093–103.

Smith R., Knight R. and Fendorf S. (2018) Overpumping leads to California groundwater arsenic threat. *Nat. Commun.* **9**, 2089.

Stahl M. O., Harvey C. F., Geen A. van, Sun J., Trang P. T. K., Lan V. M., Phuong T. M., Viet P. H. and Bostick B. C. (2016) River bank geomorphology controls groundwater arsenic concentrations in aquifers adjacent to the Red River, Hanoi Vietnam. *Water Resour. Res.* **52**, 6321–6334.

Stollenwerk K. G., Breit G. N., Welch A. H., Yount J. C., Whitney J. W., Foster A. L., Uddin M. N., Majumder R. K. and Ahmed N. (2007) Arsenic attenuation by oxidized aquifer sediments in Bangladesh. *Sci. Total Environ.* **379**, 133–150.

Stute M., Zheng Y., Schlosser P., Horneman A., Dhar R. K., Datta S., Hoque M. A., Seddique A. A., Shamsudduha M., Ahmed K. M. and van Geen A. (2007) Hydrological control of As concentrations in Bangladesh groundwater. *Water Resour. Res.* **43**, W09417.

Swartz C. H., Blute N. K., Badruzzman B., Ali A., Brabander D., Jay J., Besancon J., Islam S., Hemond H. F. and Harvey C. F. (2004) Mobility of arsenic in a Bangladesh aquifer: Inferences from geochemical profiles, leaching data, and mineralogical characterization. *Geochim. Cosmochim. Acta* **68**, 4539–4557.

Thi Hoa Mai N., Postma D., Thi Kim Trang P., Jessen S., Hung Viet P. and Larsen F. (2014) Adsorption and desorption of arsenic to aquifer sediment on the Red River floodplain at Nam Du, Vietnam. *Geochim. Cosmochim. Acta* **142**, 587–600.

Thorstenson D. C., Fisher D. W. and Croft M. G. (1979) The geochemistry of the Fox Hills-Basal Hell Creek Aquifer in southwestern North Dakota and northwestern South Dakota. *Water Resour. Res.* **15**, 1479–1498.

Thurman E. M. (Earl M. (1985) *Organic geochemistry of natural waters [electronic resource].*, Distributors for the U.S. and Canada, Kluwer Academic, Hingham, MA, USA.

Umitsu M. (1994) Late quaternary sedimentary environments and landforms in the Ganges Delta. *Sediment. Geol.* **83**, 177–186.

Umitsu M. (1987) Quaternary sedimentary environment and landform evolution in the Bengal lowland. *Geogr Rev Jpn* **B 60**, 164–78.

van Geen A., Ahmed E. B., Pitcher L., Mey J. L., Ahsan H., Graziano J. H. and Ahmed K. M. (2014) Comparison of two blanket surveys of arsenic in tubewells conducted 12 years apart in a 25 km2 area of Bangladesh. *Sci. Total Environ.* **488–489**, 484–492.

van Geen A., Bostick B. C., Thi Kim Trang P., Lan V. M., Mai N.-N., Manh P. D., Viet P. H., Radloff K., Aziz Z., Mey J. L., Stahl M. O., Harvey C. F., Oates P., Weinman B., Stengel C., Frei F., Kipfer R. and Berg M. (2013) Retardation of arsenic transport through a Pleistocene aquifer. *Nature* **501**, 204–207.

van Geen A., Rose J., Thoral S., Garnier J. M., Zheng Y. and Bottero J. Y. (2004) Decoupling of As and Fe release to Bangladesh groundwater under reducing conditions. Part II: Evidence from sediment incubations. *Geochim. Cosmochim. Acta* **68**, 3475–3486.

van Geen A., Trevisani M., Immel J., Jakariya M., Osman N., Cheng Z., Gelman A. and Ahmed K. M. (2006) Targeting Low-arsenic Groundwater with Mobile-phone Technology in Araihazar, Bangladesh. *J Health Popul Nutr* **24**, 282–297.

van Geen A., Zheng Y., Goodbred S., Horneman A., Aziz Z., Cheng Z., Stute M., Mailloux B., Weinman B., Hoque M. A., Seddique A. A., Hossain M. S., Chowdhury S. H. and Ahmed K. M. (2008) Flushing History as a Hydrogeological Control on the Regional

Distribution of Arsenic in Shallow Groundwater of the Bengal Basin. *Environ. Sci. Technol.* **42**, 2283–2288.

van Geen A., Zheng Y., Versteeg R., Stute M., Horneman A., Dhar R., Steckler M., Gelman A., Small C., Ahsan H., Graziano J. H., Hussain I. and Ahmed K. M. (2003) Spatial variability of arsenic in 6000 tube wells in a 25 km2 area of Bangladesh. *Water Resour. Res.* **39**. Available at: ://WOS:000183304800002.

van Geen A., Cheng Z., Jia Q., Seddique A. A., Rahman M. W., Rahman M. M. and Ahmed K. M. (2007) Monitoring 51 community wells in Araihazar, Bangladesh, for up to 5 years: Implications for arsenic mitigation. *J. Environ. Sci. Health Part A* **42**, 1729–1740.

Wada Y., Beek L. P. H. van, Kempen C. M. van, Reckman J. W. T. M., Vasak S. and Bierkens M. F. P. (2010) Global depletion of groundwater resources. *Geophys. Res. Lett.* **37**. Available at: https://agupubs.onlinelibrary.wiley.com/doi/abs/10.1029/2010GL044571 [Accessed October 19, 2018].

Walker S. A., Azetsu-Scott K., Normandeau C., Kelley D. E., Friedrich R., Newton R., Schlosser P., McKay J. L., Abdi W., Kerrigan E., Craig S. E. and Wallace D. W. R. (2016) Oxygen isotope measurements of seawater (18O/ 16O): A comparison of cavity ring-down spectroscopy (CRDS) and isotope ratio mass spectrometry (IRMS). *Limnol. Oceanogr. Methods* **14**, 31–38.

Weinman B., Goodbred S. L., Zheng Y., Aziz Z., Steckler M., van Geen A., Singhvi A. K. and Nagar Y. C. (2008) Contributions of floodplain stratigraphy and evolution to the spatial patterns of groundwater arsenic in Araihazar, Bangladesh. *Geol. Soc. Am. Bull.* **120**, 1567–1580.

Werner A. D., Zhang Q., Xue L., Smerdon B. D., Li X., Zhu X., Yu L. and Li L. (2013) An Initial Inventory and Indexation of Groundwater Mega-Depletion Cases. *Water Resour. Manag.* **27**, 507–533.

Whaley-Martin K. J. (2017) Examining Microbial Carbon Source Cycling in Arsenic Contaminated Bangladesh Aquifers Through Lipid and Isotopic Analyses. McMaster University.

Whaley-Martin K. J., Mailloux B. J., van Geen A., Bostick B. C., Silvern R. F., Kim C., Ahmed K. M., Choudhury I. and Slater G. F. (2016) Stimulation of Microbially Mediated Arsenic Release in Bangladesh Aquifers by Young Carbon Indicated by Radiocarbon Analysis of Sedimentary Bacterial Lipids. *Environ. Sci. Technol.* **50**, 7353–7363.

Whiticar M. J. and Faber E. (1986) Methane oxidation in sediment and water column environments—Isotope evidence. *Org. Geochem.* **10**, 759–768.

WHO (1993) *Guidelines for drinking-water quality*., World Health Organization, Geneva. Available at: http://apps.who.int/iris/bitstream/handle/10665/259956/9241544600-eng.pdf;jsessionid=6A88AB5DA4633E395E762B07AC27953A?sequence=1.

Winkel L. H. E., Trang P. T. K., Lan V. M., Stengel C., Amini M., Ha N. T., Viet P. H. and Berg M. (2011) Arsenic pollution of groundwater in Vietnam exacerbated by deep aquifer exploitation for more than a century. *Proc. Natl. Acad. Sci.* **108**, 1246–1251.

Zheng C. and Wang P. P. (1999) *MT3DMS: A Modular Three-Dimensional Multispecies Transport Model for Simulation of Advection, Dispersion, and Chemical Reactions of Contaminants in Groundwater Systems; Documentation and User's Guide*., University of Alabama prepared for US Army Corps of Engineers, Tuscaloosa, Alabama, USA. Available at: http://www.dtic.mil/dtic/tr/fulltext/u2/a373474.pdf.

Zheng Y., van Geen A., Stute M., Dhar R., Mo Z., Cheng Z., Horneman A., Gavrieli I., Simpson H. J., Versteeg R., Steckler M., Grazioli-Venier A., Goodbred S., Shahnewaz M., Shamsudduha M., Hoque M. A. and Ahmed K. M. (2005) Geochemical and hydrogeological contrasts between shallow and deeper aquifers in two villages of Araihazar, Bangladesh: Implications for deeper aquifers as drinking water sources. *Geochim. Cosmochim. Acta* **69**, 5203–5218.

Figure 4-1. The study area under the influence of Dhaka pumping. (a) Location of the study area with respect to Dhaka pumping center; the white rectangle shows the boundary of the large-scale child model of Khan et al. (2016); the perimeter of the basin-scale parent model of Michael & Voss (2008) is drawn in yellow; red cross-hatching indicates areas elevated in arsenic (As); orange polygons are the known regions of low-As Pleistocene aquifers exposed near the surface. (b) Expansion of the 9 m water level depth (maximum suction limit for hand pumped wells) over time. (c) The heterogeneous distribution of As in Araihazar based on field-testing campaign carried out in 2017-18. The rectangle shows our focus area of investigation (see *Figure 4-2)*.
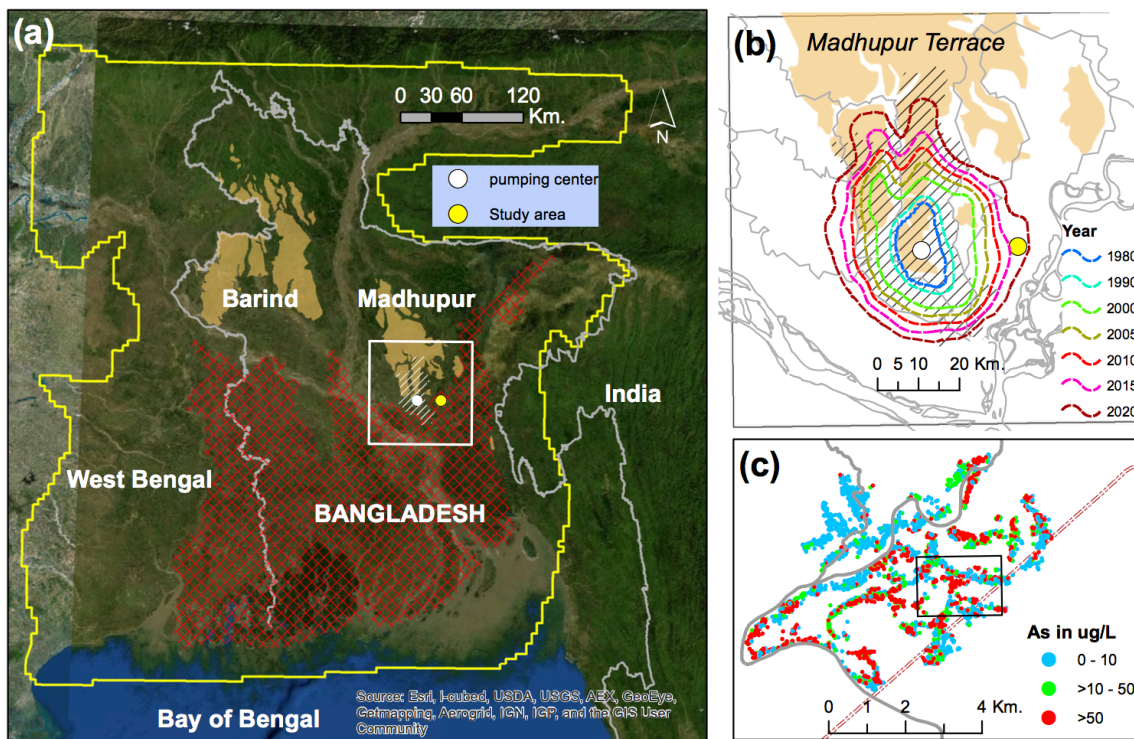
Figure 4-2. Chemical and geological heterogeneity in the study area. (a) Spatial distribution of arsenic in the intermediate aquifer (>40-100 m). (b) The proportion of sand and clay facies up to a depth of 50 m bgs. Also shown are the locations of the irrigation pumps (white filled circle) and the distribution of hand pumps (gray open circles) in the study area.
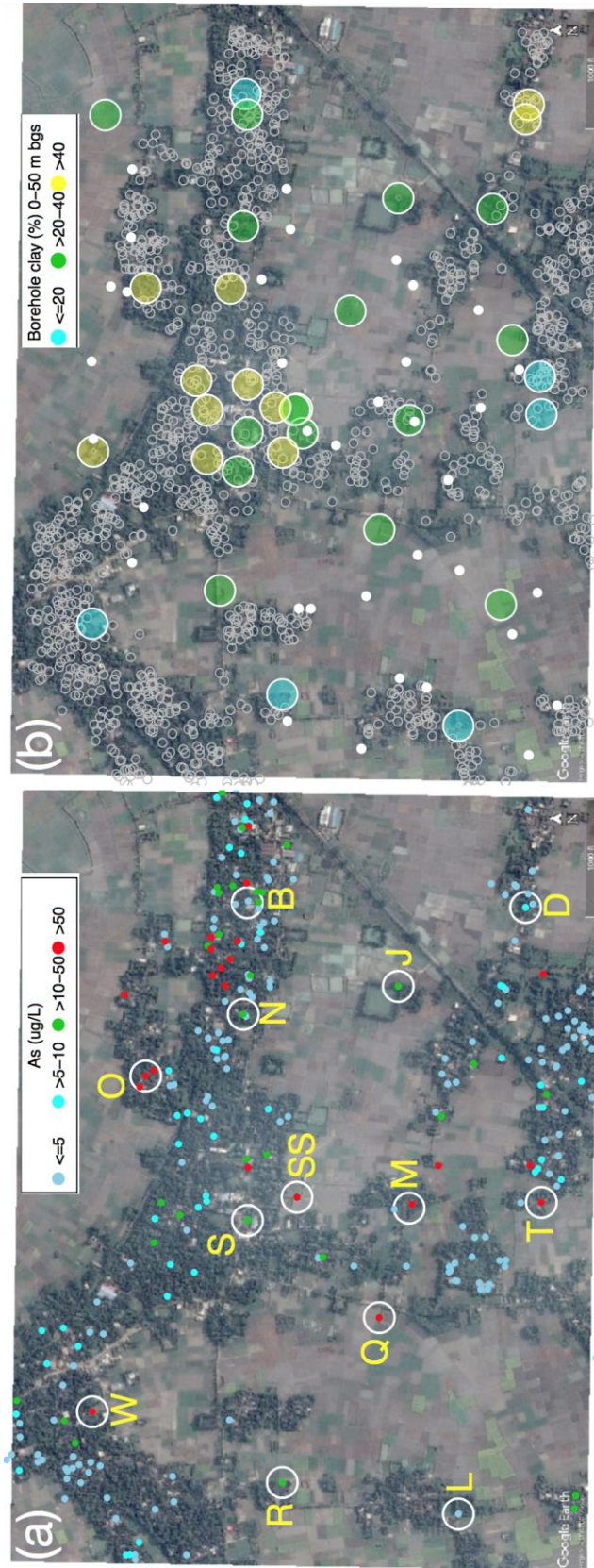
Figure 4-3. Sediment chemistry distinguishing Holocene from Pleistocene deposits. Depth profiles of Sediment age (a-b), diffuse spectral reflectance (c-d), sediment magnetic mineral content (e-f), and calcium concentrations (g-h) for the clay-capped site-S (top panel) and sandy site-T (bottom panel) in the study area (*see Figure 4-2*). The dotted horizontal gray lines indicate variations to the depth to the Pleistocene aquifer based on sediment radiocarbon dating. Typically the Holocene sediment is gray whereas oxidized Pleistocene sediment is yellowish to orange in color. The sand facies is "dotted" and the clay facies is "hatched". The black thin band at site-T indicates a peat layer.

site-S, SS, and M, respectively (*Figure 4-2*). The blue lines indicate the extent (or thickness) of the major clay aquitard capping the intermediate aquifer. The dotted horizontal gray lines indicate the approximate Holocene to Pleistocene transitional depth (Figure 4-S4b).
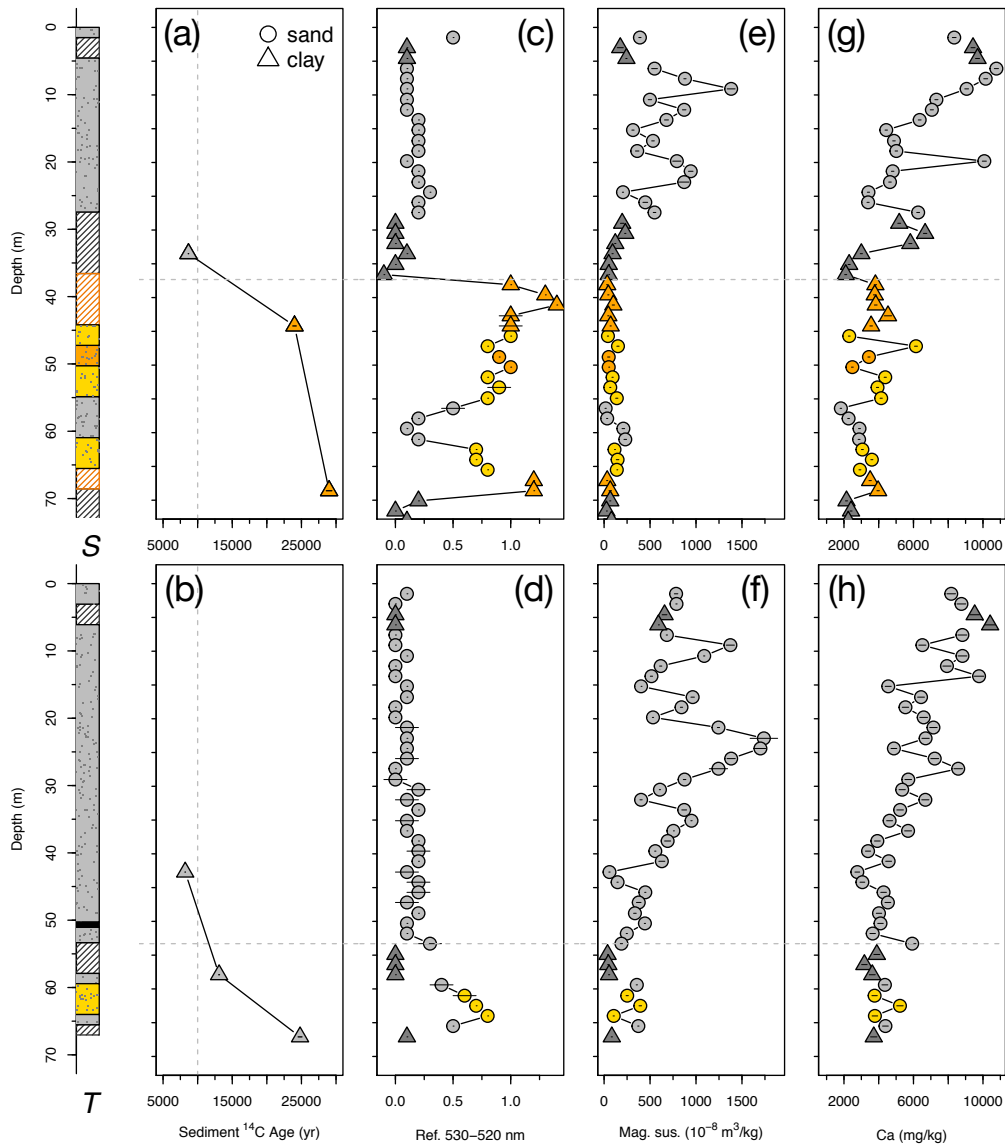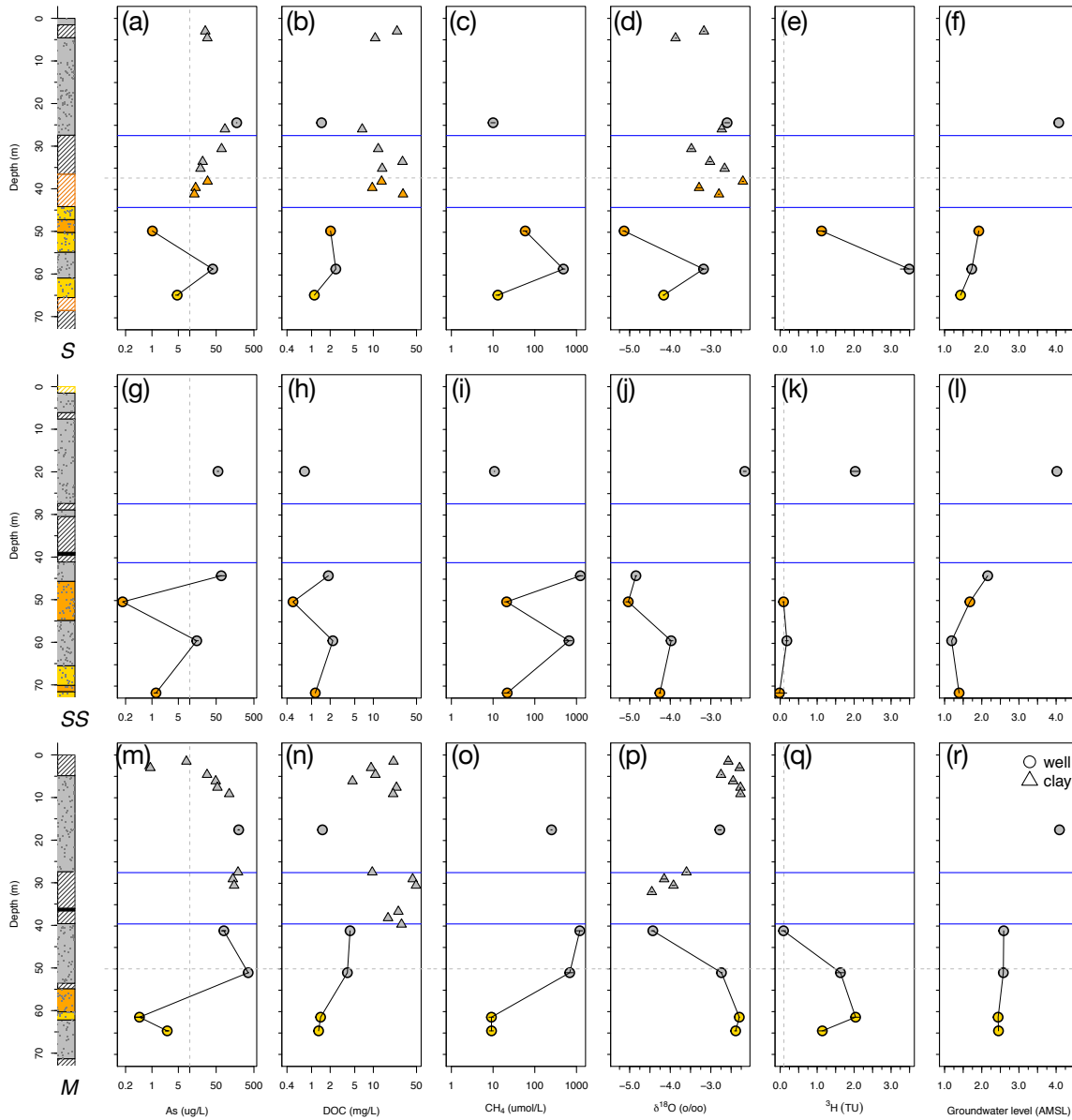
Figure 4-5. Groundwater hydrogeochemistry at two sandy sites. Depth profiles of groundwater arsenic (a, g), dissolved organic carbon (b, h), dissolved methane (c, i), stable isotope of oxygen (d, j), tritium (e, k), and hydraulic head (f, l) at the sandy site-T and R, respectively (*Figure 4-2*).
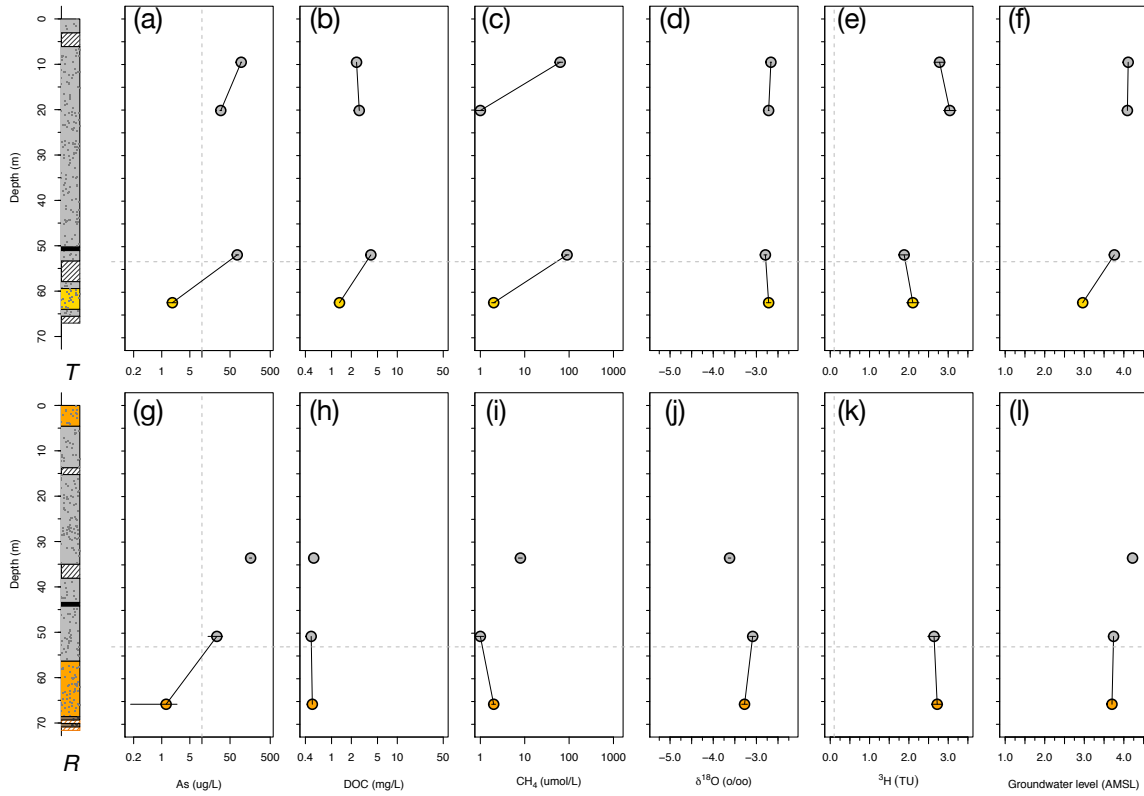
Figure 4-6. Evolution of As concentrations in the intermediate aquifer. (a) Increase (B5 and M1-4), decrease (N2), and stable (S2) As concentrations in four wells in the confined aquifer; (b) Examples of cyclic rise and fall (T3) and steady decline (T1, T2, and T4) in As concentrations in a sandy site.
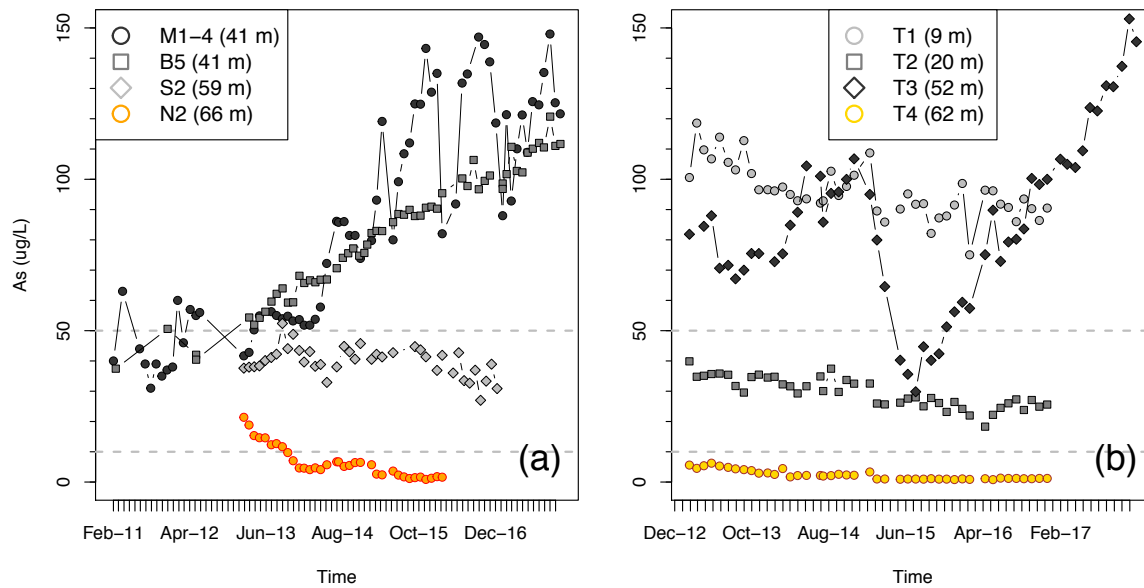
Figure 4-7. Simulated hydraulic heads in the study area. The modeled elevation of groundwater (in meters) above mean sea level (amsl) in the intermediate (a) and deep (b) aquifer under current pumping condition (*Figure 4-1*). The white circles indicate nest locations (*Figure 4-2*) with existing monitoring well(s) screened between 50 and 60 m bgs and the range of measured ^{3}H-^{3}He relative ages of groundwater containing detectable ^{3}H (Table 4-2) (a). In many cases, groundwater in the deeper intermediate wells turned out to be younger within the same nest of collocated wells as a result of mixing with old groundwater. Available deep-monitoring wells installed at 195 m bgs (b). The predicted heads are plotted against the observed head in *Figure 4-S8*.
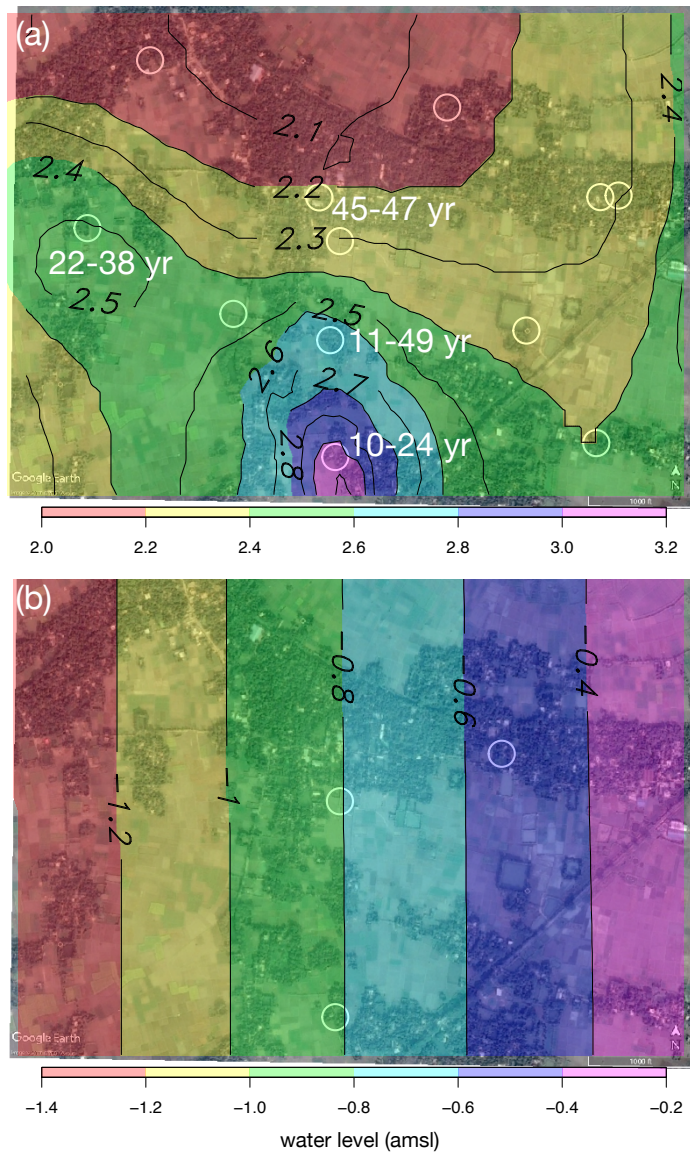
Figure 4-8. Tracing the source of groundwater and arsenic into the intermediate aquifer along a S-N transect. This is a 2D projection of the central portion of the 3D model showing (a) The distribution of As and tritium in present day shallow and intermediate aquifers along a lithological cross-section indicating the occurrence of gray and orange Pleistocene deposits; vertical white lines indicate drilling and/or groundwater monitoring locations; (b) Fifty years of backtracked particles from the As contaminated confined aquifer to the sandy recharge window under the influence of Dhaka pumping; (c) cross-section along the deeply scoured recharge window, composed of gray channel sand deposits in juxtaposition with previously uncontaminated, iron coated orange sand aquifer that has recently been reduced due to the advection of shallow groundwater; (d) Back traced particles in a hydraulically unperturbed system for 500 years. The dotted back line indicates surface elevation along the transect. The north and south boundaries are "no flow".

169
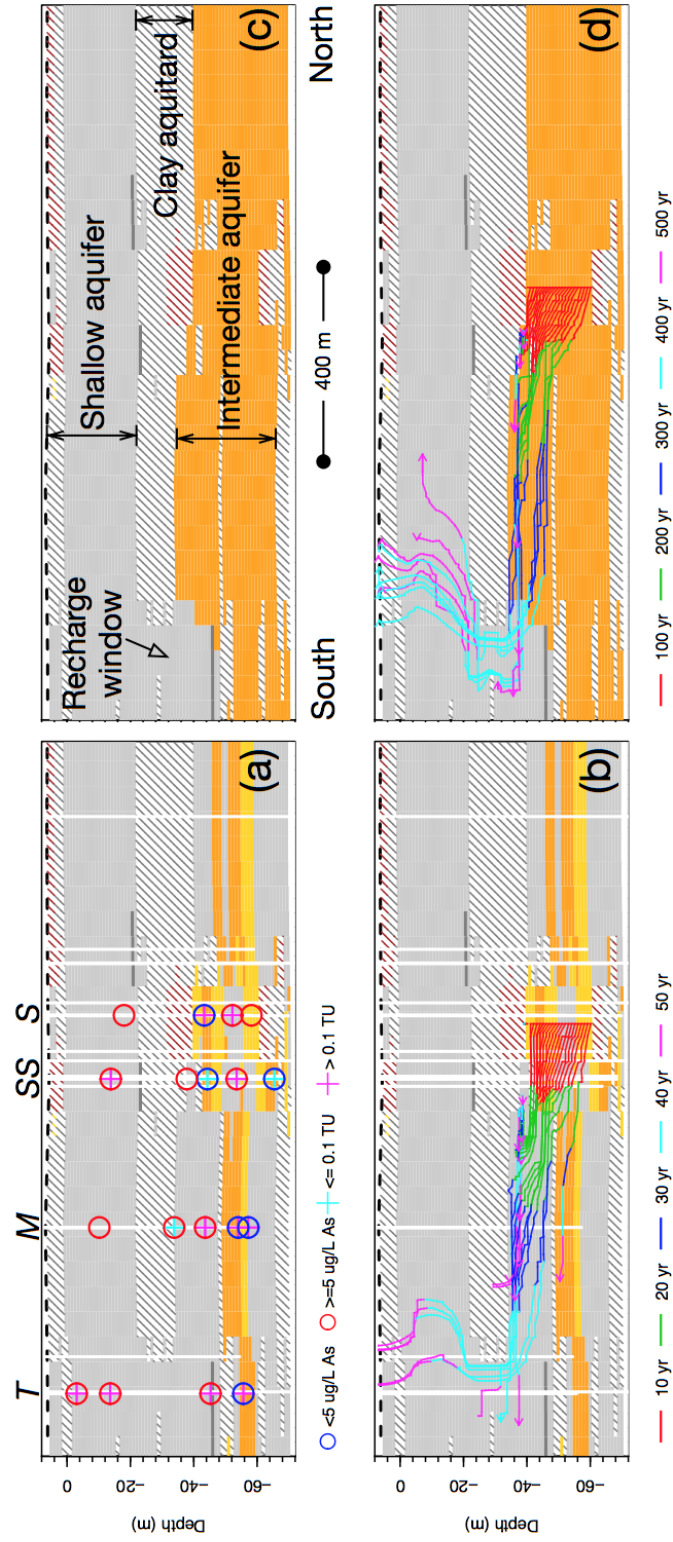
Figure 4-9. Arsenic (As) transport with retardation under pumping. The intrusion of relative As relative concentration (C/C$_0$) fronts of 0.1, 0.3, 0.5, 0.7, 0.9, and 1 through a recharge window along a S-N transect (*Figure 4-8a*) for a retardation factor of (a) 5, (b) 10, and (c) 30 after 50 years.
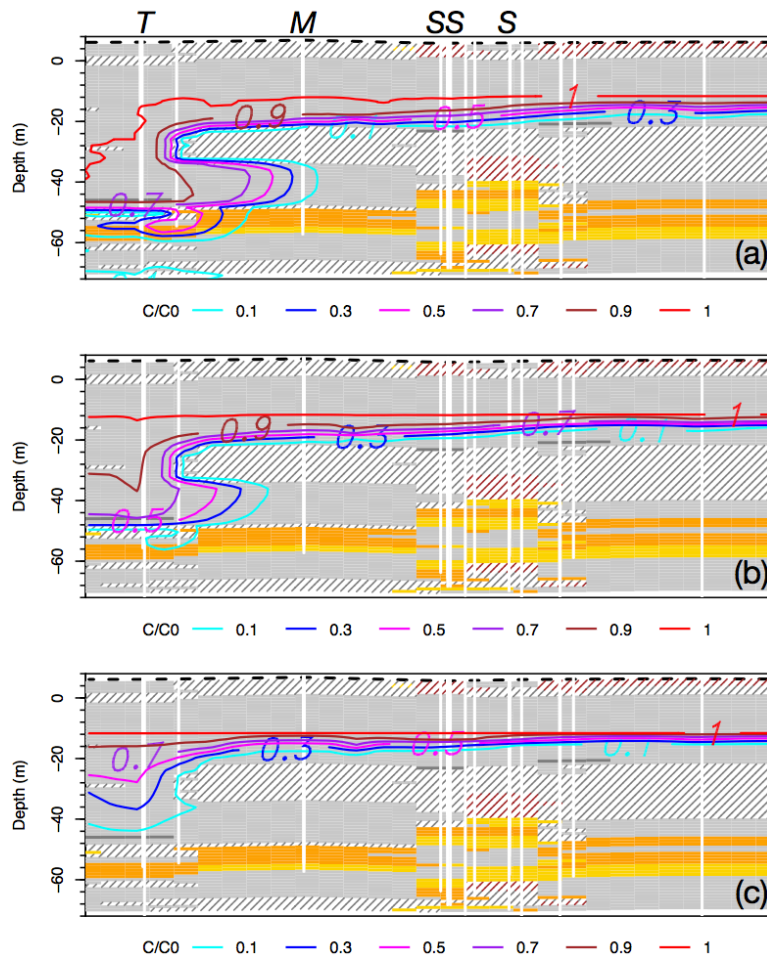
Figure 4-10. Retardation of arsenic (As) under prepumping. The intrusion of relative As concentration (C/C$_0$) front of 0.1 through a recharge window along a S-N transect (*Figure 4-8a*) for a retardation factor of (a) 5, (b) 10, and (c) 30 after 50, 100, 200, 300, 400, and 500 years of forward simulation.
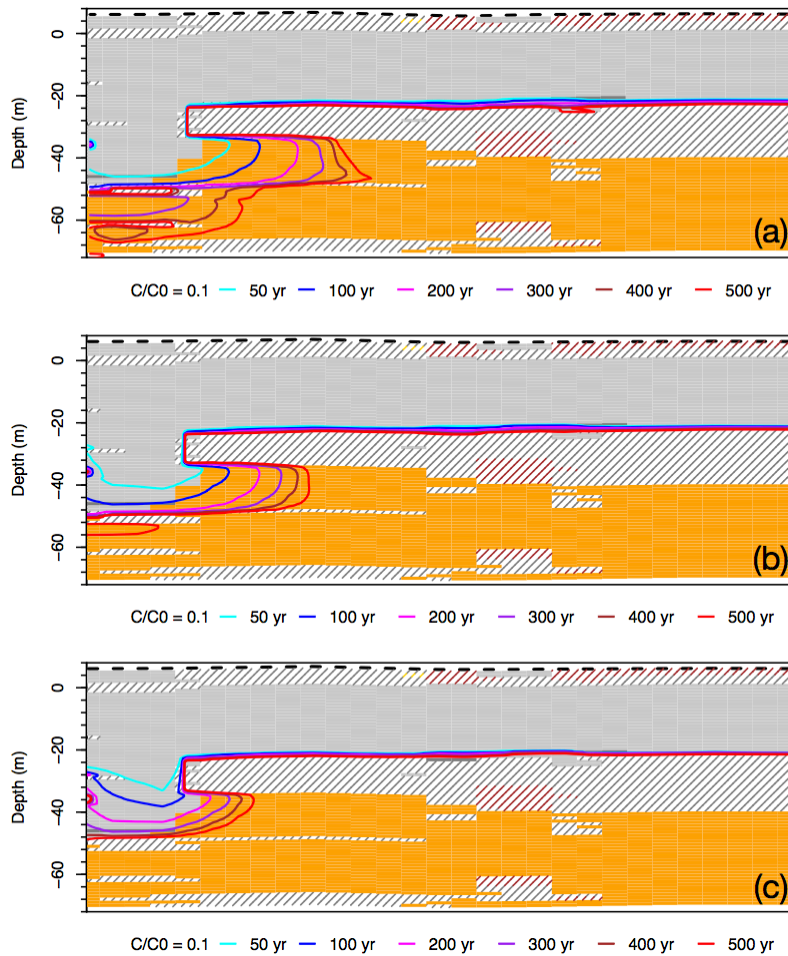
Figure 4-11. Intrusion of shallow groundwater arsenic (As) through sandy, recharge windows. (a) Relative concentrations (C/C_0) of As at 52 m bgs after 100 years of simulation for a R_f of 10 under current pumping scenario; (b) the interpolated total thickness of clay from the surface up to a depth of 50 m bgs. Also shown are the locations of intermediate monitoring wells screened between 50 & 60 m bgs.

Table 4-1: Groundwater physicochemical parameters and stable isotopic composition in sand and clay formations.

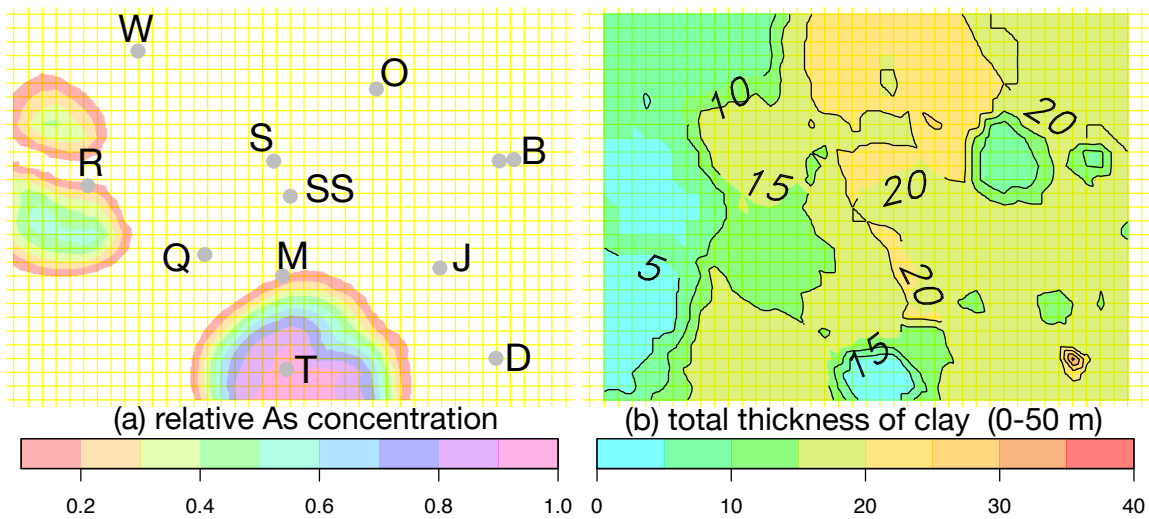| #	Well ID	Depth meters	Si mg/L	P mg/L	S mg/L	Ca mg/L	Fe mg/L	Ba µg/L	Na mg/L	Mg mg/L	K mg/L	Mn mg/L	As µg/L	Sr µg/L	F mg/L	Cl mg/L	Br mg/L	DIC mg/L	DOC mg/L	DOC* mg/L	δD ‰	δ¹⁸O ‰	Temp °C	pH	ORP mV	EC µS/cm
	Sand formations																									
1	S0	24.4	31.9	1.5	0.0	51.3	8.7	122.5	29.0	16.9	4.3	0.7	174.7	218.4	0.8	19.3	0.0	66.0	1.5		-2.6	-13.6	26.2	7.1	-51	396
2	S1	49.7	39.3	0.2	0.1	26.9	2.1	33.6	72.7	11.5	1.2	0.7	1.0	176.7	0.5	34.8	0.2	27.7	2.0		-5.1	-34.1	25.91	7.2	-50.7	459
3	S2	58.6	34.8	1.1	0.1	41.2	11.3	67.0	21.4	19.0	2.7	0.8	40.5	240.9	0.3	7.9	0.0	70.7	2.5		-3.2	-20.0	25.85	6.9	46.2	532
4	S3	64.7	44.6	0.2	0.0	32.8	0.6	48.6	46.7	14.2	1.7	0.7	4.7	224.0	0.4	9.1	0.0	70.1	1.1		-4.2	-25.7	25.95	6.6	53.8	457
5	CW-S	195	51.2	0.2	0.9	32.7	0.8	83.2	28.4	0.0	2.2	0.0	1.9	224.5	1.2	0.0	2.6	46.1	1.1		NA	NA	26.2	6.9	NA	542
6	SS0	19.8	30.5	0.8	1.0	50.3	6.0	61.4	18.6	19.2	2.7	1.1	55.9	175.9	0.7	16.7	1.7	58.6	0.8		-2.2	-12.9	26.2	7.2	-150	470
7	SS1	44.2	40.6	1.7	0.1	41.8	13.0	206.2	206.6	18.9	4.5	0.3	68.4	296.1	2.0	39.8	0.1	58.1	1.9		-4.8	-29.3	26.6	7.1	-110	569
8	SS2	50.3	36.1	0.1	0.0	36.8	0.2	37.4	62.5	14.7	1.1	1.2	0.2	222.9	2.5	34.9	0.1	65.9	0.5		-5.0	-30.6	26.7	7	30	556
9	SS3	59.4	32.8	0.2	0.0	44.3	3.6	81.5	31.3	19.6	1.8	1.0	15.3	289.4	2.0	7.8	0.0	68.0	2.2		-4.0	-23.2	26.6	7.1	-175	199
10	SS4	71.6	43.1	0.1	0.0	39.8	0.4	73.8	57.5	12.7	1.5	0.4	1.3	205.0	2.7	6.5	0.1	63.4	1.2		-4.3	-26.3	26.6	7	-165	572
11	M1-1	17.5	33.1	1.6	0.0	47.0	10.1	88.5	13.9	15.0	3.0	0.5	197.3	198.0	0.2	10.5	0.0	57.6	1.5		-2.8	-13.9	26.2	7	-49.6	418
12	M1-4	41.1	42.2	1.2	0.0	33.2	10.4	149.2	49.7	15.4	3.1	0.1	79.9	259.0	0.4	13.8	0.1	118.8	4.2		-4.4	-27.5	26.38	6.8	-22	610
13	M1-4a	50.9	31.8	1.0	0.1	66.6	11.5	196.0	19.7	20.0	3.3	0.1	352.3	436.9	0.4	24.9	0.1	85.2	3.8		-2.7	-19.8	26.36	7.4	-99.9	632
14	M1-5	61.3	38.6	0.1	0.1	63.4	0.2	126.0	13.7	24.2	1.8	0.6	0.5	423.9	0.5	15.2	0.0	96.0	1.4		-2.3	-13.3	26.36	6.7	81.6	529
15	M1-6	64.5	35.9	0.1	0.0	63.0	0.5	149.7	14.3	23.2	2.1	0.4	2.5	437.8	0.6	9.2	0.0	93.6	1.3		-2.4	-13.3	26.41	6.8	72.4	610
16	M-CW	96	54.4	0.1	0.1	32.9	0.1	96.6	26.1	0.0	2.0	0.0	0.3	267.8	1.2	6.3	NA						25.7	6.8	NA	441
17	T1	9.5	36.7	3.1	0.0	53.4	10.0	108.6	17.2	14.4	4.2	0.2	94.8	259.4	0.3	22.0	0.0	63.6	2.4		-2.7	-14.6	25.6	6.8	-60.5	513
18	T2	20.1	27.1	1.1	0.8	39.3	16.5	109.7	25.5	16.6	2.2	1.2	29.4	149.5	0.1	15.1	0.0	74.4	2.6		-2.7	-18.0	25.92	6.8	-57.1	488
19	T3	51.8	32.2	1.6	0.0	39.5	3.8	27.2	22.7	24.8	2.9	0.0	75.5	268.5	0.7	11.1	0.0	80.4	4.0		-2.8	-16.0	25.76	6.7	69	516
20	T4	62.3	30.4	0.0	0.0	38.3	0.4	13.5	16.6	25.0	2.1	1.4	1.8	239.6	0.5	17.2	0.0	64.8	1.3		-2.7	-15.4	26.01	6.8	6.9	470
21	CW-T	195	50.0	0.2	0.4	41.9	1.5	63.2	36.0	0.0	2.0	0.0	1.6	263.6	1.3	0.0	1.3	48.6	1.9		NA	NA	25	6.8	NA	630
22	R0	33.5	31.2	1.5	0.0	26.5	2.2	29.0	10.1	6.1	1.9	0.6	162.6	97.8	0.9	4.9	0.0	28.6	0.5		-3.6	-20.0	26.9	7.2	-55	301
23	R1	50.7	31.8	0.5	1.5	27.2	5.6	72.4	12.9	13.0	2.9	1.2	23.5	104.8	0.2	7.7	0.0	31.9	0.5		-3.1	-18.4	26.44	7.2	-26.2	330
24	R2	65.6	30.7	0.2	0.0	26.6	0.6	36.0	12.3	20.5	3.1	0.2	1.3	228.0	0.6	4.5	0.0	35.5	0.5		-3.3	-17.9	26.51	7.2	-0.9	325
25	N0	32	36.5	2.6	0.1	65.2	10.3	112.4	27.9	27.5	4.9	0.2	109.8	305.0	1.1	36.4	0.7	NA	NA		NA	NA	25.8	7.1	NA	822
26	N1	47.4	42.8	0.9	0.0	34.5	7.8	43.5	50.8	19.6	3.4	0.1	14.9	283.5	0.2	9.6	0.1	65.4	1.7		-4.9	-32.2	25.85	7.1	-28.9	540
27	N2	63	44.5	0.2	0.0	21.7	1.8	25.8	72.6	8.3	1.8	0.3	5.2	116.3	0.3	12.9	0.1	58.5	1.0		-3.7	-27.3	25.86	7.1	-6.1	449
28	N3	195	NA	NA	NA	NA	NA	NA	NA	NA	NA	NA	NA	NA	NA	NA	NA	49.5	1.4		NA	NA	25.9	6.8	NA	417
29	O1	56.3	24.7	0.8	0.0	41.2	9.3	142.5	19.6	21.4	2.4	0.0	54.7	346.0	0.3	16.0	0.0	53.3	1.4		-3.2	-20.1	25.76	7.2	-64.9	506
30	Q1	52.2	26.1	0.8	0.0	45.0	6.4	133.0	32.4	24.2	2.0	0.0	106.9	426.8	0.3	13.7	0.1	56.2	1.6		-5.3	-32.6	26.25	7.3	-68	575
31	Q2	58	35.3	0.6	0.2	35.3	6.6	85.3	85.9	17.2	1.8	0.6	38.8	315.2	0.3	12.3	0.1	74.2	0.8		-5.3	-32.9	26.33	7.3	-67.2	625
32	W-1	27.4	28.9	1.1	0.0	38.5	4.6	56.9	13.9	9.3	2.4	0.9	80.9	131.2	0.7	10.9	0.6	45.2	0.7		-2.9	-17.7	27.2	7.3	-76	360
33	W-2	42.7	35.9	1.8	0.0	55.8	8.0	183.6	287.4	31.5	6.0	0.1	171.5	363.7	1.5	33.0	0.0	95.6	3.0		-5.0	-30.5	27.2	7.2	-73	687
34	W-3	60	36.2	0.2	0.1	39.5	1.6	17.5	46.8	14.2	1.0	0.9	0.5	267.6	2.8	8.2	0.0	71.7	0.6		-4.9	-29.6	27.2	7.1	21	481
35	W-4	67	44.1	0.2	0.1	24.0	3.4	49.6	234.4	9.4	1.4	0.3	7.6	171.4	1.7	8.1	0.4	52.9	0.6		-4.6	-27.3	28.3	7	-7	483
36	D1	19.8	36.8	1.7	0.0	38.4	17.0	98.7	15.2	0.0	3.9	0.0	166.1	205.1	0.8	17.6	0.2	51.7	1.7		NA	NA	25.8	6.9	NA	403
37	D2	59.4	31.4	0.2	0.3	32.4	2.4	40.1	332.3	0.0	2.1	0.0	5.1	214.4	NA	0.0	1.2	51.4	0.8		NA	NA	26.1	6.8	NA	1393
38	J1	24.4	34.4	1.4	0.3	34.8	8.7	57.5	11.5	0.0	2.6	0.0	93.0	149.5	0.7	13.8	0.8	51.1	2.4		NA	NA	25.9	6.8	NA	514
39	J2	59.1	35.3	0.1	0.3	32.7	0.5	48.4	42.6	0.0	2.0	0.0	10.1	238.4	1.1	11.4	0.7	80.4	3.1		NA	NA	26	6.6	NA	662
40	L1	30.5	33.9	1.9	0.1	28.0	8.6	74.4	12.4	0.0	4.8	0.0	47.9	131.6	0.6	9.9	0.1	40.1	1.5		NA	NA	26.8	7.1	NA	413
41	L2	61.6	36.0	0.4	0.5	4.5	0.3	10.2	322.3	0.0	0.8	0.0	1.5	24.4	5.6	31.7	1.7	76.5	0.1		NA	NA	26.6	7.3	NA	750
42	B3	14.2	28.9	1.3	2.3	78.0	8.5	112.0	25.2	24.0	4.4	0.9	420.4	351.0	NA	NA	NA	NA	NA	NA	NA	NA	25.62	7.3	-103	700
43	B4	27.9	26.3	1.4	0.0	87.2	10.9	177.1	28.8	27.8	4.2	0.2	218.0	402.4	NA	NA	NA	NA	NA	NA	NA	NA	25.69	7.3	-99.7	1022
44	B5	40.1	25.9	1.3	0.0	58.5	7.7	74.9	28.5	47.8	5.4	0.0	98.6	474.1	NA	NA	NA	NA	NA	NA	NA	NA	25.82	7.3	-89.3	954
45	B6	52.7	16.2	0.3	0.0	32.1	3.4	65.8	82.6	23.2	2.4	0.3	12.3	233.0	NA	NA	NA	NA	NA	NA	NA	NA	25.86	7.4	-82.8	548
46	B7	8.1	37.0	1.7	30.5	127.6	12.6	306.8	246.7	0.1	7.5	0.0	16.4	506.2	NA	NA	NA	NA	NA	NA	NA	NA	25.56	7	-63.8	988
47	B8	11.1	39.4	2.0	10.5	92.5	13.2	203.7	57.9	0.0	4.6	0.0	211.7	393.9	NA	NA	NA	NA	NA	NA	NA	NA	25.63	7	-62.5	704
48	B9	20.3	31.7	1.2	0.0	86.5	18.3	239.3	26.5	0.0	4.3	0.0	432.9	456.0	NA	NA	NA	NA	NA	NA	NA	NA	25.69	7.4	-115	866
49	B-CW	88	37.4	0.1	0.0	34.8	1.3	80.7	26.8	0.0	2.2	0.0	0.4	267.9	0.9	23.2	0.1						25.7	7	-99	301
50	CW-3	60	36.4	0.1	0.0	43.7	0.3	116.0	50.1	0.0	3.1	0.0	1.5	331.0	1.7	10.4	0.0						NA	NA	NA	NA
	Clay formations																									
1	site-S	3	20.0	0.5	3.8	32.6	3.5	115.1	18.2	19.5	NA	1.0	25.8	113.6	0.2	11.3	2.6	24.2	12.2		-3.2	-22.1	NA	NA	NA	NA
2	site-S	4.6	23.4	0.1	1.2	49.7	1.1	122.2	17.0	38.1	NA	0.4	29.1	178.4	0.2	6.3	0.6	10.7	10.5		-3.9	-24.2	NA	NA	NA	NA
3	site-S	25.9	36.5	0.0	1.5	41.5	0.1	64.2	37.9	24.1	NA	0.2	85.4	256.9	0.4	10.5	0.9	6.6	NA		-2.7	-17.3	NA	NA	NA	NA
4	site-S	30.5	37.3	0.3	1.1	17.6	0.6	42.5	57.6	27.1	NA	0.2	69.6	207.4	0.4	9.7	0.6	12.0	7.6		-3.5	-21.7	NA	NA	NA	NA
5	site-S	33.5	9.6	0.0	1.8	11.4	0.0	74.2	77.3	5.3	NA	0.1	21.9	89.4	4.7	21.5	0.4	29.7	10.2		-3.0	-19.1	NA	NA	NA	NA
6	site-S	35.1	8.3	0.0	1.8	17.7	0.0	97.2	89.2	6.7	NA	0.1	19.2	134.7	3.7	23.8	0.9	13.9	5.4		-2.7	-18.2	NA	NA	NA	NA
7	site-S	38.1	23.3	0.0	1.3	21.9	0.0	53.0	89.5	8.2	NA	0.4	29.6	154.2	1.6	19.2	1.3	13.6	2.2		-2.2	-14.8	NA	NA	NA	NA
8	site-S	39.6	26.5	0.0	1.6	15.4	0.1	42.0	99.0	8.3	NA	0.4	14.3	131.0				9.6	4.6		-3.3	-21.0	NA	NA	NA	NA
9	site-S	41.1	28.2	0.0	2.0	15.3	0.0	39.1	86.6	6.7	NA	0.4	13.2	125.2				30.2	NA		-2.8	-18.1	NA	NA	NA	NA
10	site-M	1.5	33.6	0.6	261.0	465.8	0.0	183.7	321.4	232.0	NA	0.2	8.1	1477.1	0.1	291.7	0.0	21.2	20.4		-2.6	-14.3	NA	NA	NA	NA
11	site-M	3	26.2	0.0	19.5	89.8	0.0	77.6	75.9	43.1	NA	0.1	0.9	267.0	0.2	38.8	16.4	9.2	3.9		-2.3	-10.8	NA	NA	NA	NA
12	site-M	4.6	26.8	0.5	5.8	76.3	5.7	203.3	43.4	47.8	NA	1.4	28.7	240.9	0.3	20.6	4.6	10.8	NA		-2.8	-15.3	NA	NA	NA	NA
13	site-M	6.1	32.8	0.4	0.8	76.2	4.5	132.7	35.6	39.8	NA	1.9	48.6	274.9	NA	NA	NA	4.6	3.9		-2.5	-13.5	NA	NA	NA	NA
14	site-M	7.6	32.9	2.0	1.9	60.9	4.5	157.4	33.9	26.5	NA	0.6	53.9	242.4	0.3	12.3	1.2	23.7	14.0		-2.3	-11.3	NA	NA	NA	NA
15	site-M	9.1	34.7	2.7	1.0	56.9	3.6	126.9	56.5	23.2	NA	0.4	110.9	278.7	0.4	14.0	0.6	20.9	11.9		-2.3	-10.5	NA	NA	NA	NA
16	site-M	27.4	38.0	0.5	0.8	58.3	1.9	153.9	21.5	20.9	NA	0.2	189.6	298.1	0.5	9.6	0.9	9.6	NA		-3.6	-21.2	NA	NA	NA	NA
17	site-M	29	40.3	0.8	2.4	59.9	3.5	156.8	39.3	21.2	NA	0.2	138.2	332.1	NA	NA	NA	43.3	NA		-4.2	-24.8	NA	NA	NA	NA
18	site-M	30.5	41.1	1.8	1.1	51.1	3.6	117.3	48.8	16.9	NA	0.2	149.4	278.3	0.3	6.3	0.6	49.0	NA		-3.9	-25.5	NA	NA	NA	NA
19	site-M	32													0.4	8.1	1.0	NA	NA		-4.5	-28.1	NA	NA	NA	NA
20	site-M	36.6																25.4	19.5							
21	site-M	38.1																17.3	11.8							
22	site-M	39.6																28.6	9.7							

DOC* -clay pore water DOC measured after a year; the %reactivity is estimated from the difference between DOC and DOC*

Table 4-2: Groundwater ^{3}H concentrations and apparent ^{3}H/^{3}He ages estimated for a subset of samples.

Well_ID	Depth (m)	^{3}H ±1σ (TU)				^{3}H/^{3}He age (yr)
		2011*	2012	2017	2018	
S1	49.7			1.12 ± 0.05	0.22 ± 0.04	44.6 ± 3.2
S2	58.6				3.49 ± 0.12	46.8 ± 0.6
SS0	19.8			2.03 ± 0.06		
SS2	50.3			0.09 ± 0.01		
SS3	59.4			0.18 ± 0.02		
SS4	71.6			-0.02 ± 0.1		
S-CW	195.0			0.06 ± 0.04		
M1-4	41.1	0.09 ± 0.03				
M1-4a	50.9	1.61 ± 0.05		1.63 ± 0.05		
M1-5	61.3	2.04 ± 0.06				39.2 ± 1.9
M1-6	64.5	0.54 ± 0.03		1.14 ± 0.05		49.1 ± 1.4
M2-5	60.1	1.22 ± 0.05				27.03 ± NA
M2-6	68.6	0.13 ± 0.03				40.5 ± 1.8
M3-5	59.8	2.68 ± 0.06				10.6 ± 0
M3-6	67.4	1.21 ± 0.05				24.9 ± 0.1
M4-5	54.5	0.81 ± 0.04				25 ± 3
M4-6	63.5	0.08 ± 0.03				68.6 ± 1.2
T1	9.5		2.78 ± 0.07			
T2	20.1		3.04 ± 0.08			
T3	51.8		1.88 ± 0.06	1.88 ± 0.06	1.83 ± 0.07	24.2 ± 0.6
T4	62.3		1.48 ± 0.06		2.1 ± 0.08	14 ± 0.5
T-CW	195.0			0.07 ± 0.07		
T-CW- dup	195.0			0.04 ± 0.06		
R1	50.7			2.64 ± 0.08	2.36 ± 0.09	39.62 ± 0.6
R2	65.6			2.72 ± 0.07	2.64 ± 0.09	26.85 ± 0.5
N0	32.0			1.17 ± 0.09		
N1	47.4			-0.04 ± 0.02		
N2	63.0			-0.06 ± 0.01		
Q1	52.2			0.08 ± 0.02		
Q2	58.0			0.06 ± 0.01		
W1	27.4			2.26 ± 0.06		
W2	42.7			0.05 ± 0.02		
W4	67.7			0.04 ± 0.02		
J1	25.0			1.96 ± 0.09		
J2	59.1			0.11 ± 0.07		
L1	30.5			2.14 ± 0.1		
L2	61.6			0.25 ± 0.1		
D2	59.4			-0.02 ± 0.07		
O1	56.3			1.16 ± 0.04		
CW3	60			-0.03 ± 0.03		

*after Mihajlov et al. (in prep.)

Table 4-3: Methane and its stable isotopes in the groundwater of Araihazar, Bangladesh.

	Well ID	Depth meters	CH_4 ($\pm 1\sigma$) µmol/L	$\delta^{13}C$ ‰	δD ‰
1	S0	24.4	10+1	NA	NA
2	S1	49.7	59+4	NA	NA
3	S2	58.6	484+24	NA	NA
4	S3	64.7	13+1	NA	NA
5	ss0	19.8	11+0.1	-70.5	NA
6	ss1	44.2	1239+93	-67.3	NA
7	ss2	50.3	21+1	-72.4	NA
8	ss3	59.4	662+60	-79.6	NA
9	ss4	71.6	22+2	-62.6	NA
10	M1-1	17.5	252+5	NA	NA
11	M1-4	41.1	1199+100	NA	NA
12	M1-4a	50.9	688+70	NA	NA
13	M1-5	61.3	9+1	NA	NA
14	M1-6	64.5	9+1	NA	NA
15	T1	9.5	63*	NA	NA
16	T2	20.1	1+0.1	NA	NA
17	T3	51.8	90+5	NA	NA
18	T4	62.3	2+0.1	NA	NA
19	R0	33.5	8+0.4	NA	NA
20	R1	50.7	1+0.1	NA	NA
21	R2	65.6	2+0.1	NA	NA
22	N1	47.4	943+47	NA	NA
23	Q1	52.2	25+1	NA	NA
24	J2	59.1	44+2	NA	NA
25	L2	61.6	10+1	NA	NA
26	CW-B	88	65+2	-80.6	-109.2
27	B3	14.2	2.5+0.01	NA	NA
28	B4	27.9	208+10	-84.1	-160.8
29	B5	40.1	207+14	-85.8	-209
30	B6	52.7	331+27	-84.4	-200.5
31	B7	8.1	3+0.1	NA	NA
32	B8	11.1	11+1	NA	NA
33	B9	20.3	34+3	NA	NA

*Field measured value

175

4.8. Supporting Materials

Figure 4-S1. An increase in the installation of intermediate depth (>40-100 m deep) wells in Araihazar, Bangladesh. Spatial distribution and depth profile of As across the 25 sq. km area of Araihazar is shown 17 years apart. Arsenic concentrations are binned into <10 (cyan), 10-50 (green), and >50 µg/L (red). The vertical extent of the intermediate aquifer is identified with a blue arrow beneath the regional confining clay layer (yellow shaded area). A (gray) bar plot accompanying the As depth profile of 2017-18 indicates a decline in the proportion (normalized to 1) of wells in the vicinity of the clay aquitard. The location of study area is identified with a blue rectangle.
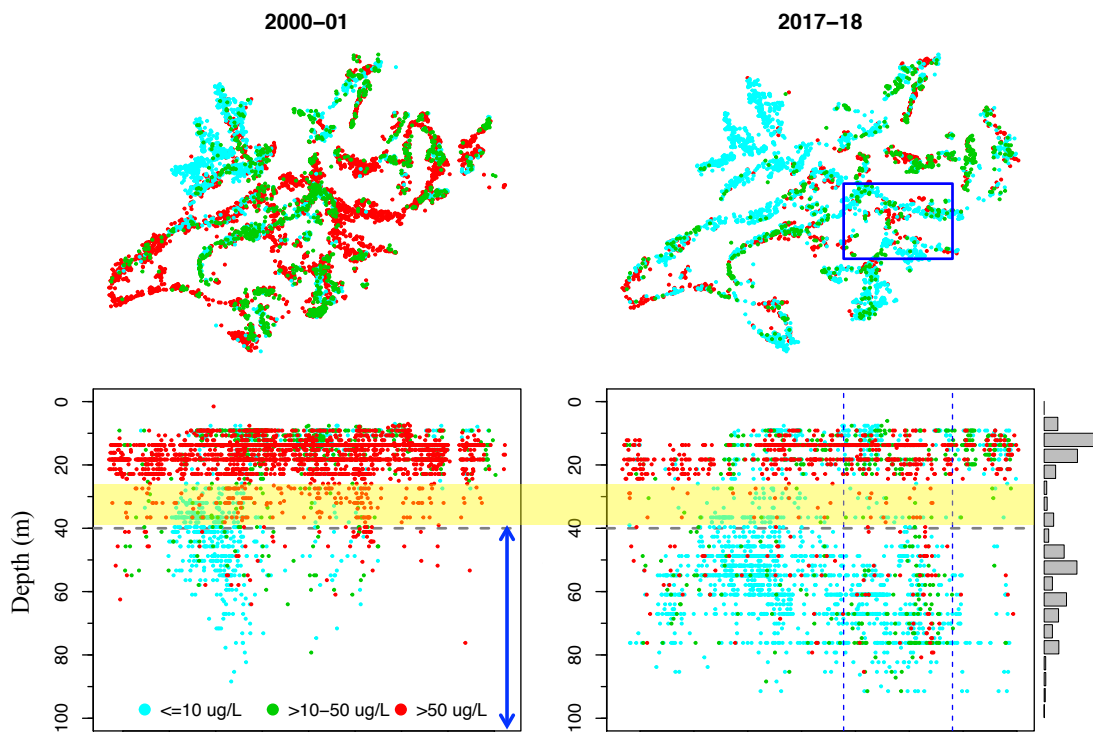
Figure 4-S2: Limited variability in shallow groundwater head across the 3 sq. km study area. (a) Temporal variability in groundwater hydraulic head with depth (8-28 m) in the shallow aquifer at site-B; (b) spatiotemporal variability of shallow head at 4 locations with long-term monitoring records (See main Figure 4-2 for the location of site-M, S, R, and T).
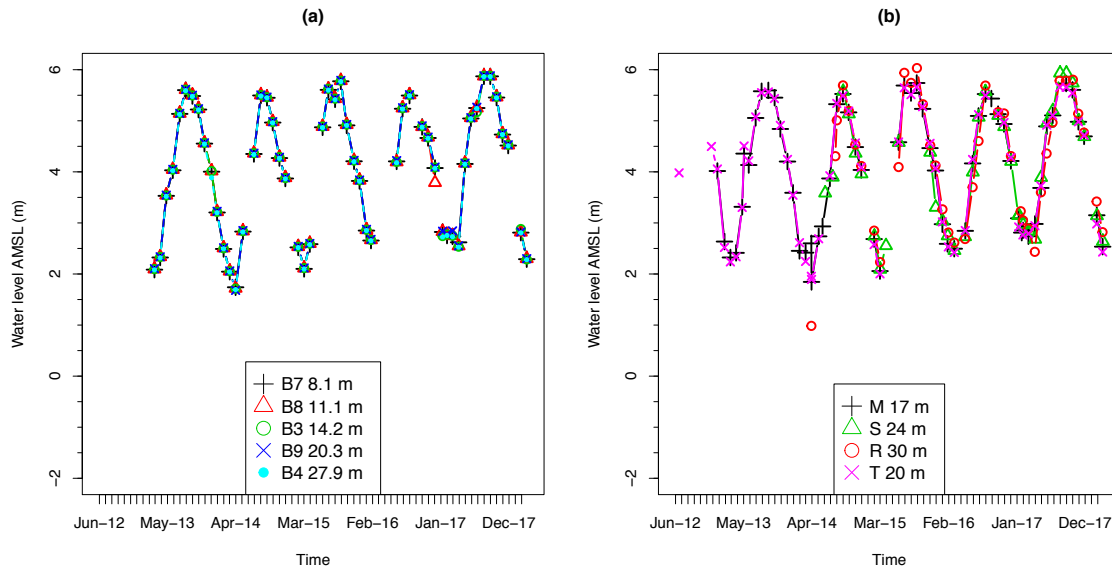
Figure 4-S3: Simulated deep aquifer reference head in the study area along the E-W transect. The transect of hydraulic head (filled circles) runs through the center of the study area and extends 10 km to the east, terminating at the boundary of Meghna River and 10 km to the west towards the Dhaka pumping center. Linear decrease (towards Dhaka) as well as increase (towards Meghna R.) of the reference heads retrieved after Khan et al. (2016) is limited up to a distance of 1 km in both directions (blue shaded area). The red dashed line indicates a linear model fit to the reference heads (red filled circles) within the study area. The longitudinal extent of the study area is shown with blue (dashed) vertical lines. The magnitude of decline in the deep aquifer head within the study area is shown with gray (dashed) horizontal lines.
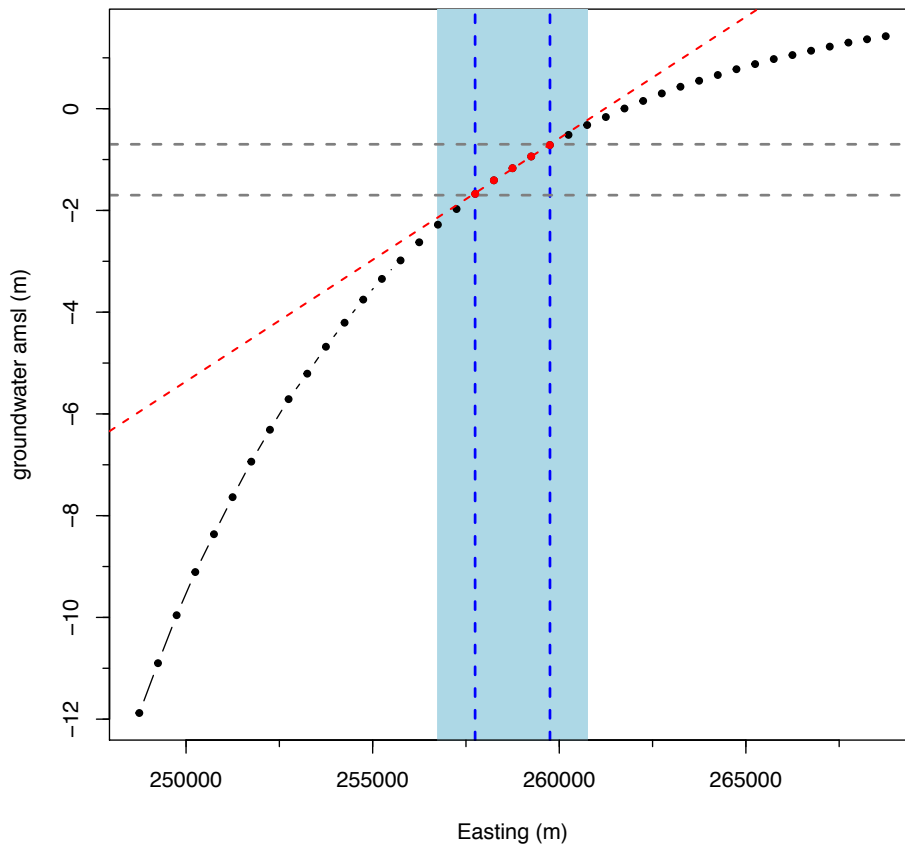
Figure 4-S4. (a) Driller's log constructed at 33 locations based on sediment cuttings retrieved every 1.5 m depth interval. The color of the sediments are categorized into 3 groups: gray, yellowish orange, and orange based on diffuse spectral reflectance (530 – 520 nm). Clay cuttings are shown as *hatching* while sand cuttings are *dotted*. The tirangles on the top of logs indicate the depth of radiocarbon (^{14}C) dated sediment; **(b)** Age of sediment with depth at 9 locations in the study area demarcating the approximate Holocene-Pleistocene transition.
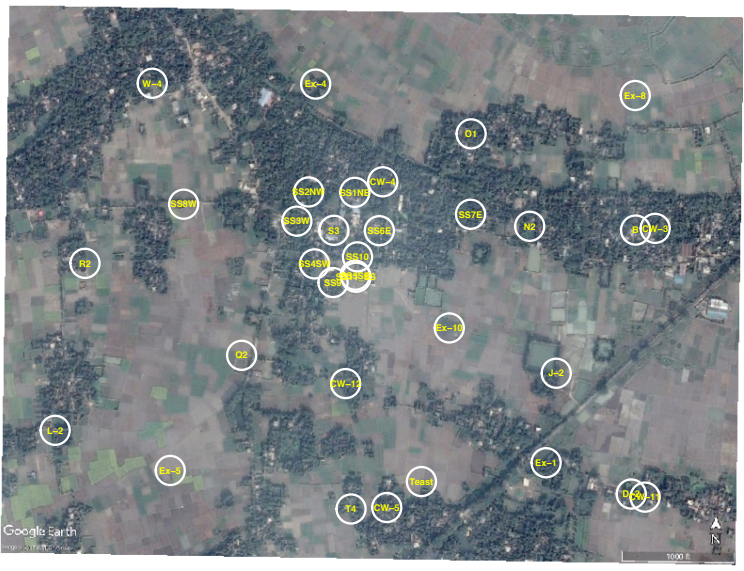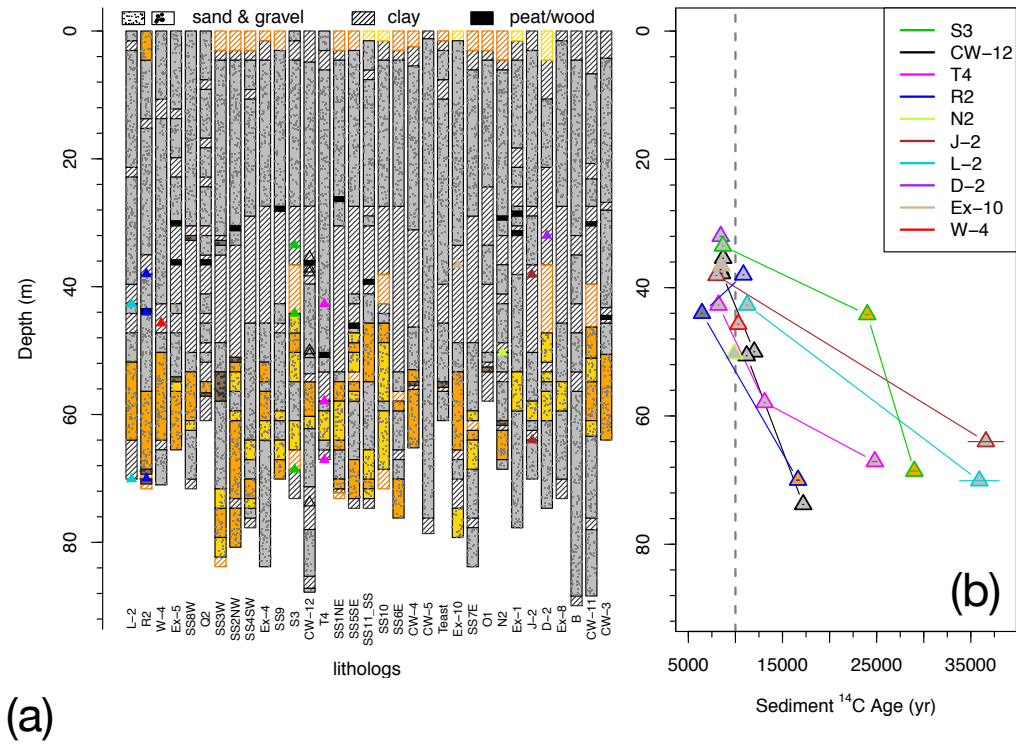
Figure 4-S5. A 3D lithostratigraphic model of the study area. The distribution of sand (violet) and clay (green) facies in the study area generated by interpolation using Rockworks15 based on data from 33 drillers log (Figure 4-S4). The model is vertically exaggerated by 10x. The southwest corner of the model is presented.
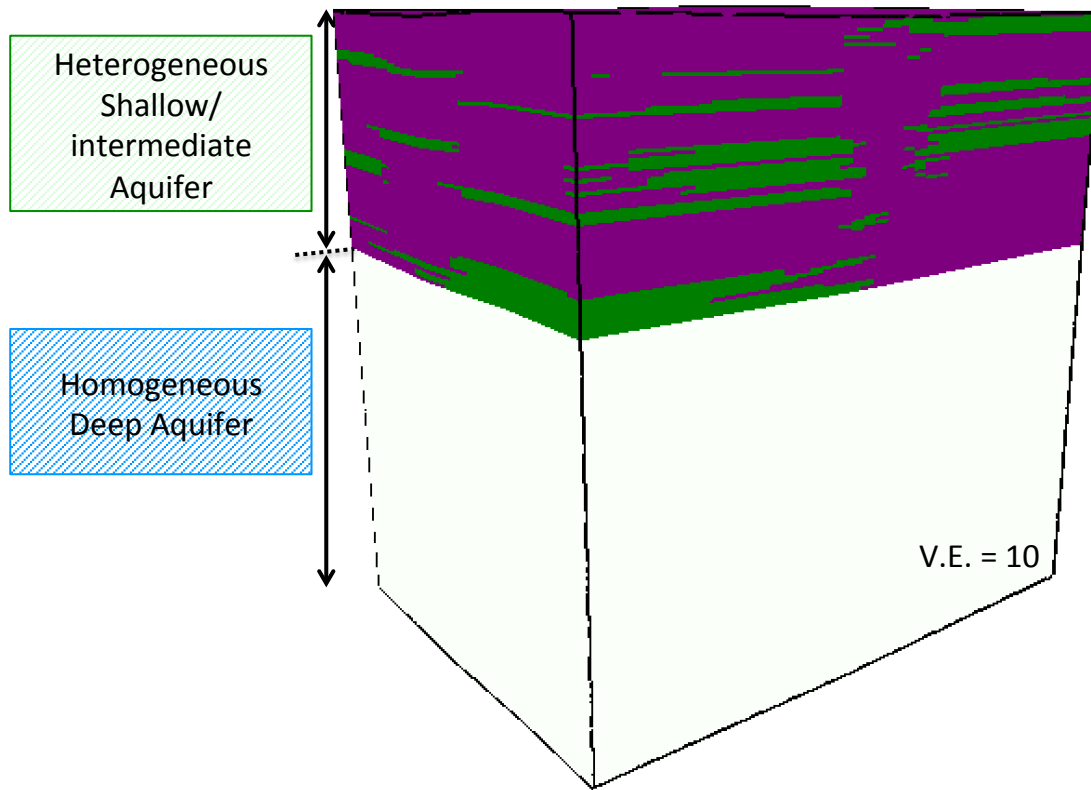
Figure 4-S6. Hydraulic conductivity determination from early drawdown data. Pumping-induced drawdown on the order of 1 to 2.5 feet (0.3 to 0.8 m) was observed in a total of 9 intermediate monitoring wells. Drawdown data in the intermediate aquifer were corrected for barometric fluctuations using a barometric efficiency of 0.1 (i.e., 90% of measured barometric pressures was subtracted), which in turn was estimated using the methods of Gonthier (2007). The data were also corrected for background seasonal fluctuations. The early-time segment (initial 100 minutes) of the corrected drawdown curves was then used to estimate the hydraulic conductivity and storativity by linear fitting of the corrected drawdown measured over time or distance from the pumping well (see Table 4-S1).
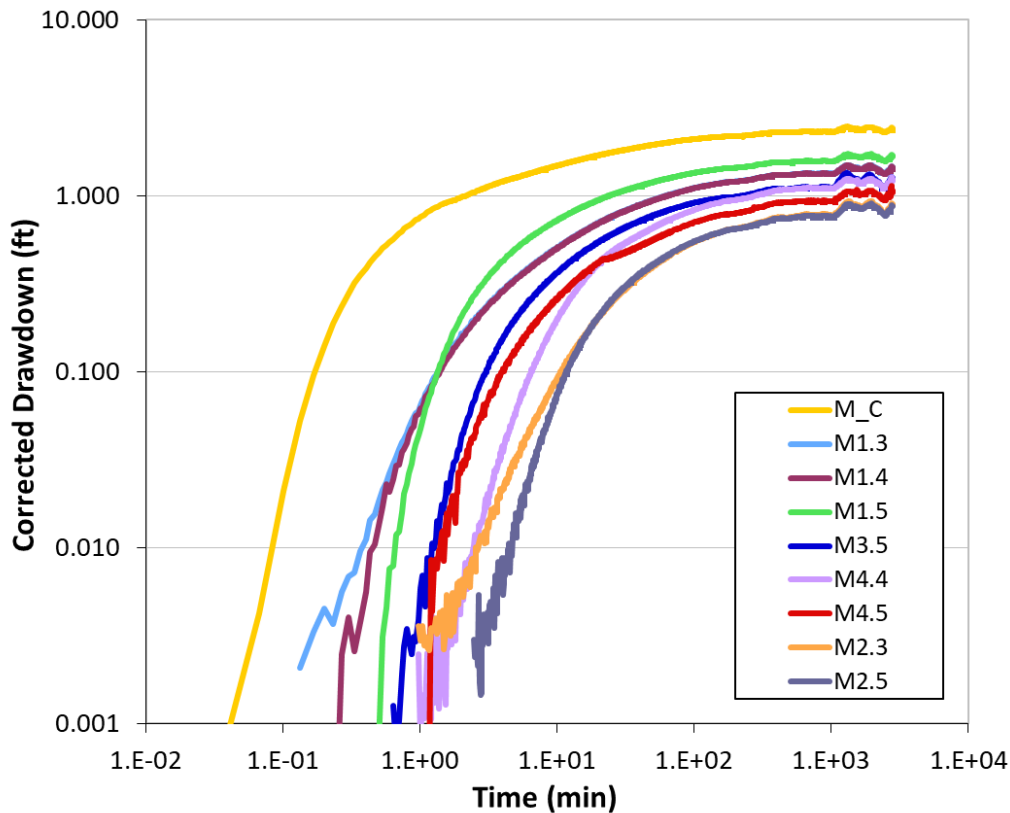
Figure 4-S7. Schematic of the model domain. The model is heterogeneous up to a depth of 75 m and homogeneous thereafter. The top of the model is simulated with a spatially uniform recharge rate or a constant head resulting in the same outcome. The drain elevation at the top of the model is set equivalent to model top. General boundary reference heads retrieved from the regional model are applied to the farthest east, west and bottom cells of the small model domain.
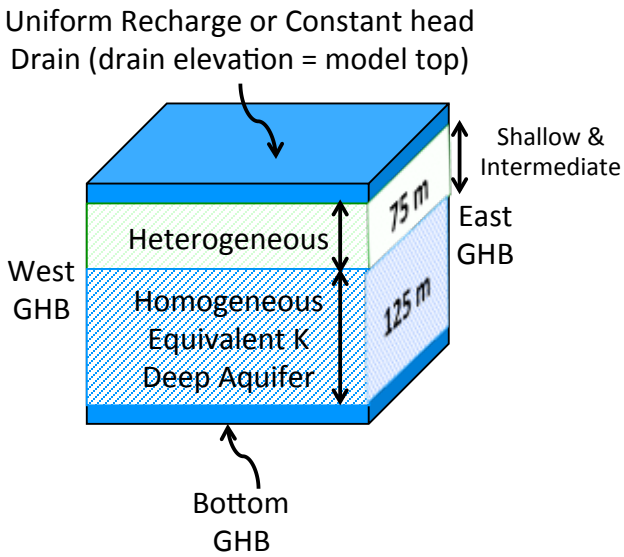
Figure 4-S8. Comparison of observed average head with simulated head. The model predicted groundwater heads are plotted as a function of the average of field observed head for 52 monitoring wells in the study area. The depths of the shallow (n = 17), intermediate (n = 30), and deep (n= 5) wells range from 8-36 m (green '+'), 41-88 m (red 'Δ'), and 100-195 m (black 'O'), respectively. The diagonal gray line represents the 1:1 line. The absolute difference between the simulated and observed heads ranged between 0.002 and 1.4 m (n = 52) with an overall root-mean-square-error (RMSE) of 0.59 m in comparison with the regional model RMSE of 3.5-10 m (Khan et al., 2016). About 60% of the predicted heads are within ±0.5 m of the observed heads. Without the 5 monitoring wells (9.6%) with more than a meter error, the RMSE is reduced to 0.47 m.
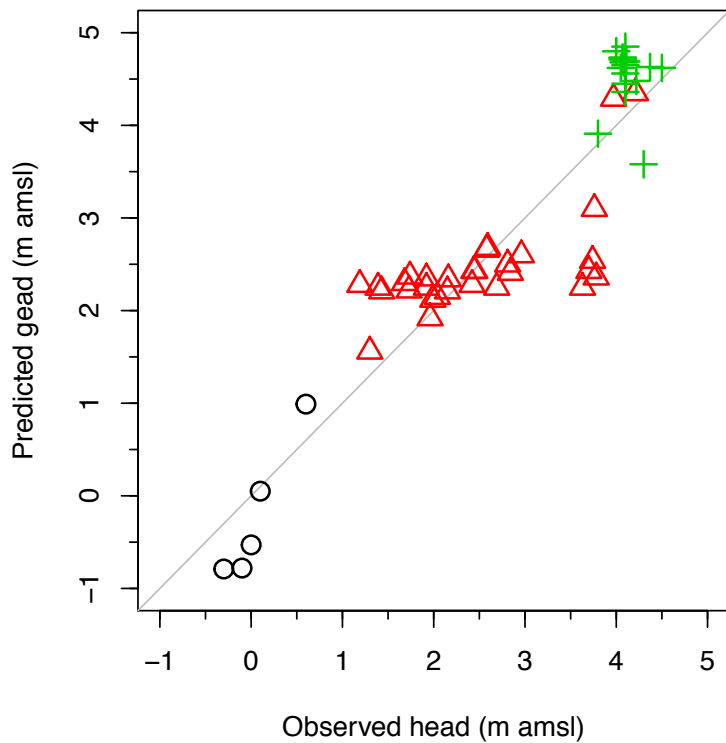
Figure 4-S9. Schematic set up for groundwater As transport simulation. A constant source of As is applied to the model top. An initial concentration of 1 was assigned to the top 20 m of the model and 0 was assigned to the rest of the modeled domain. The same partition coefficient (K_D) was applied for both sand and clay.
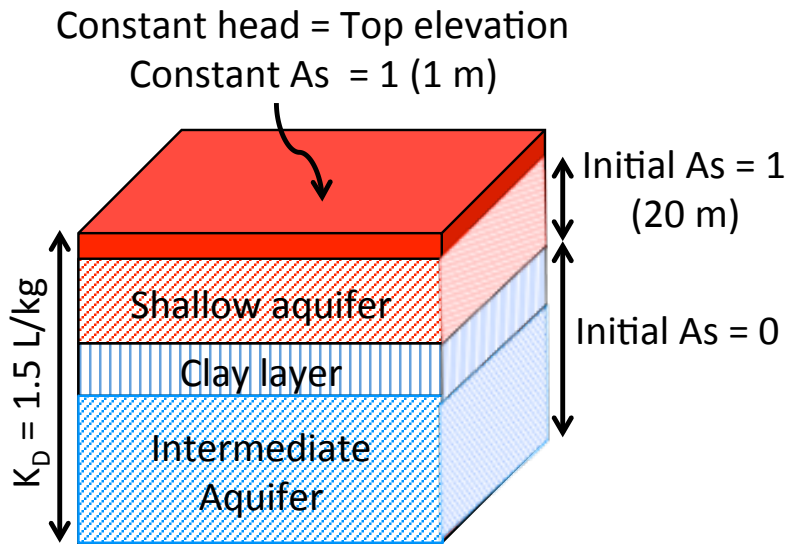
Figure 4-S10. Solid phase total organic carbon (TOC) content (%) in clay. The average TOC in the gray, Holocene clay is ~0.5% with occasionally higher concentrations whereas the orange, Pleistocene clay is typically low (<0.1%) in TOC. The horizontal dotted line demarcates the Holocene to Pleistocene transition at site-S. The upper and lower boundary of the major clay layer is shown with horizontal (solid) blue lines.
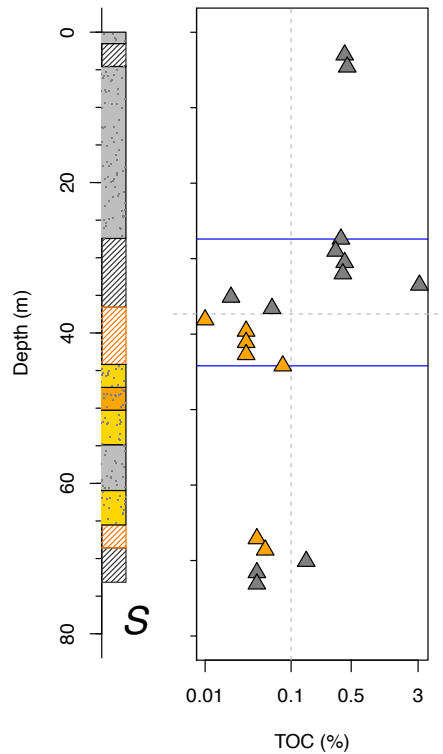
Figure 4-S11. Total tritium (^{3}H + ^{3}He$_{trit}$) concentrations in the intermediate aquifer plotted against apparent groundwater recharge in calendar year. Recharge years were estimated from ^{3}H/^{3}He ages of groundwater (see Table 4-2) and compared with the input of ^{3}H from rainfall. The solid cyan and solid brown lines indicate the annual ^{3}H in Dhaka rainfall and ^{3}H in groundwater derived from a dispersion model, respectively (Stute et al., 2007). The dotted brown lines below the ^{3}H groundwater curve (solid brown) indicate mixing of groundwater containing bomb-produced ^{3}H (% shown) with pre-bomb (^{3}H-dead) groundwater.
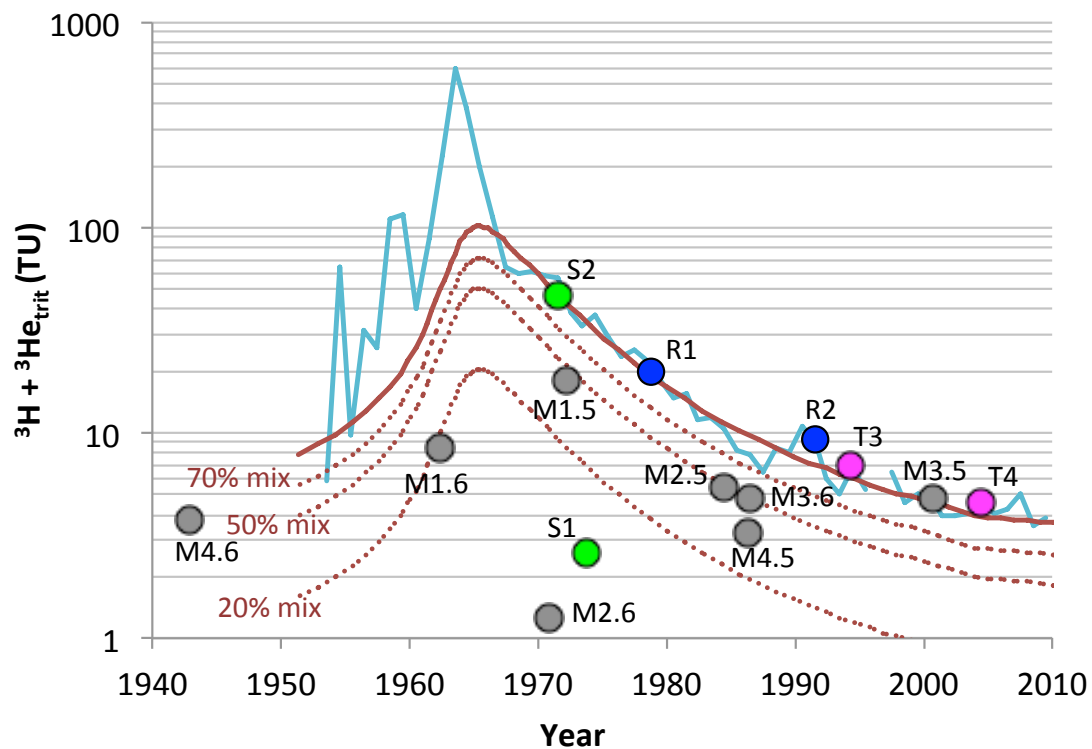
Figure 4-S12. Depth profiles of iron, Fe (a, g), phosphorus, P (b, h), sodium, Na (c, i), calcium, Ca (d, j), chloride, Cl (e, k), and bromide, Br (f, l) in groundwater and clay pore water collected at site-S and M, respectively.
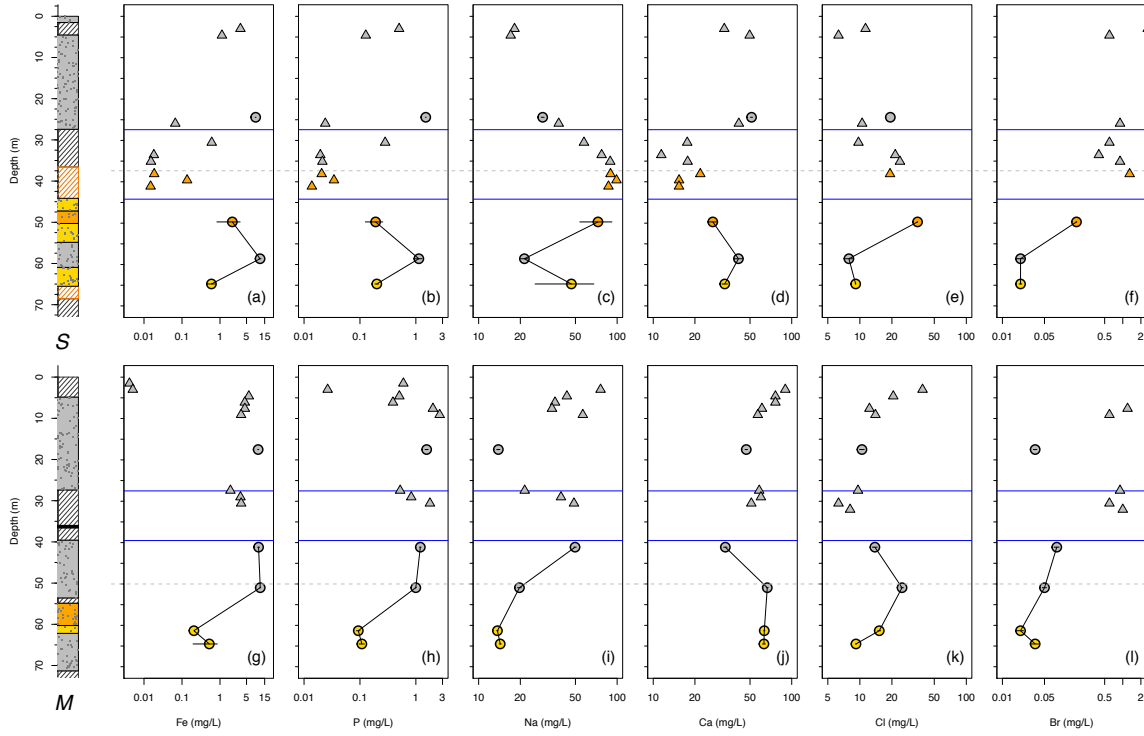
Figure 4-S13. Long-term trends of groundwater observed head in the study area. Long-term hydraulic record of level logger data in the shallow (<30 m), intermediate (>40-90 m), and deep (>90 m) wells installed at a clay-capped (a) and a sandy (b) site. Also shown is the declining groundwater head in two monitoring wells at a maximum estimated rate of 0.5 m/yr (c). The high variability of groundwater at the trough (dry season) signals the local impact of irrigation pumping for growing rice.
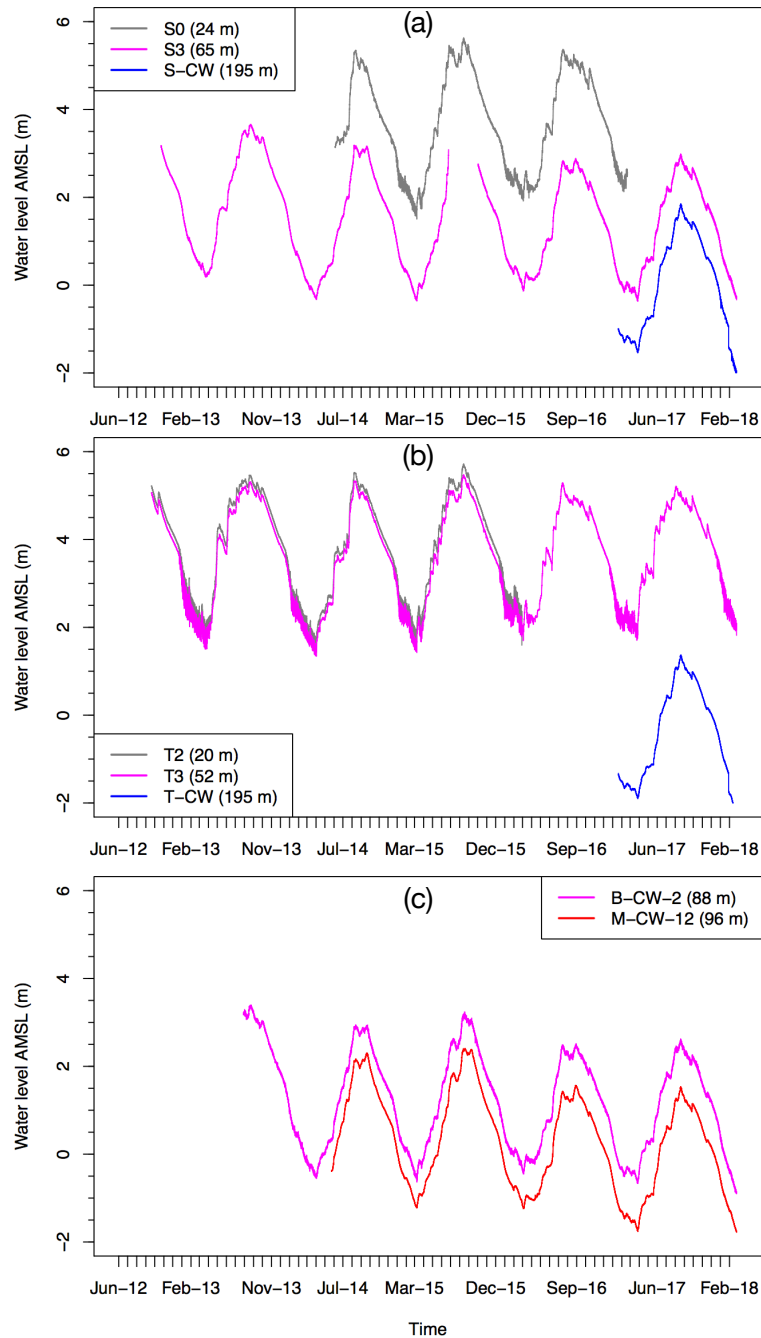
Figure 4-S14. Correlation between thickness of clay and average observed hydraulic head in the intermediate aquifer. A decrease in the average observed head with increasing overlying thickness of clay sequences. The same color convention of Figure 4-2b is used.
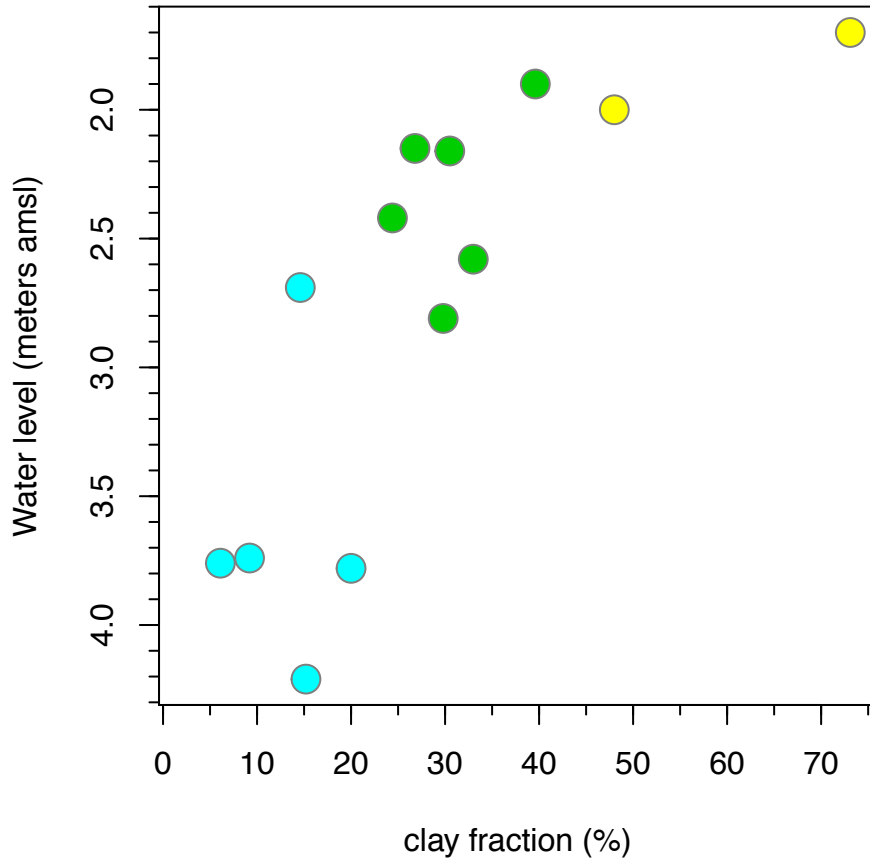
Figure 4-S15. Correlation among dissolved methane (CH$_4$), arsenic (As), tritium (^{3}H), and diffuse spectral reflectance of screened depth sediment in the intermediate aquifer. Groundwater CH$_4$ concentrations plotted as a function of As (a) and spectral reflectance (b). Also shown ^{3}H (both detectable and non-detectable) plotted as a function of As (c). The current detection limit for ^{3}H is 0.1 TU. The wells that are elevated in As and CH$_4$ are highlighted in all three plots.
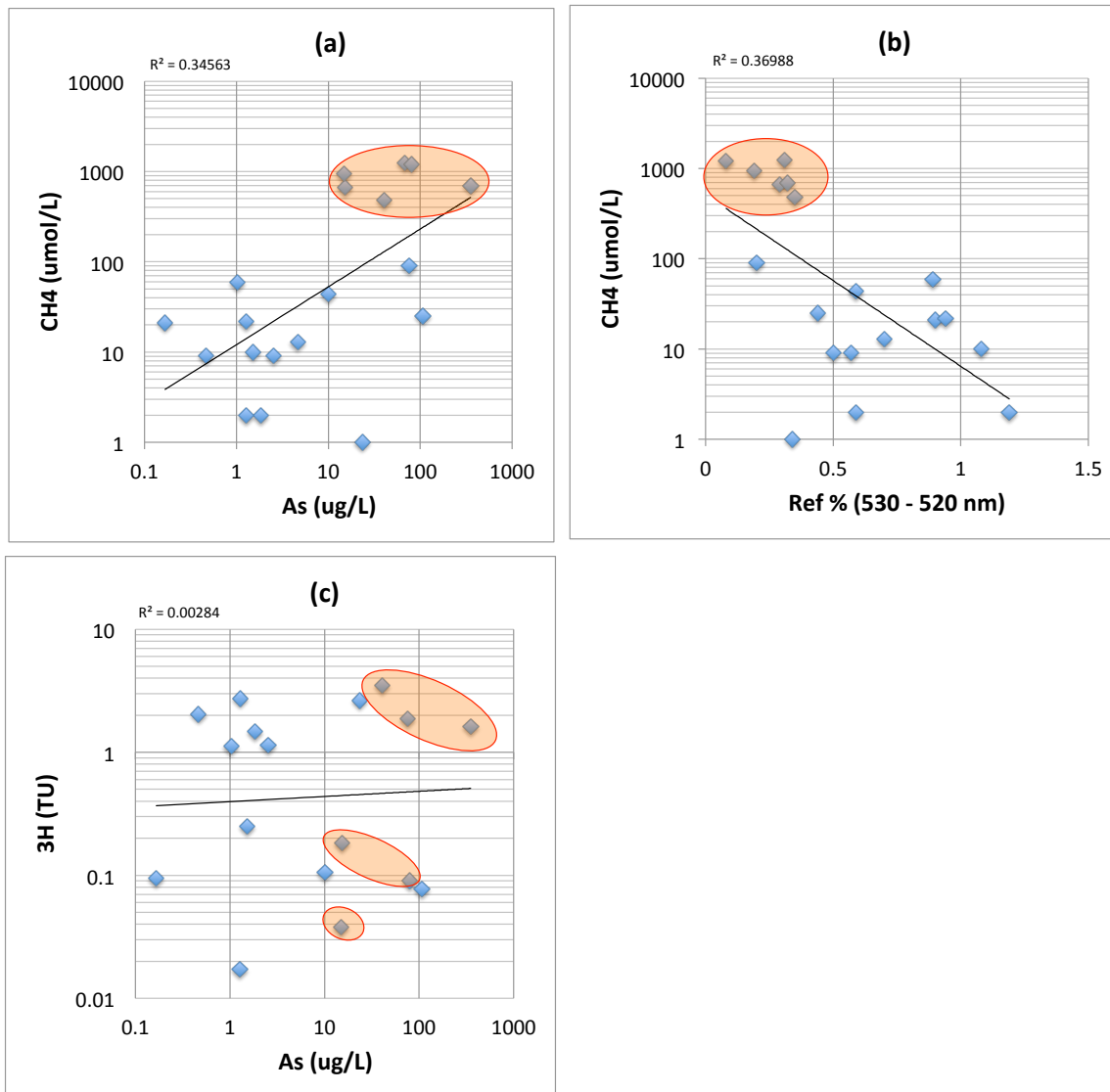
Supplementary discussion on the assumptions and calculations for the reduction of iron oxides with DOC from clay

Reduction of Fe oxides by advection of reactive carbon (DOC) from clay

The advective flow component of groundwater from the clay can be calculated using Darcy's flux written as: $Q = -K\frac{dh}{dx}A$; assuming a hydraulic gradient, $\frac{dh}{dx}$ of 0.2 (head difference of 2 m across the 10 m thick clay) and hydraulic conductivity of $K = 9 \times 10^{-9}$ m/sec (assuming $K = K_h = K_v$ for simplicity), the vertical advective flux of groundwater per sq. m would be 1.8×10^{-9} m^3/sec or 56.8 L/yr/m^2 at a Darcian velocity of 0.057 m/yr or linear average velocity of about 20 cm/year given an effective porosity is 0.3 determined based on Hg-porosimetry method. Since clay pore water contains 20 mg/L of DOC, the average flux of DOC would bring about 1.14 g of carbon per sq. meter per year, which is equivalent to 0.095 moles of C/m^2/year. Over 50 years of pumping, therefore, on the order of 5 moles/m^2 of clay-derived carbon could be advected into orange sands. This flux is sufficient to reduce 19 moles of solid phase Fe^{3+} to 19 moles of Fe^{2+}, assuming 4 moles of Fe^{2+} are produced by the reduction of 4 moles of Fe^{3+} in the expense of 1 mole of DOC (Postma et al., 2007) that is 100% reactive. Following Fe reduction, most of the Fe^{2+} would remain in the solid phase, thus changing the color from orange to gray or yellowish gray. To turn orange sand gray, if we consider the reduction of 0.2% (2000 mg/kg) solid phase Fe^{3+} to Fe^{2+} (orange sediment contain 1% Fe_{tot}), reduction of a total of 53 moles of Fe^{3+} is required to turn a meter thick orange sand aquifer into gray sand aquifer assuming an aquifer particle density of 2650 kg/m^3 and porosity of 0.3. Therefore, over the last 50 years, DOC expelled from the clay by advection could have converted a sand layer about 0.4 m thick from orange to gray in an isotropic aquifer system. With an anisotropy consistent with the 3D model ($K_h/K_v = 100$), only 0.004 m thick orange sand would convert to gray.

Reduction of Fe oxides before the onset of Dhaka pumping

To estimate the potential flux of DOC before Dhaka pumping, we assume that the thick clay aquitard overlying the intermediate aquifer always contained elevated levels of DOC (Figure 4-4). The diffusive flux of DOC from the clay aquitard to the intermediate aquifer is estimated based on Fick's first law: $J = -D \frac{\delta c}{\delta x} n$; where, D is the diffusivity of DOC; $\frac{\delta c}{\delta x}$ is the DOC concentration gradient across the aquitard-aquifer interface, and n is the effective porosity of clay. Using a diffusivity for acetate of 0.009 m^2/year (McMahon & Chappelle 1991) and a DOC gradient $(\frac{\delta c}{\delta x})$ of 0.31 mM/m, calculated at the aquifer-aquitard interface of site-M (Figure 4-4n), we estimate the DOC flux, J from the aquitard to the underlying aquifer for a range of clay porosity values assuming conservative transport of DOC within the clay aquitard (Figure 4-S16) (Put et al. 1992; Hendry et al. 2003; McCarthy et al., 1996).

The bottom of the thick gray aquitard in the study area was on average 8,800 years old based on 8 radiocarbon measurements at 6 locations (Figure 4-S4b). If reducing condition was initiated after the deposition of shallow Holocene deposits ~6,000 years ago and today's DOC concentration gradient across the aquitard-aquifer interface existed 5,000 years ago, the total flux of DOC (after 5,000 year) into the upper intermediate aquifer solely based on Fickian diffusion would be about 7 moles/m^2 assuming an upper end clay porosity of 0.5. The estimated DOC flux on geologic time scale is enough to reduce 27 moles of solid phase Fe^{3+} to 27 moles of Fe^{2+}. Thus, about 0.5 m of orange sand aquifer in contact with gray clay could have turn gray in 5000 years solely based on molecular diffusion.

Figure 4-S16. Sensitivity analyses of arsenic (As) contamination and solid phase iron (Fe) reduction near the aquifer-aquitard interface. (a) Projected aquifer As levels in the intermediate aquifer associated with diffused flux of dissolved organic carbon (DOC) from clay aquitard as a function of clay porosity, assumed contaminated aquifer thickness, and time. These estimates are based on the assumptions: (i) As:Fe molar ratio of 5.5% in the solid phase (Burnol et al., 2007), (ii) after release As is retarded by a factor of 10, and (iii) dissolved As is homogenized in an aquifer with 10 m ('o'), 20 m ('Δ'), and/or 30 m ('+') thickness. The colors corresponds to diffusion time at 1 ka year interval (between 1 ka and 5 ka); (b) Projected time required for the conversion of a meter thick orange Pleistocene aquifer to gray for the estimated DOC flux as a function of clay porosity and variation in fraction of solid phase Fe reduction.
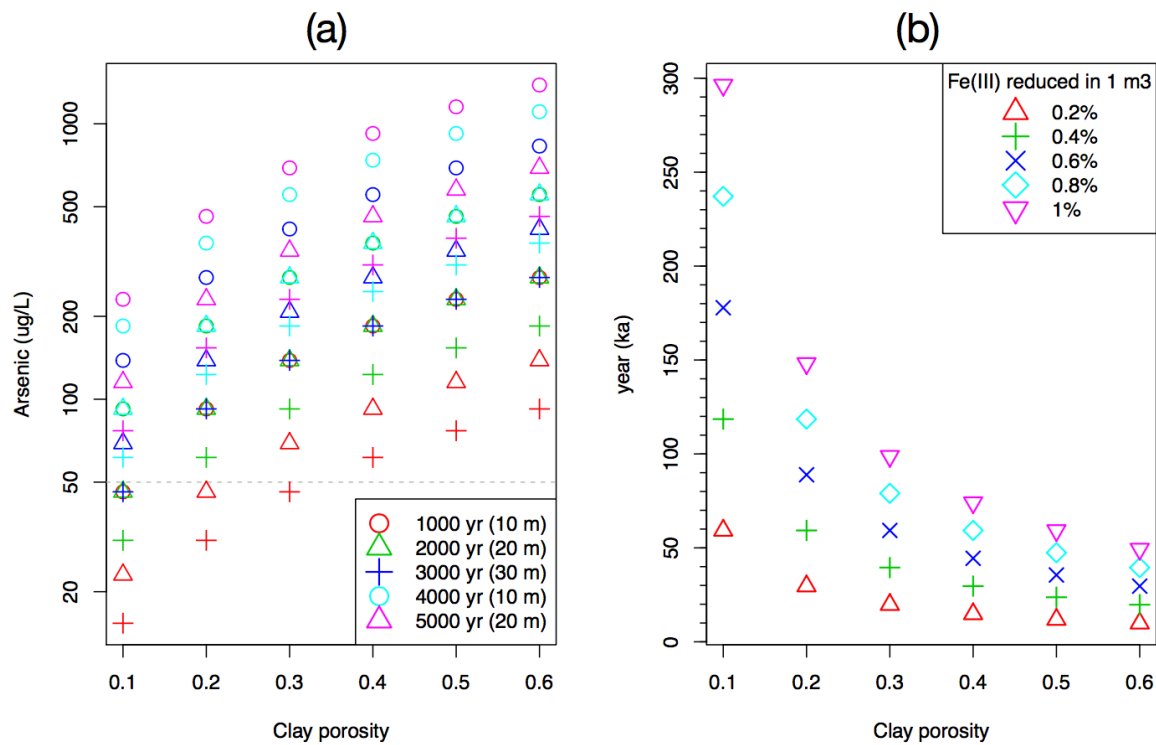
Table 4-S1. Estimated aquifer hydraulic conductivity and storativity (see Figure 4-S6).

Analysis	Well	Kh (m/s)	S
Time drawdown	C	0.98E-04	3.1E-04
	1.3	1.1E-04	7.7E-04
	1.4	1.1E-04	7.8E-04
	1.5	0.97E-04	4.1E-04
	2.3	1.4E-04	5.9E-04
	2.5	1.3E-04	5.8E-04
	3.5	1.2E-04	5.0E-04
	4.4	1.0E-04	9.4E-04
	4.5	1.5E-04	7.1E-04
	Average	1.2E-04	6.2E-04
	St. Dev.	0.2E-04	2.0E-04
Distance drawdown	n/a	0.82E-04	13E-04

References

Burnol A., Garrido F., Baranger P., Joulian C., Dictor M.-C., Bod Bod F., Morin G. and Charlet L. (2007) Decoupling of arsenic and iron release from ferrihydrite suspension under reducing conditions: a biogeochemical model. *Geochem. Trans.* **8**, 12.

Gonthier, G.J., (2007). A Graphical Method for Estimation of Barometric Efficiency from Continuous Data - Concepts and Applications to a Site in the Piedmont, Air Force Plant 6, Marietta, Georgia. *U.S. Geological Survey Scientific Investigations Report* **2007-5111**, Reston, Virginia.

Hendry M. J., Ranville J. R., Boldt-Leppin B. E. J. and Wassenaar L. I. (2003) Geochemical and transport properties of dissolved organic carbon in a clay-rich aquitard. *Water Resour. Res.* **39**. Available at: https://agupubs.onlinelibrary.wiley.com/doi/abs/10.1029/2002WR001943 [Accessed September 4, 2018].

Khan M. R., Koneshloo M., Knappett P. S. K., Ahmed K. M., Bostick B. C., Mailloux B. J., Mozumder R. H., Zahid A., Harvey C. F., Geen A. van and Michael H. A. (2016) Megacity pumping and preferential flow threaten groundwater quality. *Nat. Commun.* **7**, 12833.

McCarthy J. F., Gu B., Liang L., Mas-Pla J., Williams T. M. and Yeh T.-C. J. (1996) Field Tracer Tests on the Mobility of Natural Organic Matter in a Sandy Aquifer. *Water Resour. Res.* **32**, 1223–1238.

McMahon P. B. and Chapelle F. H. (1991) Microbial production of organic acids in aquitard sediments and its role in aquifer geochemistry. *Nature* **349**, 233–235.

Postma D., Larsen F., Minh Hue N. T., Duc M. T., Viet P. H., Nhan P. Q. and Jessen S. (2007) Arsenic in groundwater of the Red River floodplain, Vietnam: Controlling geochemical processes and reactive transport modeling. *Geochim. Cosmochim. Acta* **71**, 5054–5071.

Put M. J., Monsecour M. and Fonteyne A. (1992) Mobility of the dissolved organic material in the interstitial boom clay water. *Radiochim. Acta* **58–59**, 315–317.

Stute M., Zheng Y., Schlosser P., Horneman A., Dhar R. K., Datta S., Hoque M. A., Seddique A. A., Shamsudduha M., Ahmed K. M. and van Geen A. (2007) Hydrological control of As concentrations in Bangladesh groundwater. *Water Resour. Res.* **43**, W09417.

CHAPTER 5

SYNTHESIS

This study presents several key findings on the distribution of arsenic (As) in Bangladesh groundwater on the basis of field observations and modeling. The second chapter sheds light on the spatiotemporal evolution of As in the shallow (<30 m deep) aquifer of Bangladesh. Arsenic concentrations were compared between blanket As-testing campaigns of thousands of wells carried out 12 years apart across the same 25 sq. km area of Araihazar. Arsenic concentrations were compared in spatially paired wells (n = 271) and blocks of 300×300 m^2 areal extent (n = 346). The paired comparisons were complemented with 18 As time-series measurements from 4 locations monitored over the past 15 years. The results indicate a net decrease in the mean As for the area by about 10%, with both statistically significant increases and decreases observed for individual wells and at the block level. This moderate decline in the mean As could simply be attributed to the redistribution of As by flushing, where the export of dissolved As from the aquifer due to widespread irrigation pumping continue to deplete the inventory of sediment bound As over time in response to the buffering between the aquifer solid and aqueous phase As concentrations. Geospatial heterogeneity in the pool of exchangeable As and variations in the rate of recharge as well as pumping may explain the wide range of decline observed in dissolved As (3-300 µg/L) over the last decade. The increases in As with a similar magnitude, on the other hand, could either relate to accelerated recharge of reactive carbon promoting additional release or due to lateral advection and mixing between heterogeneously distributed high- and low-As groundwater induced by irrigation pumping. Mixing could also explain a decline in As over

196

time; however, quantifying the relative importance of flushing over mixing is beyond the scope of this thesis.

The third chapter provides new insights into the sorption and delay of As transport in the sedimentary aquifers of Bangladesh. A field column experiment was conducted with freshly collected intact cores (n = 11) and unaltered shallow groundwater to determine As retardation under controlled condition. The cored Holocene gray and Pleistocene orange sands were eluted with anoxic, high As groundwater (320 μg/L, 90% as As-III) pumped at pore water velocities (PWV) ranging between 1.5 and 9.5 cm/hour. In most of the columns, the initial breakthrough of As occurred after 50 PV. Despite high levels of Fe and P in the inflowing groundwater, the eluent from the Pleistocene orange sediment columns contained only traces of Fe and P for most part of the experiment. In contrast, a complete breakthrough of As in the gray sand columns was followed by the breakthrough of Fe and P, respectively. Sulfur concentration in the eluent declined rapidly after breakthrough at the onset of the experiment from about 3 mg/L to <0.5 mg/L between the first 30 and 100 PV, depending on PWV. The reduction of As and Fe and formation of arsenic sulfide phases was evident particularly in the orange sediment cores. A two-phase reversible kinetic model was applied to describe the initial breakthrough of As in the columns using one dimensional advection-dispersion equation. The results indicate that As transport in both the gray and orange sediment aquifers of Bangladesh is retarded by a factor of 30-35 with respect to groundwater flow.

The fourth chapter of this thesis focuses on the redistribution of As in the face of overpumping in the municipal city of Dhaka located about 25 km west to the 3 sq. km study area. A three-

dimensional groundwater flow model was developed to trace the source of As contamination in a Pleistocene intermediate aquifer (>30-90 m) that is typically low in As since much of it is capped by a thick (10-15 m) clay aquitard preventing downward migration of shallow, high As groundwater. The model predicted elevated groundwater heads in unconfined, sandy portion of the intermediate aquifer and low heads in clay-capped, confined portion of the aquifer is consistent with present day head observations. Particle tracking results suggest Dhaka pumping had accelerated the lateral advection of shallow groundwater by about 10 times along a transect from a sandy recharge window that is hydraulically connected to a clay-capped site. These results are consistent with the penetration of ^{3}H, groundwater ^{3}H-^{3}He ages, and the stable isotope composition of groundwater in the intermediate aquifer. No systematic correlation between As, ^{3}H, and sediment color suggest elevated As in the Pleistocene aquifer may not solely be linked to lateral intrusion of dissolved As, organic carbon, and/or methane. The transport (advection and diffusion) of carbon from the overlying clay aquitard could be an alternative source of reductant transforming the orange Pleistocene sand to gray. While the advection of clay-derived carbon was accelerated significantly in response to Dhaka pumping, diffusion of carbon from clay had been active for thousands of years.

In summary, the findings in this thesis put new constraints on the fate and transport of As in Bangladesh groundwater under the current pumping scenario. Geostatistical comparisons in the second chapter indicate As concentrations in the shallow aquifers perturbed by irrigation pumping are more likely to decline over time, albeit slowly. This finding, however, by no means justify encouraging households to rely on shallow, low As resources because As levels also rose significantly over the past decade. Results from field column experiments in the third chapter

indicate an earlier breakthrough of As at a higher PWV, implying accelerated groundwater flow is likely to introduce As at a faster rate in the low-As aquifers that are vulnerable to pumping. Finally, the fourth chapter provides evidence of different modes of transport of As contaminating the intermediate, low-As aquifers in the face of massive depressurization. Thousands of low-cost, private wells tapping the intermediate aquifer have already reduced human exposure to drinking water elevated in As. The government and NGOs of Bangladesh should, therefore, put more emphasis on the monitoring of the growing number of intermediate wells in parallel to the allocation of deep wells that are less vulnerable to pumping.